

**GEOLOGIC AND TECTONIC EVOLUTION OF JURASSIC
MARGINAL OCEAN BASIN LITHOSPHERE,
KLAMATH MOUNTAINS, OREGON**

Thesis by

John Douglas Yule

In Partial Fulfillment of the Requirements

for the Degree of

Doctor of Philosophy

California Institute of Technology

Pasadena, California

1996

(Submitted December 20, 1995)

ACKNOWLEDGEMENTS

This study has been conducted under the supervision of Dr. Jason B. Saleeby of the California Institute of Technology, who suggested the topic and provided financial support. I am particularly grateful to Jason for his friendship, steady encouragement, and faith in my abilities.

Support for my field work was provided by the Geological Society of America, the Oregon Department of Geology and Mineral Industries, and by the Caltech geology department with funds granted to first year graduate students. I thank these organizations for their support.

I would also like to thank the following Klamath Mountains geologists for their assistance, encouragement, and friendship during my seasons of field work. Working as a field assistant for William P. Irwin during the summer of 1983 served as my introduction to the geology of the Klamath Mountains region. I am grateful to Porter for sparking my initial curiosity about the geology of the region, an intrigue that eventually led to my pursuit of this project. My mapping benefited greatly from many discussions with Dr. Gregory D. Harper of SUNY-Albany. Greg freely shared his vast knowledge and insights of the Josephine ophiolite and the geologic and tectonic evolution of the Klamath Mountains province. I always looked forward to visiting Greg and his students at their various field “camps” where I appreciated sharing in their open exchange of ideas and geologic discoveries, particularly during spirited, if not hotly contested, games of basketball at the Gasquet elementary school courts. I am also grateful to Tom Wiley and Frank Hladky of the Oregon Department of Geology and Mineral Industries who helped support my work and were always able to take the time to offer their advice and insights. I am also thankful for a field visit from Len Ramp whose geologic maps provided the foundation for this study.

The geochronological aspects of this study were conducted at the California Institute of Technology under the direction of Dr. Jason B. Saleeby who taught me the theory and practice of U-Pb geochronology and prepared the standards used during this study. Dr. Leon T. Silver prepared the isotopic tracers used during this study.

The geochemical analyses included in this study were conducted at Texas Tech University by Dr. Calvin G. Barnes. Cal also provided the zircon separates from the Ashland, Grayback, and Thompson Ridge plutons “in exchange” for the whole rock powders used for the geochemical analyses. I am grateful to Cal for entrusting a “rookie” zirconologist to analyze his samples. $^{40}\text{Ar}/^{39}\text{Ar}$ age determinations were conducted by Dr. Bradley R. Hacker at Stanford University in Dr. M.O. McWilliams’ laboratory, and I thank them for allowing me to publish the data here. Michelle Silk at the University of California at Berkeley processed and analyzed the chert samples and generously allowed me to publish the data.

I would especially like to thank my brother, Brad Yule, for his able assistance during portions of my field seasons (the summers of 1990-1994). Without his help I would never have managed the numerous chaparral traverses, bushwhacks, and backpack excursions necessary fill the various “holes” in my map. I also enjoyed and appreciated his creative attempts to cook field meals featuring the local flora and fauna.

I also greatly appreciated field visits from a fellow Caltech graduate students Dave Sauer, Elizabeth Nagy, Rich Dissly, Lazlo Kesthelyei, Steve Leroy, Jim Spotila, Nathan Niemi, Craig Scrivner, and Tim Melbourne. And, many thanks to the Rev. Harry Dog (“and them’s my rules”) and his minstrel band of mirthmakers for welcoming me at their annual Labor Day weekend soirees at the Store Gulch campsite. Thanks also to my Illinois River friends Art Bleeker and “Bud” who maintained the Store Gulch campsite, stored my rocks samples, and looked after my belongings while I was away.

My office mates, Carey Gazis, Mihai Ducea, and Rich Wolf, provided much needed moral support and encouragement during my years at Caltech. I am particularly grateful to Mihai for his helpful comments and suggestions on early versions of this tome.

I would also like to thank my parents, John and Jean Yule, for their constant support and enthusiasm of my studies at Caltech and my field work in Oregon. Finally I thank my wife, Rebecca McGrew, for her love, patience, and understanding during the completion of this study. Without her enduring support, none of this would have been possible.

ABSTRACT

This study examines the geologic and tectonic history of the westernmost lithotectonic belt of the Klamath Mountains province, known as the western Jurassic belt (WJB). In Oregon the WJB exposes one of the world's best preserved examples of ancient marginal ocean basin lithosphere, including a complete ophiolite sequence, an arc volcano-plutonic complex, and older fragments of oceanic lithosphere that occur as screens within the ophiolite and which form the basement constructs of the arc. As such, the region provides an exceptional opportunity to directly examine the structural framework and geologic features of marginal ocean basins. Geologic mapping in the central Illinois River drainage area, Curry and Josephine Counties, Oregon has resulted in the following changes to previously reported work: 1) the discovery of a 5 x 45 km fragment of rocks correlative with the Rattlesnake Creek terrane; rocks previously known only to occur within the overthrust lithotectonic belt to the east, the western Paleozoic and Triassic belt, 2) the discovery of an intra-peridotite boundary separating pre-175 Ma serpentinized harzburgite and dunite from relatively unaltered peridotite associated with the Josephine ophiolite (166-162 Ma), and 3) a re-interpretation of the region as a fold and fault belt rather than an imbricate thrust stack of separate subterranean units. Collectively, these relations confirm the prediction of a previous model for the Jurassic tectonic evolution of the region that invokes rifting of a Middle Jurassic arc and arc basement terrane to form a paired, Late Jurassic inter-arc basin ophiolite and volcanic arc. Radiometric ages determined from rocks in the map area and from arc plutons exposed to the east, in combination with a wealth of pre-existing geochronometric data, indicate that the Klamath Mountains province experienced a continuum of arc-related magmatism from ~175-135 Ma, distinct episodes of thrusting at ~165 and ~155 Ma, and a prolonged episode of ophiolite genesis and extension from ~170-160 Ma. These features characterize the province as a batholithic belt constructed in an entirely oceanic setting and represent an archetypal example of a long-lived oceanic arc system generated at a loosely coupled ocean/ocean convergent plate boundary.

TABLE OF CONTENTS

| | |
|---|-----|
| Chapter 1: Introduction | 1 |
| References | 13 |
| | |
| Chapter 2: Generalized geologic map and structural evolution of the western Jurassic belt, Klamath Mountains, Oregon | |
| Abstract | 16 |
| Introduction | 17 |
| Geologic Framework and Previous Work | 19 |
| Josephine ophiolite | 22 |
| Rogue River island arc complex | 23 |
| Galice Formation | 24 |
| Geology of the central Illinois River drainage area | 25 |
| Northern outlier of the Josephine ophiolite | 26 |
| Crustal rocks | 26 |
| Peridotite | 39 |
| Rogue and Galice Formations | 42 |
| Rogue Formation | 42 |
| Galice Formation | 50 |
| Illinois River plutonic complex | 51 |
| Main phase rocks | 52 |
| Sills | 52 |
| Age | 66 |
| Petrography | 66 |
| Country rocks | 66 |
| New Map Units | 77 |
| Fiddler Mountain olistostrome complex | 77 |
| Lithologies | 78 |
| Detrital rocks | 78 |
| Megabreccia | 83 |
| Pelagic sediments | 84 |
| Regional correlations | 84 |
| Onion Camp complex | |
| Overview | 85 |
| General Features | 86 |
| Metavolcanic rocks | 87 |
| Red chert | 88 |
| Metasedimentary rocks | 93 |
| Mafic intrusive suite | 96 |
| Amphibolitic rocks | 99 |
| Serpentine and serpentinitized peridotite | 103 |
| Field appearance | 106 |
| Textural and structural features | 107 |
| Dikes | 115 |
| Summary and regional correlations | 115 |

| | |
|--|-----|
| Discussion of Geochemical data | 116 |
| <i>Josephine ophiolite</i> | 116 |
| Rogue Formation | 116 |
| Onion Camp complex | 120 |
| Illinois River plutonic complex | 122 |
| Discussion of U-Pb Geochronometric data | 127 |
| Samples from the Illinois River plutonic complex | 127 |
| Plagiogranite dikes cutting Onion Camp complex | 131 |
| Plagiogranite in sheeted mafic dike complex | 131 |
| Late stage dacite dike | 132 |
| Structural and Metamorphic Features | 132 |
| Deformational and Metamorphic History | 132 |
| Mesoscopic structural features | 134 |
| Regional Fold structures | 149 |
| Faults | 152 |
| Valen Lake fault | 152 |
| Extensional shear zones | 153 |
| Madstone Cabin fault | 154 |
| Chetco Pass fault system | 160 |
| Illinois River Valley fault | 162 |
| Other Nevadan faults | 165 |
| Summary | 166 |
| Conclusions | 171 |
| References | 176 |

Chapter 3: Jurassic Orogeny During 40 M.Y. of Continuous Oceanic Arc Magmatism in the Klamath Mountains Province: New Insights From Oregon

| | |
|---|-----|
| Abstract | 182 |
| Introduction | 186 |
| General Tectonic and Geologic Framework | 188 |
| Western Jurassic belt | 188 |
| Condrey Mountain Schist | 194 |
| Western Paleozoic and Triassic belt | 195 |
| Post-164 Ma plutons | 196 |
| Geochronologic Data | 197 |
| Methods and Analytical Procedures | 197 |
| Data | 205 |
| Middle and Late Jurassic Volcanoplutonic... | 207 |
| Basement rocks..... | 213 |
| Geochronologic Overview | 215 |
| Middle Jurassic to Early Cretaceous ... | 220 |
| M.to L. Jurassic ophiolite sequences | 221 |
| Metamorphic rocks | 222 |

| | |
|--|-----|
| Discussion | 224 |
| Klamath Mountains batholithic belt (KMBB) | 224 |
| Jurassic Orogeny in the Klamath Mountains prov. | 233 |
| Tectonic and paleogeographic Reconstructions | 235 |
| Summary and Conclusions | 245 |
| References | 247 |
| | |
| Chapter 4. Structural Framework of Marginal Ocean Basin Lithosphere: An Example From the Klamath Mountains, Oregon. | |
| Abstract | 251 |
| Introduction | 252 |
| Features of Marginal Ocean Basins | 253 |
| Geologic Overview of the Josephine Marginal Ocean Basin | 255 |
| Distinctive Features of the Josephine Marginal Ocean Basin | 264 |
| Intraperidotite contact | 264 |
| Inter-arc Basin Rift-edge facies | 269 |
| Oceanic arc crust | 272 |
| Conclusions | 274 |
| References | 276 |
| | |
| Appendix 1: Geologic Map Explanation of the Central Illinois River Area, Josephine and Curry Counties, Oregon. | |
| Introduction | 278 |
| General explanation of Plates 1-11 | 280 |
| Geologic Map Explanation, Plate 1 | 287 |
| Geologic Map Explanation, Plates 2-11 | 292 |
| References | 301 |
| | |
| Appendix 2: U/Pb Geochronologic Methods | |
| Laboratory Methods | 303 |
| References | 308 |

LIST OF FIGURES

| | Page |
|---|------|
| CHAPTER 1 | |
| Figure 1-1. Generalized lithotectonic map of the Klamath Mountains province and the Oregon Coast Ranges. | 2 |
| Figure 1-2. Regional geologic map of the Klamath Mountains province and the Oregon Coast Ranges showing the principal rock units and lithotectonic terranes. | 3 |
| Figure 1-3. Tectonic and physiographic maps of modern marginal ocean basins in the Marianas and Andaman Sea regions. | 7 |
| CHAPTER 2 | |
| Figure 2-1. Regional geologic map of the northern Klamath Mountains province and the Oregon Coast Ranges. | 20 |
| Figure 2-2. Photograph of Josephine pillow lavas. | 27 |
| Figure 2-3. Photograph of Eight Dollar Mountain and the boundary between the Josephine and the Onion Camp complex peridotite masses. | 40 |
| Figure 2-4. Photograph of Rogue Fm turbidites. | 44 |
| Figure 2-5. Photograph of Rogue Fm volcanic breccia. | 46 |
| Figure 2-6. Photograph of serpentinite clast breccia. | 48 |
| Figure 2-7. Photograph of Illinois River plutonic complex hornblende diorite. | 53 |
| Figure 2-8. Photograph of stream boulder of orbicular norite, Illinois River plutonic complex. | 55 |
| Figure 2-9. Photograph of flaser gabbro, Illinois River plutonic complex. | 58 |
| Figure 2-10. Photograph of the boundary between the Pearsoll Peak peridotite and the Illinois River plutonic complex. | 60 |
| Figure 2-11. Photograph of the hornblende gabbro pegmatoid, Illinois River plutonic complex. | 62 |
| Figure 2-12. Photograph of the hornblende gabbro pegmatoid with harzburgite screen, Illinois River plutonic complex. | 64 |
| Figure 2-13. Photomicrograph of partially recrystallized norite, Illinois River plutonic complex. | 67 |
| Figure 2-14. Photomicrograph of norite with undulose extinction and bent twinning lamellae, Illinois River plutonic complex. | 69 |

| | |
|---|-------------------|
| Figure 2-15. Photomicrograph of mylonitic hornblende quartz diorite from the margin of the Illinois River plutonic complex. | 71 |
| Figure 2-16. Photograph of amphibolite gneiss, Briggs Creek amphibolite unit. | 74 |
| Figure 2-17. Photograph of heterolithologic conglomerate, Fiddler Mountain olistostrome complex. | 79 |
| Figure 2-18. Photograph of heterolithologic conglomerate and silty sand, Fiddler Mountain olistostrome complex. | 81 |
| Figure 2-19. Photograph of Onion Camp complex pillow lavas (Rattlesnake Creek terrane equivalents). | 89 |
| Figure 2-20. Photograph of Triassic chert locality near Onion Camp. | 91 |
| Figure 2-21. Photograph of strongly deformed metavolcanic rocks of the Onion Camp complex. | 94 |
| Figure 2-22. Photograph of view looking along contact between OCC crustal rocks and OCC serpentized peridotite. | 104 |
| Figure 2-23. Photograph of foliated OCC peridotite. | 109 |
| Figure 2-24. Photograph of brecciated OCC peridotite. | 112 |
| Figure 2-25. Plots of P_2O_5 , MgO/FeO, and Zr versus Ti for basaltic rocks from the Rogue Fm, Josephine ophiolite, and OCC. | 118 |
| Figure 2-26. Plot of REE abundances, normalized to chondrite values, of Rogue Formation basalts. | 121 |
| Figure 2-27. Plot of REE abundances, normalized to chondrite values, of OCC basalts. | 123 |
| Figure 2-28. Variation of common oxides in IRPC rocks plotted against SiO_2 . | 124 |
| Figure 2-29. Sr vs Y of IRPC gabbro, diorite, and tonalite-trondhjemite. | 126 |
| Figure 2-30. Stacked Terra-Wasserburg concordia plots. | 128 129 130 |
| Figure 2-31. Photomicrograph of OCC metatuff. | 135 |
| Figure 2-32. Photomicrographs of Rogue Fm basalt. | 137 |
| Figure 2-33. Photomicrograph of tightly folded OCC metaargillite. | 139 |
| Figure 2-34. Photograph of well lineated OCC metachert. | 141 |

| | |
|--|-----|
| Figure 2-35a-d. Stereographic projections of structural data. | 144 |
| Figure 2-35e-g. Stereographic projections of structural data. | 146 |
| Figure 2-36. Generalized map of the primary structures of the study area. | 150 |
| Figure 2-37. Diagrammatic map and cross-section view of the IRPC and its surrounding wallrocks during pluton emplacement. | 155 |
| Figure 2-38. Diagrammatic map and cross-section view of the IRPC and its surrounding wallrocks at the time of pluton emplacement. | 158 |
| Figure 2-39. Photograph taken looking SSW along the trace of the Illinois River Valley fault. | 163 |
| Figure 2-40. Generalized reconstruction of the rocks of the study area prior to Nevadan deformation. | 167 |
| Figure 2-41. Simplified geologic cross section across the study area. | 174 |
| CHAPTER 3 | |
| Figure 3-1. Generalized lithotectonic map of the Klamath Mountains and the Oregon Coast Ranges. | 189 |
| Figure 3-2. Regional geologic map of the northern Klamath Mountains province and the Oregon Coast Ranges. | 191 |
| Figure 3-3. Stacked Terra-Wasserburg concordia diagrams. | 201 |
| Figure 3-4. Plot of published Middle Jurassic to Early Cretaceous radiometric age data from the entire Klamath Mountains province | 217 |
| Figure 3-5. Magmatic and tectonic evolution of the Klamath Mountains batholithic belt. | 227 |
| Figure 3-6A. Tectonic and Paleogeographic reconstruction at ~175-170 Ma. | 236 |
| Figure 3-6B. Tectonic and Paleogeographic reconstruction at ~170-155 Ma. | 239 |
| Figure 3-6C. Tectonic and Paleogeographic reconstruction at ~155-150 Ma. | 242 |
| CHAPTER 4 | |
| Figure 4-1. Generalized cross-section across a marginal ocean basin. | 254 |
| Figure 4-2. Geologic map of the northern half of the Klamath Mountains province | 256 |

| | |
|---|-----|
| Figure 4-3. Generalized structural geology map of the central Illinois River drainage area. | 258 |
| Figure 4-4. Plot of the known age range for the protectonic elements of the western Jurassic belt. | 261 |
| Figure 4-5. Diagrammatic columnar sections from the central Illinois River drainage area. | 262 |
| Figure 4-6. Simplified geologic cross section of the Josephine marginal ocean basin and fringing arcs. | 267 |
| APPENDIX 1 | |
| Figure A1-1. Outline of the map area with quadrangle names. | 281 |

LIST OF TABLES

CHAPTER 2

| | |
|--|-----|
| Table 2-1. U/Pb isotopic data. | 29 |
| Table 2-2. Summary of $^{40}\text{Ar}/^{39}\text{Ar}$ geochronologic ages. | 32 |
| Table 2-3. Major and trace element abundances obtained for basaltic rocks of the Rogue Formation, the Josephine ophiolite, and the Onion Camp complex, and for mafic to intermediate plutonic rocks of the Illinois River plutonic complex. | 33 |
| Table 2-4. Approximate modal mineral abundances for rocks of the Illinois River plutonic complex. | 57 |
| Table 2-5. Rare earth element concentrations obtained for basaltic Rocks of the Rogue Formation and Onion Camp complex. | 117 |

CHAPTER 3

| | |
|---|-----|
| Table 3-1. U/Pb isotopic data. | 198 |
| Table 3-2. Summary of $^{40}\text{Ar}/^{39}\text{Ar}$ geochronologic ages. | 206 |

CHAPTER 4

| | |
|---|-----|
| Table 4-1. Distinguishing features of the Josephine and Rattlesnake Creek terrane peridotite masses. | 265 |
|---|-----|

APPENDIX 1

| | |
|---|-----|
| Table A1-1. Geochemical samples and localities. | 282 |
| Table A1-2. Paleontologic samples and localities. | 285 |
| Table A1-2. Geochronologic samples and localities. | 286 |

APPENDIX 2

| | |
|--|-----|
| Table A2-1. Isotopic composition of Pb in NBS standard. | 306 |
| Table A2-1. Isotopic composition of U in NBS standard. | 307 |

LIST OF PLATES

Plate 1. Geology map (1:96,000) of the central Illinois River drainage (pocket) area with cross-sections. (See Appendix 1 for map explanation.)

Note: **Plates 2-11** are a series of adjoining 7.5' topographic quadrangle maps, numbered as shown in **Figure A1-1** (also see **Plate 1**).

Plate 2. Reconnaissance geologic map of part of the Chetco Peak 7.5' (pocket) quadrangle (1:24,000).

Plate 3. Reconnaissance geologic map of part of the Josephine (pocket) Mountain 7.5' quadrangle (1:24,000).

Plate 4. Reconnaissance geologic map of part of the Cave Junction (pocket) 7.5' quadrangle (1:24,000).

Plate 5. Geologic map of part of the Pearsoll Peak 7.5' quadrangle (pocket) (1:24,000), modified after Ramp et al. (1984).

Plate 6. Geologic map of the Eight Dollar Mountain 7.5' quadrangle (pocket) (1:24,000).

Plate 7. Reconnaissance geologic map of part of the Selma 7.5' (pocket) quadrangle (1:24,000).

Plate 8. Reconnaissance geologic map of part of the York Butte 7.5' (pocket) quadrangle (1:24,000).

Plate 9. Reconnaissance geologic map of the Chrome Ridge 7.5' (pocket) quadrangle (1:24,000).

Plate 10. Reconnaissance geologic map of the Onion Mountain 7.5' (pocket) quadrangle (1:24,000).

Plate 11. Reconnaissance geologic map of part of the Galice 7.5' (pocket) quadrangle (1:24,000).

CHAPTER 1

INTRODUCTION

The Klamath Mountains geological province is well known for its arcuate lithic belts, or terranes, that consist primarily of oceanic rocks separated from adjacent belts by shallowly eastward dipping fault zones (Figure 1-1). Irwin (1960, 1966), Davis (1969), and subsequent workers noted that the belts contain progressively younger rocks toward the west and that their geologic histories are essentially unrelated to those of the adjacent belts. These relations suggest that the Klamath Mountains record a succession of distinct events when oceanic materials were episodically underthrust beneath western North America. The westernmost lithotectonic belt, named the western Jurassic belt (WJB) by Irwin (1966), is a composite terrane consisting primarily of a Late Jurassic oceanic island arc rocks, a complete ophiolite sequence, and flysch deposits that were "subcreted" beneath the older Klamath terranes during the Late Jurassic Nevadan orogeny.

More recent work in the WJB has focused on the various prototectonic units and the structural framework of the belt (Figure 1-2). For example, rocks of the Rogue River island arc complex were described by Garcia (1979, 1982), and the arc volcanic rocks are conformably overlapped by sedimentary strata of the Galice Formation (Diller, 1907; Wells and Walker, 1953; and Imlay, 1980). Farther to the south, Dick (1976) defined the Josephine peridotite as a fragment of the mantle lithosphere. Harper (1980, 1984) documented that the Josephine peridotite was associated with an ophiolitic crustal sequence and was the first to refer to the entire sequence as the Josephine ophiolite. Harper (1984) also noted that Galice-type sediments conformably overlapped pillow lavas of the ophiolite and therefore suggested that the Rogue River arc and Josephine ophiolite formed contemporaneously as part of an arc and back-arc basin.

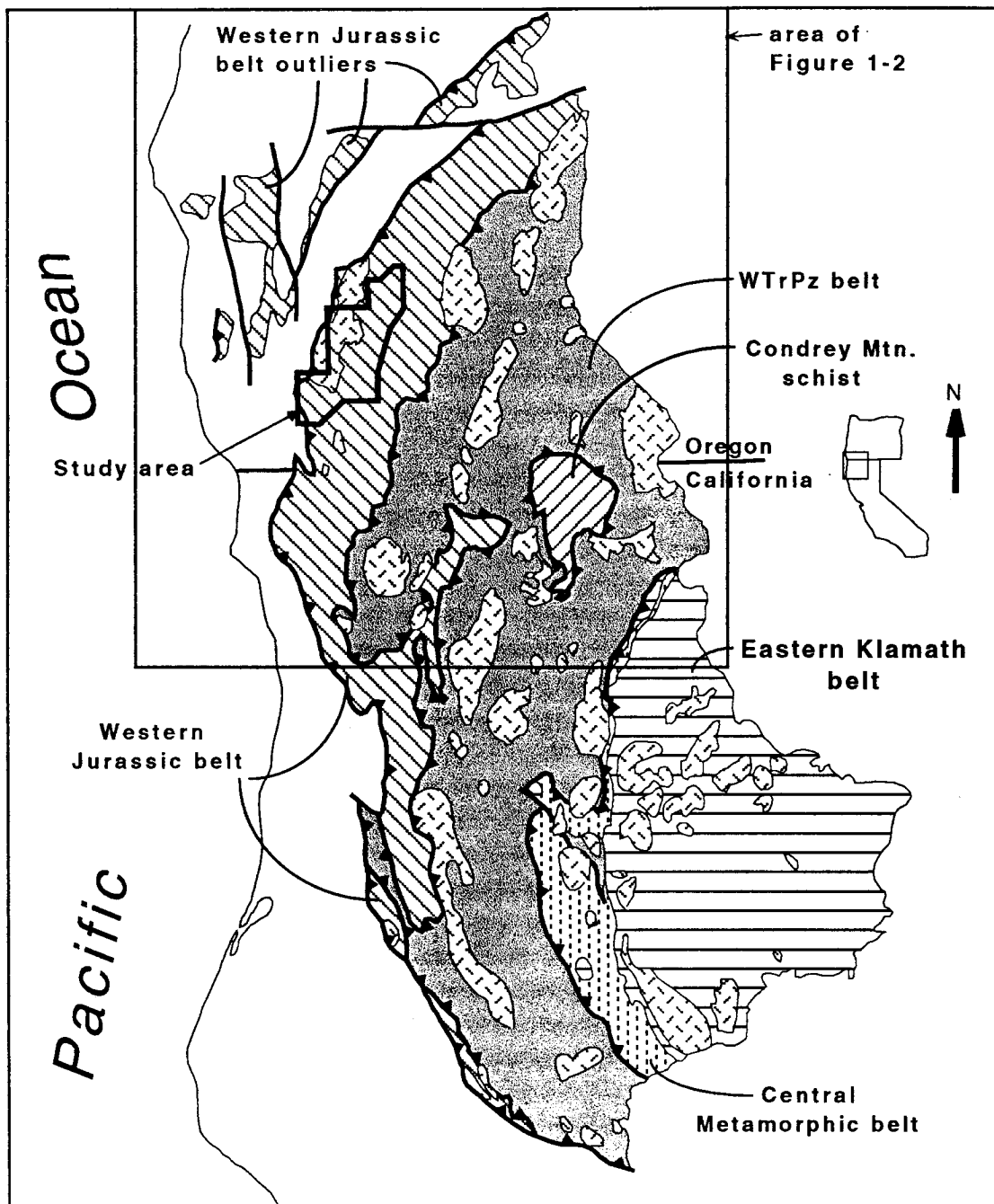
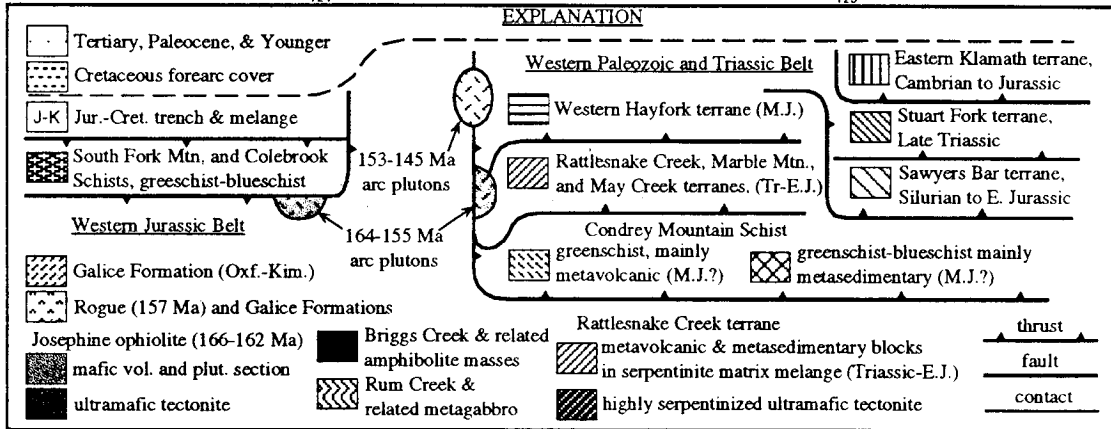
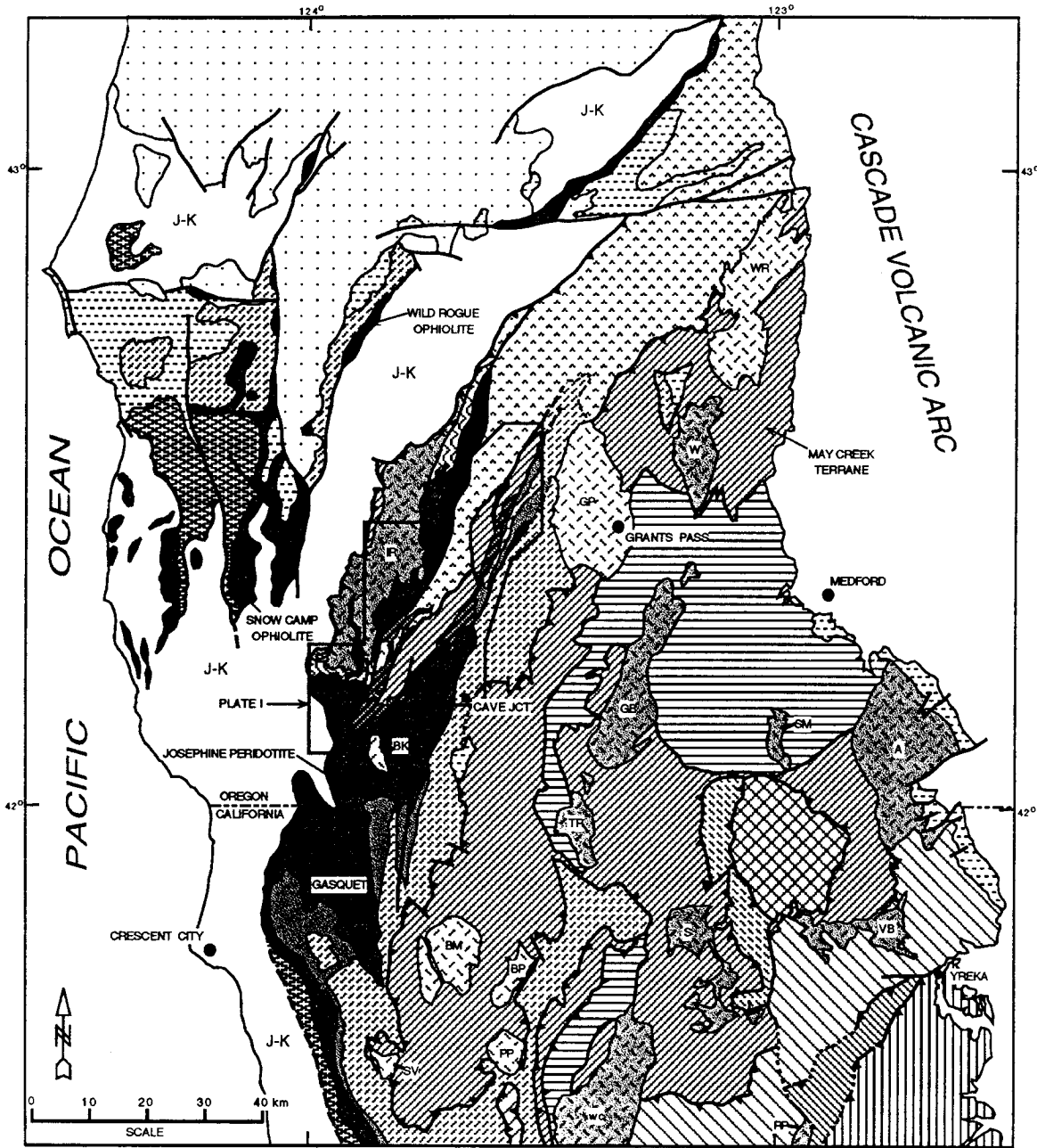


Figure 1-1. Map of the Klamath Mountains province and Oregon Coast Ranges showing the principal lithotectonic belts and plutons.

Figure 1-2. Regional geologic map of the northern Klamath Mountains province and the Oregon Coast Ranges. The map is compiled from my field studies during 1989-1994 and modified from work published by Coleman and Lanphere (1991), Hacker et al. (1995), Irwin (1994), Ramp et al. (1977), and Ramp et al.(1979).



Work to constrain the ages of the arc and ophiolitic rocks (Saleeby and others, 1982; and Saleeby, 1984) confirmed the arc and ophiolite sequences were coeval. In addition, the Galice Formation sediments were shown to contain distinctive detrital grains derived from cratonic North America and older Klamath terranes indicating that the Rogue arc and the Josephine ophiolite formed in an ocean basin fringing western North America (Snoke, 1977; Miller and Saleeby, 1987). Snoke (1977) suggested that the Josephine ophiolite formed as an older oceanic arc complex rifted apart. The "rift-edge" of the older arc is preserved in the region surrounding Preston Peak, California, and forms the western edge of the western Paleozoic and Triassic belt (WTrPz belt). This model implied that a matching rift-edge fragment of the older arc complex should occur outboard of the Josephine spreading centers, on the opposite side of the marginal basin. The report by Roure and DeWever (1983) of a Triassic chert collected from beneath the Rogue arc suggested that at least part of the WJB contains pre-Middle Jurassic rocks, consistent with the implicit prediction of Snoke (1977).

The structural complexity of the WJB has been attributed to Late Jurassic Nevadan deformation resulting from the tectonic collapse and subcretion of belt below the older Klamath terranes. The structural configuration of the WJB resulting from this deformation has been interpreted as an eastward-dipping, imbricate thrust stack of "subterranean" units (Blake et al., 1985). These subterranean units primarily include, from west to east, the plutonic complex and metaplutonic complex of the Rogue River arc, a highly deformed amphibolite belt, the volcanic rocks of the Rogue arc, and the Josephine ophiolite sequence.

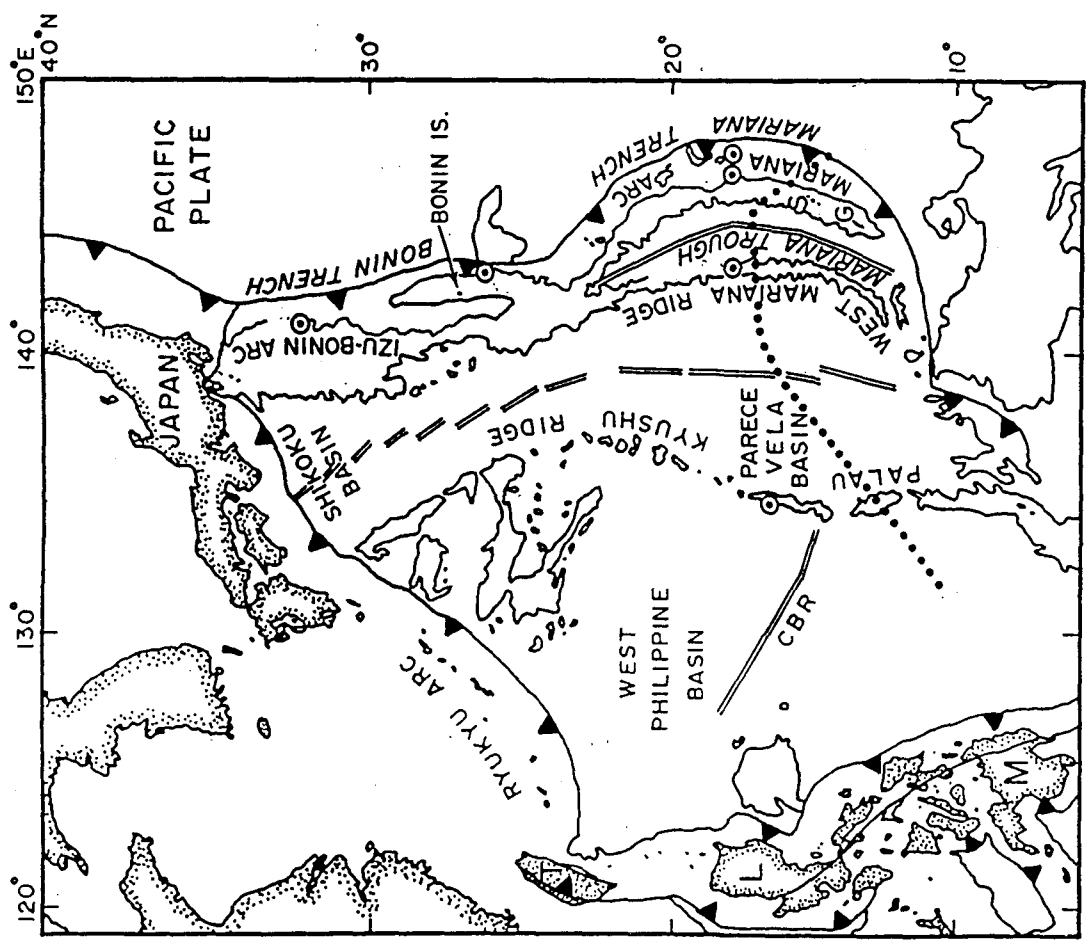
The Klamath region has experienced no significant deformation and only minor plutonism subsequent to Nevadan deformation. The province thus represents an archetypal example of the style and timing of Late Jurassic tectonism and magmatism across the western North American Cordillera. This history includes: 1) an episode of Middle

Jurassic regional deformation and low P/T metamorphism (Wright and Fahan, 1988; “Siskiyou” event of Coleman, et al., 1988) that coincided with the re-establishment of oceanic arc magmatism after an ~20 m.y. hiatus, 2) Late Middle Jurassic rifting of an older arc terrane to produce the Rogue River active arc, the Josephine inter-arc basin ophiolite, and the Middle Jurassic remnant arc, and 3) Late Jurassic tectonic collapse of the Josephine marginal ocean basin and subcretion beneath the remnant arc during the Nevadan orogeny (Snoke, 1977; Saleeby and others, 1982; Harper and Wright, 1984; and Wright and Fahan, 1988).

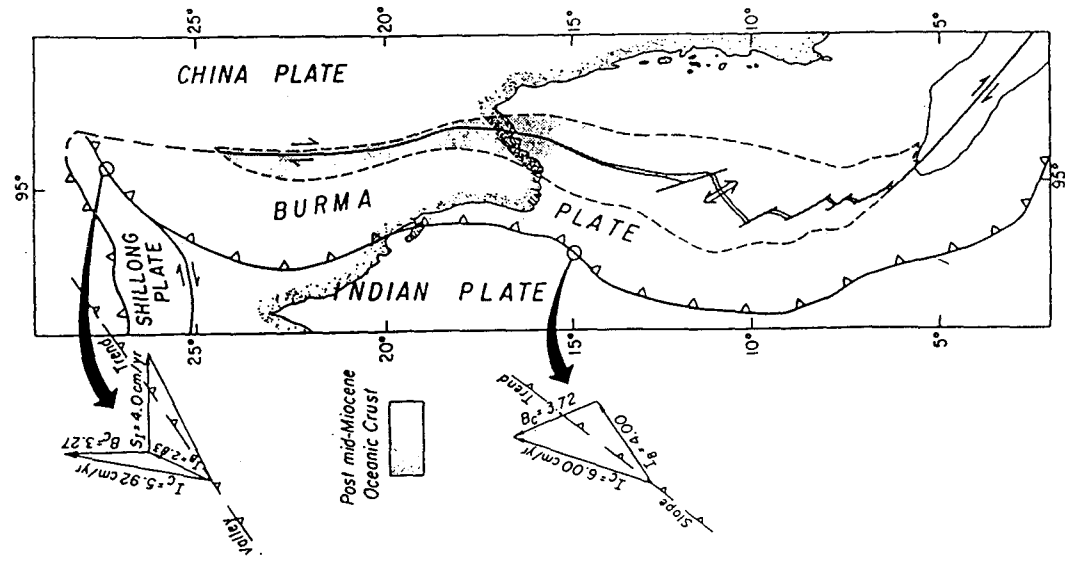
Current debate regarding Jurassic orogenic events in the region centers on their duration, and their temporal and spatial variability. One interpretation considers the Middle and Late Jurassic orogenies to be relatively short-lived regional events which result in profound changes in the style and location of magmatism (Wright and Fahan, 1988; Barnes, et al., 1992). In contrast, several other investigations suggest that the Nevadan orogeny was a long-lived event, lasting ~20 m.y. (Saleeby et al., 1989; Tobisch et al., 1989; Harper et al., 1994). A third opinion states that orogenic activity occurred continuously during the Jurassic but it varied greatly time and space throughout the province. All three arguments are rooted in observable features suggesting that at least some aspects of each reflect a fundamental tectonic and/or magmatic process that affects orogenic belts.

Modern marginal ocean basins of the western Pacific and southeast Asia probably represent likely modern analogs for the Jurassic Josephine marginal basin. For example, the Mariana and Andaman Sea basins occur above a subduction zone and have coeval oceanic island arc volcanoes and inter-arc basin spreading centers with inactive oceanic arc ridges and plateaus located on the opposite side of the spreading center from the active arc (Figure 1-3). This geometry results when extension in the overriding plate rifts apart older oceanic arc lithosphere and forms an active arc, inter-arc basin, and remnant arc triad (Karig, 1971). As illustrated by the spreading geometries in the Mariana and the Andaman

Figure 1-3. A) Tectonic and physiographic map of the Philippine Sea/Mariana arc area, taken from Stern and Bloomer, 1992. B) Tectonic and physiographic map of the Philippine Andaman Sea area, taken from Curray et al., 1977.



A



B

Sea basins (Figure 1-3), extension can be directed either orthogonal or sub-parallel to the subduction trench, and its orientation is probably dependent upon the relative motions of the overriding and subducting plates. The Andaman Sea analogy is most similar to the Josephine basin because sheeted dike orientations and faunal data from the Galice Formation suggest that spreading in the Josephine marginal ocean basin was north-south directed (Alexander and Harper, 1992; Pessagno and Blome, 1990).

Current knowledge of the structural framework of marginal basin oceanic lithosphere is based largely on seismic imaging and other remote sensing techniques. These data suggest that the thickness and the structural framework of oceanic arc and inter-arc basin crust mantle lithosphere are distinctly different. For example, the data suggest that oceanic arc crust is generally three to five times thicker than inter-arc basin ophiolite crust and mantle lithosphere (Uyeda, 1977). This increased thickness in the arc is presumably related, at least in part, to the construction of arcs on previously thickened “remnant arc” materials. The nature of the transition from relatively thin inter-arc basin lithosphere to relatively thick oceanic arc lithosphere is poorly known. Other structural features for which little direct information is available include the possible difference between the geophysical and petrologic Moho, and the possible difference in relative age and composition between the remnant arc, active-arc, and inter-arc basin mantle lithosphere. The lithosphere-scale exposures in the WJB provide an exceptional opportunity to directly observe some of these poorly understood structural features of marginal ocean basin lithosphere and to compare the findings with those from studies in the modern oceanic setting.

The WJB belt in Oregon was chosen for study because of several reasons. First, Oregon portion of the Klamath Mountains province has received less geologic attention than their California counterparts, and as a result, some of regional geologic maps displayed certain “state line effects” where map units defined in northern California mysteriously ended at the state border. Though further investigation does not in itself lead

to a better understanding, the relatively sparsely examined geology in Oregon combined with the Triassic chert reported by Roure and DeWever (1983) implied that the geology of the WJB in Oregon was more complicated than had been previously reported, and invited further study. Furthermore, if older oceanic material indeed occurs within the WJB, then it places important constraints regarding the Jurassic tectonic evolution of the Klamath Mountains and essentially verifies the model tectonic model described above (Snook, 1977; Saleeby and others, 1982; Harper and Wright, 1984). The WJB also represents one of the few places in western North America where one can examine directly the effects of Jurassic orogenic episodes and may therefore provide the least equivocal data regarding their the timing and style. Finally, due to their relatively low regional metamorphic grade, the WJB rocks preserve many of their original oceanic features and therefore provide an exceptional opportunity to directly observe the structural framework of composite marginal ocean basin lithosphere.

The thesis is organized into three main chapters and two appendices. Each main chapter has a separate abstract, introduction, and reference list. Chapter 2 refers frequently to the maps (Plates 1-11) and focuses on the geologic and structural evolution of the western Jurassic belt in the Oregon Klamath Mountains. The first part of the chapter presents the evidence identifying part of the WJB as the Rattlesnake Creek terrane, and the last part of the chapter emphasizes the new regional structural interpretation of the belt. Appendix 1 describes the map units in general. Chapter 3 provides a detailed description of much of the geochronometric data obtained during this study (from both the study area and from plutons to the east which intrude the WTrPz belt). These new data, in combination with the wealth of radiometric data from the Klamath Mountains province, are used to review the Middle Jurassic to Cretaceous magmatic history and orogeny in the province, and to propose a new tectonic and paleogeographic reconstruction for the province. Chapter 4 focuses on the structural features of the Josephine marginal basin with general insight into the structural framework of marginal ocean basin lithosphere, e.g., the nature

of the transition between inter-arc basin and oceanic island arc crust and the nature of crust/mantle lithosphere and intra mantle lithosphere boundaries. Appendix 1 contains the geologic map explanations for Plates 1-11. Finally, the U-Pb laboratory methods and age calculation procedures are outlined in Appendix 2.

The fundamental conclusions of my study are as follows.

1) The WJB contains a rifted fragment of older oceanic crust and mantle lithosphere that is correlable with rocks of the Rattlesnake Creek terrane, part of the WTrPz belt. This correlation provides unequivocal proof that the Josephine marginal ocean basin formed by the rifting apart of the Middle Jurassic oceanic arc and arc basement of the Klamath Mountains. Therefore the WJB represents part of a composite marginal ocean basin lithosphere that formed above a subduction zone and was physically connected to the western North American continental margin. The correlation of units across a major terrane boundary demonstrates that two "suspect," tectonostratigraphic terranes can exhibit shared pre-amalgamation geologic histories.

2) The Josephine peridotite massif exposed in the WJB contains at least two distinct generations of mantle peridotite, one >175 Ma and presumably related to rocks of the WTrPz belt, and another related to the Josephine ophiolite (166-160 Ma). Field relations suggest that the two peridotites were not juxtaposed during regional contractile deformation and therefore represent an oceanic feature. Thus the composite nature of the crustal rocks of the Josephine basin is also reflected in the peridotite mass.

3) The structural framework of the WJB is best described as a regional fold belt rather than an imbricate thrust stack of "subterrane" units (Blake et al., 1985). The subterrane bounding "thrust" faults either do not exist, are regionally discontinuous, or exhibit normal displacement. Thus, their usefulness is suspect. Moreover, the subterrane faults are deceptive because they misrepresents the geology of the belt. The mesoscopic and macroscopic structures observed in the field instead define the belt as a gently NE plunging fold belt with faulted and attenuated limbs.

4) The Middle Jurassic to Early Cretaceous plutons of the Klamath Mountains represent a continuum of oceanic arc magmatism that spanned ~40 m.y. that define a long-lived oceanic arc batholithic complex. The Klamath Mountains batholithic belt is distinct from the giant Cordilleran batholiths because it probably formed at a loosely coupled convergent boundary, perhaps analogous to the long-lived oceanic arc systems of the western Pacific (e.g., the Marianas).

5) Jurassic orogeny in the Klamath Mountains province can be characterized as a continuum, variable in space and time, that was punctuated by short-lived Middle and Late Jurassic thrusting episodes which had profound effects on the subsequent magmatic processes of the province.

References

- Alexander, R.J. and Harper, G.D., 1992, The Josephine ophiolite, an ancient analog for oceanic lithosphere formed at intermediate-spreading ridges, in *Ophiolites and Their Modern Oceanic Analogues*, edited by B. Parsons and P. Browning, pp. 3-38, Blackwell Scientific Publ., Oxford.
- Barnes, C.G., Petersen, S.W., Kistler, R.W., Prestvik, T., and Sundvoll, B., 1992, Tectonic implications of isotopic variation among Jurassic and Early Cretaceous plutons, Klamath Mountains, *Geol. Soc. Amer. Bull.*, **104**, 117-126.
- Blake, M.C., Jr., D.C. Engebretson, , A.S. Jayko, and D. L. Jones, 1985, Tectonostratigraphic terranes in southwest Oregon, in: *Tectonostratigraphic Terranes of the Circum-Pacific Region*, Earth Sci. Ser., edited by D.G. Howell, pp. 147-157, Circum-Pacific Council for Energy and Mineral Resources, Houston, Tex.
- Coleman, R.G., Manning, C.E., Mortimer, N., Donato, M.M., and Hill, L.B., 1988, Tectonic and regional metamorphic framework of the Klamath Mountains and adjacent Coast Ranges, California and Oregon, in: Ernst, W.G. (ed.), *Metamorphism and Crustal Evolution of the Western United States*, Rubey vol. VII, Prentice Hall, Englewood Cliffs, NJ, 1061-1096.
- Coleman, R.G., and Lanphere, M.A., 1991, The Briggs Creek amphibolite, Klamath Mountains, Oregon: Its origin and dispersal, *N. Z. J. Geol. Geophys.*, **34**, 271-284.
- Curray, J.R., Moore, D.G., and Lawver, L. A., Raitt, R.W., and Henry, M, 1979, Tectonics of the Andaman Sea and Burma, in: Watkins, J.S and others (eds.), *Geological and Geophysical Investigations of Continental Margins: Amer. Assoc. of Petroleum Geol. Mem.*, **29**, 189-198.
- Davis, G.A., 1969, Tectonic correlations, Klamath Mountains and western Sierra Nevada, California, *Geol. Soc. Am. Bull.*, **80**, 1095-1108.
- Dick, H.J.B., 1976, The origin and emplacement of the Josephine Peridotite of southwestern Oregon, Ph.D. dissertation, Yale University, 409p.
- Diller, J.S., 1907, The Mesozoic sediments of southwestern Oregon, *Am. Jour. Sci.*, **23**, 401-421.
- Garcia, M.O., 1979, Petrology of the Rogue and Galice formations, Klamath Mountains, Oregon: Identification of a Jurassic island-arc sequence, *Jour. Geol.*, **87**, 29-41.
- Garcia, M.O., 1982, Petrology of the Rogue River island-arc complex, southwest Oregon, *Amer. Jour. Sci.*, **282**, 783-807.
- Hacker, B.R., Donato, M.M., Barnes, C.G., McWilliams, M.O., and W.G. Ernst, 1995, Timescales of orogeny: Jurassic construction of the Klamath Mountains, *Tectonics*, v. 14, 677-703.
- Harper, G.D., 1980, The Josephine ophiolite-remains of a late Jurassic marginal basin in northwestern California, *Geology*, **8**, 333-337.
- Harper, G.D., 1984, The Josephine ophiolite, *Geol. Soc. Amer. Bull.* **95**, 1009-1026.

- Harper, G.D., and Wright, J.E., 1984, Middle to Late Jurassic tectonic evolution of the Klamath Mountains, California-Oregon, *Tectonics* **3**, 759-772.
- Harper, G.D., Saleeby, J.B., and Heizler, M., 1994, Formation and emplacement of the Josephine ophiolite, and the age of the Nevadan orogeny in the Klamath Mountains, California-Oregon: U/Pb zircon and $^{40}\text{Ar}/^{39}\text{Ar}$ geochronology, *J. Geophys. Res.*, **99**, 4293-4321.
- Imlay, R.W., 1980, Jurassic paleobiogeography of the western conterminous United States in its continental setting, *U.S. Geol. Sur. Professional Paper 1062*, 134 p.
- Irwin, W.P., 1960, Geologic reconnaissance of the northern Coast Ranges and Klamath Mountains, California, with a summary of the mineral resources, *Calif. Div. Mines Bull.* **179**, 80p.
- Irwin, W.P. 1966, Geology of the Klamath Mountain province, in: Bailey, E.H. (ed.), *Geology of northern California: Calif. Div. Mines Bull.*, **190**, 19-38.
- Irwin, W.P., 1994, Geologic map of the Klamath Mountains, California and Oregon, , *U.S. Geol. Survey Misc. Field Investigations I-2148*, scale 1:500,000.
- Karig, D.E., 1971, Origin and development of marginal basins in the western Pacific, *J. Geophys. Res.*, v. **76**, 2542-2560.
- Miller, M. M., and J. B. Saleeby, 1987, Detrital zircon studies of the Galice Formation: Common provenance of strata overlying the Josephine ophiolite and Rogue Island arc, western Klamath Mountains terrane, *Geol. Soc. Amer. Abs. with Programs*, **19**, 772-773.
- Pessagno, E.A., and Blome, C.D., 1990, Implications of new Jurassic stratigraphic, geochronometric, and paleolatitudinal data from the western Klamath terrane (Smith River and Rogue Valley subterrane), *Geology*, **18**, 665-668.
- Ramp, L., Schlidker, H.G., and Gray, J.J., 1977, Geology, mineral resources, and rock material of Curry County, Oregon, *Oregon Dept. Geol. and Mineral Industries Bull.*, **88**, 47p.
- Ramp, L., and Peterson, N.V., 1979, Geology and mineral resources of Josephine County, Oregon, *Oregon Dept. Geol. and Mineral Industries Bull.*, **100**, 45p.
- Roure, F., and DeWever, P., 1983, Decouverte de radiolarites du Trias dans l'unite occidentale des Klamath, sud-ouest de l'Oregon, U.S.A.: Consequences sur l'age des peridotites de Josephine, *Comptes Rendus de l'Academie des Sciences (Paris)*, **297**, 161-164.
- Saleeby, J.B., 1984, Pb/U zircon ages from the Rogue River area, western Jurassic belt, Klamath Mountains, Oregon, *Geol. Soc. Amer. Abstr. with Prog.*, **16**, 331.
- Saleeby, J.B., Harper, G.D., Snoke, A.W., and Sharp, W.D., 1982, Time relations and structural-stratigraphic patterns in ophiolite accretion, west central Klamath Mountains, California, *J. Geophys. Res.* **87**, 3831-3848.

- Saleeby, J.B., Geary, E.E., Paterson, S.R. and O.T. Tobisch, 1989, Isotopic systematics of Pb/U (zircon) and $^{40}\text{Ar}/^{39}\text{Ar}$ (biotite-hornblende) from rocks of the central Foothills terrane, Sierra Nevada, California, *Geol. Soc. Amer. Bull.*, **101**, 1481-1492.
- Snoke, A.W., 1977, A thrust plate of ophiolitic rocks in the Preston Peak area, Klamath Mountains, California, *Geol. Soc. Amer. Bull.*, **88**, 1641-1659.
- Stern, R.J., and Bloomer, S.H., Subduction zone infancy; examples from the Eocene Izu-Bonin-Mariana and Jurassic California arcs, *Geol. Soc. Amer. Bull.*, **104**, 1621-1636.
- Tobisch, O.T., Paterson, S. R., Saleeby, J.B., and Geary, E.E., 1989, Nature and timing of deformation in the Foothills terrane, central Sierra Nevada, California, *Geol. Soc. Am. Bull.*, **101**, 401-413.
- Uyeda, S., 1977, Some basic problems in the trench-arc-back arc system, in *Islands Arcs Deep Trenches and Back-arc Basins*, Maurice Ewing Series 1, edited by Manik Talwani and Walter C. Pitman, III, pp. 1-14, American Geophysical Union, Washington D.C
- Wells, F.G., and Walker, G.G., 1953, Geologic map of the Galice quadrangle, Oregon, *U.S. Geol. Survey Map GQ-25*.
- Wright, J.E., and Fahan, M.R., 1988, An expanded view of Jurassic orogenesis in the western United States Cordillera: Middle Jurassic (pre-Nevadan) regional metamorphism and thrust faulting within an active arc environment, Klamath Mountains, California, *Geol. Soc. Amer. Bull.*, **100**, 859-876.

CHAPTER 2

**GENERALIZED GEOLOGIC MAP
AND STRUCTURAL EVOLUTION OF THE
WESTERN JURASSIC BELT,
KLAMATH MOUNTAINS, OREGON**

Abstract

The western lithotectonic belt of the Klamath Mountains province, known as the western Jurassic belt (WJB), exposes one of the world's best preserved examples of composite marginal ocean basin lithosphere. The WJB consists of the Late Middle to Late Jurassic Josephine ophiolite (Harper, 1984) and broadly coeval Rogue River oceanic island arc complex (Garcia, 1982). Both the arc complex and ophiolite sequence are overlain by flysch strata of the Late Jurassic Galice Formation. The Galice sediments contain distinct detrital grains derived from cratonal North America and older terranes of the Klamath province (Miller and Saleeby, 1987). Thus the Josephine basin is interpreted to represent a Middle to Late Jurassic marginal ocean basin that once fringed western North America. Its incorporation along the margin occurred when the basin was thrust beneath the older terranes of the province during the Late Jurassic Nevadan orogeny (Harper and Wright, 1984).

Two intriguing features of the WJB in Oregon provided the primary focus for this study. The report of a Triassic chert (Roure and DeWever, 1983) suggested that older than previously suspected rocks occur within the region. In addition, Blake and others (1985) subdivided the WJB into four eastward dipping, fault bounded subterrane units, but the

regional extent of the bounding structures and their offset were only inferred. This paper reports on findings which 1) confirm the occurrence of a Triassic and Early Jurassic rocks within the WJB (named informally herein as the Onion Camp complex), and 2) reject the subterranean designation on the basis of field relations which indicate the inferred thrust faults instead are a normal fault, a deformed intrusive contact, thrust faults of limited regional extent, or altogether non-existent.

The structural framework of the WJB is reinterpreted as a regional fold belt with faulting of secondary importance. Faults generally occur along the attenuated and truncated limbs of regional folds. Synclinal regions expose rocks of the overlapping strata of the Rogue Formation, Galice Formation, and the Fiddler Mountain olistostrome complex whereas anticlinal regions expose a composite basement terrane including: 1) crust and mantle lithosphere rocks of the Onion Camp complex, and 2) rocks of the Josephine ophiolite, and 3) oceanic arc intrusive rocks of the Illinois River plutonic complex. Retrodeforming the rocks of the study area, assuming approximately 100% shortening, restores the width of the study area to about 75-100 kilometers, a width that, in modern marginal ocean basins, is sufficient to traverse the arc axis, its flanking volcanogenic apron, and beyond into regions underlain by inter-arc basin ophiolitic rocks. Thus it seems likely that the rocks of the study area represent a relatively intact, albeit structurally complex, fragment of a marginal ocean basin across the transition from ophiolitic inter-arc basin lithosphere to oceanic arc lithosphere.

Introduction

The Klamath Mountains province, California and Oregon, consists of a series of accreted oceanic terranes whose stratigraphic record spans >400 m.y. ranging from the Cambrian to the Early Cretaceous. The terranes of the province principally occur in four thrust plates which form arcuate, N-S trending, eastward dipping belts and generally

consist of younger units from east to west across the province. The youngest thrust plate, termed the western Jurassic belt (WJB) by Irwin (1966), forms the westernmost part of the province and is the focus of this study. The primary constituents of the WJB are Middle to Late Jurassic in age and include 1) the Rogue River oceanic island arc complex (Garcia, 1979;1982), 2) the Josephine ophiolite (Harper, 1980; 1984), and 3) the Galice Formation (Wells and Walker, 1953), a sequence of pelagic, hemipelagic and flysch sediments which conformably overlap the Josephine ophiolite and the Rogue arc (e.g., Imlay 1961; Harper, 1984; Pessagno and Blome, 1990).

In a surprising discovery, Roure and DeWever (1983) reported a Triassic age obtained from a radiolarian chert collected at a locality in the WJB near Onion Camp suggesting that older, pre-Middle Jurassic rocks comprised at least part of the belt and forced a re-examination of the geologic and tectonic evolution of the region. Roure and DeWever (1983) contended the Triassic chert occurred in ophiolitic basement rocks beneath the Rogue arc and that the Josephine ophiolite was Triassic in age (not Late Jurassic). However, this interpretation ignored a wealth of data collected from the type Josephine locality in support of the Late Jurassic age (e.g., Saleeby et al. 1982; Harper, 1984; Harper and Wright, 1984). Alternatively, as predicted by a model first proposed by Snoke (1977), the Triassic chert may represent part of a fragment of older oceanic rocks that occur in the WJB as a rifted fragment or "screen" in the Josephine basin, presumably rifted from correlable rocks on the opposite side of the basin.

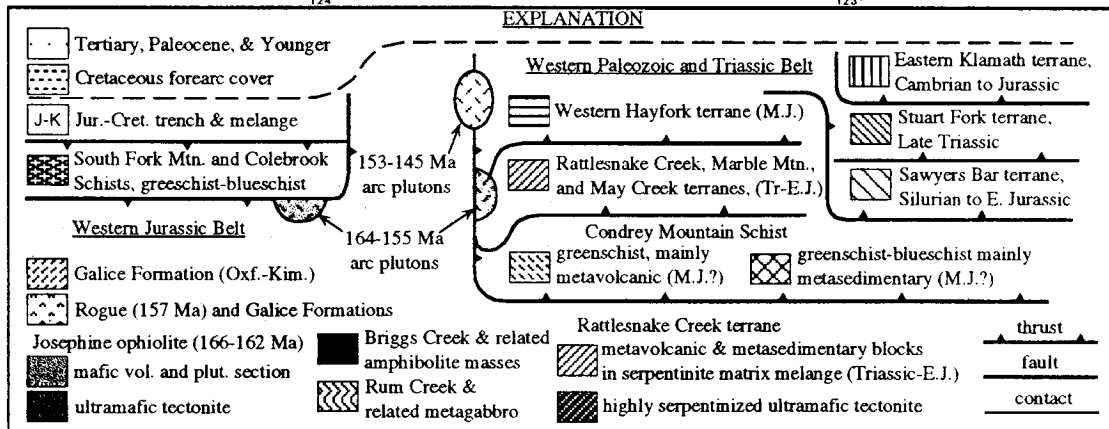
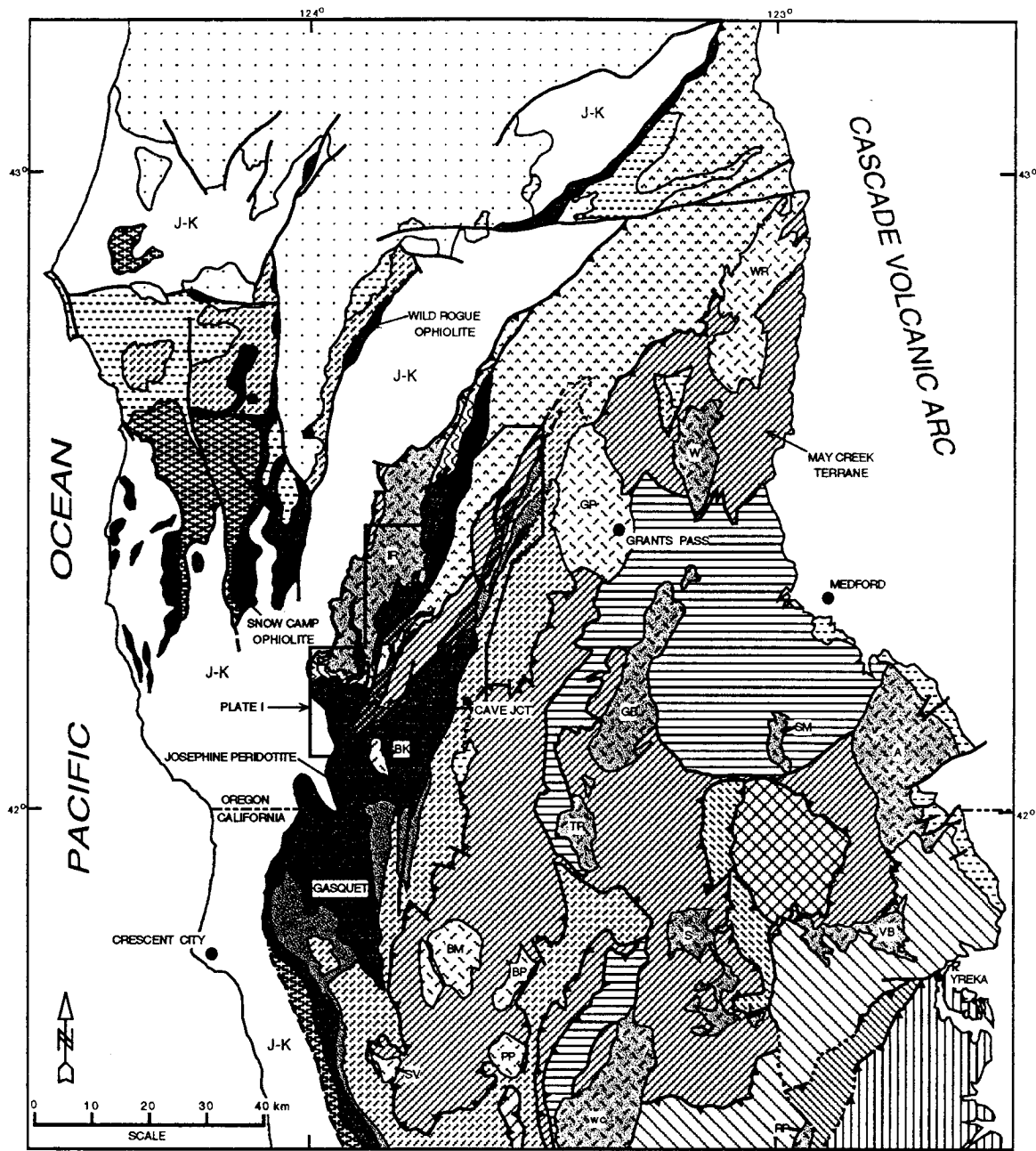
Tectonic collapse of the basin occurred during the Late Jurassic Nevadan orogeny resulted in the "subcretion" of the WJB beneath rocks of the western Paleozoic and Triassic belt (WTrPz belt; e.g., Saleeby and Harper, 1993; Harper et al., 1994). The resulting deformation is interpreted to have imbricated the WJB into an eastward dipping thrust stack of fault bounded "subterranean" units (Blake et al. 1985). However, the regional extent of the bounding thrust faults and their relative displacements is essentially unconstrained.

This chapter reports the findings of a comprehensive geologic field investigation of a portion of the WJB in Oregon (outlined in Figure 2-1). The specific aims of the field study were twofold; 1) to determine the areal extent, if any, of the Triassic chert bearing rocks and their relationship with younger units in the region, and 2) to characterize the subterranean-bounding faults and the structural framework of the region. The findings support the Triassic age of Roure and DeWever (1983) and define an elongate NE-trending belt of pre-Middle Jurassic rocks contained within the WJB. These older rocks, on the basis of distinct lithologic ties, fossil and geochronometric age data, and distinguishing geochemical signatures, correlate with rocks of the Rattlesnake Creek terrane (RCT), the westernmost component of the WTrPz belt (Figure 2-1). Secondly, the findings of this study do not support the subterranean designations (Blake et al. 1985) and suggest that their designation and usefulness is highly “suspect.” Instead the data and observed relations favor interpreting the WJB primarily as a regional fold belt with faulting of secondary importance, and suggest that the WJB, though structurally complex, represents a fragment of relatively intact Jurassic marginal ocean basin lithosphere.

Geologic Framework and Previous Work

Rocks in the western Klamath Mountains of Oregon were originally described by Diller (1907) as a belt consisting of crystalline and metamorphic rocks overlain by a Jurassic sequence of sedimentary and volcanic rocks known as the Galice Formation. Wells and Walker (1953) subdivided the sedimentary and volcanic rocks into the Galice Formation and the Rogue Formation, respectively. More recently, rocks of the WJB were grouped into distinct lithologic associations on the basis of a common petrogenetic and/or tectonic heritage. These petrotectonic elements are the Josephine ophiolite (Harper, 1980; 1984) and the Rogue River oceanic island arc complex (Garcia, 1979; 1982) which, in addition to the Rogue and Galice Formations, includes the Chetco complex (Hotz, 1971) and the Briggs Creek amphibolite (Coleman and Lanphere, 1991).

Figure 2-1. Regional geologic map of the northern Klamath Mountains province and the Oregon Coast Ranges. Note the area outlining Plate 1. The map is compiled from my field studies during 1989-1994 and modified from work published by Coleman and Lanphere (1991), Hacker et al. (1995), Irwin (1994), Ramp et al. (1977), and Ramp et al.(1979). Pluton names are as follows: WR - White Rock, W - Wimer, GP - Grants Pass, IR - Illinois River plutonic complex, BK - Buckskin Peak, GB - Grayback, SM - Squaw Mountain, A - Ashland, VB - Vesa Bluffs, S - Slinkard, TR - Thompson Ridge, BM- Bear Mountian, BP - Bear Peak, PP, Pony Peak, SV - Summit Valley, WC - Wooley Creek, RP-Russian Peak.



Josephine ophiolite

The Josephine ophiolite, the rosetta stone of Cordilleran ophiolites, is exposed over an approximately 900 km² region of the California-Oregon border region (Figure 2-1). The Josephine peridotite alone is exposed over 650 km² representing one of the largest peridotite masses in the world (Dick, 1976). In its type location in the Smith River drainage of northern California, the complete ophiolite sequence is preserved and is mildly deformed and metamorphosed to greenschist and sub-greenschist grade conditions (Harper, 1984). Radiometric ages obtained from the ophiolite include apparent ages of 162 ± 1.5 Ma, U-Pb zircon and 165 ± 5 Ma, Ar/Ar amphibole from gabbro (Saleeby and Harper, 1993). The geochemical data from crustal rocks of the ophiolite plot in a field transitional between the MORB and IAT on trace and REE discrimination diagram plots (e.g., Ti vs Zr) and are consistent with the interpretation that the ophiolite formed above a subduction zone at inter-arc spreading centers (Shervais, 1982; Pearce et al., 1984). Slow- to intermediate-spreading rates are suggested by a number structural and geometric features exhibited by the ophiolite including, tectonically thinned and rotated crustal sections, and abundant oceanic faults (Alexander and Harper, 1992).

North-south directed spreading in the Josephine basin is suggested by 1) the predominant E-W strike, corrected for Nevadan folding, of sheeted mafic dike swarms (Harper and Wright, 1984), 2) an apparent change in microfossil faunal affinities from equatorial to boreal faunas up section in Galice Formation strata (Pessagno and Blome, 1990), and 3) shallow paleomagnetic inclinations in gabbro, dikes, and lavas of the ophiolite interpreted to represent the oceanic remanent magnetization (Smith et al., in review, 1995). The fossil and paleomagnetic data suggest displacements of 500-1000 km, which correlate to 1/2 spreading rates of 5-10 cm/yr for 10 m.y. of spreading.

The ophiolite was deformed and imbricated during the Late Jurassic Nevadan orogeny when it was thrust beneath the older terranes of the Klamath Mountains province

along the Orleans/Preston Peak fault (e.g., Saleeby and Harper, 1993). Contemporaneous with its subcretion beneath the back-arc region of the Josephine, the ophiolite appears to have overthrust the plutonic complex of the Rogue River island arc along the Madstone Cabin fault (Ramp, 1975; Loney and Himmelburg, 1977). The Madstone Cabin thrust geometry is similar to the classic sole faults of large peridotite sheets (e.g., Moores, 1982; Ghent and Stout, 1981) and is interpreted by Harper et al. (1994) and Canat and Boudier (1985) to represent the sole fault of the Josephine ophiolite. Blake et al. (1985) interpret this structure as a regionally extensive structure separating the Smith River subterrane from the Rogue Valley subterrane of the WJB, though it was originally mapped as a relatively localized structure by Ramp (1975).

Rogue River island arc complex

The Rogue River island arc complex, defined by Garcia (1979, 1982), is interpreted to represent a Late Jurassic magmatic arc that formed the fringing arc of the Josephine marginal ocean basin (Snoke, 1977; Saleeby and others, 1982; Harper and Wright, 1984). The Rogue arc consists of an arc volcanoplutonic complex and various highly deformed and metamorphosed mafic and ultramafic rocks interpreted to represent the basement terrane for the arc (Garcia, 1982; Figure 2-1).

The arc plutonic complex, designated the Illinois River gabbro by Jorgenson (1970) and Illinois River batholith by Garcia (1982), is a calc-alkaline, reversely zoned, gabbroic to tonalitic plutonic complex. The country rocks of the plutonic complex include the Pearsoll Peak and Chrome Ridge peridotite masses (Ramp, 1961) and various amphibolite facies metagabbro bodies (e.g., the Rum Creek metagabbro). Hotz (1971) collectively referred to the plutonic and metamorphic rocks as the Chetco complex and obtained several K/Ar hornblende ages of ~154-155 Ma for gabbro and metagabbro in the central and northern part of the complex. Two additional K/Ar hornblende ages of ~157 and 160 Ma

(Dick, 1976) were determined for hornblende gabbro samples collected from the southern part of the complex.

Basaltic to andesitic, bedded to massive volcanic rocks of the Rogue Formation are interpreted to represent the extrusive equivalents of the Illinois River plutonic rocks based on their similar age (~157 Ma) and nearly identical mineral chemistry signatures (Garcia, 1982; and Saleeby, 1984). Rocks of the Rogue Formation occur primarily in the northern part of the Klamath Mountains province (Figure 2-1), in relative close proximity to the Illinois River plutonic rocks. However, scarce occurrences of thin volcanogenic beds are reported to the south of the main outcrop belt where they are interbedded with strata of the Galice Formation (Harper, 1984).

Amphibolite gneiss and schist, and scarce impure quartzite occur in the regions flanking the arc plutonic complex and the peridotite and metagabbro country rocks. The Briggs Creek amphibolite (BCA) body (Figure 2-1) is interpreted by Coleman and Lanphere (1991) to represent an allochthonous slice of metamorphosed oceanic crust, presumably back-arc basin ophiolitic crust, emplaced during the Nevadan orogenic event. Separate occurrences of amphibolite tectonite which are lithologically identical to the BCA are exposed beneath the Madstone Cabin thrust fault (Loney and Himmelburg, 1977; Harper et al., in press, 1995). Harper et al. (1995, in press) correlate these amphibolites with amphibolite in the RCT based on minor and trace element abundances, along with the rare occurrence of rhodonite in both bodies. Thus the high grade metamorphic rocks surrounding the arc pluton appear to have been derived from at least two types of progenitor materials.

Galice Formation

Galice Formation strata conformably overlap volcanic rocks of both the Josephine ophiolite and the Rogue Formation (Pessagno and Blome, 1990). In the Josephine section (Harper, 1984; Harper et al., 1988; Saleeby and Harper, 1993), the basal Galice Formation

strata consist of Late Callovian pelagic and hemipelagic deposits which grade upward into Oxfordian-Kimmeridgian flysch sediments (Pessagno and Blome, 1990). In the Rogue section (Wells et al., 1949; Irwin, 1966; Coleman, 1972), the pelagic and hemipelagic sediments interfinger with Rogue Formation deposits. Here, Oxfordian-Kimmeridgian flysch deposits conformably overlap the Rogue Fm volcanogenic strata (Pessagno and Blome, 1990). The Rogue and Josephine overlap sections are interpreted to represent lateral facies equivalents (Harper, 1984) of two subterranean units (Blake and others, 1985).

Detrital grains derived from older terranes of the Klamath Mountains province provide a stratigraphic linkage between the WJB and older terranes to the east (Snoko, 1977; Miller and Saleeby, 1987). Distinctive detrital grains in the flysch sediments indicate an up section waning in volcanic arc activity and a subsequent increase in material derived from the older terranes of the Klamath Mountains to the east (Miller and Saleeby, 1987; Miller and Saleeby, 1995; Snoko, 1977). This increase in detritus from the continental margin is interpreted to record deformation, uplift, and erosion of the Klamath Mountains province; interpreted as a response to the tectonic collapse and underthrusting of the Josephine marginal ocean basin during the Nevadan orogeny.

Geology of the Central Illinois River Drainage Area

The following discussion describes the geologic relations of the central Illinois River drainage. The most detailed discussion focuses on the newly recognized map units of the WJB, the Onion Camp complex and the Fiddler Mountain olistostrome. In describing the previously mentioned petrotectonic units, the emphasis is on new field relations and data observed and collected during this study. These relations provide a new perspective from which to view the regional structural framework of the WJB and provide the basis for the interpretation presented at the end of this chapter.

The following discussion of the rock units frequently refers to Plate 1, a generalized geologic map at a 1:96,000 scale, and to Plates 2-11, more detailed geologic maps drawn at

a scale of 1:24,000. In addition numerous references are made to the geochronologic and geochemical data, Tables 2-1, 2-2, and 2-3. However, a more thorough discussion of these data follow the general lithologic discussion.

PREVIOUSLY DEFINED LITHOLOGIC UNITS

Northern outliers of the Josephine ophiolite

The type locality of the Josephine ophiolite occurs ~50-75 km south of the study area in the Smith River region of northern California (Harper, 1980). The Josephine peridotite massif (Dick, 1976) connects the ophiolitic crustal rocks of the type section and the study area and suggests that the ophiolite sequences in the the Illinois River area are the northern equivalents of the Josephine ophiolite. This inference is supported by the field, geochemical, and age data described below.

Crustal rocks. Crustal rocks of the ophiolite and associated overlapping sediments primarily occur in two separate regions of the study area; one is a mostly complete ophiolite sequence exposed in the core of a northeast-trending, regional-scale syncline located northwest of the town of Selma (Plates 1, 6, 7, and 10), and the other is highly fragmented in a serpentine matrix melange exposed in the Chetco pass region in the central part of the study area (Plates 1, 3, 5, and 6).

The normal ophiolite stratigraphy is exposed near Selma complete with cumulate gabbro, massive gabbro, sheeted mafic dikes, and pillow lava Figure (2-2) and breccia from base top top. The volcanic rocks are conformably overlain by slaty argillite and impure chert typical of the basal Galice Formation. Distinctive features of the ophiolite near Selma include: 1) thin volcanic deposits, generally <5-10 meters thick, 2) multiple sets of sheeted dike orientations that are inclined at ~40-60° angles with respect to bedding in the overlying volcanic and sedimentary rocks, 3) thin cumulate sequences, generally <50-75 m thick, and 4) small scale normal faults, fragmented textures, and ubiquitous hydrothermal alteration in all crustal rocks. Many of the alteration and fragmentation structures are cut by

Figure 2-2. Roadcut exposure of pillow lava above Shan Creek. Note the elongate tube structures inclined from the upper right to lower left in the photo; suggesting that the lavas are exposed essentially parallel to bedding. This sub-vertical plane is sub-parallel to bedding planes in overlying hemipelagic strata.

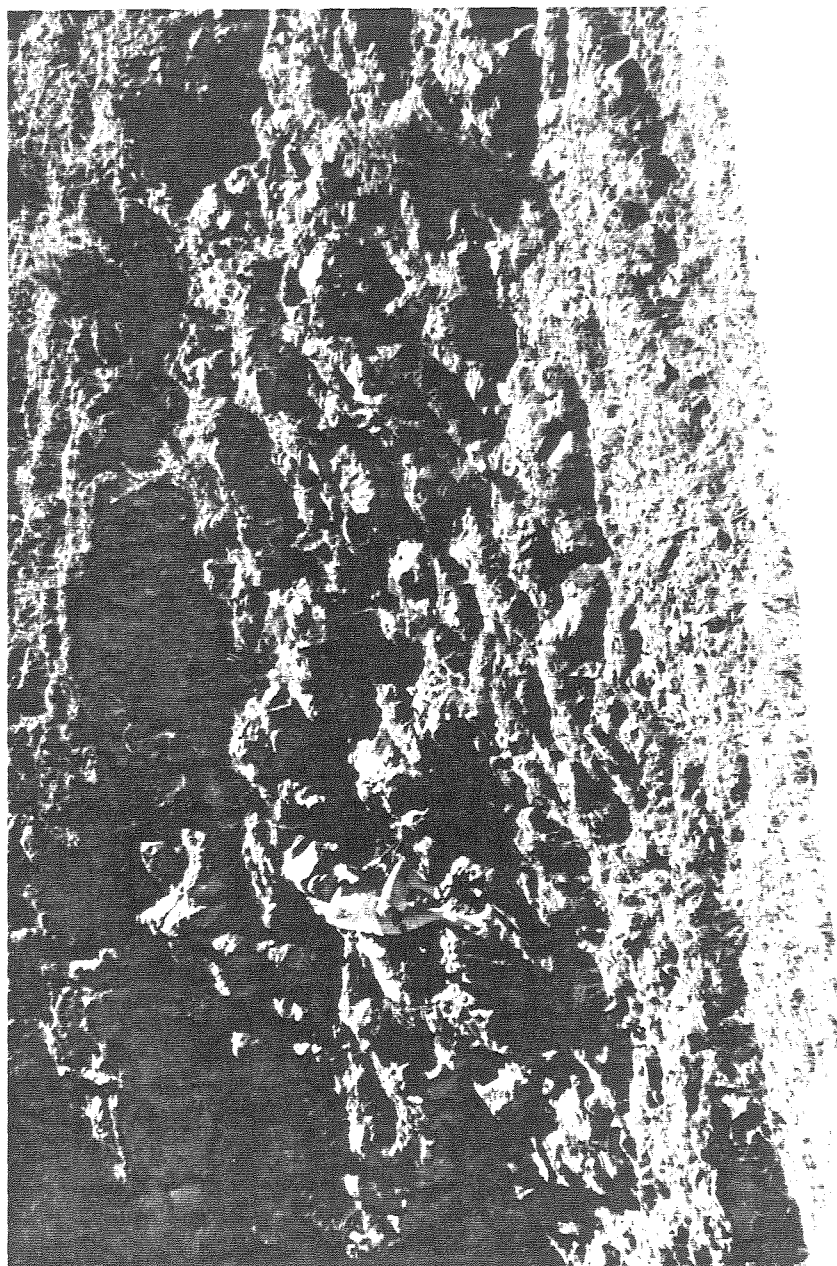


Table 2-1. URANIUM-LEAD ISOTOPIC DATA

| Size (μm) [†] | Zircon fraction properties ^{††} | Wt. (mg) [@] | U (ppm) | ²⁰⁶ Pb (ppm) | Atomic ratios | | | | | | Apparent Ages (m.y.) \S | |
|---|--|--------------------------|------------|----------------------------|---|--|--|---|--|--|--|---|
| | | | | | $\frac{^{206}\text{Pb}}{^{204}\text{Pb}}$ | $\frac{^{206}\text{Pb}^*}{^{238}\text{U}}$ | $\frac{^{207}\text{Pb}^*}{^{235}\text{U}}$ | $\frac{^{207}\text{Pb}^*}{^{206}\text{Pb}^*}$ | $\frac{^{206}\text{Pb}^*}{^{238}\text{U}}$ | $\frac{^{207}\text{Pb}^*}{^{235}\text{U}}$ | $\frac{^{207}\text{Pb}^*}{^{235}\text{U}}$ | $\frac{^{206}\text{Pb}^*}{^{206}\text{Pb}}$ |
| IR-3: Massive hornblende diorite, Illinois River plutonic complex (123°48'21" W, 42°22'18.5"). | | | | | | | | | | | | |
| 64-80 ³ | Tan w/rare incl., 2:1, Fr>Eu. | 4.2 | 118.7 | 2.55 | 5,306 | 0.02484(17) | 0.16880 | 0.04931(12) | 158.2 | 158.4 | 162 (6) | |
| 80-100 ³ | Lt. tan w/rare incl., 2:1, Fr=Eu. | 4.6 | 191.7 | 4.17 | 5,733 | 0.02513(17) | 0.17051 | 0.04922(11) | 160.0 | 159.9 | 158 (5) | |
| IR-4: Agmatic diorite, Illinois River plutonic complex (123°50'53.5" W, 42°23'19.5"). | | | | | | | | | | | | |
| 45-64 ² | Stubby prisms, lt tan. | 3.0 | 335.1 | 7.06 | 9,553 | 0.02433(16) | 0.16541 | 0.04933(18) | 155.0 | 155.4 | 163 (8) | |
| 64-80 ² | <2:1 only, clear w/rare incl. | 4.2 | 192.5 | 4.09 | 11,074 | 0.02453(16) | 0.16659 | 0.04927(19) | 156.3 | 156.5 | 160 (9) | |
| 80-100 ² | Bi-modal 95% 1:1, 5% >4:1. | 2.2 | 218.6 | 4.67 | 6,774 | 0.02468(17) | 0.16769 | 0.04931(14) | 157.2 | 157.4 | 162 (7) | |
| 93DY-YB-8: Pegmatic hornblende-biotitetonalite, Illinois River plutonic complex (123°51'44" W, 42°23'53.5"). | | | | | | | | | | | | |
| <64 ⁴ | Eu>Fr, 3:1, clear w/micro incl. | 0.95 | 185.7 | 3.96 | 2,503 | 0.02465(13) | 0.16680 | 0.04910(13) | 157.0 | 156.6 | 152 (6) | |
| IR-1: Foliated biotite tonalite, Illinois River plutonic complex (123°46'57" W, 42°21'14.5"). | | | | | | | | | | | | |
| 45-64 ⁴ | >3:1 w/clear incl., Eu>Fr. | 3.9 | 247.8 | 5.09 | 8,615 | 0.02368(16) | 0.16122 | 0.04941(15) | 150.9 | 151.8 | 167 (7) | |
| >120 ⁴ | ~3:1, w/clear incl., Eu>Fr. | 6.6 | 259.5 | 5.52 | 3,676 | 0.02456(17) | 0.16669 | 0.04925(15) | 156.4 | 156.5 | 159 (7) | |
| 91DY-PP-64: Foliated biotite tonalite, Illinois River plutonic complex (123°46'46" W, 42°19'37"). | | | | | | | | | | | | |
| 45-64 ³ | Lt. tan w/rare inclusion. | 1.5 | 609.1 | 11.94 | 10,877 | 0.02264(15) | 0.15474 | 0.04947(24) | 144.4 | 145.8 | 170 (11) | |
| 64-80 ³ | 3:1 to 5:1, Eu>Fr. | 5.1 | 366.2 | 7.70 | 4,407 | 0.02430(16) | 0.16649 | 0.04924(19) | 154.8 | 155.0 | 159 (9) | |
| IR-2: Trondhjemite gneiss layer in amphibolite, Illinois River plutonic complex (123°46'57" W, 42°21'07.5"). | | | | | | | | | | | | |
| 64-80 ² | Cloudy, opaque grains, Eu>Fr. | 4.7 | 457.8 | 9.98 | 2,735 | 0.02519(17) | 0.17087 | 0.04923(13) | 160.3 | 160.2 | 158 (6) | |
| 91DY-PP-9B: Trondhjemite dike in amphibolite-grade metamorphosed dike complex (123°46'40" W, 42°18'36"). | | | | | | | | | | | | |
| 45-64 ³ | Lt. Tan, stubby prisms. | 2.5 | 231.1 | 5.00 | 4,323 | 0.02500(17) | 0.16979 | 0.049289(15) | 159.2 | 159.2 | 161 (7) | |
| 64-80 ³ | | 5.6 | 366.2 | 8.00 | 5,292 | 0.02524(17) | 0.17127 | 0.04924(11) | 160.7 | 160.5 | 159 (5) | |
| 80-100 ³ | | 2.3 | 419.3 | 9.03 | 7,859 | 0.02489(17) | 0.16908 | 0.04929(13) | 158.5 | 158.6 | 161 (6) | |

Table 2-1 (continued). URANIUM-LEAD ISOTOPIC DATA

| Size (μm)† | Zircon fraction properties†† | Wt. (mg)@ | U (ppm) | $^{206}\text{Pb}^*$ (ppm) | Atomic ratios | | | | | | Apparent Ages (m.y.) § | |
|--|----------------------------------|--------------|------------|------------------------------|---|--|--|---|--|--|---|---|
| | | | | | $\frac{^{206}\text{Pb}}{^{204}\text{Pb}}$ | $\frac{^{206}\text{Pb}^*}{^{238}\text{U}}$ | $\frac{^{207}\text{Pb}^*}{^{235}\text{U}}$ | $\frac{^{207}\text{Pb}^*}{^{206}\text{Pb}^*}$ | $\frac{^{206}\text{Pb}^*}{^{238}\text{U}}$ | $\frac{^{207}\text{Pb}^*}{^{235}\text{U}}$ | $\frac{^{207}\text{Pb}^*}{^{206}\text{Pb}^*}$ | $\frac{^{206}\text{Pb}^*}{^{206}\text{Pb}^*}$ |
| 91DY-PP-9A: Trondhjemite gneiss in amphibolite-grade metamorphosed dike complex (123°46'40" W, 42°18'36"). | | | | | | | | | | | | |
| 45-64 ³ | Brown w/fractures, Eu=Fr. | 2.7 | 1,408 | 18.17 | 19,967 | 0.01491(14) | 0.10152 | 0.04940(07) | 95.4 | 98.2 | 166 | (3) |
| >64 ³ | Brown w/fractures, Eu=Fr. | 1.7 | 1,503 | 21.91 | 11,857 | 0.01685(13) | 0.11472 | 0.04941(07) | 107.7 | 110.3 | 167 | (3) |
| 89DY-S-3: Dacite dike cutting regional Nevadan metamorphism (123°44'30" W, 42°15'11.5"). | | | | | | | | | | | | |
| 64-80 ¹ | Zoned grains, <3:1 | 5.5 | 149.2 | 3.04 | 2,759 | 0.02357(16) | 0.15953 | 0.04910(15) | 150.2 | 150.3 | 152 | (7) |
| 80-100 ¹ iii | Clear, grains w/Eu>Fr, 3:1 | 4.2 | 66.00 | 1.34 | 6,335 | 0.02350(13) | 0.15886 | 0.04905(08) | 149.8 | 149.7 | 150 | (4) |
| 93DY-JM-10: Plagiogranite dike cutting serpentinitized peridotite of the Onion Camp complex (123°48'35.5" W, 42°14'35.5"). | | | | | | | | | | | | |
| <45 ² | Clear, Eu>Fr, 2:1 to 5:1. | 2.3 | 379.8 | 8.37 | 13,361 | 0.02547(17) | 0.17444 | 0.04970(12) | 162.1 | 163.3 | 181 | (6) |
| 45-64 ² | Clear, Eu>Fr, 2:1 to 5:1. | 1.4 | 726.6 | 16.69 | 12,111 | 0.02654(18) | 0.18107 | 0.04950(55) | 168.9 | 169.0 | 171 | (26) |
| 64-80 ² | Clear, Eu>Fr, 2:1 to 5:1. | 0.8 | 562.3 | 13.21 | 8,013 | 0.02760(17) | 0.18817 | 0.04947(18) | 175.5 | 175.1 | 170 | (8) |
| 91DY-JM-11: Plagiogranite dike cutting serpentinitized peridotite of the Onion Camp complex (123°48'35" W, 42°14'45"). | | | | | | | | | | | | |
| 45-64 ³ | 1:1 to 4:1 w/clear incl., Eu>Fr. | 2.3 | 198.3 | 4.67 | 9,855 | 0.02723(15) | 0.18604 | 0.04957(13) | 173.2 | 173.3 | 175 | (6) |
| 64-100 ³ | 1:1 to 4:1 w/clear incl., Eu>Fr. | 1.3 | 215.2 | 5.08 | 8,002 | 0.02725(15) | 0.18650 | 0.04965(15) | 173.4 | 173.6 | 178 | (7) |
| 93DY-EDM-89: Plagiogranite associated with mafic dike complex (123°43'40.5" W, 42°17'48"). | | | | | | | | | | | | |
| 45-64 ⁴ | Clear, incl. free, Eu=Fr, <4:1. | 1 | 445.0 | 6.79 | 8,358 | 0.01764(09) | 0.12091 | 0.04973(10) | 112.8 | 115.9 | 182 | (5) |
| 45-64 ⁴ | Cloudy, incl-rich, Fr>Eu. | 0.9 | 421.7 | 8.75 | 9,038 | 0.02399(13) | 0.16901 | 0.05113(07) | 152.8 | 158.6 | 246 | (3) |

Table 2-1 (continued). URANIUM-LEAD ISOTOPIC DATA

† Fractions separated by grain size and magnetic properties. Magnetic properties are given as non-magnetic split on Franz Isodynamic Separator for 1.7 amps with side/front slopes of; ¹ 0.5/20, ² 1/20, ³ 2/20, or ⁴ 5/20. Dissolution and chemical extraction technique modified from Krogh (1973).

†† All samples are hand-picked to 99.9% purity prior to dissolution. Abbreviations are: Eu=euhedral grains; Fr=fregrmented grains; ratios given are the respective length:width ratios of euhedral zircon grains; incl.=inclusion; Lt=light.

@ Due to uncertainties in weight of sample, U-Pb concentration may be in error, use of mixed ²⁰⁵Pb-²³⁰Th-²³⁵U spike ensures age of sample is correct.

* Radiogenic/nomradiogenic correction based upon 40 picogram blank Pb (1:18.78;15.61;38.50) and initial Pb approximations: 206/204=18.6; 207/204=15.6; 208/204=38.2.

§ Decay constants used in age calculation: $\lambda^{238}\text{U}=1.55125 \times 10^{10}$, $\lambda^{235}\text{U}=9.98465 \times 10^{10}$ (Jaffey and others, 1971); $^{238}\text{U}/^{235}\text{U}$ atom=137.88.

Uncertainties (\pm) in radiogenic ratios calculated by quadratic sum of total derivatives of ²³⁸U and ²⁰⁶Pb* concentration and ²⁰⁷Pb*/²⁰⁶Pb* equations with error differentials defined as follows: (1) Isotope ratio determinations from standard errors (β/n) of mass spectrometer runs plus uncertainties in fractionation corrections based on multiple runs of NBS 981, 983, and U500 standards; (2) Spike concentrations from range of deviations in multiple calibrations with normal solutions; (3) Spike compositions from external precisions of multiple isotope ratio determinations; (4) Uncertainty in natural ²³⁸U/²³⁵U from Chen and Wasserburg (1981); and (5) Nonradiogenic Pb isotopic compositions from uncertainties in isotope ratio determinations of blank Pb and uncertainties in composition of initial Pb from estimates of regional variations based on references given above and consideration of rock type.

Table 2-2. Summary of $^{40}\text{Ar}/^{39}\text{Ar}$ apparent ages.

| Lithologic Unit | Station | Lat/Long | Description | Mineral | Plateau Age ^a , Ma |
|--|------------|-----------------------------|---|------------|-------------------------------|
| <i>Rogue Formation</i> | 89-PP-4 | 42°18'10" N 123°46'51" W | Illinois River falls; crystal and lithic tuff breccia | hornblende | 153.4 ± 0.6 |
| <i>Illinois River plutonic complex</i> | 92-PP-70 | 42°15'43" N 123°52'11" W | Chetco River; norite | hornblende | 155.3 ± 0.5 |
| <i>Illinois River plutonic complex dikes</i> | 89-PP-12C | 42°18'38" N 123°46'51" W | Illinois River; hornblendite | hornblende | 156.0 ± 0.5 |
| | 89-PP-15 | 42°19'32" N 123°46'38" W | Illinois River; gneissic hornblende- biotite quartz diorite | hornblende | 156.3 ± 0.6 |
| <i>Briggs Creek amphibolite</i> | 91CR-9B | 42°24'04" N 123°44'50" W | Briggs Creek; metagabbro | hornblende | 156.8 ± 0.5 |
| | 91EDM-72A | 42°21'37" N 123°44'42" W | Soldier Creek; hornblende schist | hornblende | 157.9 ± 0.5 |
| <i>Onion Camp complex</i> | 91-EDM-81A | 42°20'40" N 123°39'40" W | Squaw Mountain; amphibolite gneiss | hornblende | 169.6 ± 0.5 |
| | 90-EDM-10 | 42°18'58" N 123°40'46" W | Squaw Mountain; hornblende schist | hornblende | 173.1 ± 0.6 |

Table 2-3. Major and trace element analyses from the western Jurassic belt, central Illinois River drainage, Oregon.

| Sample | Josephine ophiolite | | | | | | | | | | Pillow lavas | | | | | | Greenst. | | | | |
|----------------------------------|---------------------|--------|--------|--------|--------|---------|---------|-------|--------|--------|--------------|-------|--|--|--|--|----------|--|--|--|--|
| | Dikes | | | | | | | | | | | | | | | | | | | | |
| | PP-27 | PP-33 | PP-44A | OM-1A | S-2 | EDM-88A | EDM-88B | G-17B | S-1 | G-17A | W-ID | JM-6 | | | | | | | | | |
| SiO ₂ | 53.96 | 54.35 | 54.48 | 55.30 | 51.41 | 54.00 | 54.62 | 50.95 | 48.82 | 53.34 | 50.98 | 56.33 | | | | | | | | | |
| TiO ₂ | 0.43 | 0.23 | 0.35 | 1.02 | 1.28 | 0.25 | 0.52 | 0.57 | 1.83 | 0.79 | 0.93 | 0.74 | | | | | | | | | |
| Al ₂ O ₃ | 16.46 | 11.70 | 13.84 | 15.66 | 14.48 | 11.07 | | 15.44 | 16.46 | 15.53 | 16.36 | 14.34 | | | | | | | | | |
| Fe ₂ O ₃ * | 8.11 | 8.00 | 7.49 | 10.31 | 10.25 | 7.81 | 9.35 | 7.83 | 12.92 | 14.17 | 9.24 | 7.95 | | | | | | | | | |
| MnO | 0.14 | 0.16 | 0.21 | 0.17 | 0.18 | 0.14 | 0.10 | 0.15 | 0.19 | 0.23 | 0.17 | 0.19 | | | | | | | | | |
| MgO | 6.95 | 12.80 | 10.43 | 5.15 | 6.34 | 13.26 | 6.64 | 7.82 | 4.39 | 4.41 | 8.81 | 6.54 | | | | | | | | | |
| CaO | 6.35 | 8.06 | 5.90 | 7.62 | 8.85 | 6.04 | 5.15 | 6.50 | 7.97 | 3.34 | 6.77 | 6.84 | | | | | | | | | |
| Na ₂ O | 5.21 | 0.84 | 3.23 | 3.27 | 4.47 | 1.98 | 5.68 | 4.75 | 4.64 | 6.09 | 4.37 | 3.66 | | | | | | | | | |
| K ₂ O | 0.04 | 0.77 | 0.43 | 0.12 | 0.54 | 0.32 | 0.11 | 0.48 | 0.14 | 0.40 | 0.79 | 0.38 | | | | | | | | | |
| P ₂ O ₅ | 0.04 | 0.03 | 0.03 | 0.15 | 0.12 | 0.02 | 0.05 | 0.06 | 0.22 | 0.23 | 0.11 | 0.11 | | | | | | | | | |
| LOI | 3.11 | 3.87 | 3.71 | 2.19 | 2.79 | 4.32 | 2.51 | 4.62 | 3.11 | 2.46 | 2.82 | 3.52 | | | | | | | | | |
| Total | 100.81 | 100.81 | 100.09 | 100.96 | 100.72 | 99.21 | 100.64 | 99.19 | 100.68 | 100.99 | 101.34 | 100.6 | | | | | | | | | |
| <u>Trace elements in ppm</u> | | | | | | | | | | | | | | | | | | | | | |
| Rb | 2 | 11 | 7 | 4 | 9 | 6 | 3 | 6 | 4 | 8 | 13 | 3 | | | | | | | | | |
| Sr | 57 | 48 | 88 | 90 | 217 | 92 | 218 | 166 | 113 | 165 | 273 | 175 | | | | | | | | | |
| Zr | 41 | 13 | 23 | 82 | 87 | 19 | 37 | 52 | 134 | 61 | 62 | 56 | | | | | | | | | |
| Y | 13.4 | 11.5 | 13.0 | 27.6 | 34.5 | 11.6 | 15.0 | 19.3 | 47.5 | 21.0 | 24.2 | 21.3 | | | | | | | | | |
| Nb | b.d. | 1 | b.d. | 1 | 2 | b.d. | b.d. | b.d. | 1 | 1 | b.d. | 2 | | | | | | | | | |
| Ba | 12 | 26 | 45 | 36 | 36 | 44 | 13 | 41 | 16 | 351 | 150 | 49 | | | | | | | | | |
| Sc | 38.3 | 40.8 | 46.2 | 40.1 | 47.6 | 44.5 | 48.5 | 38.7 | 37.0 | 44.8 | 45.0 | 31.5 | | | | | | | | | |
| V | 238 | 191 | 195 | 297 | 281 | 193 | 289 | 224 | 385 | 353 | 231 | 220 | | | | | | | | | |
| Cr | 106 | 1116 | 386 | 81 | 86 | 1095 | 136 | 361 | 31 | 29 | 268 | 231 | | | | | | | | | |
| Ni | 25 | 247 | 87 | b.d. | 4 | 297 | 10 | 193 | b.d. | b.d. | 59 | 93 | | | | | | | | | |
| Cu | 299 | 20 | 83 | 128 | 149 | 64 | 2 | 7 | 48 | 106 | 75 | 92 | | | | | | | | | |
| Zn | 41 | 68 | 86 | 66 | 59 | 44 | 13 | 55 | 110 | 107 | 43 | 138 | | | | | | | | | |
| Ti | 2,579 | 1,379 | 2,098 | 6,115 | 7,692 | 1,493 | 3,105 | 3,439 | 10,972 | 4,736 | 5,548 | 4,450 | | | | | | | | | |

Table 2-3 (continued). Major and trace element analyses from the western Jurassic belt, central Illinois River drainage, Oregon.

| Sample | Rogue Formation | | | | | | | | | | Sills |
|----------------------------------|-----------------|---------|---------|--------|--------|--------|--------|---------|---------|--------|--------|
| | Flow units | | | | | Tufts | | | | | |
| | PP-6* | EDM-49* | EDM-51B | EDM-59 | G-9* | S-38 | S-18 | EDM-48C | EDM-51A | 6MiRd* | EDM-84 |
| SiO ₂ | 51.96 | 47.55 | 47.55 | 52.88 | 52.34 | 55.99 | 50.71 | 47.08 | 46.79 | 49.50 | 53.14 |
| TiO ₂ | 0.97 | 0.81 | 0.63 | 1.06 | 1.18 | 0.33 | 0.64 | 0.73 | 0.93 | 0.90 | 1.42 |
| Al ₂ O ₃ | 16.25 | 14.34 | 16.17 | 21.16 | 18.40 | 12.51 | 13.60 | 15.75 | 16.59 | 16.33 | 16.07 |
| Fe ₂ O ₃ * | 8.91 | 9.97 | 8.44 | 8.54 | 9.80 | 8.85 | 7.56 | 8.25 | 10.90 | 9.63 | 11.91 |
| MnO | 0.18 | 0.19 | 0.16 | 0.24 | 0.16 | 0.23 | 0.13 | 0.19 | 0.18 | 0.19 | 0.21 |
| MgO | 6.31 | 9.75 | 7.11 | 2.95 | 4.36 | 10.87 | 6.52 | 6.02 | 5.06 | 9.13 | 3.65 |
| CaO | 8.66 | 10.09 | 11.46 | 7.86 | 8.09 | 5.80 | 9.15 | 14.15 | 9.57 | 7.06 | 5.47 |
| Na ₂ O | 3.79 | 2.10 | 2.97 | 4.30 | 3.24 | 3.17 | 2.70 | 0.34 | 2.76 | 3.33 | 4.70 |
| K ₂ O | 0.55 | 1.22 | 0.38 | 0.62 | 0.85 | 0.71 | 1.63 | 0.05 | 0.49 | 0.61 | 0.85 |
| P ₂ O ₅ | 0.24 | 0.16 | 0.12 | 0.33 | 0.26 | 0.04 | 0.15 | 0.13 | 0.18 | 0.17 | 0.25 |
| LOI | 3.71 | 3.24 | 5.85 | 2.46 | 2.92 | 3.83 | 7.71 | 7.64 | 6.74 | 3.40 | 2.63 |
| Total | 101.52 | 99.42 | 100.84 | 102.40 | 101.60 | 102.34 | 100.49 | 100.33 | 100.19 | 100.24 | 100.31 |
| <u>Trace elements in ppm</u> | | | | | | | | | | | |
| Rb | 16 | 36 | 11 | 14 | 20 | 11 | 27 | 4 | 14 | 15 | 12 |
| Sr | 512 | 439 | 323 | 671 | 485 | 183 | 370 | 553 | 345 | 512 | 788 |
| Zr | 66 | 46 | 34 | 94 | 99 | 27 | 35 | 45 | 54 | 55 | 114 |
| Y | 27.2 | 23.3 | 18.3 | 35 | 29.9 | 15.3 | 1805 | 22.3 | 23.4 | 23.9 | 34.3 |
| Nb | 3 | 3 | 2 | 5 | 2 | b.d. | 3 | 3 | 3 | 4 | 1 |
| Ba | 75 | 295 | 130 | 186 | 241 | 168 | 366 | 22 | 115 | 360 | 1717 |
| Sc | 34.4 | 41 | 38.5 | 25 | 26.3 | 39.5 | 34.6 | 38.1 | 38.8 | 43.3 | 40.6 |
| V | 270 | 263 | 215 | 185 | 266 | 221 | 214 | 250 | 280 | 259 | 355 |
| Cr | 211 | 609 | 432 | 7 | 70 | 974 | 316 | 166 | 32 | 542 | 23 |
| Ni | 89 | 160 | 95 | 48 | 133 | 304 | 92 | 61 | 27 | 256 | ... |
| Cu | 57 | 97 | 73 | 24 | 47 | 71 | 71 | 68 | 97 | 19 | 63 |
| Zn | 82 | 71 | 60 | 106 | 89 | 51 | 49 | 65 | 90 | 49 | 107 |
| Ti | 5,813 | 4,850 | 3,753 | 6,348 | 7,053 | 1,969 | 3,861 | 4,396 | 5,599 | 5,407 | 8,540 |

Table 2-3 (continued). Major and trace element analyses from the western Jurassic belt, central Illinois River drainage, Oregon.

| Sample | Illinois River plutonic complex | | | | | | | | | | | | | | |
|----------------------------------|---------------------------------|--------|--------|-------|-------------------|--------|-------------------|-------------------|-----------------------|--------|--------|--------------------|--------|--------------------|-------|
| | Troctolite | | Norite | | Hornblende gabbro | | Grano-diorite | | Tonalite-trondhjemite | | Dikes | | | | |
| | CP-4 | YB-6 | PP-70 | YB-13 | YB-7 | YB-9 | IR-3 [†] | IR-4 [†] | PP-17 | PP-48 | PP-62 | PP-64 [†] | PP-69 | PP-9A [†] | PP-14 |
| SiO ₂ | 42.26 | 41.78 | 46.98 | 43.64 | 45.15 | 46.83 | 49.36 | 65.85 | 67.37 | 74.15 | 64.94 | 67.42 | 71.46 | 59.34 | 40.27 |
| TiO ₂ | 0.04 | 0.12 | 0.75 | 0.93 | 0.91 | 0.74 | 0.76 | 0.34 | 0.24 | 0.08 | 0.26 | 0.27 | 0.15 | 0.24 | 1.03 |
| Al ₂ O ₃ | 24.65 | 25.79 | 19.56 | 18.50 | 19.60 | 20.43 | 17.64 | 15.86 | 16.85 | 15.35 | 17.38 | 16.70 | 15.50 | 18.38 | 14.47 |
| Fe ₂ O ₃ * | 7.72 | 8.78 | 13.42 | 15.67 | 14.68 | 12.71 | 12.23 | 5.08 | 3.69 | 1.15 | 4.46 | 3.99 | 1.98 | 5.54 | 18.29 |
| MnO | 0.10 | 0.12 | 0.25 | 0.26 | 0.30 | 0.25 | 0.22 | 0.16 | 0.14 | 0.09 | 0.15 | 0.14 | 0.15 | 0.18 | 0.19 |
| MgO | 10.37 | 9.18 | 5.63 | 6.94 | 5.60 | 5.51 | 5.36 | 1.86 | 1.43 | 0.52 | 1.76 | 1.48 | 0.72 | 2.20 | 10.65 |
| CaO | 13.30 | 13.55 | 11.71 | 11.98 | 11.14 | 11.10 | 10.70 | 5.90 | 5.80 | 3.37 | 6.12 | 5.71 | 3.57 | 6.03 | 10.96 |
| Na ₂ O | 0.49 | 0.48 | 1.70 | 1.15 | 1.97 | 1.75 | 2.00 | 3.23 | 3.27 | 4.04 | 4.18 | 3.27 | 3.75 | 3.74 | 1.54 |
| K ₂ O | 0.07 | 0.00 | 0.16 | 0.04 | 0.07 | 0.14 | 0.29 | 1.21 | 0.74 | 0.75 | 0.52 | 0.73 | 1.05 | 2.25 | 0.47 |
| P ₂ O ₅ | 0.00 | 0.00 | 0.11 | 0.00 | 0.16 | 0.11 | 0.13 | 0.09 | 0.13 | 0.06 | 0.14 | 0.11 | 0.14 | 0.29 | 0.01 |
| LOI | 1.89 | 0.89 | 0.18 | 0.44 | 1.20 | 1.02 | 0.63 | 1.19 | 1.08 | 1.17 | 0.76 | 0.85 | 1.67 | 2.60 | 1.94 |
| Total | 100.89 | 100.70 | 100.46 | 99.55 | 100.78 | 100.58 | 99.33 | 100.77 | 100.76 | 100.73 | 100.67 | 100.66 | 100.13 | 100.80 | 99.82 |
| Trace elements in ppm | | | | | | | | | | | | | | | |
| Rb | 3 | 3 | 5 | 3 | 3 | 4 | 6 | 22 | 18 | 17 | 12 | 18 | 26 | 46 | 41 |
| Sr | 304 | 283 | 300 | 289 | 372 | 348 | 309 | 321 | 467 | 496 | 500 | 438 | 797 | 693 | 217 |
| Zr | b.d. | b.d. | 6 | 1 | 1 | 6 | 37 | 58 | 57 | 75 | 60 | 60 | 77 | 95 | 5 |
| Y | 2.3 | 1.7 | 9.9 | 7.9 | 9.9 | 18.6 | 19.7 | 13.6 | 15.9 | 8.1 | 12.3 | 13.5 | 9.8 | 10.9 | 15.0 |
| Nb | b.d. | b.d. | b.d. | b.d. | b.d. | b.d. | b.d. | 4 | 5 | 3 | 4 | 3 | 6 | 3 | b.d. |
| Ba | 28 | 10 | 62 | 33 | 44 | 68 | 114 | 541 | 394 | 381 | 328 | 365 | 673 | 894 | 111 |
| Sc | 3.0 | 3.3 | 56.8 | 66.5 | 68.7 | 54.9 | 53.8 | 12.8 | 8.9 | 1.7 | 11.7 | 8.7 | 3.4 | 9.7 | 184 |
| V | 32 | 105 | 388 | 549 | 413 | 338 | 329 | 84 | 45 | 3 | 75 | 49 | 7 | 96 | 1048 |
| Cr | 207 | 230 | 24 | 32 | 11 | 10 | 27 | 16 | 20 | 7 | 12 | 19 | 16 | 19 | 12 |
| Ni | 21 | 25 | 3 | ... | ... | ... | 16 | ... | 39 | 13 | ... | ... | 35 | ... | 32 |
| Cu | 4 | 6 | 126 | 152 | 140 | 78 | 100 | 27 | ... | ... | 18 | 3 | ... | 66 | 69 |
| Zn | 28 | 37 | 96 | 107 | 114 | 102 | 85 | 53 | 53 | 37 | 58 | 52 | 56 | 62 | 70 |
| Ti | 255 | 728 | 4,523 | 5,565 | 5,458 | 4,418 | 4,559 | 2,037 | 1,456 | 499 | 1,559 | 1,638 | 877 | 1,466 | 6,163 |

Table 2-3 (continued). Major and trace element analyses from the western Jurassic belt, central Illinois River drainage, Oregon.

| Sample | Union Camp complex | | | | | | | | | | Dike | |
|----------------------------------|--------------------|-------|---------|----------------------|--------|--------------------|--------------------|--------|-------|--------|-------|--------------------|
| | Pillow lava | | | | | Massive Greenstone | | | | | | |
| | CP-3 | OM-8 | EDM-83A | EDM-83B [#] | EDM-87 | G-14C | OM-11 [#] | OM-14 | G-14A | CP-45 | CR-22 | JM-11 [†] |
| SiO ₂ | 48.51 | 48.54 | 46.31 | 45.68 | 52.12 | 52.49 | 54.06 | 53.98 | 49.02 | 50.14 | 49.52 | 76.63 |
| TiO ₂ | 2.66 | 1.38 | 2.20 | 2.06 | 0.70 | 0.77 | 1.18 | 0.51 | 1.27 | 0.93 | 1.38 | 0.22 |
| Al ₂ O ₃ | 14.45 | 14.57 | 15.36 | 15.39 | 16.33 | 15.45 | 13.47 | 14.79 | 15.89 | 16.19 | 12.12 | 13.33 |
| Fe ₂ O ₃ * | 13.10 | 12.24 | 10.75 | 9.65 | 10.26 | 8.38 | 7.82 | 7.99 | 9.25 | 8.89 | 13.70 | 1.12 |
| MnO | 0.20 | 0.21 | 0.16 | 0.15 | 0.15 | 0.13 | 0.17 | 0.14 | 0.15 | 0.15 | 0.22 | 0.02 |
| MgO | 4.47 | 5.93 | 6.70 | 5.00 | 6.61 | 9.12 | 7.70 | 8.23 | 6.46 | 6.63 | 7.17 | 0.53 |
| CaO | 8.86 | 10.05 | 9.73 | 11.42 | 5.44 | 7.42 | 8.57 | 8.45 | 9.69 | 13.14 | 8.86 | 2.27 |
| Na ₂ O | 4.58 | 3.68 | 4.03 | 4.44 | 4.77 | 4.14 | 4.09 | 3.23 | 3.68 | 2.21 | 2.83 | 4.68 |
| K ₂ O | 0.27 | 0.42 | 0.30 | 0.48 | 0.43 | 0.12 | 0.75 | 0.34 | 0.14 | 0.03 | 0.22 | 1.06 |
| P ₂ O ₅ | 0.39 | 0.20 | 0.39 | 0.38 | 0.09 | 0.09 | 0.16 | 0.08 | 0.16 | 0.10 | 0.11 | 0.03 |
| LOI | 2.84 | 2.43 | 4.44 | 6.33 | 3.41 | 2.74 | 2.20 | 2.99 | 2.66 | 3.69 | 3.09 | 0.68 |
| Total | 100.33 | 99.66 | 100.37 | 100.97 | 100.31 | 100.85 | 100.16 | 100.75 | 98.37 | 102.11 | 99.22 | 100.57 |
| Trace elements in ppm | | | | | | | | | | | | |
| Rb | 7 | 9 | 6 | 8 | 7 | 3 | 13 | 8 | 4 | 2 | 7 | 22 |
| Sr | 225 | 245 | 361 | 419 | 145 | 137 | 90 | 156 | 256 | 56 | 100 | 121 |
| Zr | 197 | 81 | 156 | 146 | 44 | 57 | 99 | 36 | 104 | 65 | 68 | 105 |
| Y | 43.3 | 39.7 | 26.1 | 24.7 | 23.8 | 22.1 | 29.6 | 16.5 | 32.8 | 24.5 | 32.8 | 10.9 |
| Nb | 28 | 4 | 30 | 32 | 1 | 1 | 4 | b.d. | 2 | b.d. | 4 | 5 |
| Ba | 70 | 46 | 132 | 201 | 123 | 27 | 62 | 155 | 33 | 11 | 26 | 355 |
| Sc | 33.4 | 43.8 | 24.4 | 21.9 | 35.6 | 38.7 | 28.4 | 36.2 | 35.5 | 37.6 | 49.3 | 2.3 |
| V | 285 | 279 | 209 | 204 | 296 | 223 | 212 | 228 | 245 | 195 | 325 | 16 |
| Cr | 64 | 212 | 200 | 179 | 111 | 547 | 247 | 341 | 233 | 209 | 109 | 11 |
| Ni | | 53 | 138 | 121 | 91 | 252 | 97 | 101 | 90 | 75 | 50 | 20 |
| Cu | 55 | 23 | 51 | 41 | 60 | 75 | 53 | 74 | 52 | 104 | 85 | ... |
| Zn | 115 | 83 | 78 | 74 | 87 | 57 | 55 | 51 | 63 | 46 | 103 | 9 |
| Ti | 15,947 | 8,271 | 12,350 | 13,178 | 4,180 | 4,598 | 7,070 | 3,081 | 7,641 | 5,551 | 8,273 | 1,338 |

Table 2-3 (continued). Major and trace element analyses from the western Jurassic belt, central Illinois River drainage, Oregon.

Major element data given in weight %, minor and trace element data in ppm.
Greenst. = greenstone.

* Total Fe content is given as Fe_2O_3 .

† U/Pb geochronologic samples.

* Samples with REE analyses (see Table 2-5).

Note: Analyses done at Texas Tech University by ICP-MS, inductively-coupled atomic emission mass spectrometry; and, for Rb, by flame emission spectroscopy; ; indicates that no data is available; b.d., below detection limits. Some of the trace elements (Sr, Ba, Zr, and Y) were analyzed twice; once with dilute solutions used for major elements, and again with concentrated solution used for the other trace elements. Values from the two runs were averaged with the following exceptions; 1) for high Sr values the trace element run values were used, 2) for high Ba values the major element run values were used, and 3) for Y the trace element runs were used because of a better fit to standards.

Nevadan structures. These features combined with the fact that the crustal sequence is <2 km thick (Plate 1) suggests that the ophiolite was tectonically thinned, probably at least partially as a result of extension in the oceanic setting thinning prior to Nevadan deformation.

In the Chetco Pass region, tectonically dismembered blocks of ophiolitic crustal rocks occur in a northeast trending serpentine matrix melange zone. Here, impure radiolarian chert interbedded with pillow lava yielded Late Jurassic and probable Callovian radiolaria (Yule and others, 1992; Silk and Yule, unpublished data, 1992). The melange zone is nonconformably overlapped by Rogue Fm volcanogenic turbidites and volcanic breccia, dated in the Illinois River area at 153.4 ± 0.6 Ma ($^{40}\text{Ar}/^{39}\text{Ar}$, igneous hornblende). Locally, this melange zone contains mono- and heterolithologic debris flow breccias that appear to occur at the base of the volcanogenic overlap assemblage. The stratigraphic and field relations clearly demonstrate that the melange belt formed prior to Nevadan folding of the overlap sequence, perhaps along a normal, transfer, or transform fault zones in the Josephine basin.

Elsewhere, countless small bodies of massive gabbro and sheeted mafic dikes intrude rocks of the Onion Camp complex (OCC, described in detail below). These bodies are not shown on the Plate 1, but some of the larger intrusions are shown on Plate 3. They are similar in appearance to the correlative portions of the Josephine ophiolite sequence suggesting that they represent ophiolite magmas which intruded the rifted fragments of the remnant arc during Josephine age extension. Attempts to obtain a radiometric age from plagiogranite dikes and small intrusions associated with these mafic intrusions have failed (see sample EDM-89, Table 2-1). These mafic complex rocks are described in greater detail below along with other units of the OCC.

Like the type Josephine ophiolite (Alexander and Harper, 1992), the ophiolite sequences of the central Illinois River region exhibit features characteristic of slow- to intermediate-spreading including: 1) serpentine-matrix melange formation, 2) tectonically

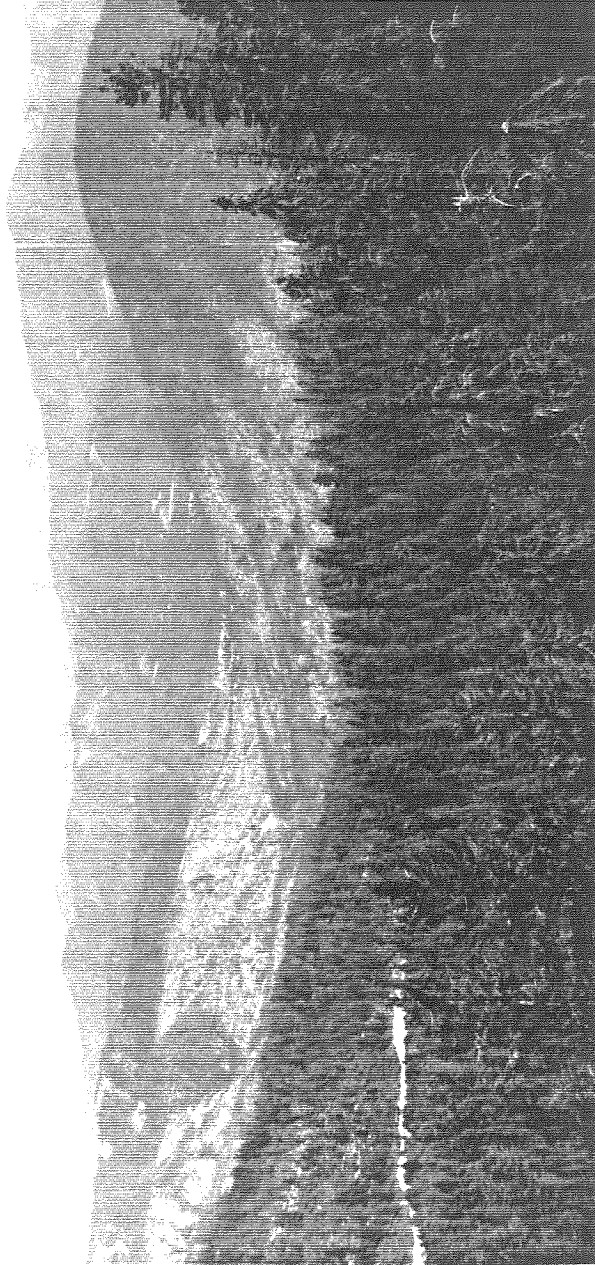
disrupted crustal sections with cumulative thicknesses generally <2 km, 3) brittle fragmentation textures, and evidence for tilting and faulting in dike complexes. Thus the crustal rocks of the Josephine ophiolite appear to have experienced relatively high degrees of tectonic disruption and alteration prior to Nevadan deformation.

Peridotite. Two peridotite units are shown on Plate 1. One represents older, highly serpentinized and sheared peridotite associated with the Onion Camp complex (discussed below) and the other corresponds to younger, moderately serpentinized to nonserpentinized Josephine peridotite. The boundary separating these two generations of peridotite is generally gradational and is often marked by a striking vegetation change (Figure 2-2).

The Josephine peridotite in the study area forms the northern portion of the largest peridotite massif exposed in North America (Dick, 1976) and consists primarily of tectonized harzburgite and dunite with subordinate amounts of lherzolite, websterite, and podiform chromitite. The peridotite is interpreted to represent the residual material formed during partial melting in upwelling mantle asthenosphere beneath the Josephine inter-arc basin spreading centers (e.g., Dick, 1976). Separate bodies of very similar peridotite occur at Pearsoll Peak and Chrome Ridge located to the north of the Madstone Cabin fault and west of the Chetco Pass fault (Plates 1, 5, 9), and are interpreted to have once been continuous with the main body of the Josephine peridotite. The Pearsoll Peak and Chrome Ridge peridotite bodies and the two northern prongs of the Josephine body at Chetco Pass and Eight Dollar Mountain are interpreted to represent the cores of northeast trending anticlinoria that reflect the regional fold patterns characteristic of this portion of the WJB.

The degree of serpentinization of the Josephine peridotite is variable throughout the study area. Highly serpentinized rocks exhibit complex alteration fabrics and cross-cutting relations suggestive of a long-lived and multi-stage serpentinization process. For example, the most highly serpentinized zones tend to occur along faults and shear zones oriented sub-parallel to the regional Nevadan foliation. Alternatively, Coulton (1995) presents

Figure 2-3. Photograph with view toward the northeast of Eight Dollar Mountain and the town of Selma. Note the distinct vegetation change on the west flank of Eight Dollar Mountain marking the boundary between highly serpentinized harzburgite and dunite of the Onion Camp complex, and relatively nonserpentinized Josephine peridotite.



evidence to indicate that some of the serpentinization in these zones of alteration and shearing occurred prior to the Nevadan deformation and probably are a product of oceanic serpentinization. It seems likely that a combination of both oceanic- and accretion-related serpentinization has affected the Josephine peridotite.

Rogue and Galice Formations

The Rogue and Galice Formations, along with the localized deposits of the Fiddler Mountains olistostrome complex (see below), comprise the overlap assemblage of the WJB. The Rogue Formation consists of an overall coarsening upward sequence of basaltic to andesitic volcanogenic sediments, tuffs, tuff breccias, and lava. These strata are intercalated with the basal Galice Formation pelagic and hemipelagic strata and are overlain by Galice Formation flysch deposits. The interdigitation between volcanogenic deposits of the Rogue Formation and argillaceous Galice strata occur at scales ranging from centimeter scale to a scale of tens of meters. Some of the larger scale interlayering occurs at a large enough scale to be shown on Plates 6,9, and 11. Previously reported ages for these rocks are 157 ± 1.5 Ma for an andesitic tuff layer in the Rogue Formation (U-Pb zircon, Saleeby, 1984) and Middle Oxfordian to Upper Kimmeridgian fossil age for the Galice Formation flysch deposits (Diller, 1907; Imlay, 1981; Pessagno and Blome, 1990). Additional age control is provided by a 153.4 ± 0.6 Ma $^{40}\text{Ar}/^{39}\text{Ar}$ hornblende age from igneous grains separated from a lithic tuff breccia collected immediately downstream from the Illinois River falls (Table 2-2).

Rogue Formation. In the study area rocks of the Rogue Formation primarily occur in an elongate belt bounded on the west by the Chetco Pass fault and on the east by a faulted depositional contact with rocks of the Onion Camp complex (e.g., Plate 1). The fault boundaries are interpreted as truncated fold limbs of a regional synclinoria cored by the Rogue Formation rocks (e.g., Plate 1). Several exposures of mylonitic Rogue

Formation rocks (mainly lithic and crystal-lithic tuffs) occur to the west of the Chetco Pass fault above low angle extensional shear zones.

The Rogue Formation in the study area, to a first order, consists of an overall coarsening upward sequence of volcanogenic sediments, flows, and breccias with proximal deposits most common in the west and north and distal facies most common in the east and south. The more distal, basal strata consist primarily of thin-bedded volcanogenic turbidite wackes and impure chert (Figure 2-4) that give way up section to more proximal deposits including thick-bedded crystal and lithic tuff, lithic tuff breccia, and lava (Figure 2-5). The coarsest deposits observed in the field area occur in the vicinity of Illinois River falls where volcanic clasts up to 50 cm occur in meter to several meter thick matrix and clast supported breccia layers. Lavas are most common to the north of the Illinois River falls.

Clinopyroxene-rich gabbroic sills commonly intrude the basal strata of the Formation. Collectively, these relations suggest the strata of the Rogue Formation in the study area formed part of a submarine volcanogenic edifice sourced from nearby areas to the north and west.

The basal strata of the Rogue Formation generally occur interbedded with platy, siliceous argillite of the Galice Formation. In the southern part of the outcrop belt, Rogue Formation strata rest nonconformably upon a variable substrate including a melange belt of Josephine ophiolite rocks (described above) and rocks of the Onion Camp complex. For example, near Whetstone Butte (Plate 3), thin-bedded turbidite wackes are exceptionally well exposed along the ridge line in striking nonconformity with massive serpentinite of the Onion Camp complex. In a few localities, the basal Rogue strata overlap ophicalcite and heterolithologic ophiolite clast, talus breccias and debris flows (Figure 2-6). Though generally poorly exposed elsewhere in this region, the general parallelism between bedding attitudes and the contact with basement rocks suggests that the contact is a depositional nonconformity and indicates that the melange belt formed prior to the deposition of the overlap sequence.

Figure 2-4. Photograph of river polished exposure of rhythmically bedded Rogue Formation volcanogenic turbidites. Individual beds contain crystal fragments (clinopyroxene, hornblende, and plagioclase), lithic clasts (tuff clasts and lava), and lapilli in a tuffaceous matrix. Graded beds are common and typically contain shale rip-up clasts and cross-stratification. The graded beds are almost always capped by hemipelagic silicic-tuffaceous argillite.



Figure 2-5. Photograph of a river boulder of Rogue Formation volcanic breccia. Clasts consist of clinopyroxene- and plagioclase-phyric, and clinopyroxene-, hornblende-, and plagioclase-phyric clasts.

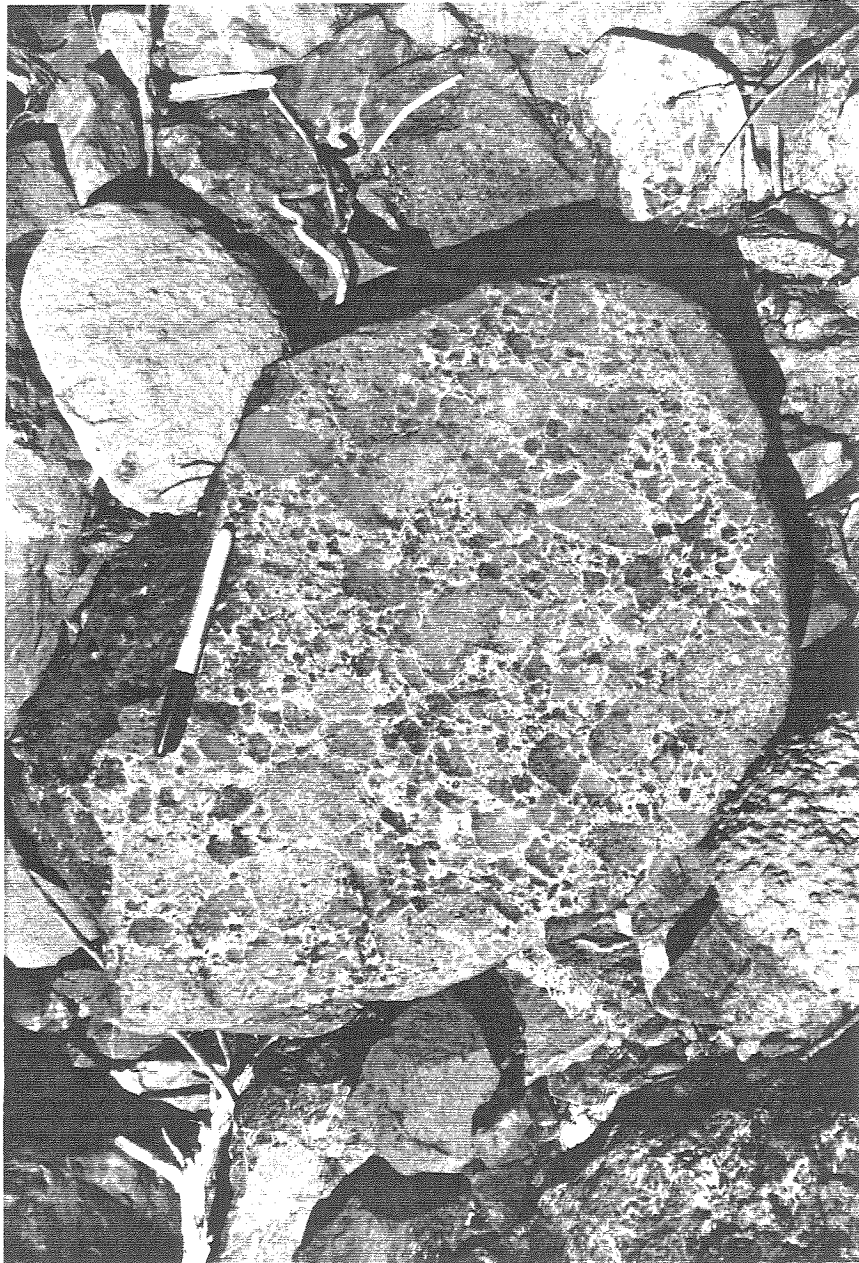
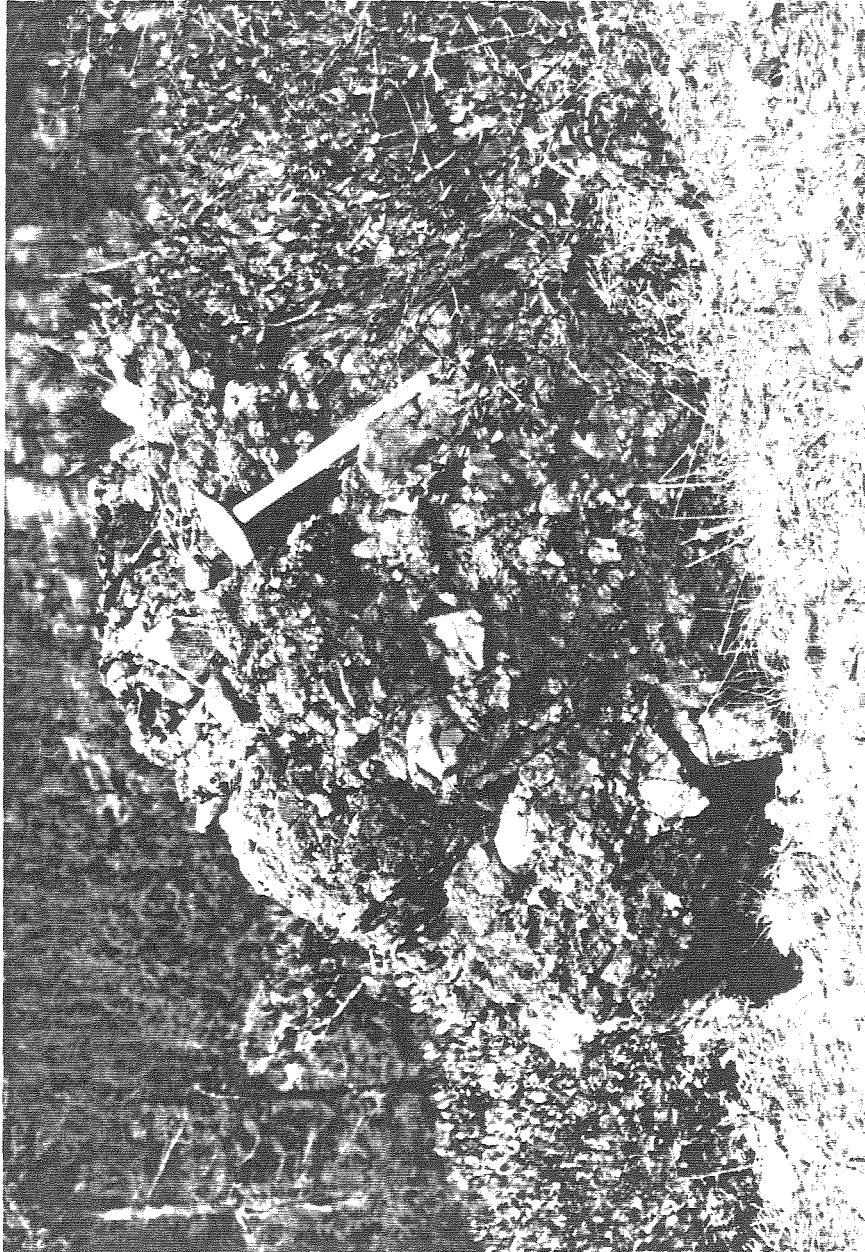


Figure 2-6. Photograph of an outcrop in the Chetco Pass region of monolithic, serpentine-clast, debris flow breccia. This deposit is interpreted to occur at the base of the overlapping Rogue Formation deposits, which are exposed nearby.



Galice Formation. Strata of the Galice Formation are exposed along the entire length of the Klamath Mountains province. In the study area, the Galice Formation strata consist primarily of interbedded argillites, siltstones, and occasional wackes. No age data exists from the study area, but the metasedimentary deposits are correlated with the basal pelagic and hemipelagic deposits that overlap the Josephine ophiolite, determined as Late Callovian to Oxfordian in age (Pessagno and Blome, 1990). This correlation is based on the general absence of sandy layers combined with their occurrence at the base of the overlap assemblage.

Like the deposits of the Rogue Formation, Galice Formation strata suggest a west to east facies transition. West of the Onion Camp complex (Plates 1, 6, and 9), black to gray slaty argillite and chert, with rare occurrences of gray pelagic limestone, are intricately interlayered with volcanogenic turbidites of the Rogue Formation. These relations suggest that the strata of this region represent the distal fringe of the Rogue Formation volcanic edifice. At the basal overlap with the Onion Camp complex, Galice strata include rare deposits of gray pelagic limestone and are interbedded with heterolithologic conglomeratic grit and breccia of the Fiddler Mountain olistostrome. Similarly, in the type Josephine section, pelagic limestone occurs in a thin stratigraphic horizon immediately overlying pillow lavas (Harper, 1983; Pessagno and Blome, 1990) providing a possible correlation between the basal Galice strata of the central Illinois River drainage and the type Josephine ophiolite.

To the east of the regional anticlinoria marked by the Onion Camp complex (Plates 1, 6, 7, and 10) the volcanogenic contribution diminishes. West of the Illinois River Valley fault (Plates 6 and 10), the Galice Formation conformably overlaps a disrupted ophiolite sequence and consists of black to buff-gray, siliceous argillite and tuffaceous siltstone. These deposits are strikingly similar to the basal pelagic and hemipelagic sequence that overlies the type Josephine ophiolite sequence of northern California (Harper, 1984; Pessagno and Blome, 1990). To the east of the Illinois River Valley Fault

(Plates 7 and 10), the Galice strata are buff-gray to buff, argillite, and siltstone and wacke flysch deposits that characterize the bulk of the Formation above the basal pelagic and hemipelagic deposits. Wackes in the flysch sequence exhibit an up-section increase continental margin material (Miller and Saleeby, 1987).

In general, the stratigraphic relations exhibited by Galice Formation strata suggest that they form part of a submarine sedimentary basinal overlap sequence that interfingered with arc volcanogenic deposits on the west and received an increasing contribution from uplifting and eroding older terranes situated to the east.

Illinois River plutonic complex

The central Illinois River flows through the middle of an elongate (1 to 10 km wide and 60 km long), heterogeneous mafic to intermediate plutonic complex that forms the western portion of the study area and extends northeastward to the Rogue River (Plates 1, 2, 3, 5, and 8). The plutonic rocks occur in the most remote region of the study area and access is primarily limited to river polished exposures in the Illinois and Chetco River drainages and along hiking trails in the Kalmiopsis Wilderness. Road access is limited to the Illinois River road and to the USFS access road 2512 to the west of Chrome Ridge. Due to its relative inaccessibility, the Illinois River plutonic complex has received relatively little attention; at least relative to other large plutons of the Klamath Mountains (e.g., Gribble et al., 1990; Barnes et al., 1992; Charlton, 1979).

The plutonic rocks are herein referred to informally as the Illinois River plutonic complex (IRPC) in place of the previous designations, the Illinois River gabbro by Jorgenson (1970) and the Illinois River batholith by Garcia (1979; 1982). This distinction is made because the plutonic complex neither consists entirely of gabbro nor contains multiple plutonic bodies as the term batholith implies. Hotz (1971) included the plutonic rocks in the Chetco complex which also consisted of metagabbro, amphibolite schist and

gneiss, and metaperidotite. However, this designation is abandoned here to emphasize the distinctly different petrogeneses of the highly deformed wallrocks and the IRPC.

Main phase rocks. The IRPC is reversely zoned with massive norite, hornblende gabbro and diorite, and sparse biotite-hornblende quartz diorite surrounding a core region consisting of coarsely crystalline, layered troctolite, norite, and hornblende gabbro (Figure 2-7 and Figure 2-8). In general, the diorite and quartz diorite occur at the margins of the complex and the rocks become more mafic toward the core (Jorgenson, 1970). The approximate modal mineralogy of samples collected during this study are shown in Table 2-4. Classification of igneous rocks is after Streckeisen (1973). The most strongly deformed rocks of the IRPC, flaser gabbro and quartz leucogabbro (Figure 2-9), are exposed along the eastern margin of the complex and are mapped as a separate unit (Plates 1, 2, and 9). These highly deformed rocks exhibit a variable foliation orientation, but a consistent moderate to shallow, NE-SW trending elongation lineation. The overall domal structure of the IRPC suggests that the complex is a doubly plunging anticlinoria with relatively highly strained limbs.

Sills. Commingled biotite tonalite and garnet, two-mica trondjemite forms an approximately 100-300 meter thick sill at the roof of the plutonic complex beneath the subhorizontal slab of the Pearsoll Peak peridotite mass (Figure 2-10) and as an inclined sill on the western margin near Pine Flat (Plates 1, 5, and 8). A late magmatic hornblende pegmatoid sill, approximately 0.5-1.0 kilometers thick, occurs at the top of the plutonic complex near Dry Butte at the southern end of the complex (Plates 1 and 2). The pegmatoid exhibits a striking layered, comb structure texture defined by centimeter to near meter sized hornblende crystals oriented perpendicular to compositional layering and the margins of the sill (Figures 2-11 and 2-12). Nondeformed to mylonitic dikes consisting of gabbro, hornblendite, quartz leucogabbro, diorite, and quartz diorite intrude the roof and wallrocks surrounding the IRPC, and are most common in the Pearsoll Peak peridotite body. Zoned reaction halos of talc-tremolite-antigorite rimmed by actinolite are often

Figure 2-7. Photograph of massive hornblende diorite with dunite xenolith. Photograph taken of a river polished outcrop at zircon locality IR-3. The massive texture exhibited here is common of most exposures in the complex, with the exception of the layered rocks in the core region, and the highly strained rocks at the margins.

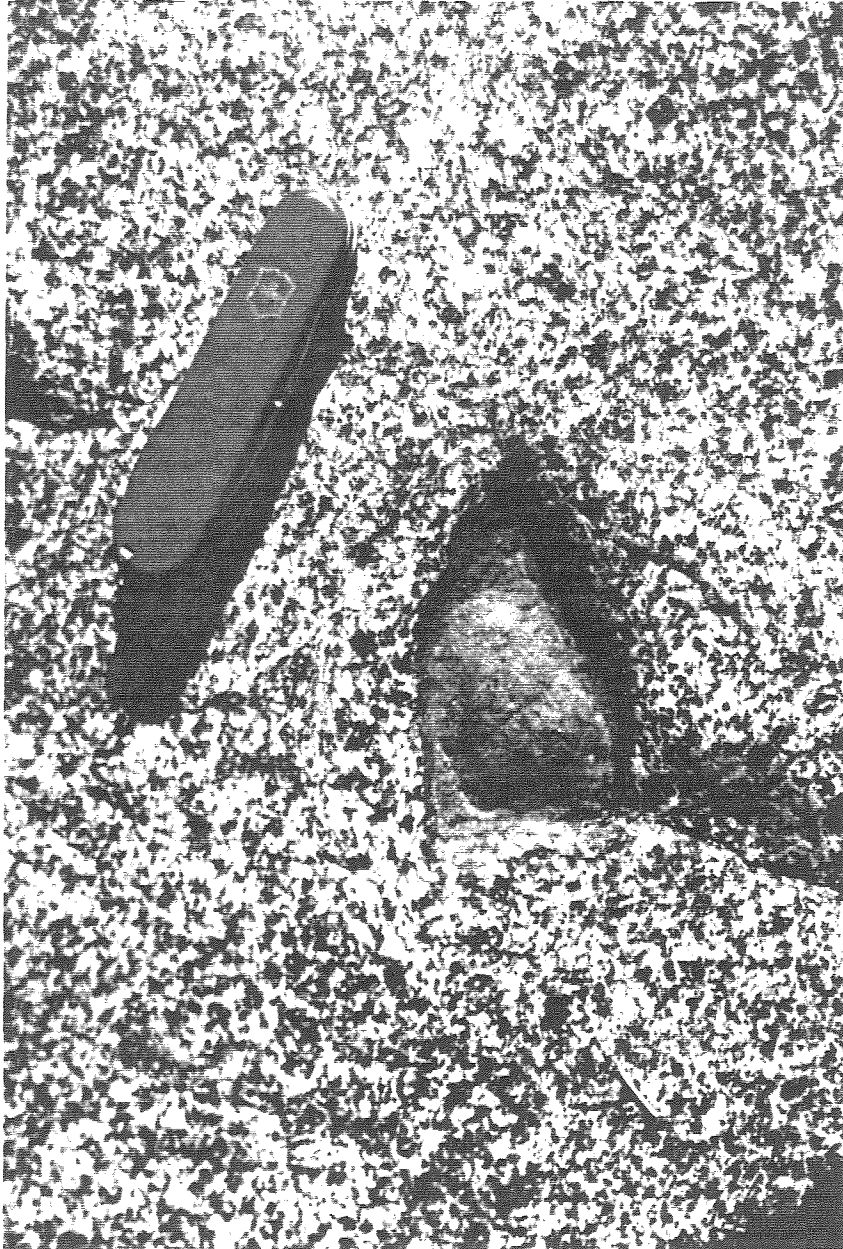


Figure 2-8. Photograph of an orbicular norite boulder at the confluence of Briggs Creek with the Illinois River. This lithology was never found in outcrop, however the restriction of boulders to the creeks draining York Butte suggest that this striking lithology occurs as part of the layered core region of the IRPC.

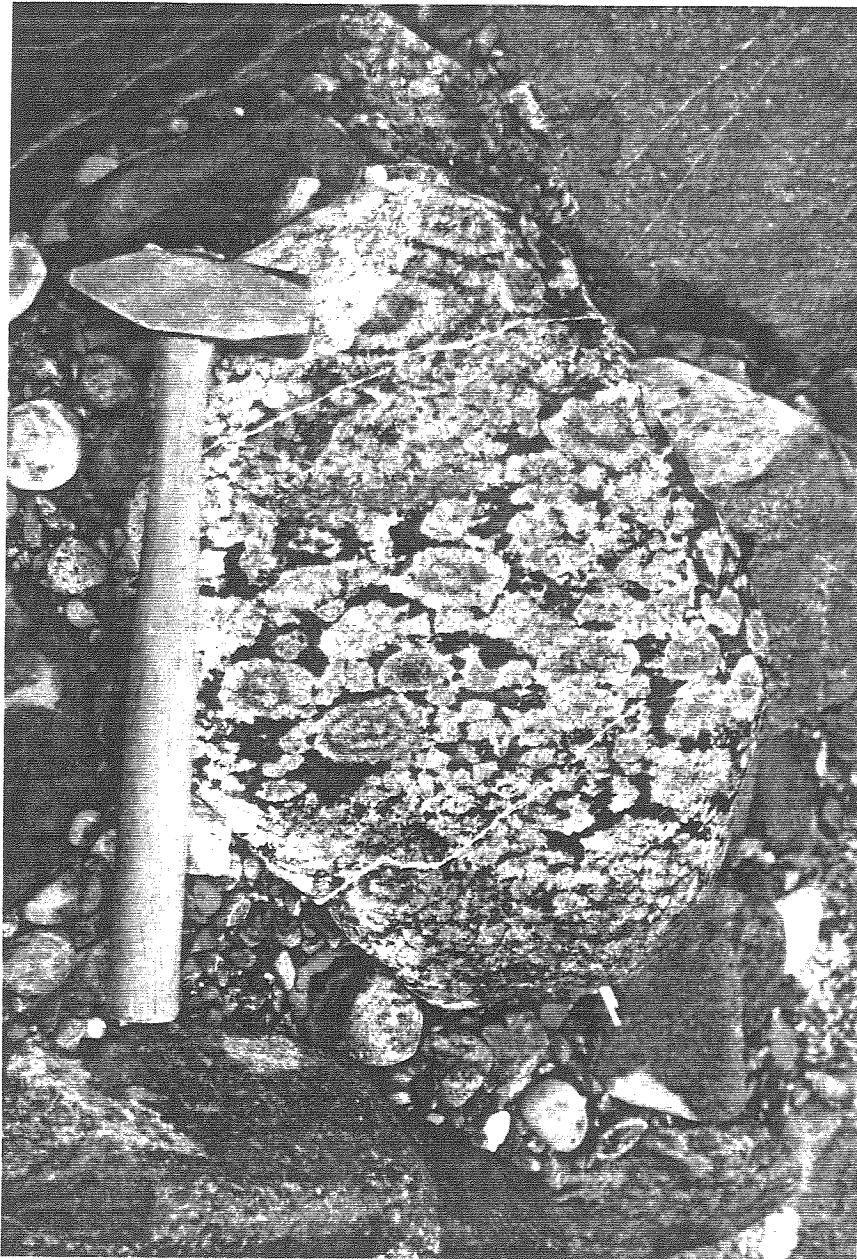


Table 2-4. Approximate range of modal mineral percentages for the primary lithologies of the Illinois River plutonic complex.

| Rock type | Quartz | Muscovite | Biotite | Plagioclase | Hornblende | Clinopyroxene | Orthopyroxene | Olivine | Accessory minerals | Secondary minerals |
|---|--------|-----------|-----------|---|------------------------------|---------------------------------------|------------------------|--------------------|--------------------------------|---|
| Troctolite (n=4) | 0% | 0% | 0% | 55-65% An 95-100 | 5-27% | 0% | <5% En 71 | 10-20% Fo 72-77 | Hercynite | Orthopyroxene Hornblende Serpentine |
| Norite (n=23) | <5% | 0% | 0% | 45-65% An 77-93 | 0-25% | <5% to 20% Fs 11-17 | <5% to 25% En 58-71 | 0% | Magnetite | Hornblende |
| Hornblende gabbro and diorite (n=28) | <10% | 0% | 0% to <2% | 40-75% An 70-95 core An 70-80 rim An 45-60 | 10-55%, but generally 40-55% | 5-40%, but generally <10% Fs 11-17 | 0% | 0% | Magnetite Apatite Zircon | Chlorite Hornblende Epidote |
| Biotite-hornblende quartz gabbro and diorite (n=12) | 10-25% | 0% | 5-10% | 45-60% core An 65-75 rim An 40-60 | 20-40% | <5% | 0% | 0% | Magnetite Apatite Zircon | Epidote Sericite Chlorite |
| Tonalite and trondhjemite (n=10) | 25-35% | 0-10% | 0-15% | 45-55% An 30-40 | 0-15% | 0% | 0% | 0% | Garnet Apatite Zircon | Epidote Sericite Chlorite |

Modal percentage values are tabulated from approximate modal estimates made for 25 samples during this study, plus more precise point counting results reported for six samples by Garcia (1982) and for 46 samples by Jorgenson (1970). Mineral compositions are taken from Jorgenson (1970). Anorthite content for plagioclase is given for nonzoned crystals unless otherwise noted.

Figure 2-9. Photograph of strongly lineated ($L \gg S$ tectonite), flaser gabbro; a texture typical of the marginal rocks of the IRPC.



Figure 2-10. Photograph of Pearsoll Peak from the air, view to the ENE (photo courtesy of Greg Harper). The distinct vegetation change on the west flank of Pearsoll Peak marks the boundary between the Pearsoll Peak peridotite body (harzburgite and dunite) and a tonalite-trondhjemite sill which forms the top of the Illinois River plutonic complex. Not obvious on the photograph is the relatively sharp boundary between the tonalite-trondhjemite sill and the underlying dioritic and gabbroic rocks which occurs approximately 100 m below the peridotite contact.



Figure 2-11. Photograph of a stream boulder in the upper Chetco River illustrating the comb structure characteristic of the hornblende gabbro pegmatoid sill exposed at the southern boundary of the IRPC.

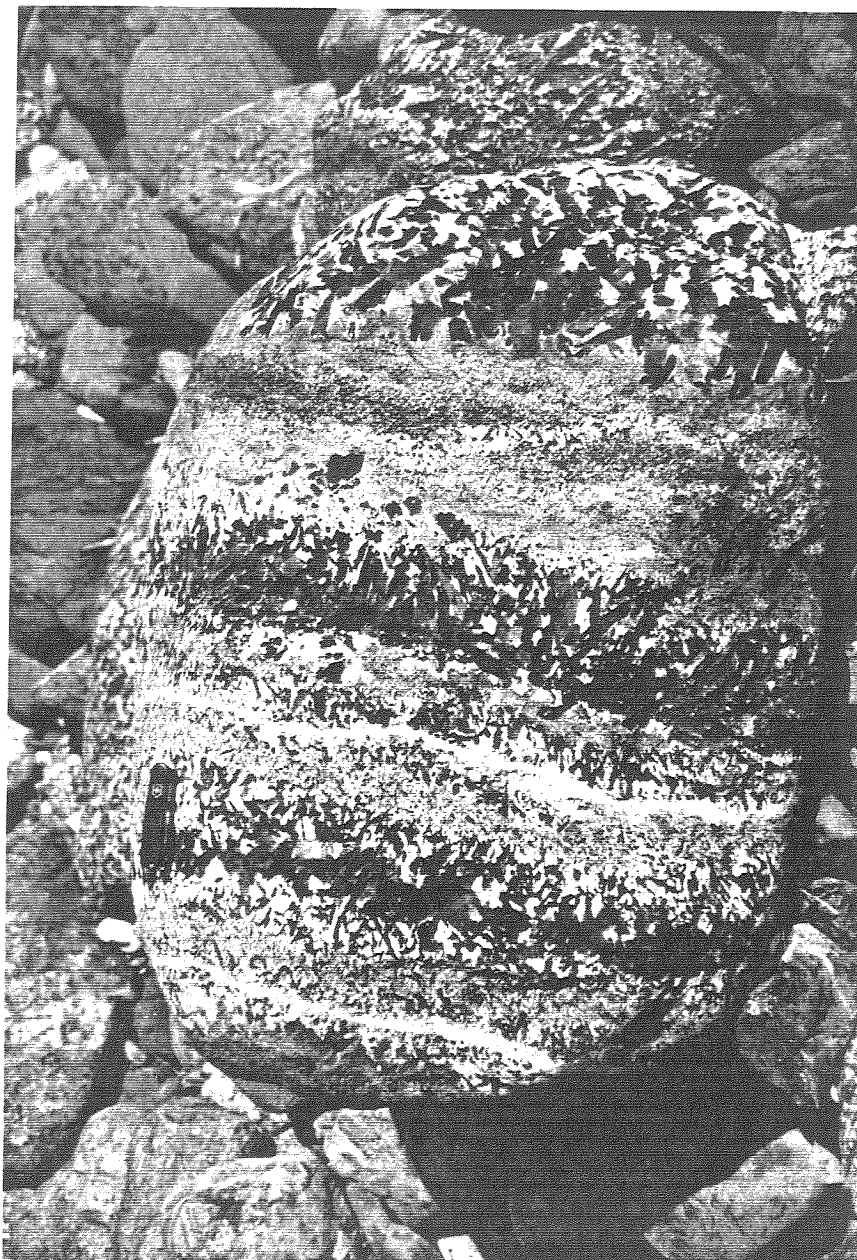
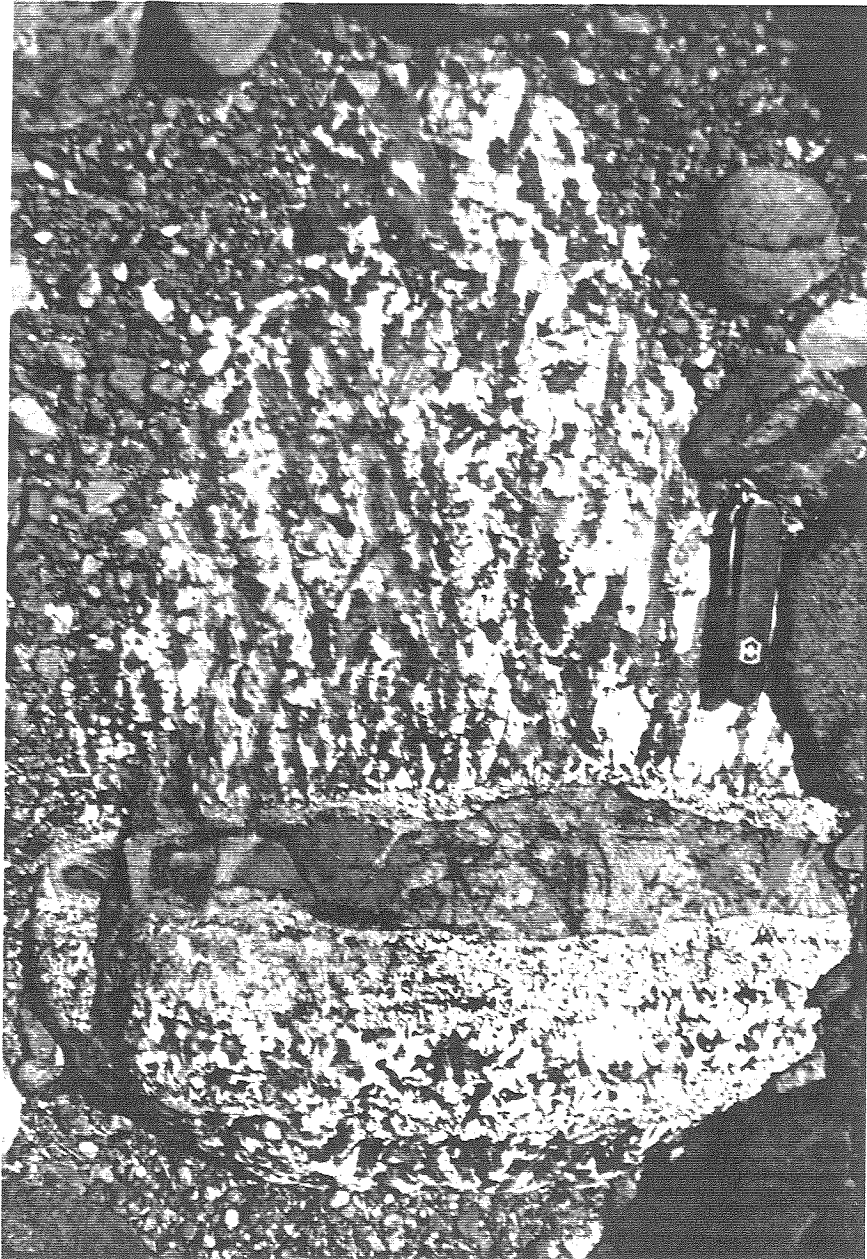


Figure 2-12. Photograph of a stream boulder in the upper Chetco River. The boulder consist of hornblende gabbro pegmatoid with a “screen” of harzburgite. Note the orientation of the hornblende megacrysts essentially perpendicular to the xenolith screen.



preserved bordering the dikes, and clearly indicate that the peridotite formed the wallrocks and roof rocks of the IRPC.

Age. U/Pb zircon apparent ages for the IRPC are 160 ± 0.5 Ma for the main phase gabbro, norite, and gabbro; and dikes which intrude the country rocks yield $\sim 160.5 \pm 0.5$ Ma; the late stage tonalite sill yields zircon apparent ages of 157-155 Ma (Table 2-1). $^{40}\text{Ar}/^{39}\text{Ar}$ hornblende plateau ages are ~ 156 -155 Ma (Table 2-2), in general agreement with previously reported ages by Dick (1976) and Hotz (1971).

Petrography. All rocks of the IRPC, with the exception of the late stage hornblende pegmatoid sill, have experienced some form of recrystallization that obscure the original igneous textures. The most common form of recrystallization texture is a static granoblastic texture with polygonal grain boundaries, sub-grain development, undulose extinction, and bent twinning lamellae (Figure 2-13). At the margins of the complex where the rocks are strongly lineated mylonites ($L \gg S$ tectonites, Figures 2-9 and 2-). IRPC rocks at the steeply inclined margins appear to have experienced distinctly higher degrees of strain than rocks which occur beneath the flat roof regions. Nonetheless, the mylonitic rocks exhibit the same types of post-metamorphic granoblastic textures as seen in the undeformed rocks.

The original igneous textures, indicated by relict and pseudomorph features, were cumulate in the core and xenomorphic- to hypidiomorphic-granular in the marginal facies of the complex. Compositional layering in the core rocks is defined by varying proportions and sizes of mafic and felsic minerals. Cumulus phases were ortho- and clinopyroxene, olivine, spinel, and anorthite with post-cumulus overgrowth by clinopyroxene, hornblende, and labradorite. Kelpytic rims are common surrounding spinel and olivine. Normally zoned plagioclase is rare in the cumulus rocks, but common in the marginal gabbros and diorites with typical cores of An_{70-95} and rims of An_{50-75} .

Country rocks of the plutonic complex. Amphibolite grade metamorphic mafic schist and gneiss to the west of the Chetco Pass fault form the wallrocks, roof rocks,

Figure 2-13. Photomicrographs of norite from the Illinois River plutonic complex; field of view ~3mm, upper photograph - plane polarized light, lower photograph - polarized light. Primary mineral phases include orthopyroxene, clinopyroxene, bytownite, and ilmenite. Note the polygonal grain boundaries and sub-grain development, particularly evident in polarized light.

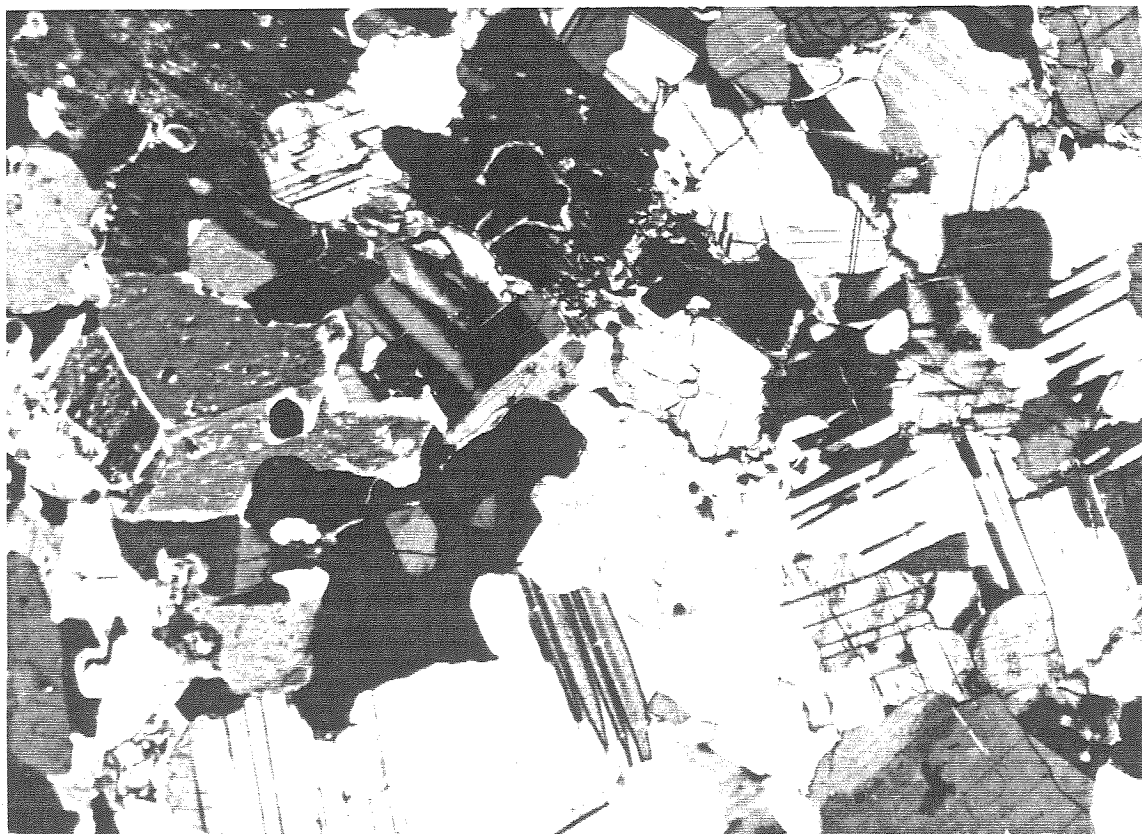
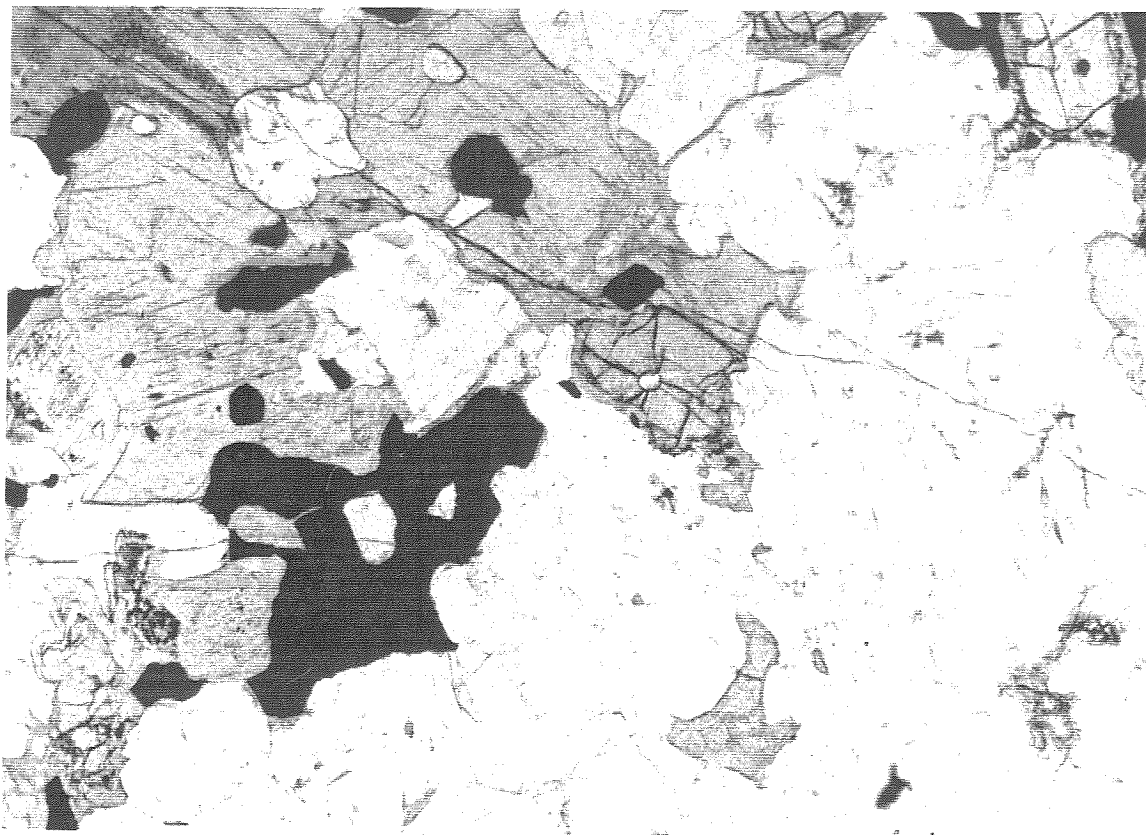


Figure 2-14. Photomicrograph of norite from the Illinois River plutonic complex; field of view ~3mm, polarized light. Note the bent plagioclase twinning lamellae.

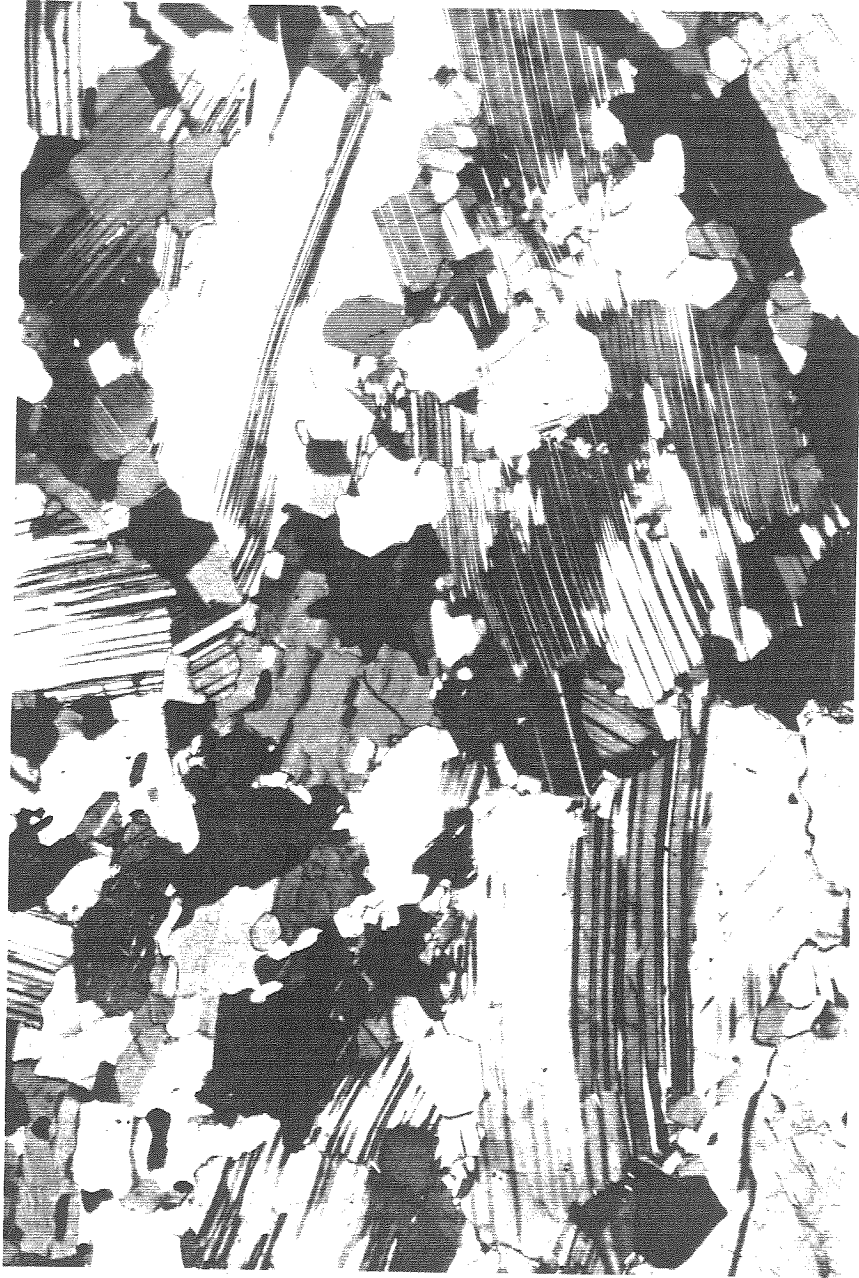
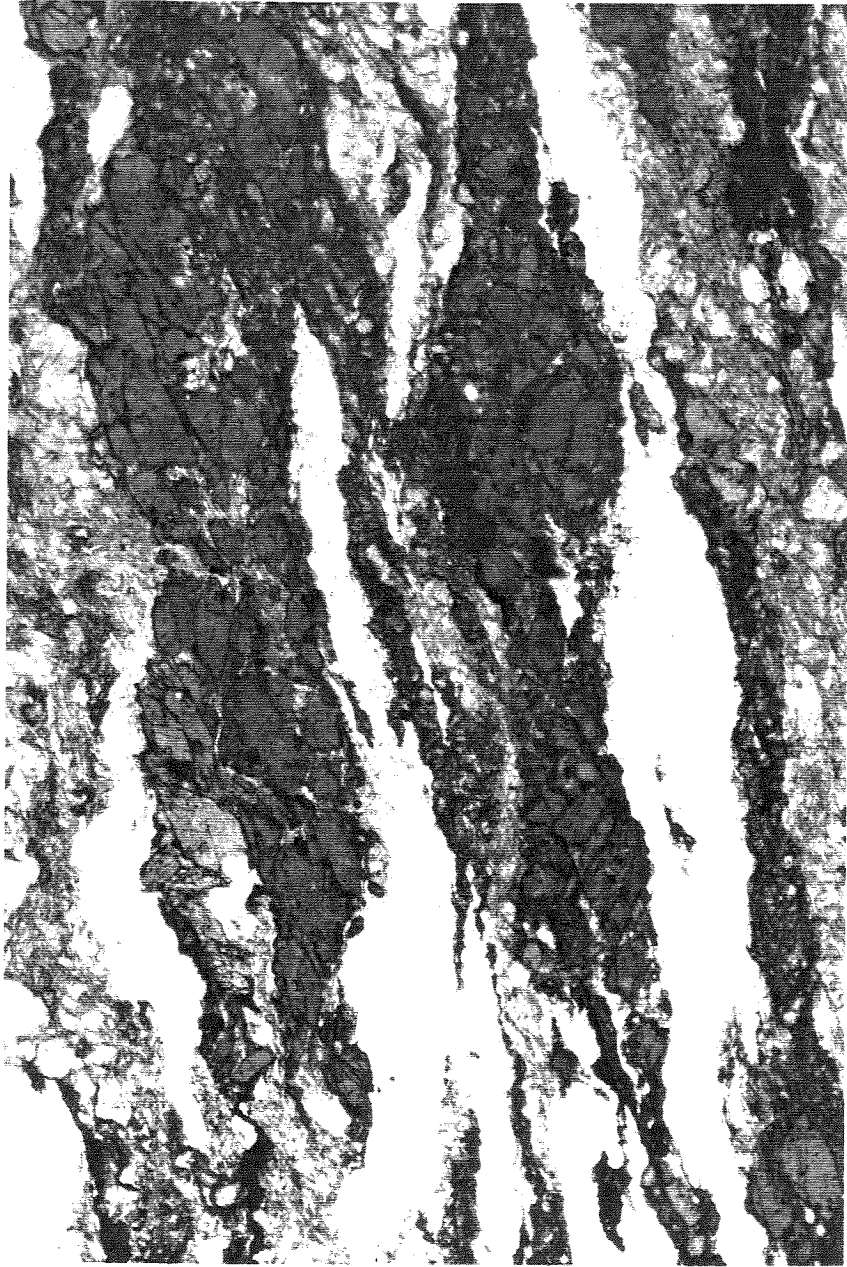


Figure 2-15. Photomicrograph of a mylonitic hornblende quartz diorite sample from the Illinois River plutonic complex; field of view ~3mm, polarized light. The principal mineral phases include hornblende, plagioclase, epidote, and quartz. The sample was collected from immediately beneath the contact with the Pearsoll Peak peridotite body. Section is oriented parallel to the mineral elongation lineation. Sense of shear is right lateral in the photomicrograph which equates to top to the northeast in the field.



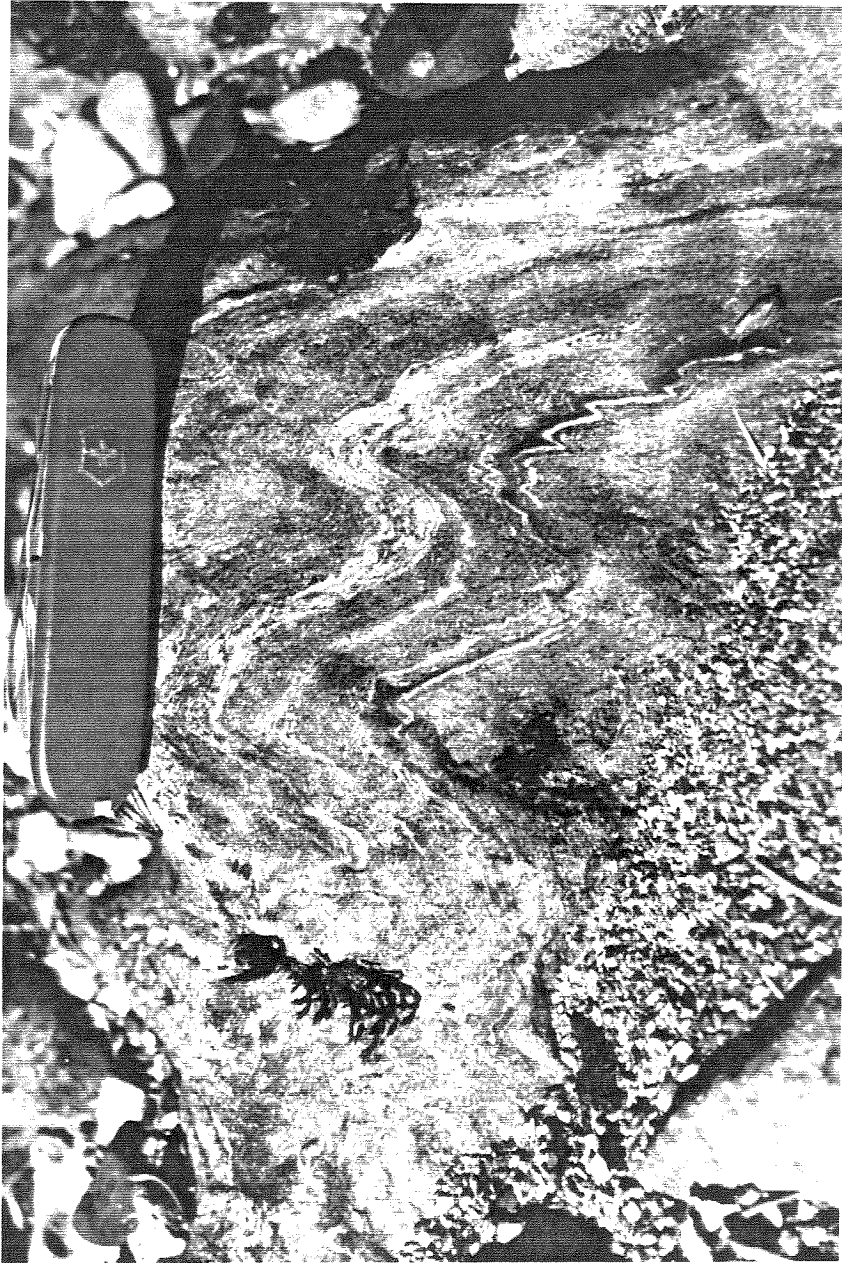
and screen-like septa of the IRPC plutonic complex. As such, they are interpreted to have been deformed and metamorphosed in a regional thermal welt surrounding the plutonic complex.

These rocks consist primarily of infolded masses of metaperidotite and amphibolite known as the Pearsoll Peak and Chrome Ridge peridotite bodies (Ramp, 1961), and the Briggs Creek amphibolite (BCA; Coleman and Lanphere, 1991: Plates 1, 6, and 9). Other amphibolite bodies occur in the southwestern corner of the study area in the footwall of the Madstone Cabin thrust (Loney and Himmelburg, 1977; Harper et al., 1995, in press; Plates 1 and 2). The hanging wall of the Madstone Cabin thrust consists of Josephine peridotite that was underthrust by the IRPC and its wallrocks during Nevadan deformation and elongation of the plutonic complex (see discussion of the Madstone Cabin thrust below).

Previously reported ages from amphibolites in the region include K/Ar mineral ages that range from 155 to 131 Ma (Garcia, 1979, 1982; Coleman and Lanphere, 1971) and an $^{40}\text{Ar}/^{39}\text{Ar}$ hornblende age of 156.4 ± 0.9 Ma from the BCA reported in Hacker et al. (1994). Several 190-200 Ma K/Ar mineral ages reported by Dick (1976) are considered anomalous and probably result from excess Argon incorporated in the hornblende. However, it is interesting to reconsider these ages in light of the discovery of Triassic and Early Jurassic rocks of the Onion Camp complex that occur nearby. Two additional BCA samples analyzed during this study yielded 157.9 ± 0.5 and 156.3 ± 0.5 Ma Ar/Ar hornblende apparent ages (Hacker and Yule, unpublished data, 1994). These ages overlap with the cooling ages obtained from the IRPC (Table 2-2). The Pearsoll Peak and Chrome Ridge peridotite bodies are considered fragments of the Josephine peridotite based on their similar field appearance and a lack of evidence for interpreting parts of these bodies with the Onion Camp serpentinite and serpentinitized peridotite (discussed below).

The orientation of structural features in the country rocks parallel the structures observed for the IRPC; e.g., variable foliations with consistently NE-SW trending mineral and intersection lineations and fold axes (Figure 2-16). An exception occurs in rocks

Figure 2-16. Photograph of folded gneissic banding typical of amphibolite in the Briggs Creek and Chetco Pead regions (Plates 1, 2, 6, and 9).



situated immediately beneath the Madstone Cabin fault where late metamorphic northeast vergent structures are evident. These structures overprint the northeast trending structures and are interpreted to be related to late motion across the fault (Loney and Himmelburg, 1977; Harper et al., 1995, in press). An important difference between structures in the country rocks and those in the IRPC is that the country rocks exhibit extremely high degrees of flattening, rather than elongation strain. Characteristic structural features include gneissic banding and schistosity defined by highly flattened mineral grains and multiple generations of roughly parallel tight to isoclinal folds. It is also important to note that the amphibolites exhibit a much higher degree of strain than the metaperidotite, though the latter has shared in the deformation.

The characteristic prograde metamorphic mineral assemblages are olivine, tremolite, talc, magnetite, and magnesian chlorite in metaperidotite, hornblende, oligoclase, epidote, quartz, garnet, titanite, and Fe oxide in metabasites, and quartz, biotite, muscovite, and Mn garnet in quartzites (metachert), and are typical of amphibolite facies metamorphic grade (Robinson and others, 1982). Retrograde mineral assemblages are mostly characteristic of the greenschist facies, e.g., albite, quartz, actinolite, epidote, and chlorite.

Likely protolith materials for the country rocks of the IRPC are peridotite, mafic volcanic and intrusive rocks, and impure chert or siliceous argillite. These progenitor materials are consistent with the interpretation of Coleman and Lanphere (1991) who, based on the geochemistry and metamorphic age of the Briggs Creek amphibolite, infer that the BCA represents a high-grade metamorphosed ophiolite, presumably the Josephine ophiolite. However, distinctive lithologic and geochemical features of the BCA and other amphibolites in the region suggest that rocks of the Rattlesnake Creek terrane (RCT) may have provided protolith materials. For example, rhodonite nodules, which are a scarce but distinctive lithology in the RCT, occur in scattered outcrops beneath the Madstone Cabin thrust fault (near Chetco Peak) and in the BCA (Len Ramp, personal communication). Also, amphibolite grade metabasalts of the BCA share distinctive geochemical trends with

greenschists of the RCT (Wright and Wild, 1994; Harper et al., 1995, in press). Furthermore, the occurrence of RCT equivalent rocks contained within the WJB, herein termed the Onion Camp complex, also contain amphibolite bodies that bear a striking resemblance to the BCA and other amphibolite country rocks of the IRPC.

If the IRPC country rocks indeed consist of composite RCT and Josephine ophiolite crust and mantle lithosphere, then a composite terrane identical to the material that occurs beneath the Rogue-Galice overlap sequence would provide suitable progenitor materials. In this scenario, the region to the west of the Chetco Pass fault would represent the high temperature thermal “welt” that formed surrounding the Illinois River arc plutonic complex. If so, the country rocks of the IRPC and the substratum for the overlap sequence would consist of the same lithologies, only at different metamorphic grades.

New Map Units

The following section describes the geologic relations that provide the basis for designating two additional distinct petrotectonic units of the WJB. These new map units, herein informally named the Onion Camp complex (OCC) and the Fiddler Mountain complex, were previously included with the Rogue Formation and the Josephine peridotite. Rocks of the OCC are correlated with the Rattlesnake Creek terrane (RCT) of the western Paleozoic and Triassic belt (WTrPz belt). The Fiddler Mountain olistostrome complex lithologies share strikingly similar geologic features with other olistostromal and ophiolite breccia deposits in the region that are also associated with the Josephine marginal ocean basin.

Fiddler Mountain olistostrome complex

Overview and general distribution. The Fiddler Mountain olistostrome complex is named for the roadcut exposures along the Babyfoot Lake-Onion Camp U.S. Forest Service access road and for natural exposures on the ridgelines and flanks of Fiddler Mountain, located in the northwestern 1/4 of the Josephine Mountain 7.5' topographic

quadrangle (Plate 3). Fiddler Mountain itself also coincides with the greatest width of the unit (Plate 1). Other widely scattered exposures of Fiddler Mountain olistostrome deposits occur at a scale too small to show on Figure 2-2, but are included on the 7.5' scale maps in the appendix (Plates 5, 6, and 11).

Internal stratigraphic layering parallels the general outcrop pattern of the main body near Fiddler Mountain and indicates that the olistostrome complex occurs as a synclinorium with a near vertical to steeply overturned eastern limb and a moderately upright western limb. A bedded chert horizon exposed on the ridgelines immediately to the north of Fiddler Mountain defines a synclinal fold nose in the inferred hinge region of the olistostrome complex (Plate 3). The greatest width of the outcrop belt at Fiddler Mountain is a function of the topography, while the northern and southern terminations are structurally controlled. The northern termination is controlled by a west-northwest trending anticlinal cross structure centered approximately on Squaw Mountain, and the southern termination is controlled by the overall gentle northeasterly plunge of the synclinoria.

Lithologies. The Fiddler Mountain olistostrome deposits are mostly sedimentary deposits, not volcanogenic as originally believed, and consist primarily of poorly sorted, clast and matrix supported heterolithologic megabreccia, breccia, conglomeratic grit, lithic wacke, and lithic arenite. Impure chert and tuffaceous argillite are secondary. The deposits are laterally discontinuous, always occur at the base of the overlapping sedimentary and volcanogenic sequence (the Rogue and Galice Formations), and are deposited on a variable substratum comprised of both Onion Camp complex and Josephine ophiolite sequence lithologies.

Detrital rocks. The breccias, conglomerates, and sandstones contain a wide variety of distinctive clast lithologies that are generally ophiolitic in character (Figures 2-17, and 2-18). The dominant clast lithologies are aphyric to phyric green to gray metabasalt, fine- to medium- grained metadiabase, and medium- to coarse-grained gabbro. Secondary clast lithologies include chert, argillite, serpentinite, and serpentinitized peridotite

Figure 2-17. Photograph of a slabbed sample of heterolithologic conglomerate, a typical constituent of the Fiddler Mountain breccia. The clasts in this examples consist entirely of gabbro, diabase, and greenstone.

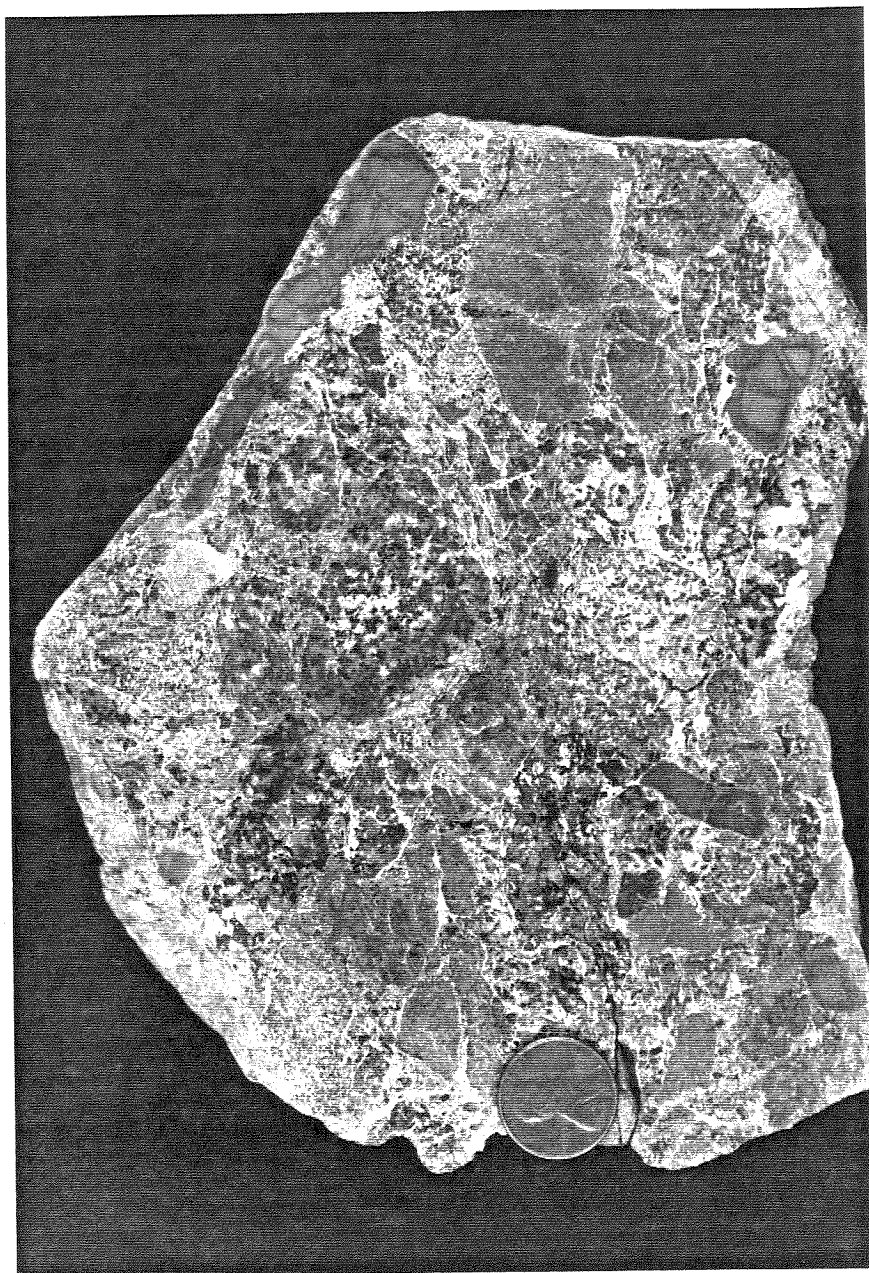
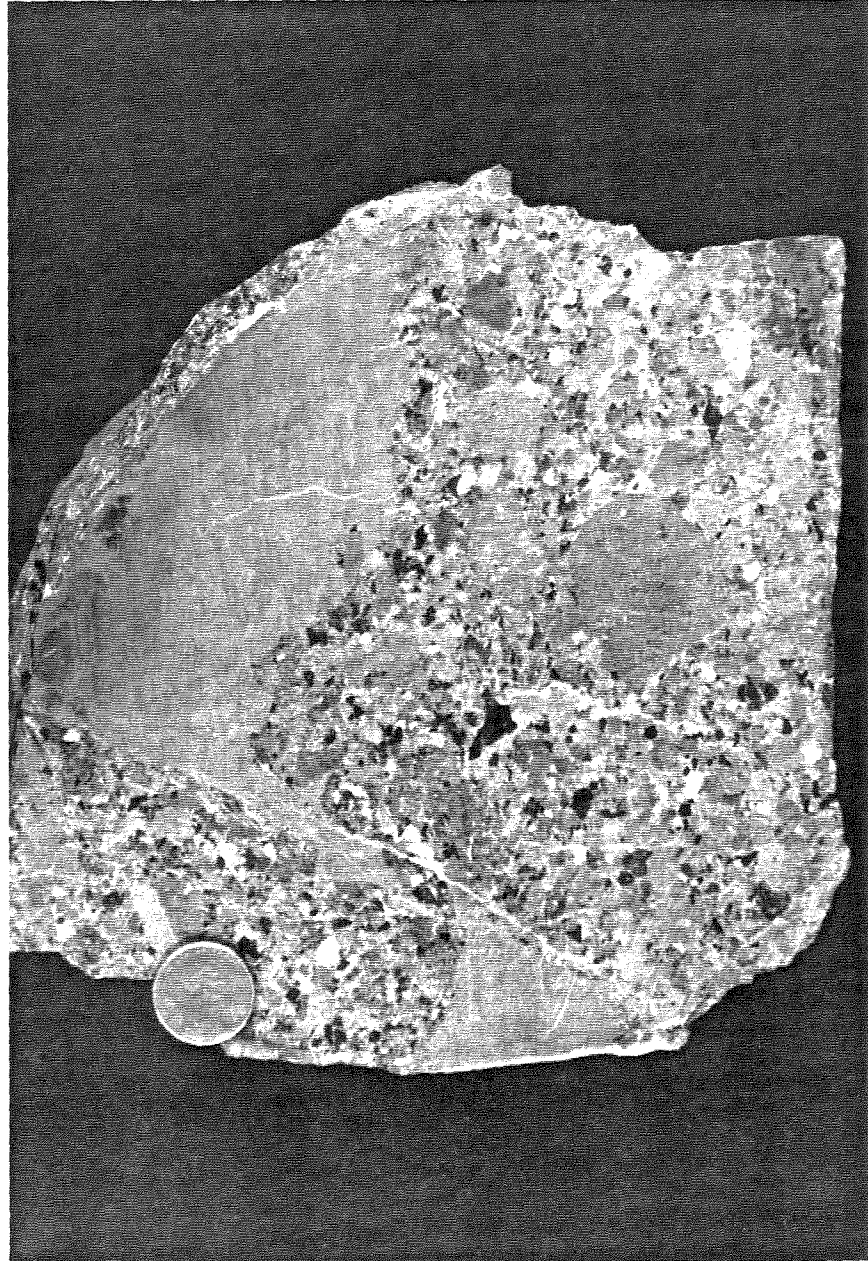


Figure 2-18. Photograph of heterolithologic conglomerate with a medium-grained silty sand interlayer. Clast lithologies in this example primarily include diabase, greenstone, chert, with secondary chert clasts (small white clasts throughout), and serpentinite clasts (e.g., black clast near the center of the photo). Note the offset of the silty sand layer. Where observed in outcrop, these small faults consistently indicate normal displacements.



and rare occurrences of quartzite, chlorite schist, phyllonite, and amphibolite. In cases where the olistostromal rocks are deposited upon serpentinized peridotite, the breccias contain entirely serpentinite and serpentinized peridotite clasts (Figure 2-6). A rare but distinctive opicalcite breccia, exposed in a roadcut near Store Gulch, consists of matrix supported serpentine clasts in a hematitic and calcareous (micritic) serpentine silt and mud matrix. The matrix materials in general consist of clay- to angular sand-size and coarser grains derived from the same material as the clasts.

The clast lithologies in essence represent a collection of most, if not all, lithologies that comprise the Josephine ophiolite and the Onion Camp complex, and clearly were derived from these basement materials. However, the overwhelming majority of clast lithologies are ophiolitic in character suggesting that the Josephine ophiolite was the primary source terrane.

Distinctive deformation and alteration textures exhibited by the clasts also match those of the host lithologies. For example, many clasts display cataclastic shears and textures, vein fillings, and static greenschist grade, hydrothermal alteration commonly observed in the fragmented and altered bedrock exposures of the Josephine ophiolite and in the mafic intrusive complex of the Onion Camp complex.

Grain sizes in the detrital rocks range from silt-sized to >100 meters, but most commonly contain boulder and smaller sized clasts with the most common clast size approximately 1-10 centimeters. Matrix materials in these deposits range from silt size on up to centimeter size depending on the coarseness of the clasts. Matrix to clast ratios are highly variable but are typically less than 10%. Pebble-sized and coarser deposits are typically massive but stratification is common in the sands and conglomerates. The layering is often cut by small offset faults and cataclastic shear zones with both normal displacements apparent most often (Figure 2-18).

Megabreccia. “Megabreccia” deposits comprise roughly half of the olistostrome complex at Fiddler Mountain. The term megabreccia is used here to describe the part of the

Fiddler Mountain olistostrome complex where huge blocks (some >100 meters in dimension) occur surrounded by finer-grained deposits of the complex, i.e., boulder breccia, conglomerate, argillite, and chert. Because the typical outcrop is smaller than the apparent megabreccia blocks, one might mistakenly interpret the unit as a heterogeneous intrusive complex or a tectonic melange zone if not for the occurrence boulder and smaller clast size breccia deposits. Altered and fragmented gabbro and diabase are the most common megabreccia clast lithology.

Pelagic sediments. Platy argillite and white to gray bedded chert layers comprise <10% of the complex and generally occur as distinct bedded horizons within the complex. These strata probably accumulated during pelagic depositional periods which separated episodes of catastrophic deposition of the megabreccia and breccia deposits. Radiolarian chert yield a poorly constrained Late Jurassic (possible Kimmeridgian?) age for these deposits (Silk and Yule, unpublished data, 1992). The Late Jurassic age combined with the stratigraphic position of these deposits at the base of the WJB overlap sequence suggests that the pelagic rocks of the olistostrome complex are correlative with the similar pelagic and hemipelagic sequence of the basal Galice Formation.

Regional correlations. Deposits similar to those of the Fiddler Mountain olistostrome complex are described from various localities throughout the Klamath Mountains and California Coast Ranges where they generally occur as deposits at the base of the Galice Formation and the Great Valley sedimentary overlap sequences (e.g., the Lems Ridge olistostrome, Ohr, 1987; the Devil's Elbow ophiolite section, Wyld and Wright, 1988; Coast Range ophiolite near Paskenta, CA, Blake and others, 1987; the Preston Peak ophiolite, Snoke, 1977; and in the Bolan Lake area, Donato et al., in review). Like the Fiddler Mountain olistostrome, these deposits are closely associated with the RCT and the Josephine ophiolite. The widespread occurrence of these deposits suggests that the Josephine and Coast Range marginal ocean basins formed when an older oceanic arc complex rifted apart. These basins, prior to their overlap by Galice Formation and Great

Valley sequence strata, must have contained localized areas of considerable topographic relief, probably as a result of extensional, transfer, and/or transform faulting. This depositional environment is consistent with the slow-spreading interpretation for the Josephine ocean basin dominated by faulting (Alexander and Harper, 1992).

Onion Camp complex

Overview. The Onion Camp complex (OCC) is named herein for an association of Late Triassic to Early Jurassic rocks that were first recognized near Onion Camp located in the northwestern corner of the Fiddler Mountain 7.5' topographic quadrangle, Josephine County, Oregon. The rocks primarily occur in an elongate NE-SW belt 3-5 kilometers wide and approximately 40 km long that extends from the Canyon Peak region west of Cave Junction, Oregon, northward to the Hellgate Canyon of the Rogue River (Plate 1). Rich soils develop on the mafic rocks of the complex and support a lush flora, particularly in bogs at higher elevations that develop in the headscarps of landslides. Wild Onions (and certain illegal crops) flourish in these settings, hence the names Onion Camp and Onion Mountain. Consequently, "Onion Camp" provided a logical choice for a name to distinguish these rocks from the surrounding units. Other exposures of the OCC occur in a small isolated patch near the center of the study area along the Chetco Pass Fault and in a narrow sliver along the western margin of the Illinois River plutonic complex (Plates 1, 6, and 8).

Rocks of the OCC were formerly considered part of the Rogue Formation by Wells and Walker (1953). Subsequent workers noted differences between the type Rogue Formation rocks and the metavolcanic rocks in the region of Onion Camp, but still considered them part of the Rogue Formation rather than part of a lithologically distant unit (e.g., Wise, 1969; Dick, 1976; Page and others, 1981; Ramp and others, 1977, 1979, Ramp, 1984). The first, hard evidence to suggest that a distinctly different unit occurs in

the region came from Roure and DeWever (1983) who reported a Triassic age from a single chert sample collected near Onion Camp.

General features. OCC rocks are generally the most poorly exposed lithologies in the map area. The best exposures occur along the Illinois and Rogue Rivers with up to 500 meters of continuous outcrop in places. Other relatively large scale exposures occur in road gravel quarries hosted in metabasaltic rocks near Onion Camp and north of Onion Mountain. However, most outcrops of OCC rocks occur in degraded roadcuts and along ridgelines.

The complex consists primarily of mafic metavolcanic rocks, largely recrystallized chert, and argillaceous metasediments, a heterogeneous mafic intrusive complex, and serpentized harzburgite and dunite. Less common lithologies include hornblende schist, amphibolite gneiss, garnet-mica quartzite, and lenses and variably sheared serpentinite. Of the crustal rocks in the complex, metavolcanic and metasedimentary rocks comprise >50% of the exposures, and cross-cutting intrusive rocks of the mafic complex, about one third of the exposures. A small proportion of the OCC consists of amphibolitic rocks that are most common near Squaw Mountain in the central part of the complex.

Several episodes of metamorphism and deformation affected the rocks of OCC. Peak regional metamorphic conditions of greenschist to amphibolite grade were achieved during the earliest deformational episode. Subsequent deformational episodes occurred at lower temperature conditions and include: 1) an intermediate episode characterized by brittle fragmentation and hydrothermal alteration, and 2) a latest episode characterized by regional lowest greenschist and sub-greenschist facies metamorphism and deformation.

Hillslopes underlain by rocks of the OCC are among the most rugged and densely vegetated in the region. The limited exposures in combination with their complex metamorphic and deformational history conceal most original igneous and sedimentary features and make it difficult, if not impossible, to distinguish the original stratigraphic sequence. Despite the complexities of the complex, the following rock associations are

clear. The metavolcanic and metasedimentary rocks generally occur in two distinct associations. One association consists primarily of metabasalt, sills, and dikes that exhibit MORB geochemical signatures, and lenses and thin intercalations of red chert, and tuffaceous metasediments. The second association includes relatively thick sequences of interbedded impure chert, tuffaceous siltstone and argillite. To the south of Squaw Mountain (Plate 6), the metavolcanic rocks generally predominate to the west of the Fiddler Mountain olistostromal deposits and metasedimentary rocks predominate to the east. No such generalized exposure patterns were noticed to the north of Squaw Mountain.

Both the metabasaltic and metasediment-rich associations are crosscut by a heterogeneous mafic to intermediate intrusive complex, though the intrusive rocks are most commonly associated with predominantly metavolcanic rocks sequences. Belts of amphibolite gneiss, hornblende schist, and impure quartzite are often “sandwiched” between serpentized mantle peridotite and crustal rocks of the OCC. A relatively sharp metamorphic gradient occurs between the amphibolite to greenschist grade rocks and suggests that greenschistic rocks served as the protolith for the amphibolitic rocks. The geologic relations define a crude, highly disrupted ophiolite stratigraphy for OCC with a) serpentized mantle peridotite beneath b) a primarily mafic crustal sequence consisting of amphibolite grade metamorphosed materials that are overlain with a sharp metamorphic gradient by c) greenschist grade MORB metavolcanic rocks and interlayered (and perhaps overlying) metasedimentary rocks.

Metavolcanic rocks. Most of the metavolcanic rocks in the OCC comprise a poorly exposed heterogeneous sequence of faintly to highly strained greenstone, phyllonite, and phyllonite mylonite. In all cases, the metavolcanic rocks break along a weakly to well developed rock cleavage oriented parallel to the regional foliation. The rocks range in color from various shades of green to dark and light gray. They are completely recrystallized to greenschist facies and contain epidote+ chlorite+ albite+ calcite± actinolite± quartz with secondary Fe-oxide and pyrite. Spene is a ubiquitous

accessory mineral. Abundant prehnite, quartz+prehnite and quartz+calcite veins cut all exposures. Where distinguishing features are present, the predominant lithologies are flows with subordinate dikes and sills, lava breccia, and mafic tuff and tuff-breccia. Altered clasts in the breccias were plag>cpx-phyric based on metamorphic mineral pseudomorphs. Some exposures display pillow structures and amygdules and vesicles are common in many of the specimens collected (Figure 2-19). Chilled dike and sill margins are present at a few localities. The fragmental volcanic rocks contain moderately to highly flattened and altered lithic clasts and lapilli. Some of the best exposures occur in road gravel quarries near Onion Camp and Onion Mountain, and in bold outcrops surrounding Babyfoot Lake, along the Illinois River between Snailback and Sixmile Creeks, and in the Hellgate Canyon section of the Rogue River (Plates 1, 3, 6, 10, and 11).

Red chert. Roure and DeWever (1983) report a Triassic age for a chert sample interbedded with Onion Camp metabasalt collected near Onion Camp. In order to confirm the Triassic age determination and to strengthen the case for older rocks in the western Jurassic belt, a chert locality near Onion Camp (Figure 2-20) was collected on two separate occasions and processed for radiolaria by two independent labs. The red chert collected for this study was taken from a well-bedded red chert outcrop exposed in a logging roadcut located approximately 0.5 km to the northeast of Onion Camp and matches the description given by Roure (personal communication) for the appearance and general location of the chert reported in the 1983 study. Though the hillslopes surrounding Onion Camp contain numerous small outcrops of red chert plus innumerable fragments of loose chert in float, it is virtually certain that the locality shown in Figure 2-20 is the same locality that reported by Roure and DeWever (1983).

The age determinations for chert samples from the Onion Camp chert locality collected for this study differ in detail from those of Roure and DeWever (1983), but in general they support a pre-Middle Jurassic age for chert of the Onion Camp complex (see Appendix 1). One sample yielded mostly amorphous forms with the exception of a

Figure 2-19. Photograph of river polished exposure of pillow lavas of the Onion Camp complex, station EDM-83 located on the banks of the Illinois River. Two samples collected from this outcrop were analyzed for major and trace element abundances (Table 2-3). One sample was analyzed for REE abundances which show a pronounce LREE pattern typical of ocean island or within plate basalts.

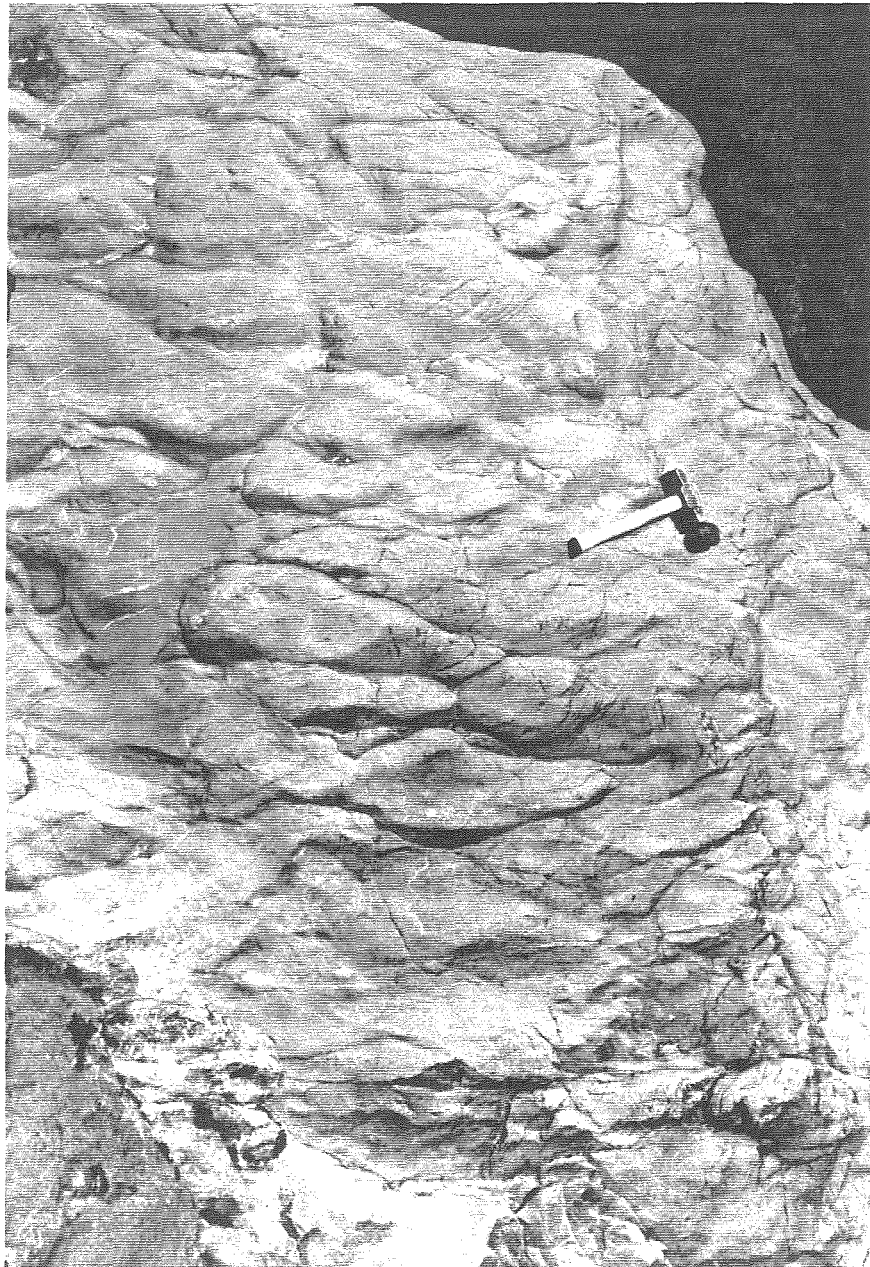


Figure 2-20. Photograph of Triassic chert locality near Onion Camp. Bedding is oriented at ~N20E, 39SE, inclined toward the left in the photo. Numerous chert exposures occur in this region closely associated with massive and pillow metabasalt.



possible Late Triassic radiolarian form (*Canoptum* sp., M. Silk, 1992, personal communication). Two additional samples collected from the same locality yielded scarce Jurassic with no Triassic forms (C. Blome, personal communication). Though the new radiolarian data do not in themselves confirm the report of Roure and DeWever (1983), the Late Triassic to Jurassic age range is consistent with ages reported from cherts collected from throughout the western Paleozoic and Triassic belt (Irwin and others, 1982).

Metasedimentary rocks. The metasedimentary rocks occur as isolated lenses and intercalations within the metavolcanic rocks and as more continuous, thick sequences along poorly defined elongate belts generally confined to the eastern part of the complex (e.g., a belt extending southwest from near Squaw Mountain, another belt extending south from near Onion Mountain to near Four Corners, and one more belt centered on Buckhorn Mountain in the northern part of the terrane; Plates 1, 3, 4, 6, and 10). They are characterized by an imperfect platy cleavage and include impure chert, argillite, and tuffaceous siltstone and rare poly lithologic sandstone, conglomerate, and conglomerate grit. The metasedimentary rocks are well indurated, highly strained, and structurally interdigitated (Figure 2-21). Original stratification is rarely apparent, but when found it is generally parallel or nearly parallel to the cleavage. Flattening strains of >20:1 are locally indicated by line length to width ratios measured where original stratification occurs oblique to the cleavage (Ramsay and Huber, 1983). Boudinage of chert and silicic argillite layers is common and also indicates relatively high degrees of flattening strain.

Exposures of relatively undeformed, banded red chert similar to the "Onion Camp locality" are most commonly associated with metabasalts and are locally abundant throughout the complex, particularly in the vicinity of Onion Camp and Babyfoot Lake, and between Four Corners and Onion Mountain. Red, white and gray chert and cherty layers are equally common in the thicker metasedimentary sections, but are highly strained and often thoroughly recrystallized. Relict multigrain ovoids, probably recrystallized radiolaria, are common in the less deformed boudins. Siliceous argillites consist essentially of quartz,

Figure 2-21. Photograph of well foliated metasedimentary rocks of the Onion Camp complex in a river polished exposure along the Illinois River. Lithologies include gray siliceous argillite, light green tuffaceous argillite, and red to maroon chert. Note the boudin of chert above the lens cap.



phyllosilicates, and opaque oxides with secondary carbonate, albite, pyrite, and accessory minerals including zircon, apatite, and sphene. Tuffaceous layers are typically green and contain chlorite, minor epidote, and albite porphyroclasts.

A distinctive but relatively scarce polymictic conglomeratic grit occurs as meter to several meter thick interbeds in predominantly wacke, siltstone, and argillite sequences. Poorly to moderately sorted sand grains and pebble to cobble-sized rock clasts are angular to sub-angular. The coarser-grained conglomerates are generally matrix supported. Clast lithologies in the sandstones and conglomerates are diverse and include wacke, siltstone, siliceous argillite, recrystallized chert (with relict radiolaria), sugary quartzite, monocrystalline quartz, mafic volcanic rocks (with porphyritic, intergranular, and spherulitic textures), and recrystallized limestone. Siliceous sediment and chert are by far the most abundant clast lithologies. Volcanic clasts, though present, never occur in greater percentage than sedimentary clast fragments. The conglomeratic grit is therefore distinct from other polymict deposits in the region that contain mostly volcanic fragments, e.g., breccias and conglomerates of the Fiddler Mountain olistostromal complex and the Rogue Formation. In addition the conglomeratic grit is very similar to deposits in the Bear Basin Road sequence of Snoke (1977) and provides a lithologic link between rocks of the Onion Camp terrane and the Rattlesnake Creek terrane.

Mafic intrusive suite. A heterogeneous assemblage of altered mafic intrusive rocks occur in close association with the metavolcanic and metasedimentary rocks of the OCC. The mafic intrusive rocks usually occur as relatively small equidimensional to elongate bodies that cover areas ranging from less than 1 km² to approximately 10 km² (below the resolution of Plate 1, some of the larger bodies are shown on Plate 3). In total they comprise approximately one quarter to one third of the exposures in the OCC excluding the amphibolite and ultramafic rocks. In outcrop the rocks are massive, nonschistose, and extremely tough. The distinct regional foliation that occurs in all other greenschist grade metamorphosed rocks of the OCC is absent in mafic intrusive rocks

except for cataclastic shear bands interpreted to represent reactivated hydrofractures and veins (see below).

The mafic intrusive suite consists predominantly of metadiabase and aphanitic greenstone with subordinate altered gabbro, diorite, and rare plagiogranite distinguished by their relict igneous textures (aphanitic, aphanitic-porphyritic, sub-ophitic, hypidiomorphic granular) and the relative abundances of feldspar to mafic mineral pseudomorphs. Metamorphism and alteration of these rocks is characterized by a static, ubiquitous greenschist facies and sub-greenschist facies hydrothermal alteration. The primary mineral constituents in mafic rocks are actinolitic amphibole, altered plagioclase, epidote, chlorite, sulfide minerals, and partially to wholly altered ilmenite (leucosene). Relict cores of clinopyroxene and hornblende are locally preserved in gabbro and diorite. Plagiogranite has been altered to sausseritized plagioclase, quartz, and chlorite (replacing biotite), and minor opaque oxides.

Distinctive features of the mafic intrusive lithologies include an intricate network of mineralogically distinct vein systems and patchworks of healed cataclasite and mafic-clast breccia hosted in otherwise nondeformed yet recrystallized rock. Vein mineralogies are diverse and include epidote, epidote (and clinozoisite)-quartz, prehnite, prehnite-quartz, quartz-epidote-chlorite, and quartz-calcite. As mentioned above, the cataclasite and brecciated zones are locally sheared, but are often nondeformed. The breccia clast lithologies match the adjacent nondeformed host lithology and are generally encased in vein materials and subordinate amounts of cataclastic matrix. The cataclasite consists of angular coarse sand- to clay-sized rock and mineral fragments that also were clearly derived from the host lithology. Previous workers described these breccias (and other mafic clast sedimentary breccias of the Fiddler Mountain olistostrome, see below) as volcanic breccias (Page and others, 1981). However, the veining combined with their apparent host-derived nature suggest that these breccias formed in situ resulting from tensile forces and hydrofracturing associated with circulating hydrothermal fluids. Throughout the study

area, this distinctive “hydrofracture” texture is most commonly observed in mafic intrusive rocks, but also occurs locally in all other lithologies of the OCC and in the crustal rocks of the Josephine ophiolite.

The hydrothermal alteration and accompanying brittle fragmentation textures preserved in these lithologies are interpreted to have formed during the extensional tectonic episode that led to the formation of the Josephine marginal basin (record the Josephine orogeny). Similar textures and features have been described elsewhere in the Josephine ophiolite and are considered to be diagnostic of ophiolite genesis at slow- to intermediate-spreading centers (Alexander and Harper, 1992; Macdonald 1982, 1983; Lagabrielle and Cannat, 1990).

The contacts of the mafic intrusive suite are rarely exposed. A few outcrops show metadiabase and aphanitic greenstone dikes with chilled margins cutting rocks of the metavolcanic and metasedimentary sequence. Multiple chilled dike margins are also common in metadiabase outcrops. Also, numerous small bodies (<1 kilometer in the longest dimension) of metadiabase and altered diorite and gabbro occur scattered throughout regions that otherwise consist of metabasalt and intercalated chert. These outcrop patterns suggest that the boundary of the mafic intrusive suite is either an irregular intrusive contact, a complexly folded stratigraphic/structural boundary, or a combination of both. Based on the available evidence, it seems likely that at least part of the mafic complex intrudes the metavolcanic and metasedimentary sequence. However, without knowing their absolute ages, a complexly folded (and faulted) ophiolite stratigraphy with the mafic complex underlying the metavolcanic and metasedimentary sequence remains a possibility.

Some of the best places to view the gross lithologic and textural features of the mafic intrusive suite occur 1) along the roadcuts and cliff exposures in the Hellgate Canyon portion of the Rogue River (Plate 11), 2) in the Clear Creek drainage northwest of Selma (Plates 6 and 7), and 3) in the roadcut and ridgeline exposures between Onion Camp and Hungry Hill, and along the trails, ridgelines, and drainages south of Canyon Peak (Plate

3). Near Canyon Peak, the mafic complex rocks are distinct from the relatively unaltered, younger, post-150 Ma intrusive rocks of calc-alkaline affinity that are common in the region (Dick, 1976; Harper et al., 1994).

The rocks of the mafic intrusive suite are very similar to the sheeted dike and massive gabbro portion of the northern outliers of the Josephine ophiolite (Plates 1, 3, 5, 6, 7, and 10). One possible interpretation is that the mafic intrusive complex is equivalent in age to the Josephine ophiolite, and has intruded older oceanic crust of the OCC during the initial phase of Josephine-related rifting. Alternatively the mafic intrusive rocks may represent part of a Triassic ophiolite sequence that includes the metavolcanic metasedimentary rocks of the OCC. However, without definitive age data, it remains unclear which interpretation is correct. The former scenario seems most likely based on the available field observations and interpretations. In addition, rocks of the mafic intrusive suite exposed in the OCC share numerous distinct geologic features with the “mafic complex” exposed in the Preston Peak area (Snoke, 1977). Field relations and U-Pb zircon apparent age data suggest that the Preston Peak mafic suite represents Josephine-type magmas that intruded into the Rattlesnake Creek terrane and therefore represent the eastern “rift-edge” of the Josephine marginal basin (Snoke, 1977; Saleeby and others, 1982). By analogy, the rocks of the mafic intrusive suite and other rocks of OCC could represent the western “rift-edge” or an isolated rift fragment in the Josephine basin.

Amphibolitic rocks. Discontinuous and irregular belts of amphibolite and amphibolite gneiss with subordinate impure quartzite are scattered throughout the OCC near Squaw Mountain, south of Onion Mountain, near Hawk’s Rest, and to the west of Eight Dollar Mountain (Plates 1 and 6). The amphibolite typically forms steep hillslopes covered by loose boulders and brushy chaparral that contrast the old growth pine and cedar forests that are common to hillslopes underlain by greenschist facies metavolcanic and metasedimentary rocks of the complex. Amphibolitic rocks of the OCC consists primarily of distinctly foliated rocks with subordinate massive, amphibolite grade metamorphosed

gabbro and diabase. Ubiquitous retrograde greenschist and lower grade alterations and vein systems penetrate most outcrops, particularly the smaller, isolated masses of amphibolite. Previous workers described these rocks as “gnessic migmatite” (Wells and others, 1949), “metagabbro” (Ramp, 1977), and “gabbroic rocks and dike complexes” (Page and others, 1981) and interpreted them as intrusive and metamorphic rocks related to and derived from rocks of the Rogue Formation. However, the field, petrographic, and age relations described below indicate that the amphibolite gneiss and schist represent higher grade metamorphosed equivalents of the OCC metavolcanic, metasedimentary and mafic intrusive rocks.

All of the amphibolite bodies are at least partially bounded by serpentized peridotite that is variably sheared at the contact. In addition, slivers of sheared serpentinite occur locally within the amphibolite. The smaller masses of amphibolitic rocks are extensively altered and have highly sheared and discordant contacts with serpentized peridotite suggesting that a history of tectonic fragmentation and disruption followed high grade metamorphism. In contrast the larger amphibolitic belts display little postmetamorphic shearing at the peridotite-amphibolite contact. Moreover, the metamorphic foliations found in the peridotite, amphibolite, and greenschist facies rocks are parallel suggesting that the amphibolite is part of a large amalgamated block of tectonic crustal rocks and serpentized mantle peridotite.

Texturally the amphibolitic rocks can be subdivided into two groups based on the absence or presence of a distinct foliation. Massive amphibolites are characterized by relict hypidiomorphic granular, sub-ophitic, and ophitic textures and amphibolite grade pseudomorphs. Foliated amphibolites contain granoblastic grains with a strong preferred orientation of flattened mineral grains, most commonly hornblende. Coarser-grained varieties are often gneissose and display a faint intersection lineation, while the more fine-grained varieties are schistose with a well-developed intersection lineation. Alternating plagioclase-rich and hornblende-rich layers, generally <3 millimeters thick, define the

gneissic layering. The deformed amphibolitic rocks display at least two styles of folding. One style is characterized by tight to isoclinal, similar folds with highly attenuated limbs oriented parallel to the foliation and probably represent syn-metamorphic folds that developed during amphibolite facies metamorphism. A post-metamorphic fold phase is characterized by open to tight, similar folding of the foliation and gneissic layering.

The amphibolitic rocks are intruded by relatively unaltered mafic dikes and younger intermediate dikes. The mafic dikes display textures and mineralogy similar to rocks of the mafic intrusive suite, and the younger intermediate dikes are always hornblende phyric (usually acicular in habit) and are very similar appearance and composition to dikes in the region dated at approximately 150 Ma (this study; Dick, 1976; Lanphere et al., 1968). In a few exposures, plagiogranite dikelets and segregations in the amphibolite cut the distinctly foliated amphibolite. It remains unclear whether these felsic rocks represent melts derived from the surrounding amphibolite or more evolved melts of the mafic intrusive suite.

The typical amphibolite consists of hornblende and plagioclase with subordinate of epidote, titanite, and opaque oxides (mostly ilmenite). Common alteration minerals include chlorite, epidote, clinozoisite, prehnite, green amphibole, white mica, and quartz (sausserite). Hornblende usually comprises 60% to 80% of the rock. Plagioclase is untwinned and ranges from albite to intermediate oligoclase in composition based on refractive indexes ranging from slightly lower than balsam in epidote amphibolites to slightly higher than balsam in epidote-absent amphibolites. Fresh, brown pleochroic amphibole (hornblende) separated from two different samples collected near Squaw Mountain yielded Ar/Ar plateau cooling ages of 173 ± 0.6 Ma and 169.6 ± 0.7 Ma (Table 2-2, Hacker et al., 1995).

Impure quartzite accounts for <5% of the amphibolitic rocks in outcrop, and consists of 60%-90% quartz with secondary cummingtonite, almandine, biotite, white mica, and opaque oxides. Quartzose layers are most abundant in the amphibolite masses near Squaw Mountain (Plates 1 and 6) where they occur as infolded layers within outcrops

consisting mostly of hornblende schist and amphibolite gneiss. In hand samples and in thin sections, the quartzites are fine- to medium-grained, banded, well-foliated and lineated rocks that display a sugary recrystallized texture.

The following parageneses were noted in the amphibolitic rocks: 1) brown hornblende-oligoclase-clinopyroxene-titanite, 2) green hornblende-oligoclase-titanite, 3) green hornblende-epidote-albite-titanite, 4) quartz-cummingtonite-biotite-almandine, and 5) quartz-biotite-white mica-almandine. These assemblages indicate epidote-amphibolite to upper amphibolite facies metamorphic conditions and provide the following rough estimates of the metamorphic pressure and temperature conditions. Experimental data and the apparent range in amphibole composition (based on petrographic observation) constrain epidote-amphibolite facies to >4 kb and $\sim 550^{\circ}$ C to 650° C (Apted and Liou, 1983; Thompson, 1976). The greenschist and lower metamorphic grade alteration and vein mineral assemblages are very similar to those noted for the mafic intrusive suite and are interpreted to have formed during the same episode of extension and hydrothermal alteration. It seems likely that apparent hornblende ages record cooling during this extensional episode as the amphibolites were denuded from the 4 kb environment.

Some of the less altered amphibolite bodies exposed near Squaw Mountain exhibit a general metamorphic gradient from epidote-amphibolite facies rocks at the boundary with greenschist grade rocks to upper amphibolite facies rocks near the boundary with serpentized peridotite. The greenschist-amphibolite contact is essentially a preserved metamorphic "hornblende-in" isograd and marks the change in metabasaltic mineral assemblages from actinolite-chlorite-epidote-albite to hornblende-epidote-albite. In addition the rocks become more coarsely crystalline and more highly strained across this reaction boundary. For instance actinolite-chlorite schist, metabasalt, and impure chert become hornblende schist, gneissic amphibolite, and impure quartzite. Where directly observed, the facies transition is a narrow zone about 1-2 meters in width. These relations clearly

indicate that the protolith materials for the amphibolite were the metavolcanic and metasedimentary rocks of the OCC.

Serpentinite and serpentized peridotite. Roughly one third to one half of the ultrabasic rocks that occur in the study area consist of sheared serpentinite (slickenite) and highly serpentized peridotite. These rocks occur as small lenses and smears of highly sheared serpentinite in the crustal sections east of the Chetco Pass fault, and as massively serpentized peridotite that forms the northeastern prong of the Josephine peridotite sheet (Dick, 1976). However, the highly serpentized rocks which are spatially associated with the OCC crustal rocks are given a separate designation. This is because their apparent age and field relations are distinct from the relatively unshaped and unaltered peridotite that characterizes the Josephine peridotite massif. A gradational serpentization boundary apparently forms the lower boundary with the relatively pristine Josephine peridotite. The upper contact is variable ranging from a conformable depositional contact beneath volcanogenic and olistostromal sediments (e.g., the Rogue Formation and Fiddler Mountain complex) to a variably sheared boundary with crustal rocks of the Onion Camp complex and the Josephine(?) ophiolite (Figure 2-3 and Figure 2-22).

The boundary between the Josephine peridotite and the serpentized peridotite of the OCC is typically marked by a break in slope and a distinct change in hillslope vegetation that is conspicuous on air photos and is easily visible in the field (e.g., Figure 2-3). The unshaped Josephine peridotite forms blocky, resistant outcrops and extremely rugged topography whereas the serpentinite forms smooth, subdued topography with sparse vegetation that is subject to landslides and other downslope movements. Previous workers (e.g., Dick, 1976; and Ramp, 1986) noticed this boundary and interpreted it to have formed during the emplacement and deformation of the peridotite during the Nevadan orogeny and subsequent deformational events. Dick (1976) noted that the sheared belts of serpentinite were oriented parallel to the Nevadan regional deformation fabric whereas Ramp (1986) pointed out that the serpentinite typically occurred at lower elevations and

Figure 2-22. Photograph of view looking to the northeast along the contact between the heavily vegetated crustal rocks of the Onion Camp complex on the northwest, and the relatively sparsely vegetated hillslopes of Onion Camp complex serpentinitized peridotite on the southeast. The small patches of barren slopes in the upper left of the photograph represent small areas of complexly folded serpentinite exposed on the flanks of Squaw Mountain (see Plates 1 and 6). For reference, the northwestern flank of Eight Dollar Mountain is seen in the middle right of the photo, and the Illinois River flows north along its base.



suggested that it might reflect deformation and serpentinization along low angle structures located at relatively shallow depths beneath the region. Recent work by Coulton (1995) in serpentinized portions of the Josephine peridotite indicates that alteration of the peridotite occurred during Josephine-age magmatism and mid-ocean spreading (at about 160 Ma). The geologic relations described below indicate that the serpentinite and serpentinized peridotite of the OCC experienced a much earlier metamorphic history and were at least partly altered and deformed prior to ~175 Ma.

Field appearance. Exposures of ultramafic rocks in the OCC range from massive and blocky outcrops unaffected by shearing, to incoherent outcrops of highly sheared, platy serpentinite. The massive outcrops generally weather brown to reddish-orange with weathered surfaces studded by aggregates of primary mineral grains, now mostly to wholly pseudomorphed by serpentine-group minerals. Some massive weathering exposures weather to blue-gray color. Sheared serpentinite (slickenite) varies in appearance depending on the degree of shearing. Moderately sheared serpentinite is generally dark green or blue-green in outcrop, whereas highly sheared varieties are polished black or metallic blue in appearance. In general, the degree of shearing increases along known faults (e.g., the Illinois River fault), in the axial planar regions of regional scale folds (e.g., the Hellgate Canyon of the Rogue River, Plate 11), and toward contacts with crustal rocks. The central portions of large blocks of serpentinized peridotite tend to be the least altered; however, small lenses and smears of slickenite crop out throughout the interior portions of the ultramafic body.

Nearly all ultramafic rocks in the OCC are intensely serpentinized making an estimation of the relative percentages of primary minerals uncertain. Relict mineral grains, most commonly olivine kernels, occur in variable percentages ranging from about 5%-20% in the more massively serpentinized rocks but are scarce to absent in sheared serpentinites. Pyroxene is rarely preserved and most often occurs as a bastite, pseudomorph made of serpentine-group minerals with a bronze-like metallic lustre, or uralite, a light blue-green

fibrous amphibole of undetermined composition. The low temperature serpentine-group minerals (lizardite and chrysotile) generally comprise >75% of the rocks and occur as both massive replacement minerals and in intricate vein networks indicative of multiple episodes of serpentinization and alteration. Higher temperature minerals (>300° C) such as antigorite with tremolite occur as fragmented, irregular patches in sheared serpentinite and occasionally border fragmented mafic dikes suggesting a complex history of tectonic disruption and formation relatively early in the alteration history. Magnetite is ubiquitous and provides an indication to the degree of serpentinization with the more highly serpentinized rocks being generally more strongly magnetic.

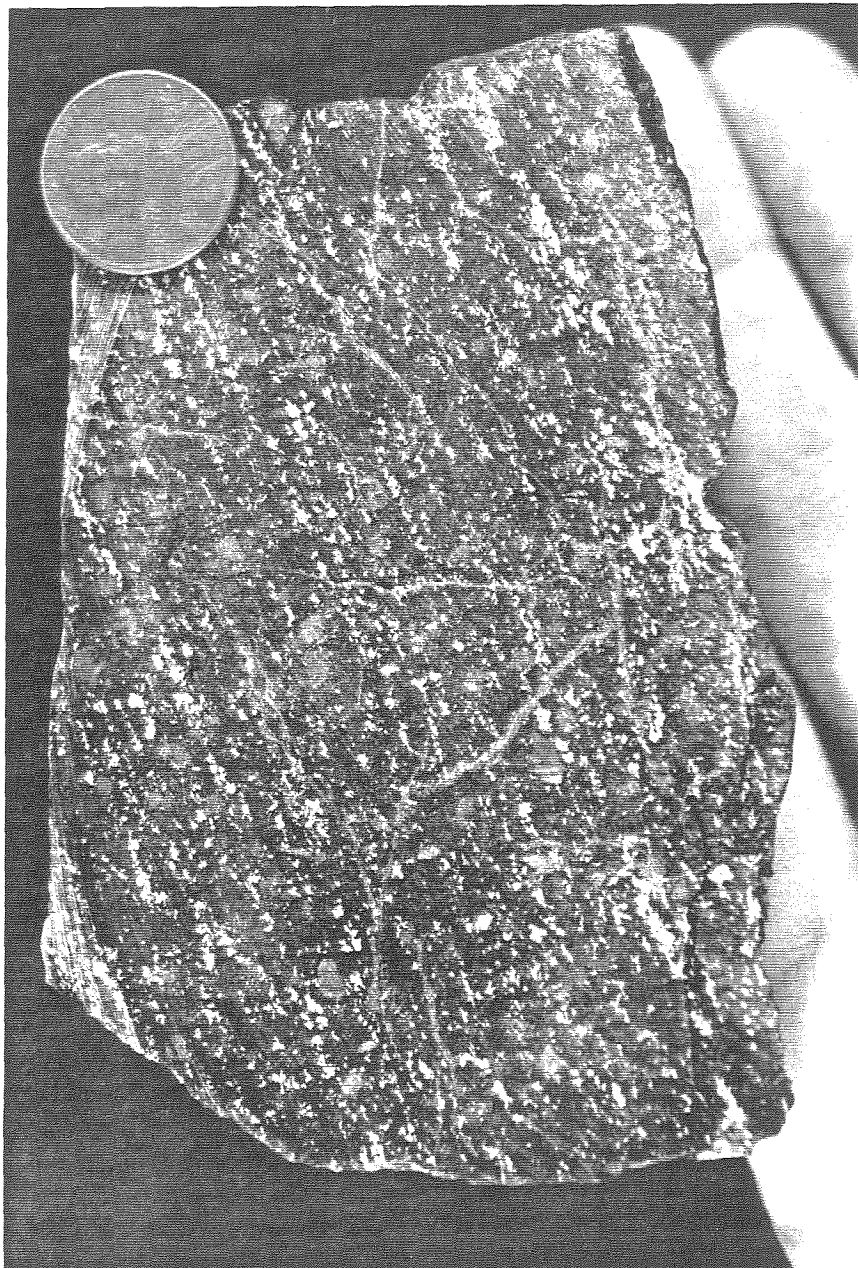
Based on estimates of primary mineral abundances, harzburgite, dunite, and relatively scarce pyroxenite are the original lithologic constituents of the OCC ultramafic rocks. Podiform chrome ore deposits are conspicuously scarce in comparison to those associated with the surrounding peridotite bodies; i.e., the Pearsoll Peak and Chrome Ridge peridotite bodies located west of the Chetco Pass fault, and the main body of the Josephine peridotite located to the south. Olivine of about Fo₉₀ is the most abundant primary mineral constituent of the Onion Camp complex ultramafic rocks (based on centered optic axis figures on a flat stage microscope), originally forming about 75% to 95% of the rock. The other major mineral constituent was pyroxene. The relative orthopyroxene:clinopyroxene abundances are unknown because of intense alteration, but probably were exceedingly high (>95%) based on similarities with the Josephine peridotite (Dick, 1976; Harper, 1980). Chrome spinel octahedra are still visible on weathered surfaces of massive outcrops, but are largely pseudomorphed by magnetite.

Textural and structural features. The ultramafic rocks of the Onion Camp complex preserve at least four texturally distinct deformation and alteration episodes that, overall, record decreasing metamorphic temperature conditions over time. The earliest episode is rare in occurrence and is characterized by a mesoscopic foliation defined by flattened and elongated aggregates of primary mineral grains. Blastomylonites with

moderately to well developed S-C fabrics occur locally in otherwise structureless massive and blocky exposures. Structureless peridotite contains equigranular mineral grains suggestive of annealing recrystallization and grain growth that may have obliterated evidence of a high temperature ductile deformation history. Weathered rock faces that display the mylonitic fabric show multi-grain porphyroclastic augens of olivine and pyroxene in a fine-grained, xenoblastic matrix of mostly olivine. The porphyroclasts invariably show pronounced strain effects such as kink bands, deformed exsolution lamellae, and undulatory extinction. Most alpine-type peridotite masses experienced a similar deep-seated deformational episode (Moore, 1982) presumably in response to asthenospheric mantle upwelling at ocean spreading centers.

Another distinct textural feature of the ultramafic rocks in the Onion Camp complex is a serpentine foliation and lineation that is best developed in massive outcrops near the amphibolite-peridotite contact (e.g., in the vicinity of Squaw Mountain), but also occurs in scattered exposures throughout the unit. The foliation is defined by semi-continuous bands of light green serpentine spaced at about 1-3 mm intervals in an otherwise dark green, massively serpentinized peridotite, formerly harzburgite and dunite. The alternating light green and dark green bands give the serpentinite a gneissose appearance (Figure 2-23). A poor to moderate rock cleavage occurs along throughgoing shear bands spaced about one centimeter apart that intersect the light green serpentine foliation at about a 25° angle. The resulting intersection lineation and foliation parallel similar features in the adjoining amphibolite masses and suggest that the peridotite and amphibolite experienced the same metamorphic and deformational episode (at approximately 170 Ma). However, the mineral assemblage associated with the serpentine “gneiss” indicate lower metamorphic temperatures than those of the amphibolite and, given a shared history, require that the current mineral assemblage is the result of a later, low-temperature alteration products of an amphibolite grade mineral assemblage (e.g., talc-tremolite-antigorite). This scenario seems likely since extensive low temperature metamorphic conditions characterize the subsequent

Figure 2-23. Photograph of a slabbed hand sample of serpentinized peridotite showing the metamorphic foliation interpreted to be associated with the amphibolite facies metamorphism observed in the crustal sequence. The foliation shown parallels gneissic layering in hornblende schist and gneiss exposed nearby. The light colored bands consist of light -green serpentine group minerals (probably lizardite). Also note the medium-gray bastite pseudomorphs of pyroxene grains in a dark-gray matrix of thoroughly serpentinized olivine.

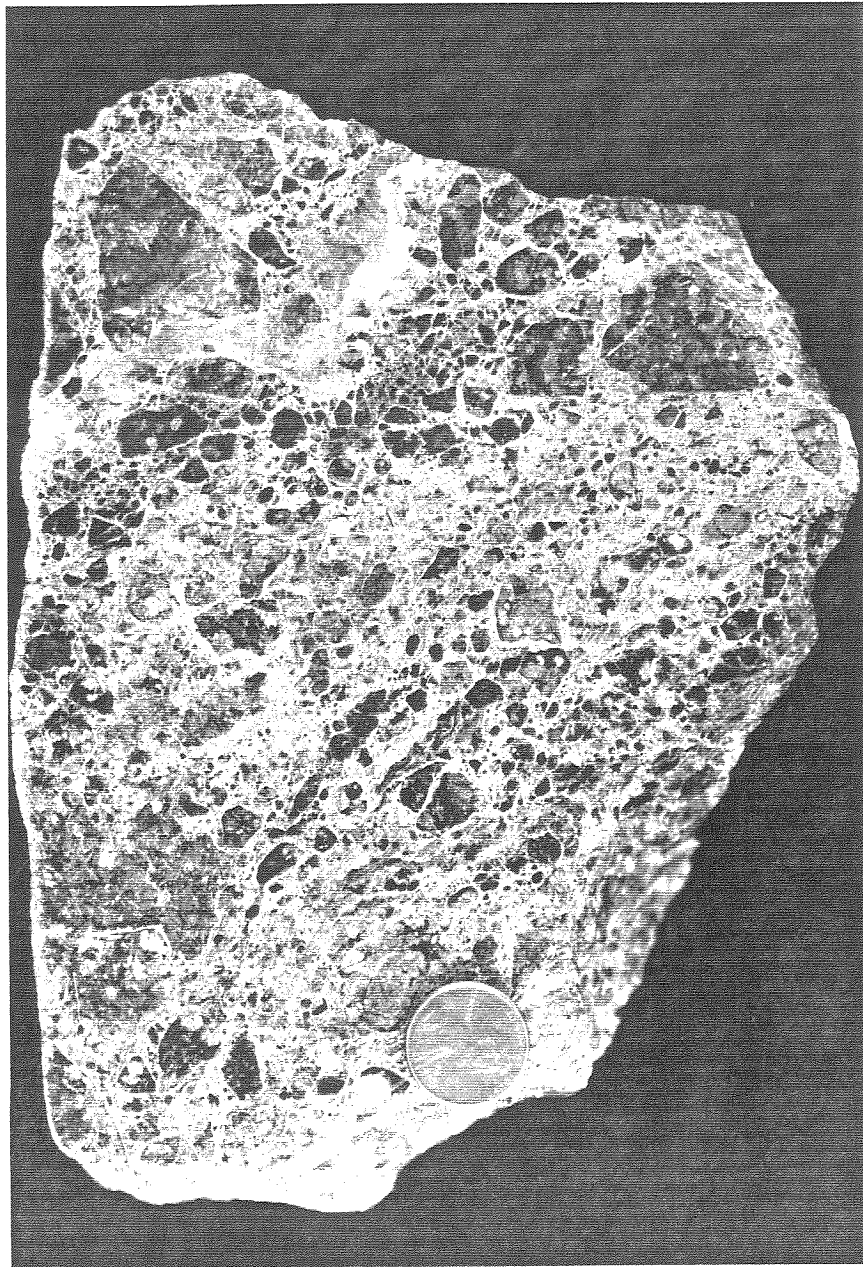


regional alteration and deformation episodes. Similar amphibolite-peridotite relations are described from parts of the western Paleozoic and Triassic belt (Kays, 1992; Donato, 1992) and provide another lithologic linkage between rocks of the Onion Camp complex and the Rattlesnake Creek terrane.

A third type of alteration and deformation is characterized by ubiquitous low-temperature static serpentinization, intricate vein networks, and healed fragmentary breccia zones. These textures clearly cut the mylonite and the serpentinite gneiss fabrics described above and indicate a distinct change from earlier penetrative episodes of deformation to an episode of general static alteration with extensive veining and localized fragmentation. Locally some serpentinites exhibit intricate patchwork textures of veins and fragmental textures that resemble serpentinite “marble” (ophicalcite) quarried from the world famous serpentinite belts of the Mediterranean region (Figure 2-24; and e.g., Bonatti et al., 1974; Lemoine, 1980; Lagabrielle and Cannat, 1990). These textures, alterations, and veining relations are similar to those that occur in the mafic intrusive complex and are probably related to the same deformation and alteration episode.

Static replacement minerals include serpentine-group minerals, lizardite and chrysotile, with secondary uralite (fibrous amphibole), and magnetite. The serpentinite hosts a great diversity of other alteration products and vein mineralogies including lizardite, chrysotile, and local occurrences of calcite, malachite, limonite, hematitic-siliceous micrite, barite, and various sulfide-group minerals including pyrrhotite, chalcopyrite, chalcocite, and sphalerite. The carbonate, sulfide, and sulfate deposits occur in serpentinite that is nonconformably overlain by submarine volcanogenic strata of the Rogue Formation. It therefore seems likely that the ultramafic rocks were exposed on the seafloor, perhaps along a low-angle normal fault, where they hosted hydrothermal vent systems. A relatively high concentration of these mineralized zones occur in the highly disrupted serpentinite melange belt bordering the Chetco Pass region to the southeast where they have been prospected for small amounts of Au and Cu (Plate 5; Ramp, 1984). Similar mineral

Figure 2-24. Photograph of a slabbed hand sample of brecciated serpentized peridotite collected from near Squaw Mountain (Plate 6). The outcrop occurs as a 1-2 meter wide zone of breccia in otherwise intact serpentized peridotite and is interpreted to represent a healed hydrothermal fracture. The serpentized peridotite clasts are supported by a serpentine mud matrix.



deposits occur as stratiform (Kuroko-type) massive sulfide deposits in the Rogue Formation (Koski and Derky; 1981; Wood 1987). Constraints on the timing and duration of the hydrothermal alteration are few, but field relations suggest that it accompanied Late Jurassic ophiolite genesis and arc magmatism.

The latest structural and textural features of the ultramafic rocks are sets of anastomosing shear bands whose orientations, on average, parallel the north-northeast striking and east dipping regional foliation and are cut by 150 Ma mafic to intermediate dikes (Dick, 1976). Rhombohedra-shaped augens of massive serpentinite occupy the regions between shear surfaces. The augens flatten and subparallel the shear bands with increasing strain. Shear surfaces either display a black to dark green lustrous polish, or contain lineated, stepped serpentine fibers that indicate the shear direction. Most exposures display both types of surface. However, the former type of shear surface is most common in isolated, small masses of serpentinite that occur within the Onion Camp complex (e.g., see Plate 6) whereas fiber-filled surfaces are most common in the main serpentinitized peridotite mass. The absence of serpentine fibers probably reflect increased shearing, the absence of fluids, or a combination of both. Shear zones occur at essentially all scales. For example, in the field and at map scale, careful attention to the augen and boudinage patterns in the ultramafic masses helped to discern the regional scale fold belt structures that define the map area (Plate 1). At the outcrop scale (and at microscopic scale), low strain shear zones have a widely spaced, anastomosing schistosity (0.5m - 1.0 m) and equidimensional augens whereas high strain zones generally have a centimeter-scale, parallel schistosity and highly flattened serpentine augens. In extremely high strain cases, generally along fault zones, the serpentinite appears as a platy schist with a distinct metallic blue luster. Excellent exposures and opportunities to view these high strain zones occur in the map scale fold hinge zones in the Hellgate Canyon of the Rogue River and near Squaw Mountain (Plates 1 and 11).

Dikes. A variety of dike lithologies ranging from ultramafic to intermediate in composition intrude the ultramafic rocks of the Onion Camp complex. All dikes have experienced varying degrees of alteration but are rarely altered to rodingite suggesting that the peridotite was already largely serpentized. Dike lithologies include pegmatitic websterite and gabbro, plagiogranite, diabase, aphanitic basalt, and acicular hornblende-phyric diorite. The websterite and gabbro dikes contain individual clinopyroxene crystals that reach 50 cm in length but are now largely replaced by fibrous amphibole (uralite). Generally the dikes are rarely continuous for more than 10 meters and essentially occur as mega “porphyroclasts” and as boudins in serpentinite. In addition, dike orientations are random reflecting multiple episodes of intrusion and subsequent folding.

Cross-cutting relations are not evident in the field due to a lack of exposure and the relatively high degree of disruption; however, the following distinctions are possible. Plagiogranite dikes are probably the oldest based on their ~173-175 Ma U/Pb zircon ages (Table 2-1) and are generally the most highly altered of the dike lithologies. The diabase and aphanitic basaltic dikes resemble sheeted mafic dike lithologies of the nearby ophiolite sequence exposed at Eagle Mountain that contains pillow lava interbedded with Callovian chert (M. Silk, personal communication). The websterite and gabbro dikes appear to be related to gabbros of the IRPC (~160 Ma). Finally, the distinctive acicular hornblende-phyric dikes resemble other 150 Ma dikes in the region (Dick, 1976) and are considered to represent the youngest dikes. Thus the OCC peridotite appears to have been intruded by four separate episodes of dikes ranging from the Middle to Late Jurassic.

Summary and regional correlations. The rocks of the Onion Camp complex comprise a lithologically distinct petrotectonic unit previously unrecognized in the WJB. Their age, geochemistry, and deformational and metamorphic features unequivocally link the Onion Camp complex to the Rattlesnake Creek terrane. The OCC rocks seem most similar to the lower melange unit of the RCT as defined by Wright and Wyld (1994). The OCC rocks, based on field relations, are strikingly similar to the RCT rocks exposed in the

Preston Peak region of northern California. The distinctive lithologic ties between the OCC rocks and the Preston Peak region include a chert-clast conglomeratic grit, a heterogeneous mafic intrusive complex, composite blocks of amphibolite and metaperidotite, and overlapping heterolithologic breccia deposits. Snoke (1977) described the Preston Peak rocks as the eastern (or inboard) rift-edge facies of the Josephine marginal ocean basin. By analogy, the OCC rocks are interpreted as the western (or outboard) rift-edge facies of the Josephine basin.

Discussion of Geochemical data

A wealth of geochemical data exists for volcanic rocks from the various lithotectonic units of the Klamath Mountains province (Barnes et al., 1995, in press). The dataset is complete enough such that the characteristic geochemical signatures of numerous lithotectonic units are well defined. Three such rock associations, the crustal sequence of the Josephine ophiolite, the Rogue Formation, and the RCT exhibit important differences in their diagnostic geochemical signatures. These distinctions are evident in major and trace element data presented in Table 2-3 and also in the REE data presented in Table 2-5. The following discussion focuses on these data to see if they support the distinctions between units based on the field relations described above.

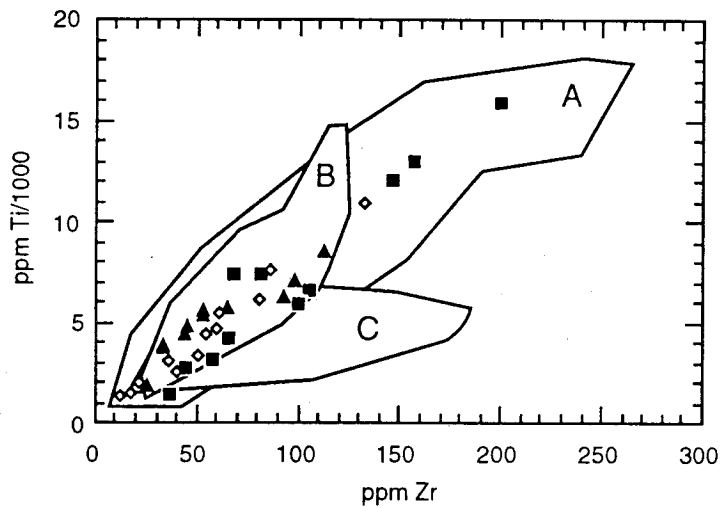
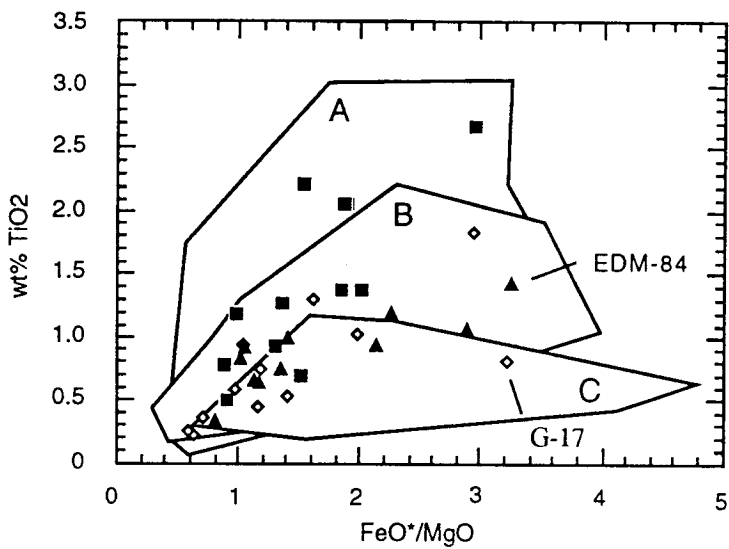
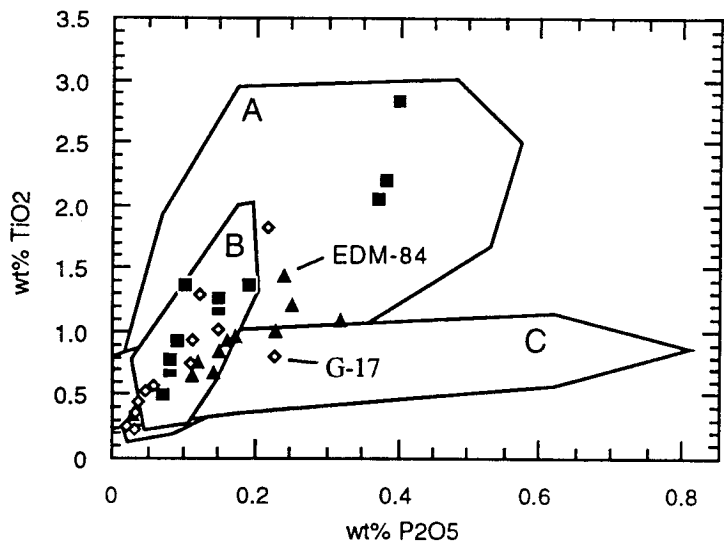
Josephine ophiolite. The minor and trace element abundances of dikes and pillow lavas of the central Illinois River drainage ophiolitic rocks (Table 2-3) match the data obtained from the type Josephine ophiolite, with the notable exception of one sample (sample G-17, Figure 2-25). The data from rocks of the study area overlap with the fields defined from the type Josephine ophiolite crust and are characteristic of transitional between MORB and IAT basalts (Harper, et al., 1995, in press).

Rogue Formation. Minor and trace element abundances for rocks of the Rogue Formation exhibit strong calc-alkaline and transitional island arc tholeiite/calc-alkaline (IAT-CA) affinities (Garcia, 1979, 1982; Barnes and others, in review, 1995). The data

Table 2-5. Rare-earth element compositions (in ppm) of selected basalts.

| <u>Sample</u> | <u>La</u> | <u>Ce</u> | <u>Nd</u> | <u>Sm</u> | <u>Eu</u> | <u>Tb</u> | <u>Yb</u> | <u>Lu</u> |
|----------------------------------|-----------|-----------|-----------|-----------|-----------|-----------|-----------|-----------|
| <u>Rogue Formation</u> | | | | | | | | |
| 89-DY-PP-6 | 10.9 | 21.6 | 14.3 | 3.8 | 1.30 | 0.66 | 2.52 | 0.38 |
| 90-DY-6MiRd | 7.8 | 15.8 | 9.5 | 3.0 | 0.97 | 0.56 | 2.03 | 0.31 |
| 91-DY-EDM-49 | 8.1 | 16.2 | 11.2 | 3.1 | 1.09 | 0.57 | 2.00 | 0.31 |
| 92-DY-G-9 | 11.0 | 23.9 | 15.6 | 4.2 | 1.17 | 0.69 | 2.73 | 0.42 |
| <u>Onion Camp complex</u> | | | | | | | | |
| 92-DY-EDM-83B | 21.5 | 41.4 | 23 | 5.3 | 1.50 | 0.81 | 2.07 | 0.31 |
| 92DY-OM-11 | 4.2 | 11.1 | 8.9 | 2.9 | 1.00 | 0.67 | 2.51 | 0.40 |

Figure 2-25. Plots of P_2O_5 , FeO^*/MgO , and Zr versus Ti abundance/concentrations for basaltic rocks of the study area. Fields A, B, and C are fields for the entire Klamath Mountains province defined by data obtained from rocks of the Rattlesnake Creek terrane, the Josephine ophiolite, and the Rogue Formation, respectively.



| | KLAMATH MOUNTAINS PROVINCE | STUDY AREA |
|---------------------------|----------------------------|------------|
| Rattlesnake Creek terrane | A | ■ |
| Josephine Ophiolite | B | ◇ |
| Rogue Formation | C | ▲ |

acquired from rocks of the central Illinois River drainage (Figure 2-25, Tables 2-3 and 2-5) exhibit relatively high TiO_2 concentrations relative to P_2O_5 , FeO/MgO , and Zr with respect to the previously defined Rogue Formation field. It should be noted that no intermediate to silicic rocks, which define the flat trajectories with respect to Ti in Figure 2-25, were collected for analysis during this study. No intermediate composition volcanic rocks were collected during this study, largely because the Rogue Formation in the study area consists almost entirely of basaltic and basaltic-andesite rocks. It is possible a regional trend may occur from south to north along the strike of the Rogue Formation outcrop belt with IAT magmas in the south and more calc-alkaline magmas in the north. It is also interesting to speculate that the apparent overlap in data between the Rogue and Josephine rocks may reflect a genetic linkage between inter-arc basin ophiolite and primitive oceanic arc magmas. More data is needed to test these intriguing possibilities.

In addition to the major and trace element analyses, four Rogue Formation basalts were analyzed for eight rare earth elements (REE) by instrumental neutron activation analysis (INAA). Figure 2-26 is a typical spider plot of the data normalized to chondrite values and shows slight REE patterns for the Rogue Formation basalts, typical of IAT lavas. However, these samples show slightly less enrichment than the more typical calc-alkaline patterns reported by Garcia (1976). Thus, the REE data also suggest a south to north transition from more primitive to more evolved magmas within the unit, perhaps a distinctive characteristic in the Rogue Formation worth further examination.

Onion Camp complex. Ten greenstone and pillow lava from the metavolcanic sequence were analyzed for major and trace element abundances (Table 2-3) with rare-earth element abundances determined for two of these samples (Table 2-5). Though the major elements may be mobile during metamorphism, most trace and rare-earth elements are considered immobile at greenschist and lower metamorphic grades (e.g., Shervais, 1982).

An extensive database of geochemical data (Barnes and others, in press, 1995) for metavolcanic and volcanoclastic rocks of the Klamath Mountains provides the criteria to

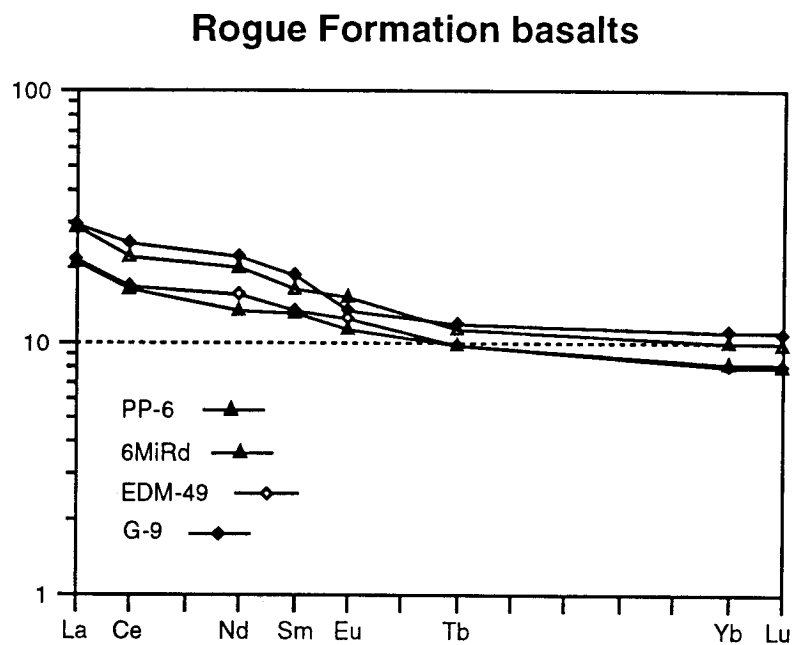


Figure 2-26. REE abundances of Rogue Formation basalts (in ppm), normalized to chondrite values, showing LREE pattern of 20-30 times chondrite values. These enrichments are slightly less than those obtained from Rogue Formation basalts collected from the Rogue Formation to the north of the study area (Garcia, 1976).

evaluate the possible correlatives to the Onion Camp complex. In support of the age and lithologic similarities, the geochemical data in Tables 2-3 and 2-5 and Figure 2-25 exhibit trends that clearly correlate the metavolcanic rocks of the Onion Camp complex with the lower melange unit of the Rattlesnake Creek terrane (Wright and Wyld, 1994).

Specifically, the mafic rocks of the Rattlesnake Creek terrane and the OCC fall in the compositional range between 46% to 55% SiO₂ and display a wide range of FeO/MgO values and generally high TiO₂ concentrations (Wyld and Wright, 1988; Wright and Wyld, 1994; Barnes and others, 1995). Also, the OCC metavolcanic rocks plot within the same fields as RCT lower melange unit on trace element discrimination diagram plots (e.g., Pearce, 1980, 1982; Wood, 1980; Shervais, 1982). In addition the REE data (Figure 2-27) from OCC pillow basalts (outcrop shown in Figure 2-19) shows a strong enrichment in light REE typical of an alkalic within-plate basalt (WPB). This is identical to the red chert-basalt breccia association of the RCT lower melange unit described by Wright and Wyld (1994). The greenstone block (OM-11) shows a flat REE pattern typical of normal tholeiitic mid-ocean-ridge basalt (N-MORB), also diagnostic of metabasalt blocks in the lower RCT melange unit (Wright and Wyld, 1994).

Illinois River plutonic complex. Previously Jorgenson (1970) and Garcia (1976, 1982) reported major element data obtained primarily from the gabbroic rocks of the complex. Analyses conducted during this study of gabbroic through tonalitic rocks help test whether the gabbroic to tonalitic composition of the complex resulted from normal fractional crystallization, magma mixing, or as a result of some other process. Though the data are as yet inconclusive, they suggest that the main phase gabbro through quartz diorite probably resulted from fractional crystallization or magma mixing processes, but that the main phase rocks and the tonalite-trondhjemite sill may represent two distinct magmas (Figure 2-28). For example, the sill rocks are much higher in Sr concentrations than the main phase rocks (Table 2-3 and Figure 2-29). The silicic rocks have values which are similar to other tonalite-trondhjemite plutonic bodies exposed elsewhere in the Klamath

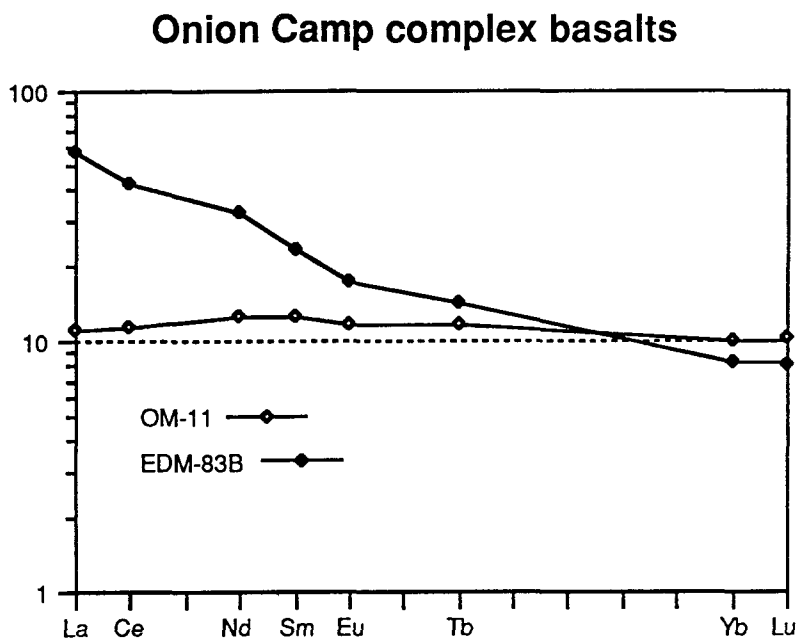
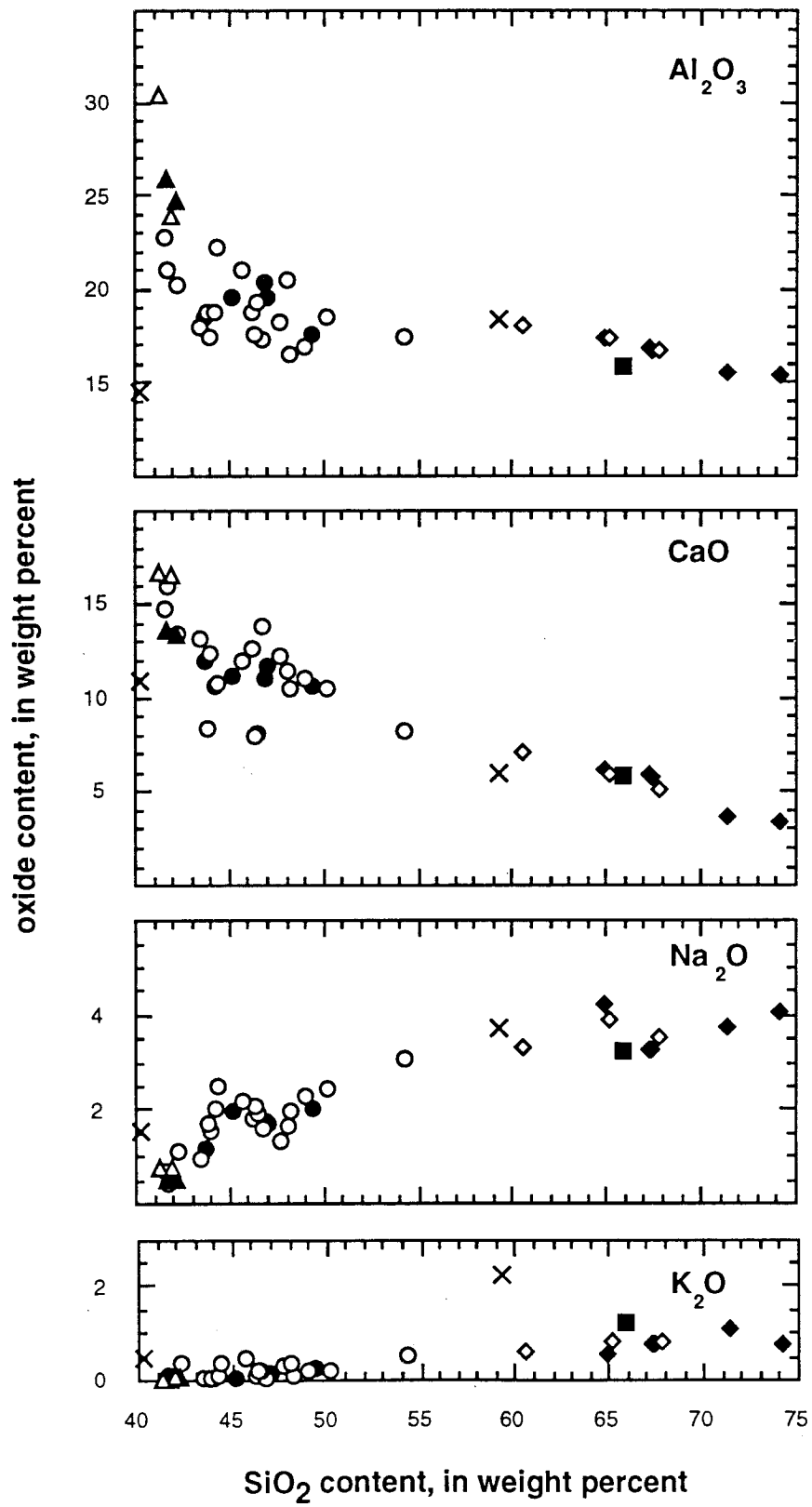


Figure 2-27. REE abundances of Rogue Formation basalts (in ppm), normalized to chondrite values, showing a two distinctly different pattern. Sample OM-11 exhibits a flat, MORB-like pattern and sample EDM-83B exhibits a strongly LREE pattern, typical of alkalic within-plate basalts. Both of these patterns are characteristic of the lower melange unit of the RCT (Wright and Wyld, 1994).

Figure 2-28. Variation of common oxides in rocks of the Illinois River plutonic complex plotted against SiO_2 . Note the gap in the data between high and low silica contents. Also note the notable change in the trends defined by of the mafic rocks versus the silicic rocks. Open symbols are data from Jorgenson (1970) and Garcia (1976), solid symbols are data obtained during from this study (see Table 2-3). Triangles = troctolite, circles = norite and gabbro, square = granodiorite, diamond = tonalite-trondhjemite, and "x" = dikes



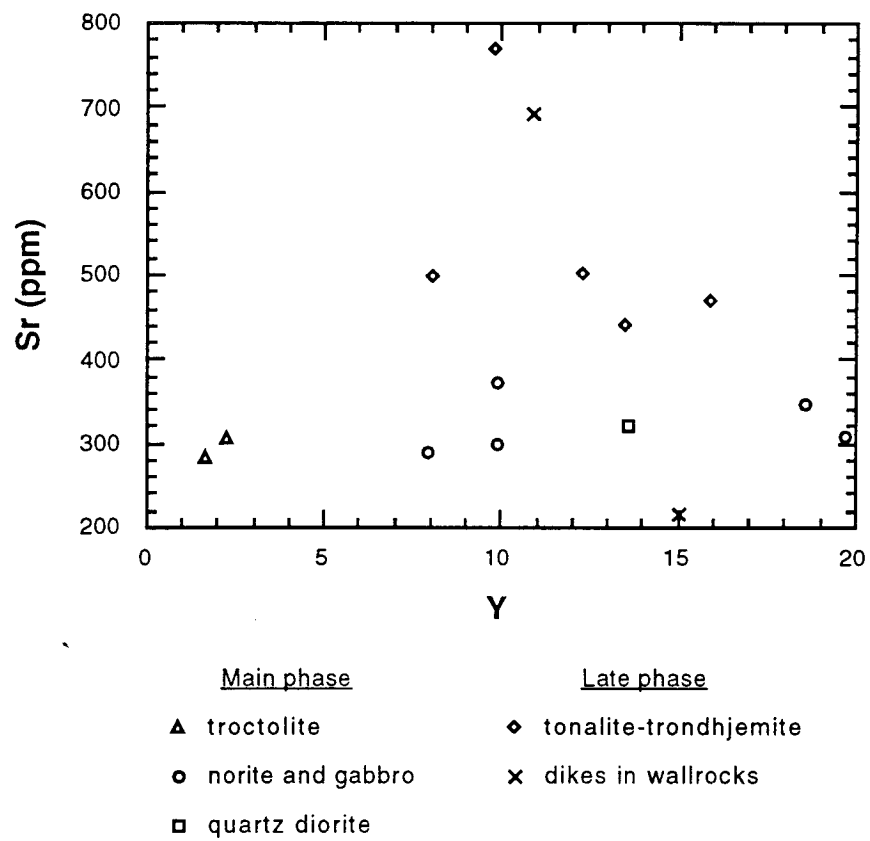


Figure 2-29. Plot of Sr versus Y concentrations (in ppm). Data are from Table (2-3).

Mountains province, e.g., the White Rock pluton. In these plutons, Barnes et al. (1992) suggest that these felsic bodies represent partial melts of a low-K tholeiite (with a garnet-amphibole as residuum). It is interesting to speculate that partial melting in the wallrocks of the IRPC, which happen to contain low-K tholeiitic amphibolite masses, may have produced the tonalite-trondhjemite sill. However, it is equally likely that the sill may represent a partial melt of subducted oceanic crust. In either case, further isotopic and REE analyses may help to define the apparent differences between the main phase and sill rocks of the IRPC.

Discussion of U-Pb Geochronometric data

Of the twelve samples analyzed from the WJB, ten yield concordant U-Pb zircon apparent ages, where concordance is recognized on Tera and Wasserburg (1971) concordia diagrams by overlap (at the 95% level) of individual zircon fraction with concordia (Table 2-1, and Figure 2-30). Samples which yield discordant dates, i.e., a lack of overlap of individual zircon grains with concordia, include the plagiogranite body from Josephine sheeted mafic dikes (sample EDM-89) and the meta-plagiogranite dike (sample PP-9A, Figure 2-30). The following discussion of the U-Pb data is organized according to rocktype.

Samples from the Illinois River plutonic complex. The degree of discordance in the IRPC samples seems related to both the proximity of sample to the Chetco Pass fault and to lithology. For instance, the three samples that were collected at a distance >5 km from the Chetco Pass fault, samples IR-3, IR-4, and YB-8 all yield concordant apparent ages (Figure 2-30). The other two samples, PP-64 and IR-1 were collected at distance <1 km from the Chetco Pass fault system, and display relatively disturbed patterns suggestive of Pb loss.

Field relations clearly indicate that the bulk of the plutonic complex (gabbro and diorite of IR-3 and IR-4) crystallized prior to the tonalite-trondhjemite sill (YB-8, IR-1, and

Figure 2-30.

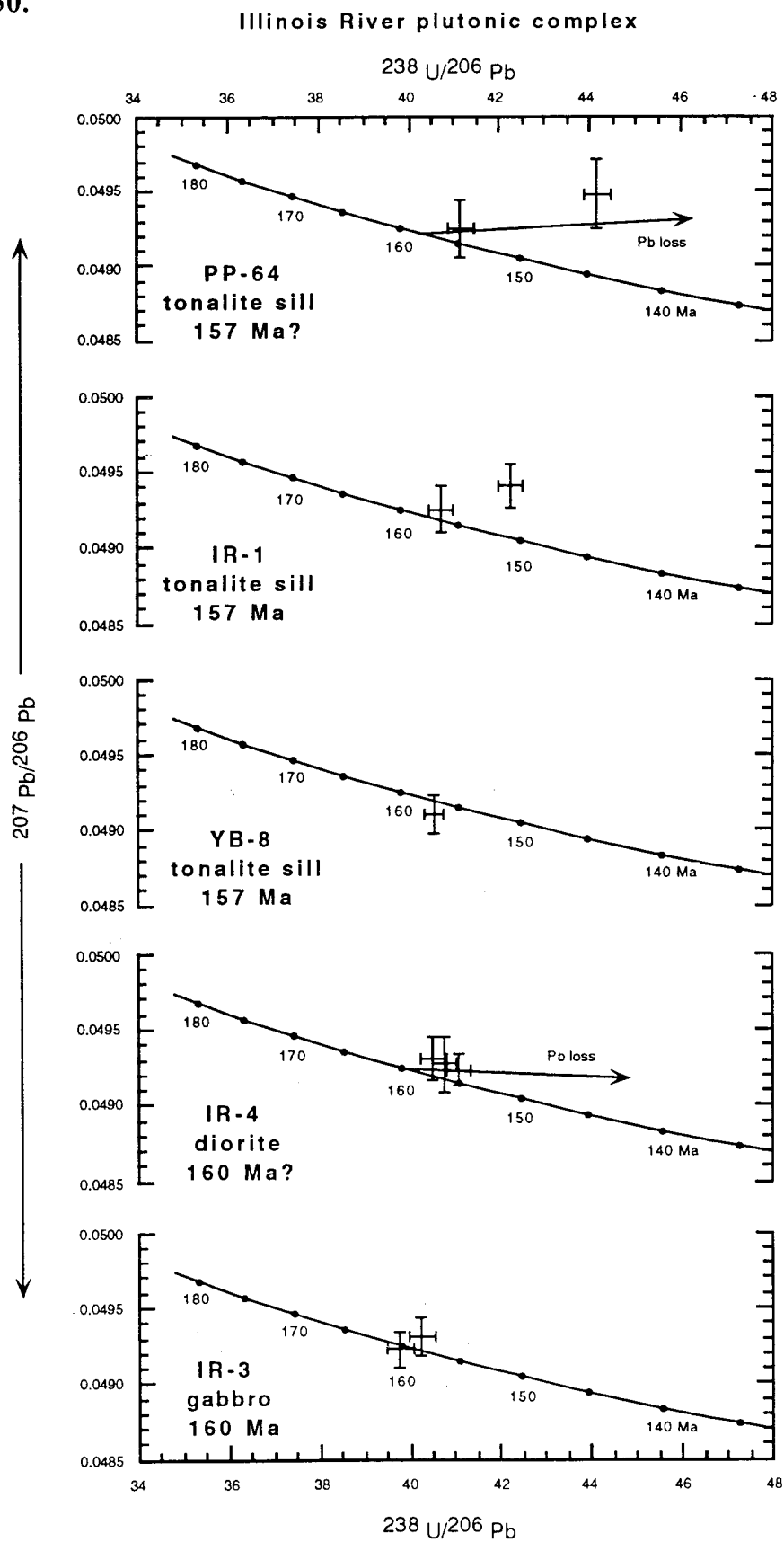


Figure 2-30 (cont).

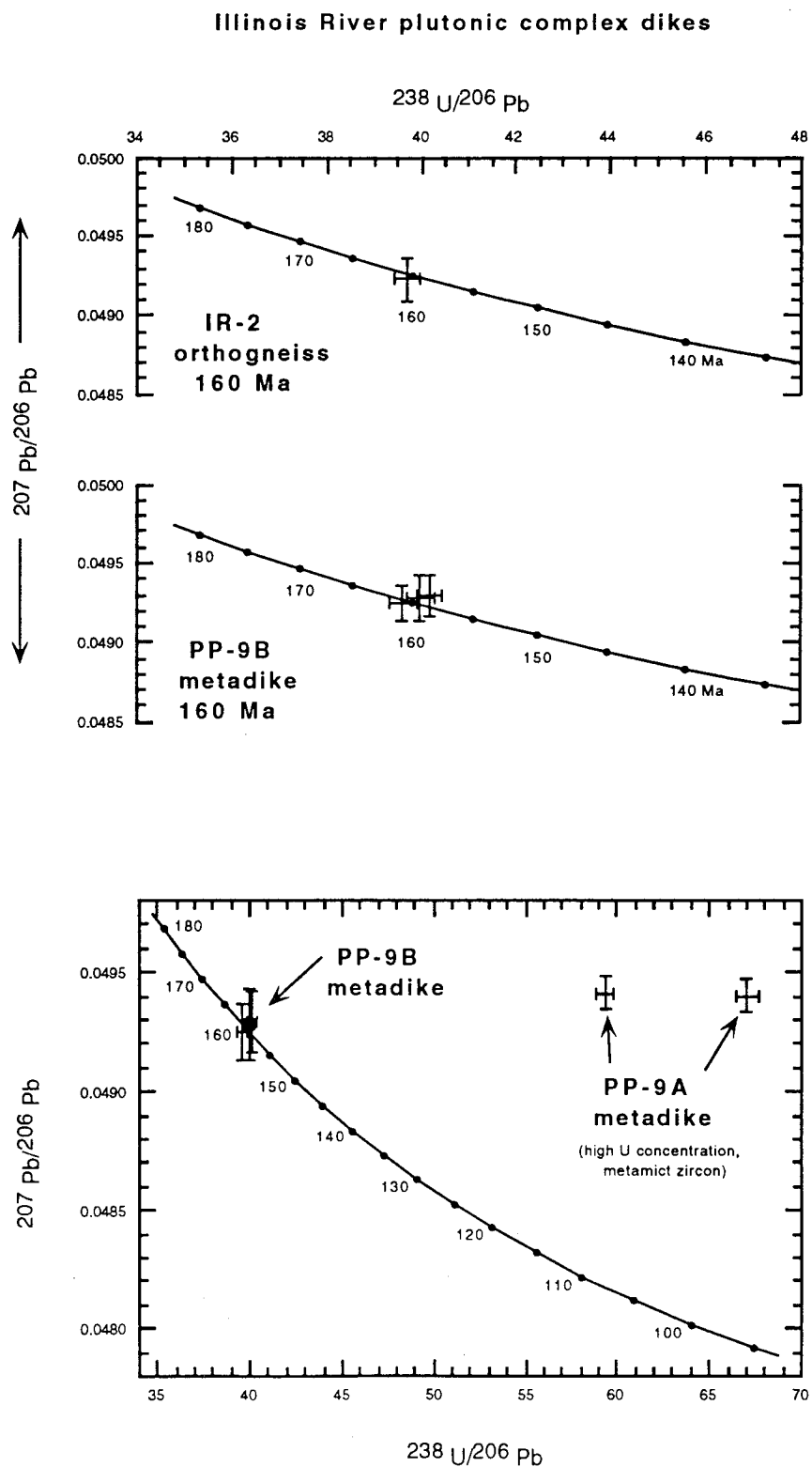
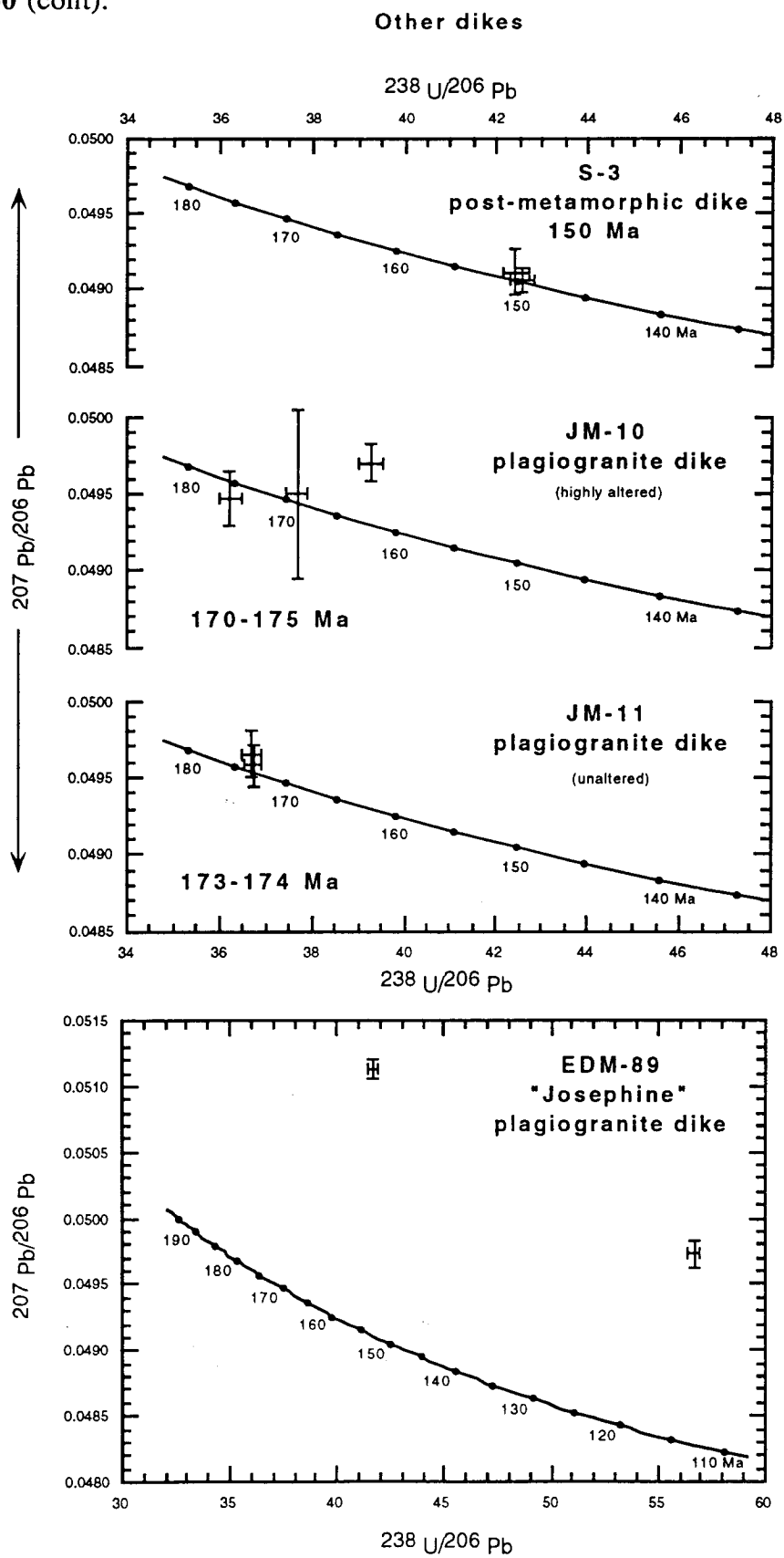


Figure 2-30 (cont).



PP-64). The U-Pb age data are consistent with this observation. Specifically, the main phase of the complex yields apparent ages of ~159-160 Ma, whereas the tonalite-trondjemite sill yields apparent ages of ~157 Ma (Figure 2-30).

Samples IR-2, PP-9A, and PP-9B were collected from two separate dikes at the margin and at the core, respectively, of the same sheeted dike outcrop which forms a resistant block in sheared serpentinite along a splay of the Chetco Pass fault. These dikes are interpreted to represent early stage trondjemitic dikes intruded into the roof rock (Pearsoll Peak peridotite) of the IRPC and subsequently metamorphosed. The 160 Ma concordant apparent age of sample PP-9B (Figure 2-30) supports this interpretation. Sample PP-9A exhibits relatively extreme Pb loss with an intercept age of approximately 162 Ma, in agreement with PP-9B (Figure 2-30). Thus, the Pb disturbance exhibited by sample PP-9A appears to be related to metamictization and deformation along the margin of the block, while sample PP-9B remained relatively undisturbed at the core of the block.

Plagiogranite dikes cutting Onion Camp complex peridotite. Samples JM-10 and JM-11 were collected from separate outcrops of plagiogranite that occur as resistant, isolated blocks in massive Onion Camp complex peridotite near Whetstone Butte (Plate 3). Their field relations suggest that the outcrops are part of a dismembered dike or related dikes that intruded peridotite that had previously been mostly serpentinitized. The outcrop at sample locality JM-10 displays brittle fragmentation textures and is highly altered relative to the outcrop at sample locality JM-11. This deformational and textural difference helps to explain the concordance of sample JM-11 and the apparent Pb loss component of the discordance pattern of sample JM-10 (Figure 2-30). The approximately “intercept” age ranging from 171 to 179 Ma of sample JM-10 agrees with the concordant ages at 173-174 Ma of sample JM-10 (Table 2-30) and is consistent with this interpretation.

Plagiogranite body in sheeted mafic dike complex. The highly disturbed discordance pattern of sample EDM-89 suggests isotope systematics affected by a combination of Pb loss and the inheritance of radiogenic Pb. The sample was collected

from a plagiogranite body in a mafic dike complex that intrudes metavolcanic and metasedimentary rocks of the Onion Camp complex. Brittle faulting is evident nearby along the contact between the Rogue Formation and the Onion Camp complex. Wright and Wyld (1986) report a xenocrystic Precambrian zircon inheritance in plagiogranite of the Devil's Elbow ophiolite, interpreted to have formed during the initial rifting of the Rattlesnake Creek terrane, the correlative unit of the Onion Camp complex. By analogy, the discordance pattern displayed by sample EDM-89 (Figure 2-30) can be explained by Pb loss disturbing zircon grains whose undisturbed pattern would define an inheritance trajectory with a lower intercept age of approximately 160-165 Ma and a Late Proterozoic upper intercept age. The analyses of additional zircon fractions should test the validity of this interpretation.

Late stage dacite dike. Sample S-3 was collected from a dacite dike that is part of a post-metamorphic dike swarm that cuts the regional Nevadan foliation. Dick (1976) reported numerous K-Ar ages of these dikes ranging in age from 145-150 Ma. The concordant U-Pb zircon analyses of 150 ma (Figure 2-30) agrees with these data.

Structural and Metamorphic Features

Deformational and metamorphic history

The structural and textural features exhibited by the rocks of the study area reflect the multi-stage evolution of the WJB and distinguish a total of four distinct deformational episodes.

Phase 1. The first deformational episode is recorded only locally in the peridotite of the Onion Camp complex and is defined by a pseudomorphed blastomylonitic texture interpreted to record deformation during subsolidus plastic flow of mantle lithosphere beneath a spreading center. Presumably, this deformation accompanied the construction of an ophiolite or primitive arc sequence represented by the volcanic rocks of the Onion Camp

complex in the Triassic and Early Jurassic. The mylonitic foliation is cut by all subsequent structural and textural features.

Phase 2. The second deformational episode is characterized by greenschist to amphibolite facies regional metamorphism of the OCC and produced its tiered metamorphic facies stratigraphy with greenschist grade materials underlain by amphibolite gneiss and schist which are in turn underlain by amphibolite grade serpentinite. $^{40}\text{Ar}/^{39}\text{Ar}$ ages of ~173-169 Ma and cross-cutting dikes of ~175 Ma constrain the deformation and metamorphism to the Middle Jurassic. These ages roughly coincide with the age of Middle Jurassic deformational in the Klamath Mountains province described by Wright and Fahan (1988).

Phase 3. Brittle fragmentation, cataclasis, and pervasive greenschist grade and lower hydrothermal alteration followed the Middle Jurassic deformational episode. Characteristic features of this phase occur in all lithologies of the Onion Camp complex and the Josephine ophiolite, but are distinctly absent in slightly younger arc plutonic rocks, the Briggs Creek amphibolite, and overlap sequence. This deformational episode is therefore interpreted to record the extension-related fragmentation and alteration associated with the inter-arc rifting of the Onion Camp complex and the formation of the Late Middle to Late Jurassic ophiolite.

Phase 4. Late Jurassic contractile deformation related to the tectonic collapse of the Josephine basin resulted in regional metamorphism and deformation 1) at greenschist to sub-greenschist facies in rocks located to the east of the Chetco Pass fault, and 2) at amphibolite facies conditions in rocks to the west of the Chetco Pass fault. This deformation produced the regionally extensive folds and faults apparent on the geologic maps (Plates 1-11). Subsequent reactivation of some of the Nevadan faults has probably occurred in Tertiary and Quaternary time during ongoing uplift and erosion of the region.

Mesoscopic structural features

The mesoscopic structural features exhibited by rocks in the study area include multiple generations of folds, metamorphic and shear foliations, mineral and intersection lineations, and fragmental textures and shears associated with the Middle Jurassic and Late Jurassic contractile deformation (phases 2 and 4 above).

Middle Jurassic structures. Middle Jurassic deformation (phase 2 above) is restricted to the rocks of the OCC except for the mafic intrusive complex rocks. The primary structural feature is a well- to moderately-developed gneissose to schistose foliation defined by the alignment of metamorphic mineral grains, e.g., mica, platy amphibole, and quartz ribbons (Figure 2-31). This contrasts sharply with the nondeformed and nonmetamorphosed volcanic and sedimentary stratas of the Rogue-Galice-Fiddler Mountain overlap sequence (Figure 2-32).

Where preserved, sedimentary layering in the OCC rocks is almost always oriented parallel to the foliation. Tight intrafolial folds are locally preserved in outcrops comprised of millimeter-scale laminated, siliceous and tuffaceous meta-argillite (Figure 2-33). High flattening strains are suggested in the tight fold regions where the line length of the sedimentary lamination is generally >20 times the intrafolial width. High flattening strains are also indicated by the highly flattened, equant shapes of metamorphic mineral grains, e.g., hornblende in amphibolite schist, and by the isolated boudins of chert and basalt blocks in the banded metatuff and meta-argillite outcrops (Figure 2-21). Often, the foliation in greenschist facies rocks of the OCC is oriented sub-parallel to the Late Jurassic regional foliation suggesting that the earlier feature has been transposed.

Linear features of the Middle Jurassic deformational event are less conspicuous. Mineral lineations were only locally observed in some amphibolite tectonite outcrops. However, an intersection lineation is common in schistose rocks of the OCC, probably resulting from the intersection of the Middle Jurassic foliation and the Late Jurassic regional foliation (Figure 2-34). At least two and possibly three generations of folds are evident in

Figure 2-31. Photomicrograph of highly strained, greenschist metavolcanic tuff from the Onion Camp complex (polarized light, field of view ~3 mm). The rock consists of chlorite-actinolite-quartz-albite-oxide. Note the well-developed foliation and compare it to the relatively nondeformed rocks of the overlap sequence (figure 2-32).



Figure 2-32. Photomicrograph of clinopyroxene- and plagioclase-phyric basalt typical of Rogue Formation basalts (plane light above and polarized light below, field of view ~3 mm). Note the complete lack of evidence for deformation, especially when compared to the highly strained metavolcanic rocks of the OCC (Figure 2-31).

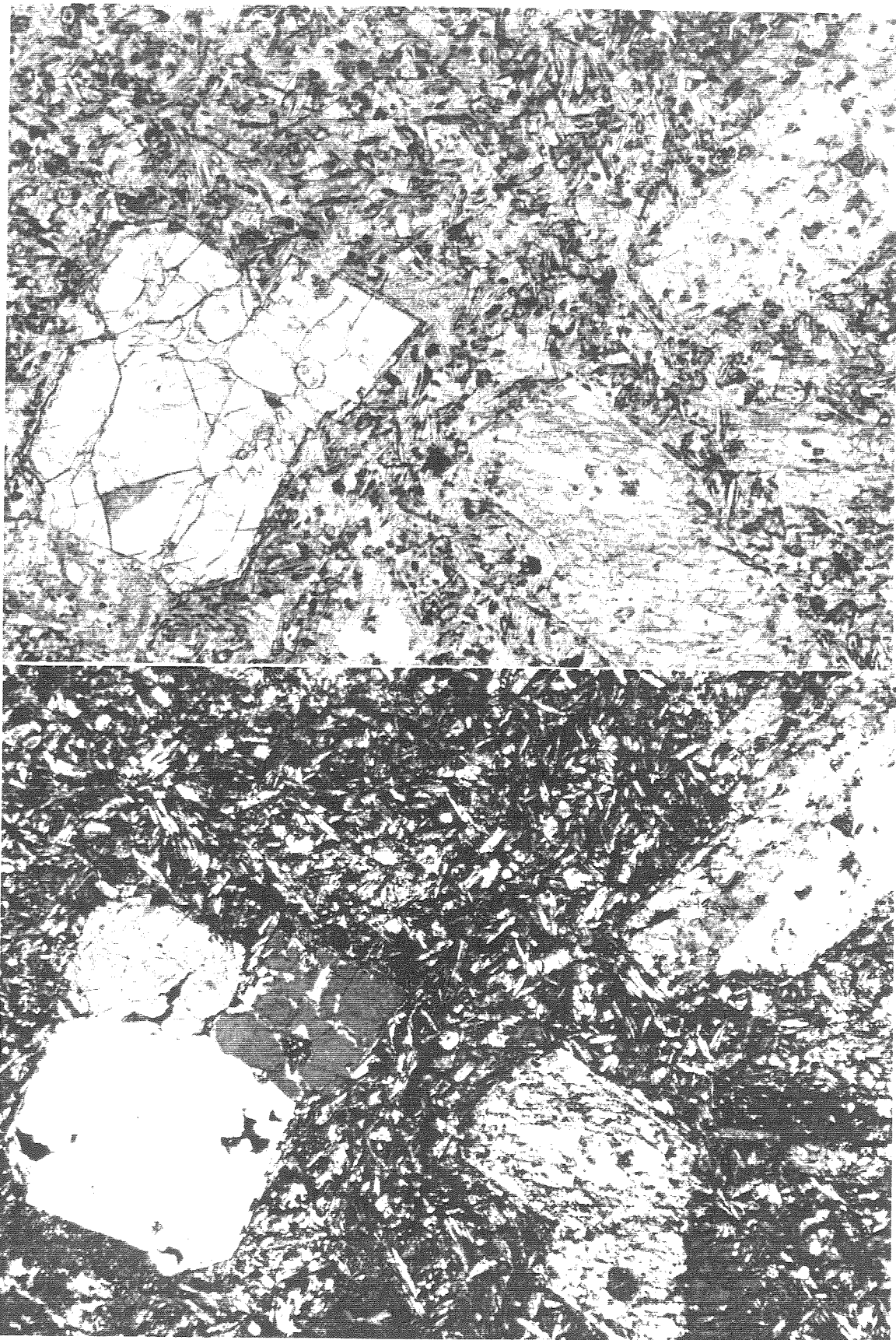
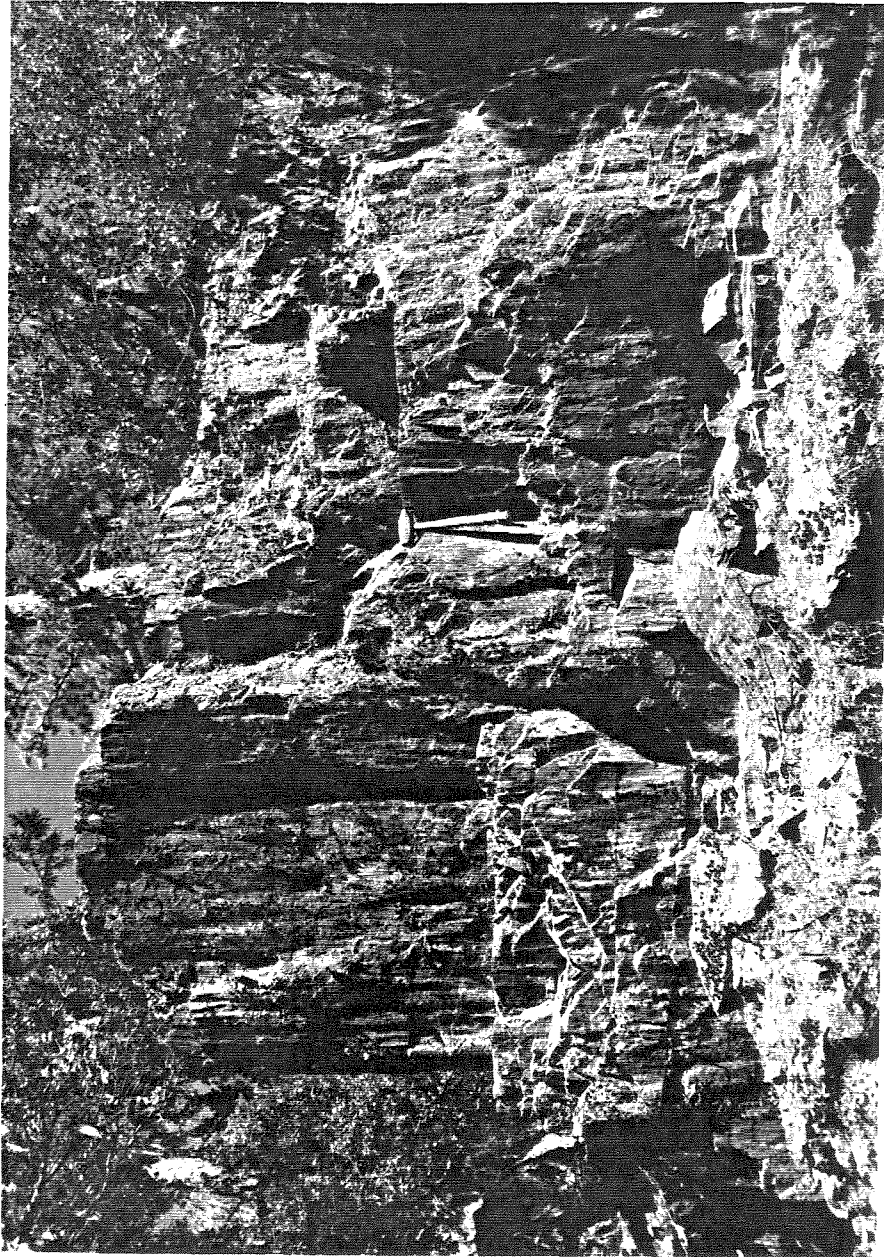


Figure 2-33. Photomicrograph of a highly strained silicic argillite from the OCC showing a tightly folded compositional boundary between a quartz-rich and argillaceous layer (plane light above and polarized light below, field of view ~3 mm).



Figure 2-34. Photograph of an outcrop of metachert in the OCC (note hammer for scale). The outcrop illustrates the steeply inclined intersection lineation typical of metavolcanic and metasedimentary rocks of the OCC.



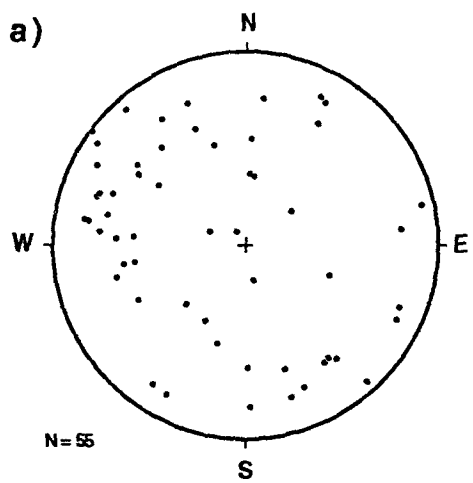
some chert outcrops, but it is unclear to which deformational episode these relate. In either case, the OCC rocks appear to have experienced multiple episodes of folding.

Stereographic plots of OCC structural features are shown in Figure 2-35a-b, and illustrate a multi-deformational history for the complex. Figure 2-35a shows the apparent random dispersal of amphibolite foliations, probably the result of at least two later folding events (F1, F2, and F3, see below). In Figure 2-35b, the intersection lineation described above plots in a scattered pattern, most likely the result of dispersal by F3 folds (see below).

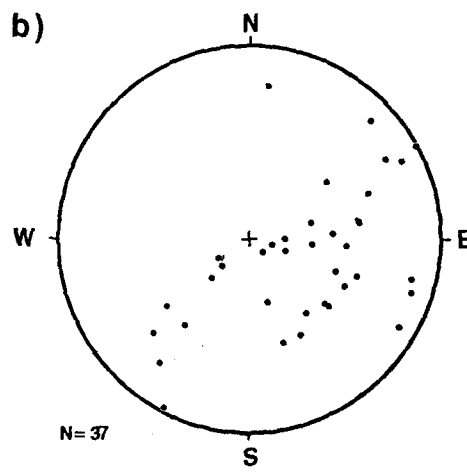
Late Jurassic (Nevadan) structures. Late Jurassic structures occur in all rocks of the study area and include a northeast striking, southeast dipping regional foliation (S1), a co-planar, locally developed syn-metamorphic foliation (S2), syn-metamorphic shallowly NE-SW plunging, tight F1 and F2 folds; post-metamorphic moderately east plunging, open F3 folds, and kink bands (Figures 2-35c-g). Regional foliations (S1 and S2) range from well-developed to absent depending on the rock type. The foliation is defined by 1) gneissose layering in the Briggs Creek amphibolite, 2) planar augen bounded by anastomosing shear bands in sheared peridotite, and 3) platy mineral alignment and a slaty cleavage in fine-grained, greenschist facies sediments and tuffaceous volcanic rocks of the OCC and the overlap sequence (Rogue, Galice, and Fiddler Mountain olistostromal complex). Massive lava and breccia units generally do not exhibit a Late Jurassic foliation (e.g., Figure 2-32). The S2 foliation is rare and is restricted to the slaty rocks and where it occurs in the axial planar regions of tight F2 folds which fold S1.

The styles of these features may vary between map units, but the structural orientations are the same illustrating how all rocks of the region were deformed under the same regional stresses. For example, the regional foliation in both the OCC and the overlap sequence is essentially coplanar (Figures 2-35c-d). The predominant orientation of the Late Jurassic foliations in the BCA and the peridotite units is also NE-striking and SE-dipping, though more scatter in the data exist. The scatter is produced by well-developed

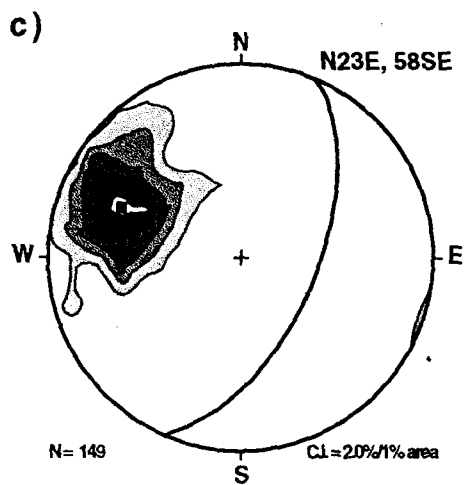
Figure 2-35a-d. Stereographic projections of structural data: a) poles to amphibolite gneiss of the OCC, b) intersection lineation between the Middle Jurassic and Late Jurassic metamorphic foliations, c) poles to regional Nevada foliation in the OCC, d) poles to regional Nevada foliation in the overlap assemblage. See text for more details.



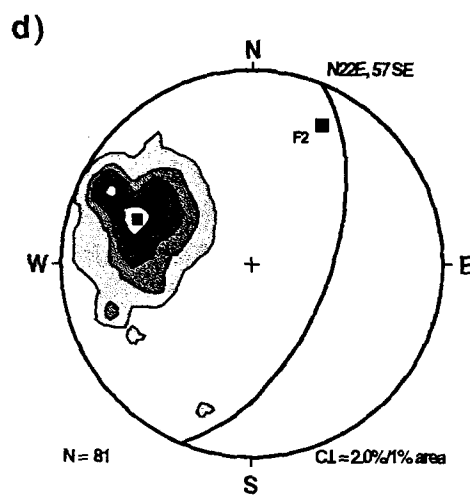
Poles to amphibolite foliation -
Onion Camp complex



Intersection lineation -
Onion Camp complex

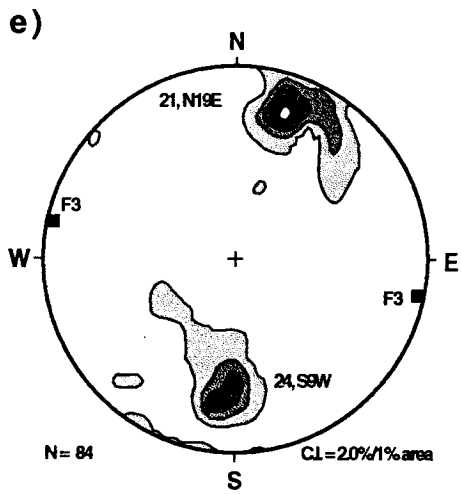


Poles to regional foliation -
Onion Camp complex

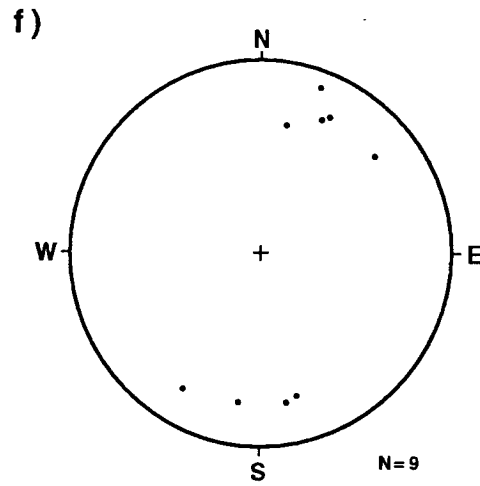


Poles to regional foliation -
Overlap assemblage

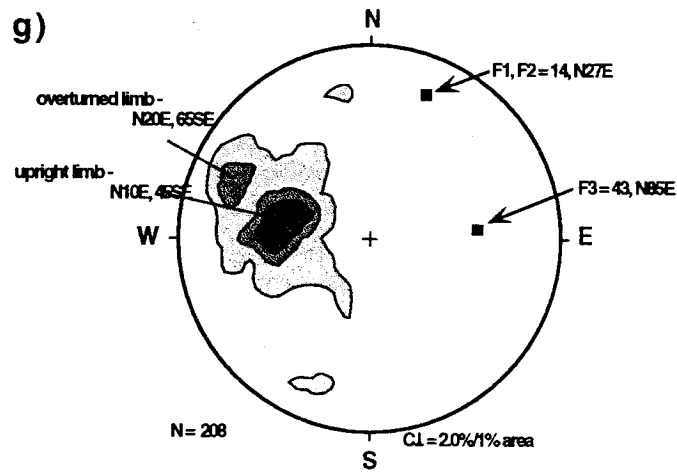
Figure 2-35e-g. Stereographic projections of structural data: e) F1 and F2 fold axes, intersection lineations, and mineral lineations measured in the BCA, f) F1 and F2 fold axes measured in the Galice Formation, g) poles to bedding measured in the Rogue Formation. See text for more details.



Fold axes and stretching lineations -
Briggs Creek amphibolite
(F1, F2, L_{min}, L_{int})



F1 and F2 Fold axes - Galice Formation



Poles to bedding - Rogue Formation

folding (F2) of the S1 foliation in the BCA, and by the anastomosing style of foliations and shears in the peridotite units.

The syn-metamorphic folds and linear structural features of the study area are generally NE-SW trending. Folds are most commonly observed in the BCA where two generations of folds deform the gneissic banding (S1). Fold styles span a wide range and include tight chevron, similar, and similar isoclinal with attenuated and slipped out limbs. BCA fold axes, mineral and intersection lineations define two distinct maxima, one plunging gently NNE and the other gently SSW. The dispersal is consistent with open folding of an originally NNE-SSW trending linear features about a shallowly plunging E-W trending folds (F3).

A similar geometry of folding is apparent from the overlap sequence. F1 and F2 type folds are scarce in the field due to a combination of poor exposure and because the fold limbs are often truncated. Where observed they are tight, similar folds with truncated limbs that plunge gently NNE-SSW (Figure 2-35f). These folds show west-vergence and generally have one moderately to steeply overturned limb and a moderately inclined upright limb. A plot of all bedding orientations collected from throughout the overlap sequence also define a shallow NNE-plunging west-vergent fold (Figure 2-35g). Note that the primary maxima defined by the poles to the regional foliation in the overlap sequence (Figure 2-35d) coincide with the axial plane to this fold pattern. These data also show a subtle dispersion about a moderately eastward-plunging fold axis, similar to the orientations of open F3-style folds observed in the field. In Figure 2-35d, the secondary maxima in the data is interpreted as a cluster of "overturned" S1 foliations which, together with the primary maxima, define the F2 folds. Thus the F1 and F2 folds are approximately coaxial and probably formed during one deformational event.

In summary, the Late Jurassic (Nevadan) mesoscopic structural features are remarkably consistent across the study area. The principal features are 1) NNE-SSW

trending synmetamorphic folds with moderately SE dipping axial planes, and 2) post metamorphic shallowly to moderately east plunging open folds.

Regional fold structures.

An understanding of the mesoscopic structures, highlighted in Figure 2-36, helps to explain the regional fold patterns that define the map outcrop pattern (Plates 1-11). In addition to the previously mentioned regional Nevadan fold patterns, at least two other sets of fold structures occur in the study area. One of these is distinctly pre-Nevadan, probably related to the Middle Jurassic deformational (Siskiyou) event, and is only observed in the Onion Camp complex map units. Another is a series of upright, open folds that trend at high angles to the dominant northeast trending regional structures and are interpreted as late- or post-Nevadan deformational features. The superposition of these three fold styles has produced, in part, the complex patterns of Plate 1 and the larger scale geologic maps (e.g., Plates 3 and 6).

For example, the post-metamorphic open (F3) folds produce the kinks in the overall northeast trend of the faults and lithologic contacts about moderately east plunging axes (Plate 1 and Figure 2-36). Map scale examples of these folds are best illustrated by the basal contact of the overlap assemblage strata (Plate 1).





The complex map patterns observed near Squaw Mountain (Plates 1 and 6) are examples of structures that are unique to the rocks of the Onion Camp complex. The map patterns are interpreted as fold interference patterns resulting from the superposition of northeast trending Nevadan folds on pre-existing Middle Jurassic structures. The orientation of these older structures is poorly constrained, but is inferred to be highly oblique to the Nevada structures based on the northwest trending outcrop patterns defined by the amphibolite/serpentinite contacts.

The northeast trending Nevadan structures (Figures 2-35 and 2-36) are the dominant structures controlling the map outcrop patterns in the study area. In general, the


Figure 2-36. Small scale, generalized map of Plate 1 showing the primary structural features. Note that, for the sake of clarity, antiformal axial traces have been omitted from the map. In general, an anticlinal regional structure accompanies each synclinal trace. Refer to text for a detailed discussion.

EXPLANATION



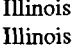
Upper structural layer - overlap sequence

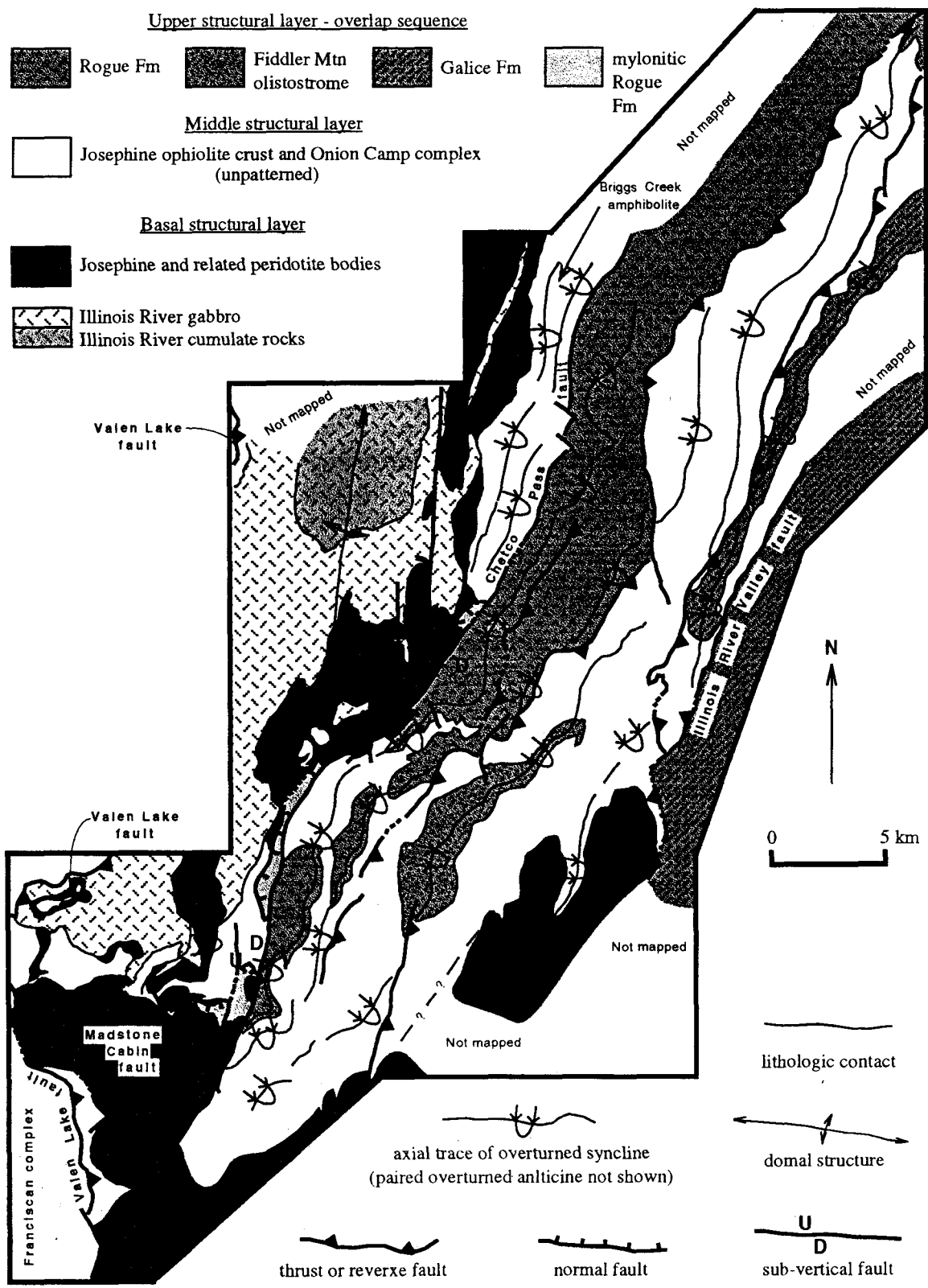
-  Rogue Fm
-  Fiddler Mtn olistostrome
-  Galice Fm
-  mylonitic Rogue Fm

Middle structural layer

-  Josephine ophiolite crust and Onion Camp complex (unpatterned)

Basal structural layer

-  Josephine and related peridotite bodies
-  Illinois River gabbro
-  Illinois River cumulate rocks



— lithologic contact

↔ domal structure

U
D
— sub-vertical fault

— axial trace of overturned syncline (paired overturned anticline not shown)

— thrust or reverse fault

— normal fault

WJB between the Valen Lake thrust and the Illinois River Valley fault consist of four alternating anticlinorial and synclinorial regions from west to east as follows (Plate 1); an anticlinorial region centered on the Illinois River plutonic complex anticlinoria, a synclinorial region centered in the Rogue Formation immediately east of the Chetco Pass fault, an anticlinoria centered on the Onion Camp complex, and a synclinoria centered on the Josephine ophiolite outcrop belt west of Selma. Each of these regions contains smaller magnitude regional scale folds (Figure 2-36). In the region between the Illinois River Valley fault and the Chetco Pass fault, the map patterns are controlled by 1) gently northeastward plunging folds, and 2) steeply eastward dipping axial planar faults that truncate the limbs of the regional folds. The following sequence of events can explain the development of these Nevadan structures: first tight to open folds form with slightly faulted limbs, then the folds tighten with a more pronounced faulting and attenuation of the fold limbs, and finally the slightly oblique cross-faulting and boudinage structures result from more extreme contraction and flattening.

Faults

Valen Lake fault. The Valen Lake fault is an eastward-dipping thrust fault that separates the Latest Jurassic (Tithonian) to Cretaceous Dothan Formation from a hanging-wall plate of the western Jurassic belt (WJB). The fault has not been examined in detail during this study and is only mentioned here because it bounds the western part of the study area. The fault, originally named by Ramp (1975) for convenience in describing the local geology of the upper Chetco River drainage, can be traced to the north and south of the study area over a distance of approximately 400 km. In California, the fault is known as the South Fork fault (Irwin, 1994). Together, the Valen Lake/South Fork fault forms the bounding structure of the Klamath Mountains geological province.

The age and displacement history of the fault are poorly constrained but probably initiated in the Latest Jurassic. The footwall rocks are correlable with Late Jurassic to Early

Cretaceous rocks of the Franciscan complex in California and the Otter Point Formation in Oregon (Coleman, 1972) and are considered to have formed part of an accretionary tectonic prism above an eastward dipping subduction zone. The WJB comprises the hanging wall. The Valen Lake/South Fork fault is therefore interpreted to represent the bounding structure separating rocks of the accretionary complex from the marginal ocean basin arc and ophiolitic rocks and probably was active during the formation of much, if not all, of the accretionary complex. Related structures probably include the Coast Range thrust in California that places the Coast Range ophiolite over rocks of the Franciscan complex and the thrust klippe exposed to the northwest of the study area that emplace ophiolitic materials, e.g., the Snow Camp ophiolite (Blake and others, 1985) over rocks of the Colebrook schist and Otter Point Formation (see Figure 2-1).

Extensional shear zones bordering the Illinois River plutonic complex. Low angle faults occur to the west of the Chetco Pass and to the north of the Madstone Cabin faults (Plates 1, 2, 3, and 5). These structures provide subtle, yet very important clues regarding the emplacement of the Illinois River plutonic complex (IRPC) and the structural evolution of its wallrocks. The footwalls of these low angle faults consist of either IRPC gabbro, massive wehrlite, or tectonized dunite and harzburgite. Their hanging walls essentially contain highly attenuated oceanic crust that includes, from base to top, gneissic metagabbro, and mylonitic greenstone, chert, and fragmental volcanic rocks. The mylonitic rocks exhibit a pronounced foliation and a weak lineation. These sections are interpreted to represent attenuated rocks of the Josephine ophiolite, OCC, and overlying Rogue Formation.

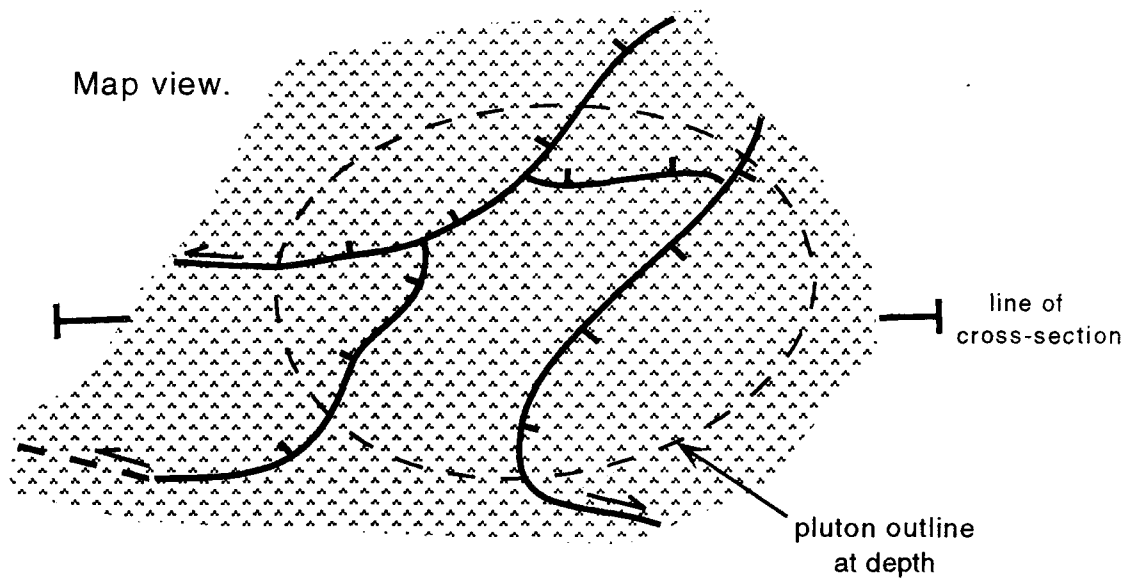
The structural evolution of these shear zones is interpreted to relate to the intrusion of the IRPC based on the following observations: 1) a thin layer of mantle peridotite commonly separates the IRPC from amphibolitic crustal rocks suggesting that the complex was emplaced just below the base of the crust, 2) greatly thickened amphibolitic crustal rocks occur along the boundaries of the plutonic complex, and 3) highly attenuated crust

and extensional shear zones occur in the roof regions of the IRPC. These features suggest a “return flow” mechanism for pluton emplacement whereby thermally weakened basal crust overlying the IRPC begins to attenuate and migrate toward the margins of the inflating plutonic complex (Figure 2-37). For some reason the peridotite remains “attached” to the roof of the complex and serves as a barrier beneath which the hornblende pegmatite and tonalite-trondjemite sills of the IRPC accumulate. Separation across these structures is estimated at approximately 5 kilometers or less based on the average estimated thickness of oceanic crust. Displacements of approximately twice the separation seem likely considering the characteristic low angle of the faults. The age of displacement is constrained to post- or syn-IRPC (161-157 Ma) and pre-Chetco Pass faulting.

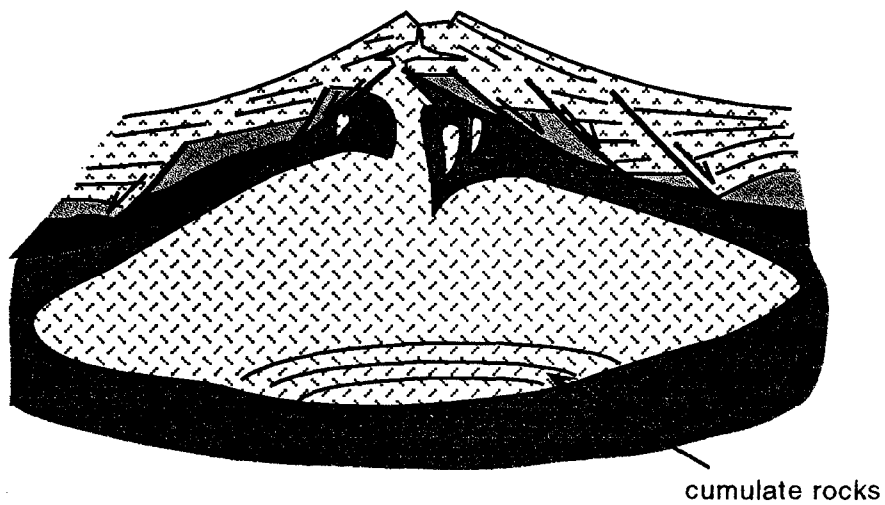
Madstone Cabin fault. The Madstone Cabin thrust fault (MCT) is a very distinctive feature in the southwestern part of the study area and separates mostly unserpentinized Josephine peridotite from underlying amphibolite gneiss and schist and metaplutonic rocks of the IRPC. Ramp (1975), who named the fault, noticed that a thin slice of Rogue Formation volcanic rocks occurred immediately beneath the fault near Emilly (sic) Cabin suggesting that the MCT emplaced the Josephine peridotite over the rocks of the IRPC and the Rogue Formation. However, Ramp (1975) did not extend the MCT beyond the Emilly Cabin region, and noted the extreme complexity of the geology at the northeastern extent of the MCT and encouraged “more thorough study” to “work out the details of this structural problem” (p. 19, Ramp, 1975). Subsequent workers (e.g., Page and others, 1981) extended the MCT to the east and northeast along several splay faults that border the northeast trending finger-like extensions of the Josephine peridotite (Plate 1). The resulting map pattern and interpretation suggested that the geologically complex Emilly Cabin region “spawned” an imbricate thrust stack above the Illinois River plutonic complex and its wallrocks.

Blake and others (1985) used this interpretation to propose that the MCT is a regionally extensive thrust fault that separates the Josephine ophiolite from the Rogue River

Figure 2-37. Diagrammatic map and cross-section view of the Illinois River plutonic complex (IRPC) and surrounding wallrocks at the time of emplacement. The figure shows how the roof region of the complex is thinned and attenuated along ductile, extensional shear zones as the plutonic complex is emplaced. This helps to explain the low-angle, highly attenuated crustal section which occur locally in the roof region of the IRPC. Refer to text for discussion.



Cross-section view.



EXPLANATION

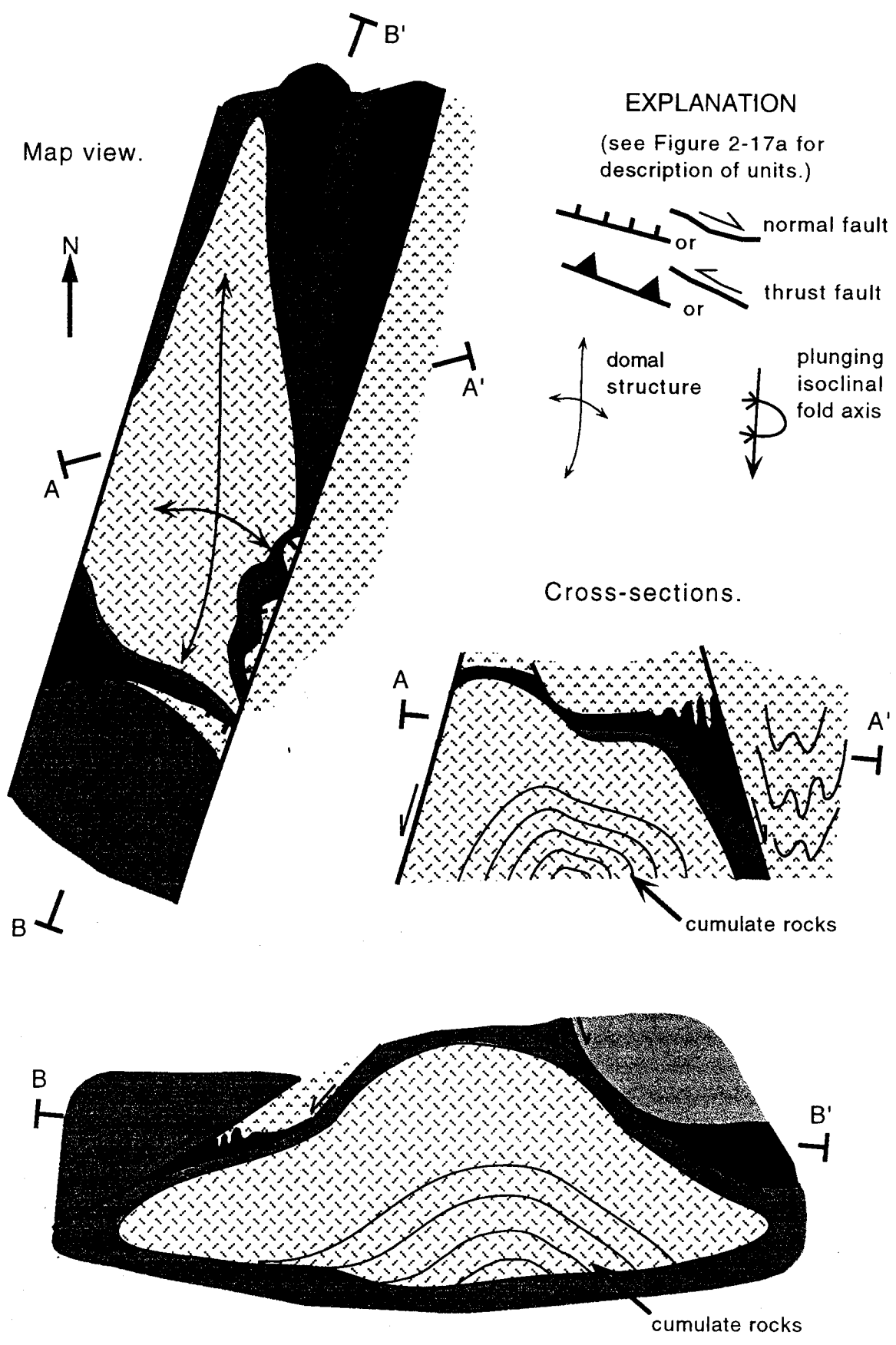
- | | | | |
|--|---|--|--|
| | arc volcanic rocks, Rogue Formation | | Composite oceanic crustal sequence, Josephine ophiolite and Rattlesnake Creek terrane |
| | arc plutonic rocks, Illinois River plutonic complex | | greenschist facies |
| | | | amphibolite facies |
| | | | depleted mantle peridotite, Josephine peridotite |
| | normal fault, map view | | normal fault, cross-section view |

Island arc complex of Garcia (1982). To Cannat and Boudier (1985) and Harper et al., in press (1995), this regionally extensive structure at the base of a large peridotite sheet resembled many of the large thrust faults which are believed to have emplaced ophiolite sheets continental margins (e.g., Ghent and Stout, 1981). By analogy, the MCT was interpreted as the emplacement fault of the Josephine ophiolite as it was thrust over the Rogue River island arc complex.

The findings of this study sharply contrast with the regional thrust interpretation for the MCT and agree with the original mapping of Ramp (1975). The Madstone Cabin thrust (MCT) does not appear to extend east of the Emilly Cabin region where it is truncated by the Chetco Pass fault (CPF). Specific field relations in support of this new interpretation include: 1) a splay fault of the CPF, exposed at the confluence of Henry Creek and the Little Chetco River, exhibits subvertical shear bands in serpentinite that clearly truncate subhorizontal foliation in amphibolitic orthogneiss oriented parallel to the trace of the MCT; and 2) to the west of the CPF planar structures in the footwall of the MCT strike east-west and are shallowly inclined to subhorizontal, but to the east, planar structures strike NNE and are moderately to steeply inclined, sub-parallel to the axial planes of regional folds; and 3) the truncation of the MCT by the CPF in combination with the interpretation of the regional fold patterns described above eliminates the need for the various splay faults and subterranean bounding structures. These relations resolve the heretofore unexplained "disappearance" of these structures along strike toward the NE as shown on previous regional geologic maps (e.g., Blake and others, 1985; Page and others, 1981; Irwin, 1994).

Rather than an emplacement structure, the MCT is herein interpreted to represent a localized structure that formed above during the deformation and elongation of the IRPC (Figure 2-38). The coincidence in the width of the IRPC and the extent of the thrust suggest that the fault formed as the IRPC and its wallrocks were thrust beneath a relatively small fragment of Josephine peridotite, probably as the IRPC was deformed and elongated

Figure 2-38. Diagrammatic map view and cross-sections of the IRPC and its wallrocks at ~157 Ma, during the onset of regional Nevadan deformation. The Madstone Cabin fault (the thrust overriding the southern end of the IRPC) and the Chetco Pass fault (the high angle structure bounding the complex on the east) are related structures forming in response to WNW-ESE directed shortening and NNE-SSW directed elongation of the IRPC. This scenario incorporates the structural data observed in the field (e.g. Figure 2-35e).



at about 155-157 Ma. Radiometric age data from the footwall of the MCT constrain displacement to have ended by about 151 Ma (Harper et al., 1994).

Chetco Pass fault system. The CPF, and its related structures, exhibit the greatest demonstrable offset of any faults in the WJB. The main trace of the fault separates shallow level, sub-greenschist facies rocks from amphibolite grade rocks of the IRPC and BCA. The fault zone is informally named herein for convenience after its geomorphic expression in Chetco Pass, the lowest elevation saddle on the ridgeline separating the upper Chetco River drainage from the central Illinois River drainage. Previous workers have interpreted this structure as a high angle subterranean bounding “thrust” (e.g., Blake and others, 1985), upthrown on the east and truncated by the MCT. However, the findings of this study indicate exactly the opposite, the fault is downthrown on the east and truncates the MCT.

The CPF zone has probably experienced a protracted displacement history with evidence of both Nevadan offset (discussed below) and more recent reactivation related to the uplift history of the region. For example, the fault zone is an inherent zone of weakness in the region with geomorphic expression along its entire trend as ridgeline saddles and waterfalls, e.g., Illinois River Falls and Rainie Falls in the Rogue River. Another peculiar geomorphic feature consists of a series of elevated river gravels preserved on ridgelines and old gravels in Briggs Valley that essentially follow the trend of the fault from the Illinois River to the Rogue River (e.g., see maps of the Eight Dollar Mountain and Chrome Ridge 7.5 ‘ quadrangles; also see “aureliferous gravels of the second cycle of erosion,” Diller, 1914; and descriptions in Wells and others, 1949). It is interesting to speculate that these gravels were deposited by the “proto-Illinois River” that, instead of flowing west-northwest, once flowed northeast along the trend of the CPF and joined the Rogue River near the present day village of Galice. This scenario suggests that the CPF once bounded an alluviated valley similar to the Illinois River valley and its bounding Illinois River Valley fault (see discussion below).

The main trace of the CPF is the only fault internal to the WJB that traverses the entire belt. It is truncated at both ends by the Valen Lake thrust. The main trace fault zone is characterized by a crush zone of variable width that typically measures between 1-10 meters wide and is widest where the fault occurs in serpentinite. Orientations of shear foliations and map outcrop patterns indicate that the fault is a subvertical to steeply inclined, with dips ranging from approximately 70° NW to 60° SE. Numerous secondary splay faults and parallel faults are associated with the main trace fault. Only the larger of these are shown on the geologic maps (Plates 1, 2, 3, and 5). Like the main trace fault, the secondary faults are typically high angle and often bound narrow slivers of crustal rocks.

Systematic differences in the displacement history across the main fault are evident from south to north along the trend of the fault. At its southern extent, the fault separates relatively un-serpentinized Josephine peridotite from moderately to highly serpentinized Josephine peridotite and Onion Camp complex serpentinite, and also truncates the southern extent of the amphibolite tectonite body exposed beneath the MCT. In the region of Chetco Pass, the fault separates relatively un-serpentinized Pearsoll Peak peridotite from a tectonic melange of serpentinite, ophiolitic crustal rocks and strata of the Rogue-Galice-Fiddler Mountain overlap sequence. Finally, in the northern part of the study area and extending northward beyond it, the fault separates the Briggs Creek amphibolite from rocks of the Rogue Formation. The south to north progression from mantle lithosphere, into ophiolitic melange overlain by surficial deposits of the Rogue Formation, suggests that the region to the east of the fault represents a gently northeast plunging, natural cross-section through composite oceanic lithosphere. No such systematic change in structural level exists in the terrane to the west of the fault implying that displacement across the CPF increases significantly from south to north, and must have rotated about a pivot point located to the south of its truncation by the Valen Lake thrust.

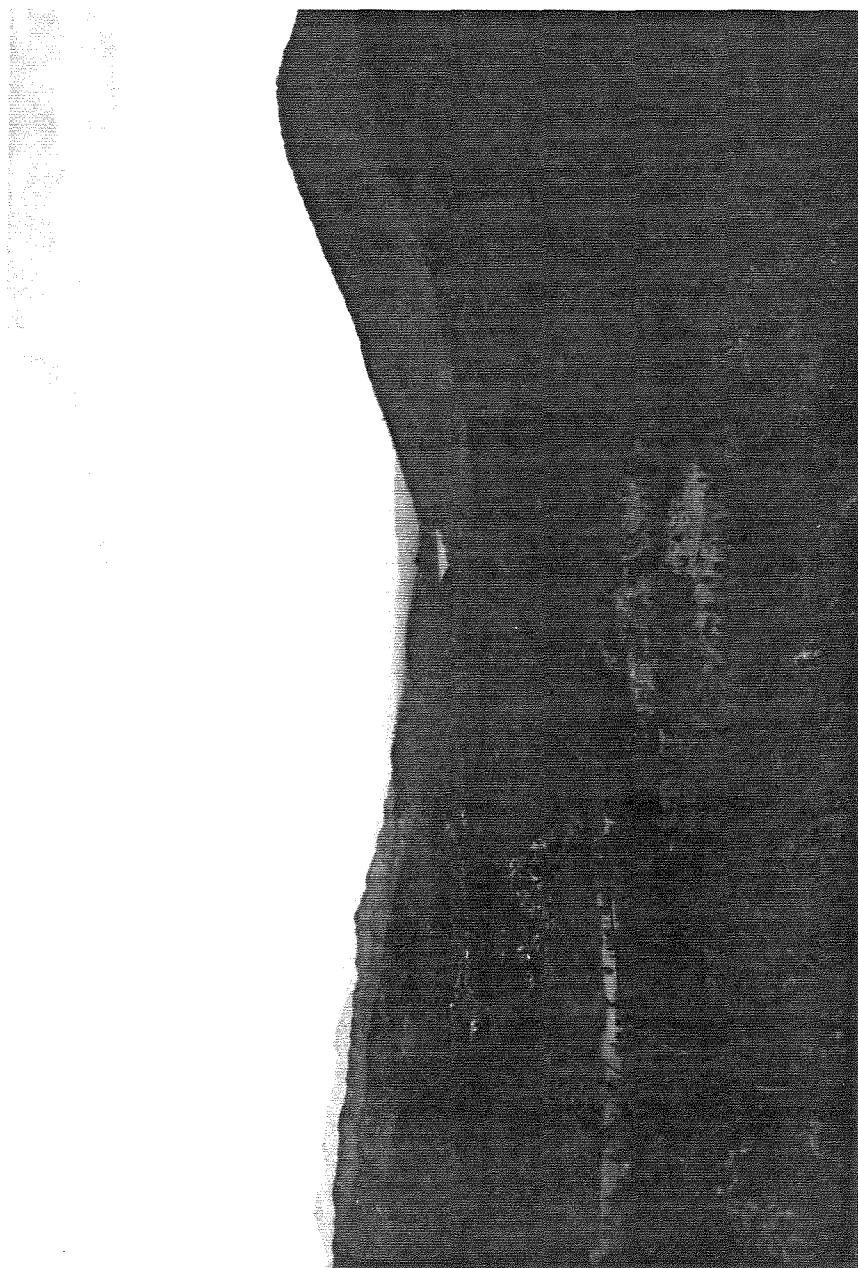
The displacement across CPF zone is constrained to ~2-4 km at its southern extent, enough to truncate the amphibolite body beneath Chetco Peak, and ~10-15 kilometers at the

northern part of the study area, enough to juxtapose the amphibolite facies rocks of the BCA (3-5 kb) and the sub-greenschist grade rocks of the Rogue Formation. The amount of lateral displacement is nonconstrained, but is probably no greater than the vertical displacement. If displacement was primarily vertical, the observation that the CPF separates an elongate domal structure in the IRPC from a regional synclinoria in the Rogue Formation supports the interpretation that the CPF is the faulted limb of a regional fold and is probably initiated as a Nevadan structure.

Illinois River Valley fault. The Illinois River Valley and Deer Creek Valley are bounded on their west sides by a high angle fault, called the Illinois River Valley fault (IRVF) in this report, that separates strata of the Galice Formation on the east from the Josephine ophiolite and OCC peridotite mass on the west. The fault zone is marked by highly sheared serpentinite with anastomosing shear bands that strike NE-SW and are variably inclined ranging from subvertical to moderately west dipping. Field measurements and map outcrop patterns of the shear zone indicates that the fault dips shallowly to moderately to the west (also see Ramp, 1986). The occurrence of deeper level rocks on the west combined with the structural data suggests that the fault is a westward dipping thrust and reverse fault.

The overall parallel trend of the IRVF with the Nevadan structural grain of the WJB suggests that the fault originated as a Nevadan structure, probably as a faulted fold limb. However, its anomalous westward inclination combined with several lines of geomorphic evidence suggest that the fault has experienced Quaternary, if not Holocene, offset. Quaternary expression of the fault includes: 1) broad alluviated plains in the footwall (Figure 2-39), 2) several levels of bench river gravels to the west of the fault that range from ~100-800 feet above the present stream (aureiferous gravels of the third cycle of erosion, Diller, 1914) (Plate 6), and 3) the fault coincides with a break in the otherwise gradual regional topographic slope defined by a decrease in maximum elevations from west to east across the region (Figure 2-39).

Figure 2-39. Photograph looking SSW along the trace of the Illinois River Valley fault. The fault runs along the break in slope at the base of Eight Dollar Mountain (the conical shaped mountain at the right of the photo) and at a more subtle break in slope at the foot of the hills in the foreground. The fault separates the alluviated lowlands of the area around Selma from the Josephine peridotite of Eight Dollar Mountain. The high Siskiyou Mountains form the horizon in the center of the photo.



In contrast to a tectonic explanation, the occurrence of the low-lying alluviated valleys may have resulted simply from the differential weathering and erosion of the Galice Formation lithologies relative to the peridotite and ophiolitic crustal rocks. However, in the northeastern corner of the study area, the trend is defined by the western extent of these alluviated plains that cuts obliquely across the lithologic belts. It therefore seems likely that the IRVF system at least experienced Quaternary offset, and is worthy of closer study to determine whether it may pose a modern seismic risk.

Other Nevadan faults. Numerous irregular, generally northeast trending, unnamed faults occur in the region bounded by the IRVF and CPF. These faults occur along the borders of serpentinitized peridotite bodies and are often marked by sheared serpentinite where they cut crustal units. It must be noted that essentially every body of serpentinite and peridotite occurring in this region exhibits evidence of shearing at its border. The dominant orientation of these structures is approximately N30E and 55-70° SE parallel to the regional foliation and rock cleavage exhibited by all lithologies of this portion of the WJB, but variations from this trend do occur where, along parts of their individual traces, some faults are oriented slightly oblique to the regional structural trend.

The faults whose orientations generally parallel the regional structural grain tend to occur along lithologic contacts and regional fold limbs, and are interpreted to represent shear zones that developed during Nevadan contractional deformation. The slightly oblique faults truncate regional fold trends (Plate 1) and are interpreted to have formed as relatively late Nevadan features and form regional boudinage structures reflecting the relatively high degrees of flattening strain that affected the region. Little evidence exists to constrain the amounts of displacement across these faults except for the fact that similar map units occur on either side of most faults. These relations constrain displacements to 1-2 kilometers at most with considerably less displacement likely.

Summary

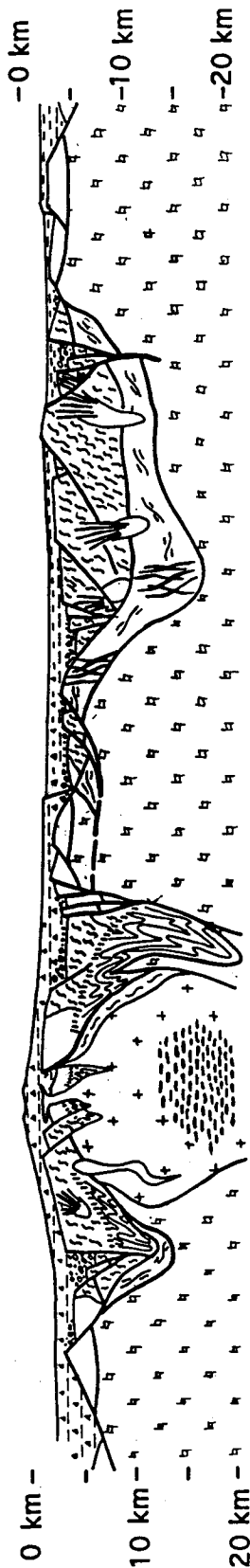
The stratigraphic record of the WJB in the southern Oregon Klamath Mountains province spans the Late Triassic-Early Jurassic to Late Jurassic and records the multi phase evolution of oceanic lithosphere that formed primarily along the western North American margin. The principal elements of the belt include 1) the Late Triassic to Early Jurassic Onion Camp complex (OCC), 2) the Middle to Late Jurassic Josephine ophiolite, 3) the Late Jurassic Rogue River oceanic island arc plutonic complex (IRPC), and 4) a Late Callovian to Kimmeridgian sedimentary and volcanogenic cover sequence. Structural and stratigraphic relations indicate that the Josephine ophiolite and OCC together comprise the basement substratum and country rock for the Rogue River arc rocks and the cover sequence (Figure 2-40). Thus the WJB defines a crude three-layered stratigraphy intruded by the IRPC, with 1) OCC and Josephine mantle peridotite forming the basal layer, 2) Josephine and OCC crust the intermediate layer, and 3) the cover sequence the upper layer (Figure 2-40).

Onion Camp complex. The OCC is a composite fragment of oceanic lithosphere. It consist of variably serpentinized and sheared peridotite, heterogeneous mafic intrusive rocks, N-MORB and WPB pillow lavas and massive greenstone, Late Triassic-Early Jurassic chert, and intercalated chert, silicic argillite, and mafic to intermediate tuff. The age, lithologic, and field relations combined with distinctive geochemical signatures unequivocally correlate the OCC with the RCT and the WTrPz belt. Therefore, the OCC is an allochthonous block within the WJB that provides important information regarding the geologic and tectonic evolution of the region.

OCC rocks have experienced multiple episodes of deformation and alteration including: 1) a Middle Jurassic greenschist to amphibolite facies regional metamorphism and penetrative deformation, 2) Late Middle to Late Jurassic hydrothermal alteration and brittle fragmentation, and 3) Late Jurassic lower greenschist to sub-greenschist facies regionally metamorphism and locally penetrative deformation.

Figure 2-40. Reconstructed cross-section cartoon of the central Illinois River drainage area immediately prior to Late Jurassic (Nevadan) deformation.

RECONSTRUCTION OF THE ROGUE RIVER ARC SYSTEM



arc volcanic deposits interlayered with marginal basin flysch deposits



basal ophiolite clast breccia and mega breccia deposits



arc plutonic complex



rifted fragments of pre-Josephine oceanic crust



rifted fragments of pre-Josephine mantle peridotite



amphibolite tectonite



mafic dikes



Josephine ophiolite mantle peridotite

Rocks of the OCC are overlain by volcanogenic, pelagic, and olistostromal deposits of the cover sequence, intruded by Josephine mafic dike complexes and gabbros, and bordered at its base and margins by the Josephine peridotite. The OCC is therefore considered to occur in the WJB as a screen of older, composite oceanic lithosphere contained within the Josephine ophiolite and overlapped by interfingering oceanic arc and rift basin deposits.

Josephine ophiolite. The partial to complete ophiolite sequences of the study area are considered outliers of the Josephine ophiolites based on: 1) their association with the Josephine peridotite which connects the type Josephine ophiolite to the central Illinois River area, and 2) their similar age, geochemistry (transitional IAT-MORB signature), field appearance, and overlap by strata of the Galice Formation. Three belts of the ophiolite occur in the study area: 1) the westernmost belt forms part of an amphibolite grade metamorphosed terrane surrounding the IRPC, 2) a central belt occurs as a serpentinite matrix tectonic melange overlain by interbedded ophiolite-derived olistostromal deposits and arc-derived volcanogenic deposits, and 3) an eastern belt that forms a tight syncline with faulted limbs. The age of the ophiolite in the study area is constrained by Callovian radiolarian chert and limestone interbedded with pillow lavas and by a U/Pb zircon age from the Rum Creek metagabbro (Saleeby, 1984), interpreted to represent part of a metamorphosed ophiolite in the country rocks of the IRPC.

Illinois River plutonic complex (IRPC). The IRPC forms the plutonic roots of the arc and consists of 1) ~160-157 Ma main phase troctolite, norite, hornblende gabbro, and diorite-quartz diorite, and 2) a ~157-155 Ma late phase tonalite-trondhjemite sill, and 3) a post-tectonic (post-155 Ma) hornblende gabbro pegmatite sill. Layered cumulates occur at the core of the complex and are mantled by massive gabbro and diorite. Both sills occur beneath sub-horizontal slabs of depleted mantle peridotite interpreted to form the roof of the plutonic complex. Gabbroic and dioritic dikes are common in the roof region and in the surrounding country rocks. The country rocks include the mantle

peridotite correlated with the Josephine peridotite and amphibolite facies metagabbro, amphibolite gneiss and schist, and rare quartzite and are considered to represent composite OCC/Josephine ophiolite crust and mantle lithosphere (Plate 1, cross sections).

Relatively high Sr concentrations suggests that the tonalite-trondhjemite sill is probably not a product of fractional crystallization of the main phase magma, but may represent a partial melt of a low-K tholeiite. No data is available to determine the genetic relationship between the gabbro sill and the earlier intrusions.

Except for the post-tectonic gabbro sill, the plutonic complex was deformed into an elongate domal structure, thoroughly recrystallized at and highly ductilely deformed along its margins (Plate 1, cross sections). Concordant structures in the country rocks indicate that the IRPC and its country rock were deformed together. These relations suggest that the IRPC intruded the uppermost mantle lithosphere where it formed as a layered complex, was itself intruded by a slightly younger tonalite-trondhjemite sill of distinctly different composition, and deformed into an elongate domal structure.

Cover sequence. The cover sequence includes stratified rocks of the Galice and Rogue Formations, and the Fiddler Mountain olistostrome complex. The Galice deposits consist of a basal pelagic and hemipelagic sequence that grades upward into Oxfordian-Kimmeridgian flysch containing detrital grains derived from the older Klamath terranes to the east. The pelagic-hemipelagic sequence conformably overlies the Josephine ophiolite, nonconformably overlies the OCC, and interfingers with olistostromal and distal volcanogenic strata. Olistostromal deposits consist primarily of ophiolite derived clasts and are most common at the base of the cover sequence overlapping the OCC. The Rogue Formation in the study area consists of an overall upward coarsening, west to east prograding, submarine volcanic apron deposited upon a variable substratum. Basal strata are generally fine-grained volcanogenic turbidites interbedded with argillite and chert. Upsection and to the west and northwest, the rocks become coarser-grained with an

increase in lava, sills, and volcanic breccia. Trace and rare-earth element abundances characterize these rocks as transitional IAT to calc-alkaline volcanic rocks.

Conclusions

This study of WJB rocks has resulted in a substantial revision of the local and regional geologic maps. The specific changes include 1) the designation of two new map units, the Fiddler Mountain olistostrome complex and the Onion Camp complex, and 2) the reinterpretation of the WJB as a regional fold belt with faulted fold limbs.

Fiddler Mountain olistostrome complex. Previously included with the volcanogenic deposits of the Rogue Formation, the Fiddler Mountains olistostrome deposits are 1) mostly sedimentary deposits, and consist primarily of polymictic megabreccia, breccia and conglomeratic grit with secondary impure chert, and argillite; 2) are laterally discontinuous, always occur at the base of an overlapping sedimentary and volcanogenic sequence otherwise comprised of the Rogue and Galice Formations, and 3) are deposited on a variable substratum comprised of Onion Camp complex and Josephine ophiolite sequence lithologies. A loosely constrained Late Jurassic age from a radiolarian chert interbed is consistent with the inferred stratigraphic age and suggests that deposition of the Fiddler Mountain deposits coincided with the early phases of extension and ophiolite generation in the Josephine basin.

Deposits similar to those of the Fiddler Mountain olistostrome complex occur throughout the Klamath Mountains province at the base of the Galice Formation deposited upon tectonically disrupted portions of the Josephine and Coast Range ophiolites and the Rattlesnake Creek terrane (Ohr, 1987; Wyld and Wright, 1988; Blake and others, 1987; Snoke, 1977; Donato et al., 1995, in review). The regional extent of these deposits and their close association with the ophiolite sequences and the remnant arc suggests that the Josephine marginal ocean basin formed as an older oceanic arc complex rifted apart.

During the early phases of overlap by Galice Formation, the Josephine basin must have contained considerable topographic relief probably as a result of extensional and/or transform faulting.

Onion Camp complex. Rocks of the OCC were previously considered part Rogue Formation. However, the field appearance, lithologic character, age, geochemistry, and deformational histories correlate these rocks with the Rattlesnake Creek terrane, a terrane that forms the western portion of the western Paleozoic and Triassic belt (WTrPz belt). The correlation of the Onion Camp complex with rocks of the Rattlesnake Creek terrane crosses a major terrane bounding fault, the Orleans-Preston Peak thrust, and has the following important implications.

First, the discovery of OCC rocks incorporated within the WJB links two of the original Cordilleran “suspect terranes,” the WJB and the WTrPz belt (Coney et al., 1980). This linkage demonstrates that the criteria for terrane designation, characteristic “internal homogeneity and continuity of stratigraphy, tectonic style and history” and “fundamental discontinuities in stratigraphy” across their boundaries (Coney et al., 1980), are not alone sufficient to infer the suspect character of fault-bounded tectonostratigraphic terranes.

Secondly, the occurrence of OCC rocks in the WJB confirms, without question, the model for the Jurassic tectonic evolution of the western Klamath Mountains province (Snoke, 1977; Saleeby and others, 1982; and Wright and Fahan, 1988). This model invokes rifting across part of a Middle Jurassic oceanic arc and arc basement complex in the WTrPz belt, to form a Late Middle to Late Jurassic marginal ocean basin with the coeval Rogue River oceanic island arc complex and the Josephine inter-arc basin ophiolite sequence. As a result a fragment Middle Jurassic arc basement, the OCC was split off from the province and was carried outboard of Josephine spreading centers where it partly served as the basement for the Rogue arc.

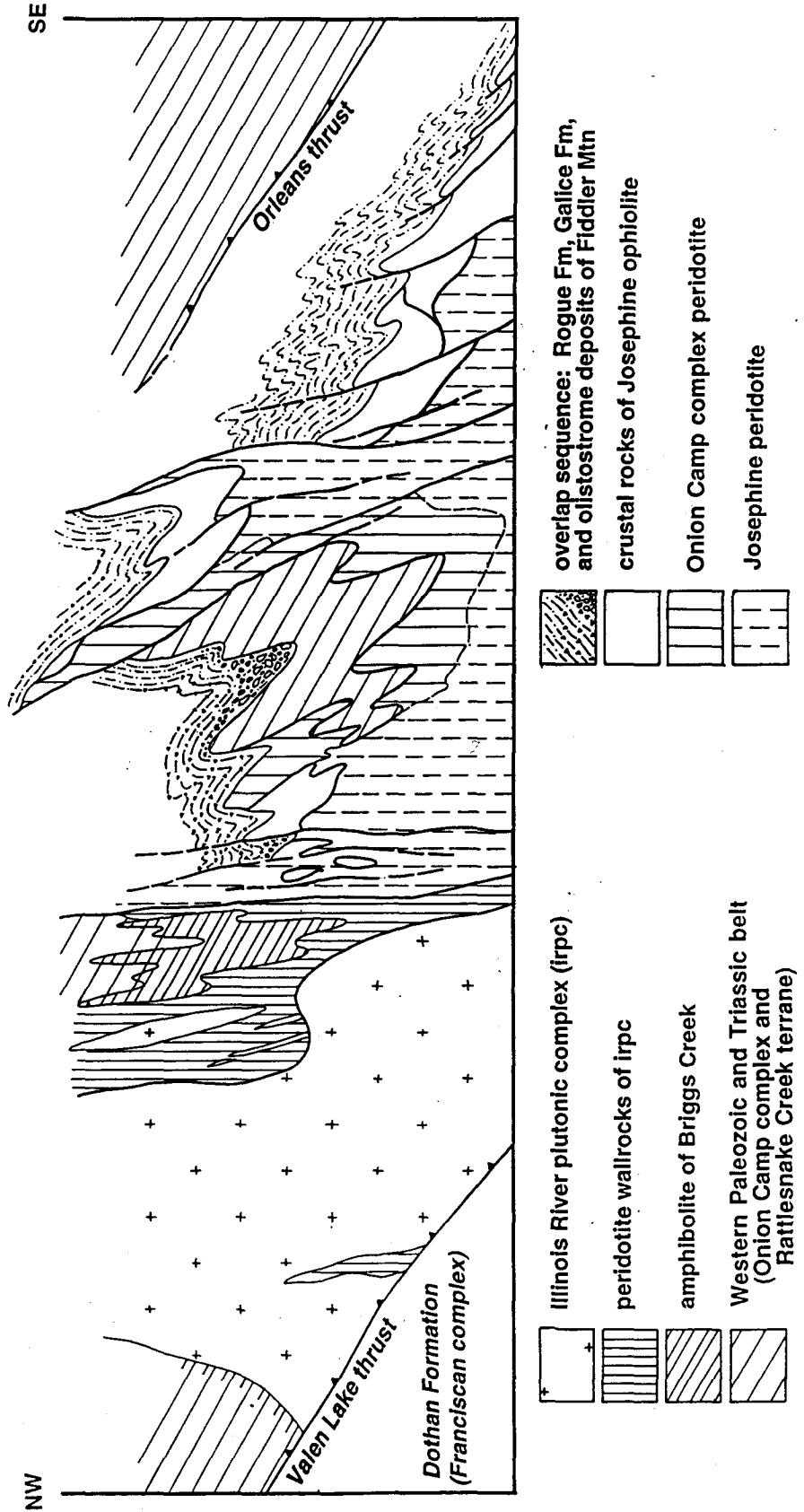
Regional structural interpretation. The regional scale structure of the WJB is best characterized as a fold belt with faulted limbs rather than a series of eastward dipping, thrust bounded “subterranean” units (Blake and others, 1985). The WJB is therefore considered to be a relatively intact, though structurally and stratigraphically complex, fragment of composite marginal basin oceanic lithosphere.

The primary Late Jurassic structures which control the map outcrop patterns within the WJB are: 1) shallowly NE plunging F1 folds, 2) a regional foliation striking ~N20-30E and dipping ~60SE and is oriented axial planar to the regional folds, 3) NE-striking, moderately to steeply SE-dipping high angle faults and are interpreted to truncate the regional fold axes, 4) moderately E plunging F2 folds that “kink” the regional NE-SW trend, 5) interference fold patterns in the OCC created by the intersection of F1 and F2 folds with Middle Jurassic structures whose original orientation is unknown.

When viewed as a thrust belt with regional, shallowly NE-plunging folds, the WJB in southwestern Oregon can be viewed as a natural cross-section through composite oceanic lithosphere. A simplified down plunge view, drawn parallel to the NE-trending regional folds, is shown in Figure 2-41 and illustrates the tight folding patterns with truncated reverse and normal slip faults.

Figure 2-41. Simplified, diagrammatic geologic cross-section of the central Illinois River drainage area, drawn approximately perpendicular to the NNE-SSW regional structural trend and modeled after the geology exposed across the central portion of the study area (Plate 1). The section illustrates the general structural style of the region and its characteristic tight regional folds and faulted fold limbs.

SIMPLIFIED GEOLOGIC CROSS SECTION



References

- Alexander, R.J. and Harper, G.D., 1992, The Josephine ophiolite, an ancient analog for oceanic lithosphere formed at intermediate-spreading ridges, in *Ophiolites and Their Modern Oceanic Analogues*, edited by B. Parsons and P. Browning, pp. 3-38, Blackwell Scientific Publ., Oxford.
- Apted, M.J. and Liou, J.G., 1983, Phase relations among greenschist, epidote-amphibolite, and amphibolite in a basaltic system: *American Journal of Science*, 283-A, 328-354.
- Barnes, C.G., Petersen, S.W., Kistler, R.W., Prestvik, T., and Sundvoll, B., 1992, Tectonic implications of isotopic variation among Jurassic and Early Cretaceous plutons, Klamath Mountains, *Geol. Soc. Amer. Bull.*, **104**, 117-126.
- Barnes, C.G., Donato, M.M., Barnes, M.A., Yule, J.D., Hacker, B.R., and Helper, M.A., 1995, Geochemical compositions of metavolcanic and metasedimentary rocks, western Jurassic and western Paleozoic and Triassic belts, Klamath Mountains, Oregon and California, *U.S. Geol. Surv. Open-file Rept. 95-227-A*, 63 pp.
- Blake, M.C., Jr., D.C. Engebretson, A.S. Jayko, and D. L. Jones, 1985, Tectonostratigraphic terranes in southwest Oregon, in: *Tectonostratigraphic Terranes of the Circum-Pacific Region*, Earth Sci. Ser., edited by D.G. Howell, pp. 147-157, Circum-Pacific Council for Energy and Mineral Resources, Houston, Texas.
- Bonatti, E., and four others, 1974, Ultra-mafic-carbonate breccias from the equatorial Mid-Atlantic ridge, *Marine Geology*, **16**, 83-102.
- Charleton, D.W., 1979, Geology of part of the Ironside Mountain quadrangle, northern California, Klamath Mountains, Ph.D. dissertation, 542pp., UCSB.
- Chen, J.H., and Wasserburg, G.J., 1981, Isotopic determination of uranium in picomole and subpicomole quantities, *Anal. Chem.*, **53**, 2060-2067.
- Coleman, R.G., 1972, The Colebrooke Schist of southwestern Oregon and its relation to the tectonic evolution of the region, *U.S. Geol. Survey Bull.* **1339**, 61p.
- Coleman, R.G., and Lanphere, M.A., 1971, Distribution and age of high-grade blueschists, associated eclogites, and amphibolites from Oregon and California, *Geol. Soc. Amer. Bull.*, **82**, 2397-2412.
- Coleman, R.G., and Lanphere, M.A., 1991, The Briggs Creek amphibolite, Klamath Mountains, Oregon: Its origin and dispersal, *N. Z. J. Geol. Geophys.*, **34**, 271-284.
- Coney, P.J., et. al., 1980, Cordilleran suspect terranes, *Nature*, **288**, 329-333.
- Coulton, A.J., 1995, Fault related oceanic and emplacement age serpentinization in the Josephine ophiolite, NW California and SW Oregon, Ph.D. thesis, State Univ. New York at Albany, 251 pp.
- Dick, H.J.B., 1976, The origin and emplacement of the Josephine Peridotite of southwestern Oregon, Ph.D. dissertation, Yale University, 409p.

- Diller, J.S., 1907, The Mesozoic sediments of southwestern Oregon, *Am. Jour. Sci.*, **23**, 401-421.
- Diller, J.S., 1914, Mineral resources of southwestern Oregon, *U.S. Geol. Sur. Bull.*, **546**, 147 p.
- Donato, M.M., 1992, A newly recognized ductile shear zone in the northern Klamath Mountains, Oregon, *U.S. Geol. Survey Bull.*, **2028**, p.
- Donato, M.M., Barnes, C.G., and Tomlinson, S.L., 1995, The Enigmatic Applegate group of southwestern Oregon: age, correlation, and tectonic affinity, *Oregon Geology*, in review.
- Garcia, M.O., 1979, Petrology of the Rogue and Galice formations, Klamath Mountains, Oregon: Identification of a Jurassic island-arc sequence, *Jour. Geol.*, **87**, 29-41.
- Garcia, M.O., 1982, Petrology of the Rogue River island-arc complex, southwest Oregon, *Amer. Jour. Sci.*, **282**, 783-807.
- Ghent, E.D., and M.Z. Stout, 1981, Metamorphism at the base of the Semail ophiolite, Southeastern Oman Mountains, *J. Geophys. Res.*, **86**, 2557-2572.
- Gribble, R.F., Barnes, C.G., Donato, M.M., Hoover, J.D., and Kistler, R.W., 1990, Geochemistry and intrusive history of the Ashland pluton, Klamath Mountains, California and Oregon, *Journal of Petrology*, **31**, 883-923.
- Hacker, B.R., Donato, M.M., Barnes, C.G., McWilliams, M.O., and W.G. Ernst, 1995, Timescales of orogeny: Jurassic construction of the Klamath Mountains, *tectonics*, v. 14, 677-703.
- Hamilton, W., 1978, Mesozoic tectonics of the western United States, in *Mesozoic Paleogeography of the Western United States*, edited by D.G. Howell and K.A. McCougall, pp. 33-70, Society of Economic Paleontologists and Mineralogists, Pacific Section, Los Angeles, Calif.
- Harper, G.D., 1980, The Josephine ophiolite-remains of a late Jurassic marginal basin in northwestern California, *Geology*, **8**, 333-337.
- Harper, G.D., 1983, A depositional contact between the Galice Formation and a Late Jurassic ophiolite in northwestern California and southwestern Oregon, *Oregon Geology*, **45**, 3-9.
- Harper, G.D., 1984, The Josephine ophiolite, *Geol. Soc. Amer. Bull.* **95**, 1009-1026.
- Harper, G.D., and Wright, J.E., 1984, Middle to Late Jurassic tectonic evolution of the Klamath Mountains, California-Oregon, *Tectonics* **3**, 759-772.
- Harper, G.D., Bowman, J.R., and Kuhns, R., 1988, A field, chemical and stable isotope study of subseafloor metamorphism of the Josephine ophiolite, California-Oregon, *J. Geophys. Res.* **93**, 4625-4656.
- Harper, G.D., Saleeby, J.B., and Heizler, M., 1994, Formation and emplacement of the

- Josephine ophiolite, and the age of the Nevadan orogeny in the Klamath Mountains, California-Oregon: U/Pb zircon and $^{40}\text{Ar}/^{39}\text{Ar}$ geochronology, *J. Geophys. Res.*, 99, 4293-4321.
- Hotz, P.E., 1971a, Geology of lode gold districts in the Klamath Mountains, California and Oregon, *U.S. Geol. Survey Bull.*, 1290, 91p.
- Imlay, R.W., 1961, Late Jurassic ammonites from the western Sierra Nevada, California, *U.S. Geol. Sur. Professional Paper 347-D*, 30 p.
- Imlay, R.W., 1980, Jurassic paleobiogeography of the western conterminous United States in its continental setting, *U.S. Geol. Sur. Professional Paper 1062*, 134 p.
- Irwin, W.P. 1966, Geology of the Klamath Mountain province, in: Bailey, E.H. (ed.), *Geology of northern California: Calif. Div. Mines Bull.*, 190, 19-38.
- Irwin, W.P., 1994, Geologic map of the Klamath Mountains, California and Oregon, *U.S. Geol. Survey Misc. Field Investigations I-2148*, scale 1:500,000.
- Irwin, W.P., Jones, D.L., and Blome, C.D., 1982, Map showing radiolarian localities in the western Paleozoic and Triassic belt, Klamath Mountains, California, *U.S. Geol. Survey Misc. Field Investigations, MF-1399*.
- Jaffey, A.H., Flynn, K.F., Glendenin, L.E., Bentley, W.C., and Essling, A.M., 1971, Precision measurement of half-lives and specific activities of ^{235}U and ^{238}U : *Physical Reviews C*, v. 4, p. 1889-1906.
- Jorgenson, D.B., 1970, Petrology and Origin of the Illinois River Gabbro, a part of the Josephine Peridotite-Gabbro Complex, Klamath Mountains, Southwestern Oregon, Ph.D., University of California, Santa Barbara, 195 pp.
- Kays, M.A., 1992, Geologic guide for the northern Klamath Mountains, 1, Cow Creek to Red Mountain, *Oreg. Geol.*, 54, 2, 27-33.
- Koski, R.A., and Derkey, R.E., 1981, Massive sulfide deposits in oceanic-crust and island-arc terranes of southwestern Oregon, *Oreg. Geol.*, 43, 119-129.
- Krogh, T.E., 1973, A low contamination method for the hydrothermal decomposition of zircon and extraction of U and Pb for isotopic age determinations, *Geochim. Cosmochim. Acta*, v. 37, 485-494.
- Lagabrielle, Y. and Cannat, M., 1990, Alpine Jurassic ophiolites resemble the modern central Atlantic basement, *Geology*, 18, 319-322.
- Lanphere, M.A., Irwin, W.P., and Hotz, P.E., 1968, Isotopic age of the Nevadan orogeny and older plutonic and metamorphic events in the Klamath Mountains, California, *Geol. Soc. Amer. Bull.*, 79, 1027-1052.
- Lemoine, M., 1980, Serpentinites, gabbros, and ophiolites in the Piemont-Ligurian domain of the western Alps: Possible indicators of oceanic fracture zones and of associated serpentinite protrusions in the Jurassic-Cretaceous Tethys, *Ach. Sc. Geneve*, 33, 103-115.

- Loney, R.A., and Himmelberg, G.R., 1977, The geology of the gabbroic complex along the northern border of the Josephine peridotite, Vulcan Peak area, southwestern Oregon, *U.S. Geol. Survey Journal of Res.*, **5**, 761-781.
- Mattinson, J.M., 1994, A study of complex discordance in zircons using step-wise dissolution techniques, *Contrib. Mineral. Petrol.*, **116**, 117-129.
- Miller, M. M., and J. B. Saleeby, 1987, Detrital zircon studies of the Galice Formation: Common provenance of strata overlying the Josephine ophiolite and Rogue Island arc, western Klamath Mountains terrane, *Geol. Soc. Amer. Abs. with Programs*, **19**, 772-773.
- Miller, M. M., and J. B. Saleeby, 1995, U-Pb geochronology of detrital zircon from Upper Jurassic synorogenic turbidites, Galice Formation, and related rocks, western Klamath Mountains: Correlation and Klamath Mountains provenance, *Jour. of Geophys. Res.*, **100 B9**, 18,045-18,058.
- Moores, E. M., 1982, Origin and emplacement of ophiolites, *Rev. Geophys. and Space Phys.*, **20**, 735-760.
- Ohr, M., 1987, Geology, geochemistry and geochronology of the Lems Ridge olistostrome, Klamath Mountains, California, M.S. thesis, SUNY Albany, 278p.
- Page, N.J., Gray, F., Cannon, J.K., Foose, M.P., Lipin, B., Moring, B.C., Nicholson, S.W., Sawline, M.G., Till, A., and W.P. Ziemianski, 1981, Geologic map of the Kalmiopsis wilderness area, Oregon, *U. S. Geol. Surv. Misc. Field Studies Map MF-1240-A*.
- Pearce, J. A., Lippard, S.J., and S. Roberts, 1984, Characteristics and tectonic significance of suprasubduction zone ophiolites, in *Marginal Basin Geology*, edited by B.P. Kokelaar and M.F. Howells, Blackwell, London, *Geol. Soc. Spec. Publ.* **16**, 77-94.
- Pessagno, E.A., and Blome, C.D., 1990, Implications of new Jurassic stratigraphic, geochronometric, and paleolatitudinal data from the western Klamath terrane (Smith River and Rogue Valley subterranean), *Geology*, **18**, 665-668.
- Ramp, L., 1961, Chromite in southwestern Oregon, *Oregon Dept. Geol. and Mineral Industries Bull.*, **52**, 169 p.
- Ramp, L., 1975, Geology and mineral resources of the upper Chetco drainage area, Oregon, *Oregon Dept. Geol. and Mineral Industries Bull.*, **93**, 79p.
- Ramp, L., 1977, Geology, mineral resources, and rock material of Curry County, Oregon, *Oregon Dept. Geol. and Mineral Industries Bull.*, **88**, 47p.
- Ramp, L., 1984, Geologic map of the southeast quarter of the Pearsoll Peak quadrangle, Curry and Josephine Counties, Oregon, *Oregon Dept. Of Geol. And Mineral Industries Geol. Map Series GMS-30*, scale 1:24,000.
- Ramp, 1986 Geologic map of the northwest quarter of the Cave Junction quadrangle, Josephine County, Oregon, *Oregon Dept. Of Geol. And Mineral Industries Geol. Map Series GMS-38*, scale 1:24,000.

- Ramp, L. and Peterson, N.V., 1979, Geology and mineral resources of Josephine County, Oregon, *Oregon Dept. Geol. and Mineral Industries Bull.*, 100, 45 p.
- Ramsay, J.G., and Huber, M.I., 1983, Techniques of Modern Structural Geology, Vol. 1: Strain Analysis, Academic Press, Inc., London.
- Roure, F., and DeWever, P., 1983, Decouverte de radiolarites du Trias dans l'unité occidentale des Klamath, sud-ouest de l'Oregon, U.S.A.: Consequences sur l'âge des peridotites de Josephine, *Comptes Rendus de l'Académie des Sciences (Paris)*, 297, 161-164.
- Saleeby, J.B., 1984, Pb-U zircon ages from the Rogue River area, western Jurassic belt, Klamath Mountains, Oregon, *Geol. Soc. Amer. Abstr. with Prog.*, 16, 331.
- Saleeby, J.B., Harper, G.D., Snoke, A.W., and Sharp, W.D., 1982, Time relations and structural-stratigraphic patterns in ophiolite accretion, west central Klamath Mountains, California, *J. Geophys. Res.* 87, 3831-3848.
- Saleeby, J.B. and G.D. Harper, 1993, Tectonic relations between the Galice Formation and the schists of Condrey Mountain, Klamath Mountains, northern California, in *Mesozoic Paleogeography of the Western United States*, vol. II, edited by G. Dunne and K. McDougall, pp.61-80, Society of Economic Paleontologists and Mineralogists, Pacific Section, Los Angeles, California.
- Shervais, J.W., 1982, Ti-V plots and the petrogenesis of modern and ophiolitic lavas, *Earth and Planet. Science Lett.*, 59, 101-118.
- Smith, G.M., Harper, G.D., and Sun, S., 1995, Paleomagnetism of the Josephine ophiolite complex: Northwestern California, in review.
- Snoke, A.W., 1977, A thrust plate of ophiolitic rocks in the Preston Peak area, Klamath Mountains, California, *Geol. Soc. Amer. Bull.*, 88, 1641-1659.
- Streckeisen, A., 1973, To each plutonic rocks its proper name: *Earth Science Reviews*, v. 12, pp. 1-33.
- Terra, F., and Wasserburg, G.J., 1972, U-Th-Pb systematics in three Apollo 14 basalts and the problems of initial Pb in lunar rocks, *Earth and Planet. Science Letters*, v. 14, p. 281-304.
- Thompson, A. B., 1976, Mineral reactions in pelitic rocks: I Prediction of P-T-X (Fe₂Mg) phase relations: *Amer. Jour. Sci.*, v.276, 401-424.
- Wells, F.G., Hotz, P.E., and Cater, F.W., Jr., 1949, Preliminary description of the geology of the Kerby quadrangle Oregon, *Oregon Dept. Geology and Mineral Industries Bull.*, 40, 23p.
- Wells, F.G., and Walker, G.W., 1953, Geology of the Galice quadrangle, Oregon, U.S. *Geol. Survey Quadrangle Map GQ-25, scale 1:62,500.*
- Wise, J. P., 1969, Geology and petrography of a portion of the Jurassic Galice Formation, Babyfoot Lake area, southwestern Oregon: Idaho State University, Master's thesis, 108 p.

- Wood, D.A., 1980, The application of a Th-Hf-Ta diagram to problems of tectonomagmatic classification and to establish the nature of crustal contamination of basaltic lavas of the British Tertiary Volcanic Province, *Earth Planet. Sci. Lett.*, 50 11-30.
- Wright, J.E., and Fahan, M.R., 1988, An expanded view of Jurassic orogenesis in the western United States Cordillera: Middle Jurassic (pre-Nevadan) regional metamorphism and thrust faulting within an active arc environment, Klamath Mountains, California, *Geol. Soc. Amer. Bull.*, **100**, 859-876.
- Wright, J. E., and S. J. Wyld, 1994, The Rattlesnake Creek terrane, Klamath Mountains, California: an early Mesozoic volcanic arc and its basement of tectonically disrupted oceanic crust, *Geol. Soc. Am. Bull.*, *106*, 1033-1056.
- Wyld, S.J., and Wright, J.E., 1988, The Devils Elbow ophiolite remnant and overlying Galice Formation: New constraints on the Middle to Late Jurassic evolution of the Klamath Mountains, California, *Geol. Soc. Amer. Bull.*, **100**, 29-44.
- Yule, J.D., Saleeby, J.B., Jones, D.L., and Silk, M., 1992, Correlation of basement terranes across the Late Jurassic Josephine inter-arc basin, southwestern Oregon and northern California, *Geol. Soc. Amer. Abs. with Programs*, 24, 5, 93.
- Yule, J.D., and Saleeby, J.B., 1993, Highly extended oceanic lithosphere: The basement and wallrocks for the Late Jurassic Rogue-Chetco oceanic arc, Oregon Klamath Mountains, *Geol. Soc. Amer. Abs. with Programs*, v. 25, 169.

CHAPTER 3

JURASSIC OROGENY DURING 40 M.Y. OF CONTINUOUS OCEANIC ARC MAGMATISM IN THE KLAMATH MOUNTAINS PROVINCE: NEW INSIGHTS FROM OREGON

Abstract

Radiometric ages for most of the principal rock units in the Klamath Mountains province have been determined, the result of almost 30 years of work by numerous investigators. However, in the Oregon Klamaths, the coverage is relatively thin to absent, particularly with regard to U/Pb zircon age data of the large plutonic bodies. The first half of this article presents radiometric age data in an attempt to erase this “state line effect” and fill in some of the gaps in the data by reporting U/Pb zircon apparent ages determined for the Illinois River plutonic complex (IRPC), and the Greyback, Thompson Ridge, Ashland, and Wimer plutons. The findings indicate that all five plutons overlap in age from ~162-156 Ma, a somewhat surprising result considering these plutons were included in four separate, northeast trending plutonic belts termed the Chetco, Grants Pass, Greyback, and Wooley Creek belts by Irwin (1985). As a result, these plutons are reinterpreted to represent a single, broadly NW-trending plutonic belt which includes plutons of ~164-155 Ma.

In addition to the pluton age determinations, this article presents U/Pb zircon and $^{40}\text{Ar}/^{39}\text{Ar}$ age data from the Briggs Creek amphibolite (BCA) and the Onion Camp complex (OCC) (chapter 2) of the western Jurassic belt (WJB). These data confirm field

observational data and indicate that 1) the BCA, whose $^{40}\text{Ar}/^{39}\text{Ar}$ ages pre-date those of the IRPC by 1-2 m.y., cooled in the regional thermal aureole surrounding the IRPC, and 2) the rocks of the OCC are pre-Middle Jurassic in age and probably correlable with the Rattlesnake Creek terrane (RCT). The documentation of a fragment of the RCT contained within the WJB provides a lithotectonic link between two of the composite terranes of the province, the WJB and the WTrPz, and confirms the tectonic model for the Jurassic tectonic evolution of the region (Snook, 1977; Saleeby et al., 1982; Harper and Wright, 1984). This model invokes rifting across the Middle Jurassic Klamath arc and arc basement (RCT of the WTrPz belt) to form the Josephine marginal ocean basin (WJB). The model predicts that a rifted fragment of the WTrPz belt is carried outboard of the Josephine ocean spreading centers, a scenario that is reinforced by the new age and observational data from the WJB.

With the addition of the new age data reported herein, the second part of this article reviews the Middle Jurassic to Cretaceous geochronometric data according to gross lithology and age dating methods. By assuming the data set is essentially complete, some intriguing first order patterns emerge from the data set: 1) arc magmatism in the province appears to have occurred continuously from ~175-135 Ma, 2) ophiolite genesis in the WJB and in outliers in southwestern Oregon occurred from ~170-160 Ma, and 3) regional metamorphic cooling ages in amphibolite terranes occurred during two distinct episodes; one small grouping of ages occur at ~175-169 Ma and another large grouping occurs at ~157-145 Ma. A second order feature is defined by short amagmatic gaps which are apparent in U/Pb zircon ages occurring at ~167-164 Ma and at ~153-150 Ma. Also, a systematic variation in age is evident in the amphibolite cooling data with ~158-156 Ma cooling in the WJB, ~153-148 Ma cooling in the central WTrPz belt (Marble Mountains terrane), and ~148-145 Ma in the northern WTrPz belt (May Creek terrane). It is particularly intriguing to note that the amagmatic breaks overlap with known episodes of regional thrust faulting in the Klamath Mountains province, specifically a Middle Jurassic

thrusting event defined by Wright and Fahan at ~169-164 Ma, and the Late Jurassic Nevadan thrusting event (e.g., Harper et al., 1994) active from ~155-150 Ma. In addition, the available geochemical and isotopic data from plutons in the province indicate fundamental changes in the composition of the deep crust accompanied these thrusting events (Barnes et al., 1992).

In light of the apparent region-wide coincidence in the age, geochemistry, and tectonic history, the following reinterpretations of the Middle Jurassic to Early Cretaceous geologic and tectonic history of the Klamath Mountains province are proposed:

- 1) The province represents a long-lived oceanic arc batholithic system, active from 175-135 Ma, that was punctuated by two distinct contractile episodes which profoundly affected the geochemistry and distribution of arc plutons. The “Klamath Mountains batholithic belt” can therefore be subdivided into three magmatic phases. Phase I consists of 175-167 Ma, calc-alkaline plutons and volcanic rocks characterized by relatively high K_2O and Rb, and relatively low ϵSr (Barnes et al., 1992) and represents the re-establishment of arc magmatism in the province after an ~20 m.y. hiatus. The amalgamation of WTrPz belt terranes, the initial genesis of Josephine ophiolite *sensu lato*, and localized metamorphic cooling of amphibolites also occurred during this time. Phase II consists of 164-153 Ma, calc-alkaline to calcic plutons characterized by relatively low K_2O and Rb, and relatively high ϵSr (Barnes et al., 1992). The distribution trend of phase II plutons is approximately 30-45° counterclockwise from the trend of phase I plutons suggesting that the province rotated clockwise (relatively) between phases I and II. This rotation may reflect differential rates of spreading across the strike of the Josephine basin. Phase III consists of 150-135 Ma, calc-alkaline plutons characterized by relatively low K_2O and Rb, and relatively low ϵSr (Barnes et al., 1992) which occur throughout all terranes of

the province and appear to get younger in age progressively from west to east across the province.

2) Tectonic and paleogeographic reconstructions for the Middle and Late Jurassic are similar to previous versions in that spreading in the Josephine ophiolite is directed parallel to the continental margin, but differ in the following fundamental ways. A) The Rogue arc is placed far to the north of the province at ~160 Ma where it is constructed upon a rifted RCT fragment carried north consistent with the spreading direction (Harper and Wright, 1984). This permits the phase II WTrPz belt plutons (e.g., Greyback-Wooley Creek-Ashland plutons) to remain in the active arc region of the Josephine marginal basin; therefore, the Rogue and phase II WTrPz belt plutons represent along strike equivalents of the same arc-subduction system. B) The Late Jurassic tectonic collapse of the Josephine basin is accommodated by highly left-oblique thrusting in order to juxtapose the Rogue and phase II WTrPz belt plutons. North directed thrust displacements as great as 500-1000 km are conceivable and may accommodate the large left-lateral truncation displacements suggested to have occurred at this time along the Mojave-Sonora megashear(s) (Silver and Anderson, 1974).

3) Jurassic orogeny in the province is considered to be a product of the variable tectonic and magmatic processes that actively shaped the province from 175-135 Ma thereby helping to resolve the debate regarding the timing and duration of orogenic episodes in the region. Specifically, Jurassic orogeny in the province is viewed as having three contributing processes, namely arc magmatism, contractile deformation, and extensional tectonism, and will therefore reflect the spatial and temporal characteristics of each process. In this sense, orogenic features which appear to show considerable spatial and temporal variation probably reflect the widely variable timing and duration of arc magmatic patterns in the province. Secondly, the regional orogenic features of the same age probably reflect the distinct thrusting events which occurred in the Middle and Late Jurassic. Therefore, Jurassic orogeny, though temporally and spatially variable, is

considered to have occurred continuously in the Klamath Mountains province from the Middle Jurassic to the Early Cretaceous, but it was punctuated by Middle and Late Jurassic thrusting events which had profound regional effects.

Introduction

The construction of the Klamath Mountains province is generally considered to have occurred in relatively close proximity to western North America in an oceanic setting above an east dipping subduction zone (e.g., Burchfiel and Davis, 1981; Davis and others, 1978; Harper and Wright, 1984; Wright and Fahan, 1988; Wright and Wyld, 1994). The region has been the focus of comprehensive study for the past 30 years which has produced a wealth of information regarding the processes that have affected western North America. Though the stratigraphic history spans nearly 400 m.y., the data suggest that much of the province was assembled in the Middle and Late Jurassic. This paper will focus on new geochronometric data which relate to the Jurassic geologic and tectonic evolution of the province.

Numerous geologic investigations of Middle Jurassic to Cretaceous subduction-related plutons in the Klamath Mountains province have produced an extensive database of radiometric and geochemical analyses (e.g., Barnes, 1982; Barnes et al., 1986a; Barnes et al., 1986b; Barnes et al., 1992a; Barnes et al., 1992b; Charlton, 1979; Hacker and Ernst, 1993; Hacker et al., 1995). These data reveal a number of intriguing general patterns within the province. For example, Irwin (1985) noted that the available radiometric age data and geologic relations suggested the plutons occurred in five discrete belts. However, it remains unclear as to what may have caused this apparent temporal and spatial variation in magmatism. In the Oregon Klamaths, subsequent workers have noted that two of these belts, the Chetco and the Greyback belts, overlap in apparent age but appear to have formed in distinctly different tectonic settings, the former in the active arc region and the latter in

remnant arc crust of the Josephine basin (e.g., Barnes et al., 1992a; Hacker et al., 1995). Hacker et al. (1995) explain this apparent paradox by invoking extension across the remnant arc. An alternative explanation, discussed in detail below, is that the Chetco and Greyback belts were once part of the same oceanic island arc, but were subsequently juxtaposed in an apparent arc and “back-arc” configuration by left-oblique displacement across the Orleans-Preston Peak fault. Another peculiarity is a threefold systematic temporal variation of certain geochemical and isotopic traits of the plutons that is presumably an effect of tectonism in the province (Barnes et al., 1992). Thus, though much is known in detail, the fundamental reasons for the temporal and spatial variation of Middle Jurassic to Cretaceous arc magmatism remain unresolved.

Similarly, the fundamental cause or causes of Jurassic orogeny in the province are poorly understood with two principal competing interpretations. One invokes relatively short-lived events with differential deformation, magmatism, sedimentation, and regional metamorphism. The other suggests that orogenic activity was spatially and temporally variable. This article reconsiders the timing and location of orogenic features in the province in light of new U/Pb and $^{40}\text{Ar}/^{39}\text{Ar}$ ages. The conclusion accepts aspects of both views for Jurassic orogenesis in the province. Specifically, Jurassic orogeny in the Klamath Mountains province is considered a product of two relatively short-lived regional deformational events that punctuate a continuum of deformation, metamorphism, and sedimentation which varies in space and time. The latter style of orogenic activity is probably related to oceanic arc and inter-arc basin magmatism in the region which spans an ~40 m.y. period from 175-135 Ma. In this view the Middle Jurassic to Early Cretaceous geologic and tectonic history of the province represents a relatively long-lived orogenic cycle transitional between the relatively short-lived Paleozoic and Early Mesozoic orogenies (e.g., Antler and Sonoman) and the long-lived Cretaceous to Tertiary Andean-type convergent margin along the western North American margin.

General Tectonic and Geologic Framework

The Klamath Mountains consist of a series of moderately to gently eastward dipping thrust plates whose ages generally increase from Late Jurassic on the west to Early Paleozoic in the east. Plates contain primarily oceanic rock types, with east dipping foliations, west-vergent folds, and are separated by west-directed faults. This paper focuses on the Middle Jurassic to Early Cretaceous geologic and tectonic evolution of the Klamaths, specifically on the rocks that comprise the western two belts of province, the western Jurassic belt (WJB) and the western Paleozoic and Triassic belt (WTrPz belt) (Figure 3-1).

Western Jurassic belt

The WJB consists primarily of the coeval Late Middle to Late Jurassic Josephine ophiolite (Harper, 1980; 1984) and Rogue River island arc complex (Garcia, 1979; 1982), which are both overlapped by the Middle Oxfordian to Late Kimmeridgian Galice Formation (Pessagno and Blome, 1990), a flysch sequence with distinct provenance ties to both the Rogue River island arc and to older terranes of the Klamath Mountains (Miller and Saleeby, 1987). Other distinct rock associations of the WJB include the Briggs Creek amphibolite body (Coleman and Lanphere, 1992), olistostromal deposits associated with the basal strata of the Rogue-Galice overlap sequence, and an elongate ~5x50 km belt comprised of pre-Middle Jurassic oceanic crust and mantle peridotite that correlate with rocks of the Rattlesnake Creek terrane (RCT), the westernmost terrane of the WTrPz belt (Figure 3-2; e.g., Wright and Wyld, 1994).

The occurrence of RCT rocks within the WJB confirms the prediction of a previously proposed model for the Jurassic tectonic evolution of the Klamath Mountains province originally proposed by Snoke (1977) and later modified by Saleeby et al. (1982) and Harper and Wright (1984). This model considers WJB rocks representative of a Late Jurassic marginal ocean basin fringing western North America that formed in response to

Figure 3-1. Generalized lithotectonic map of the Klamath Mountains and Oregon Coast Ranges province (after Irwin, 1985; and Blake et al., 1985).

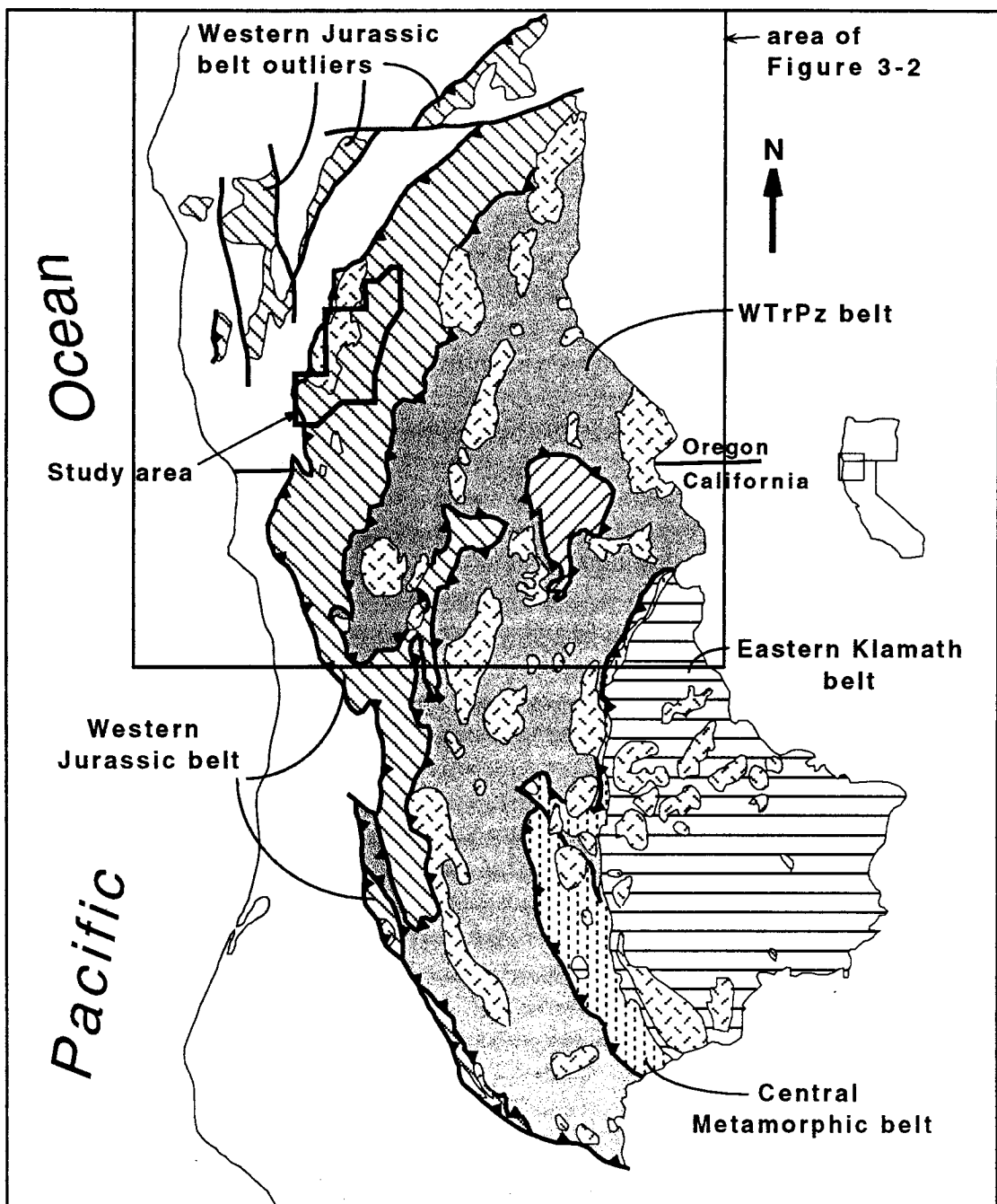
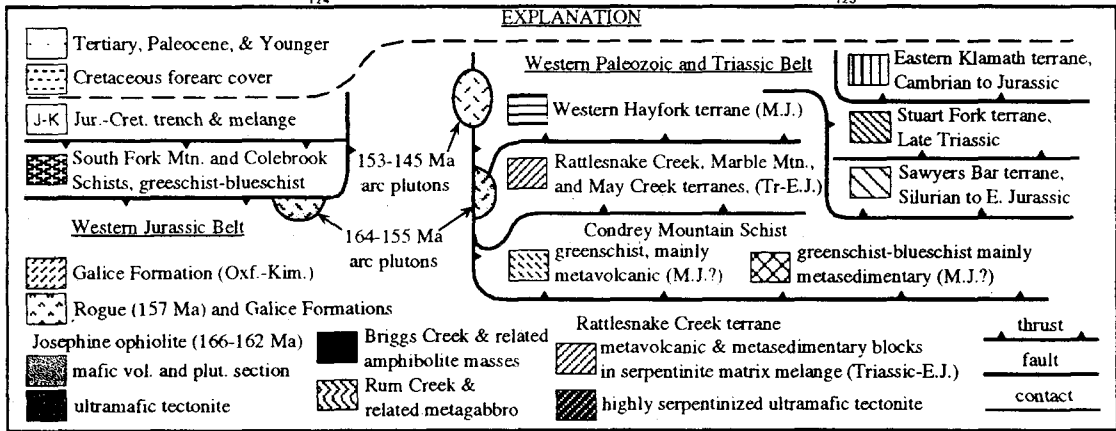
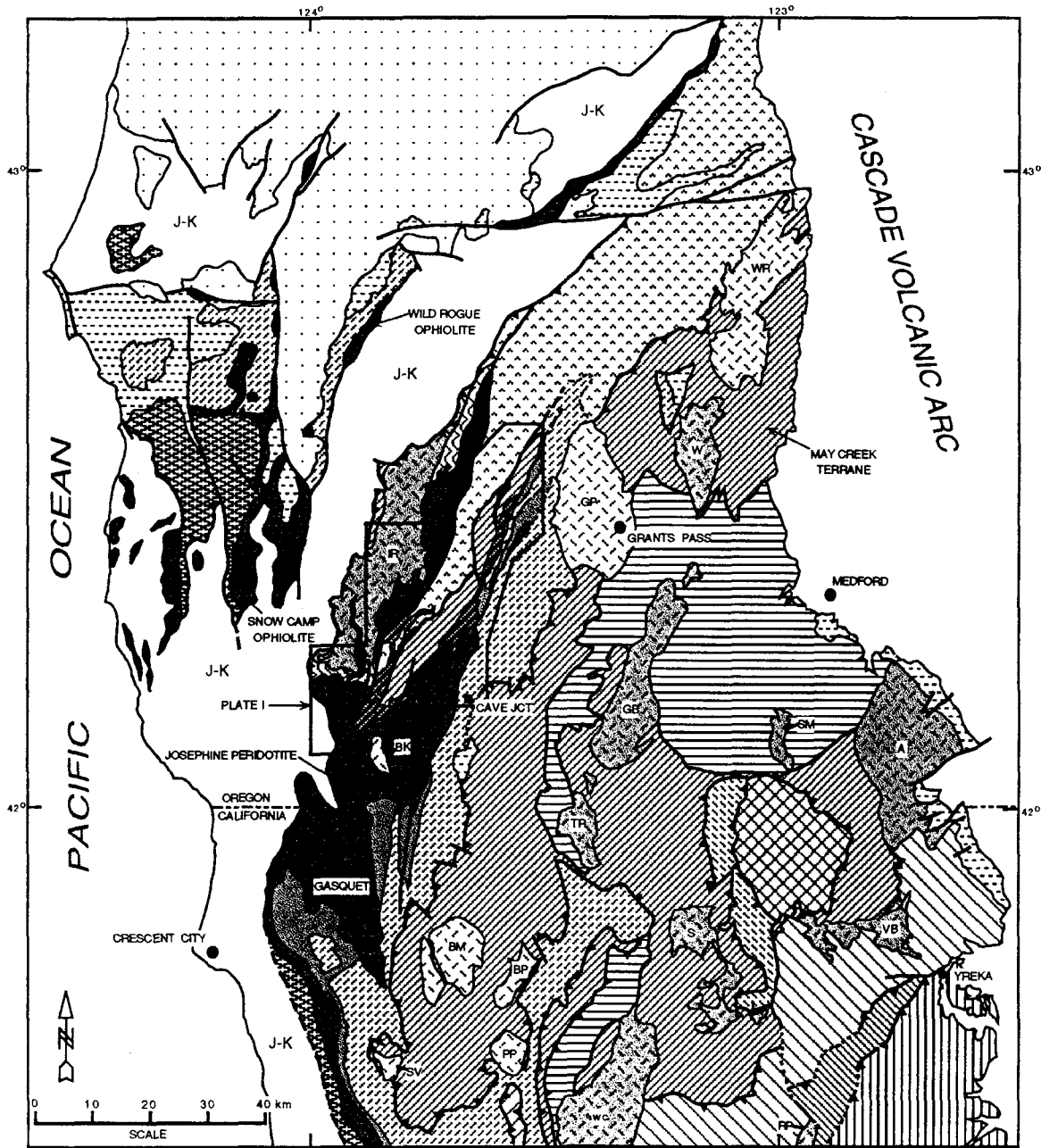


Figure 3-2. Generalized regional geologic map of the northern Klamath Mountains province and the Oregon Coast Ranges. The map is compiled from my field studies during 1989-1994 and modified from work published by Coleman and Lanphere (1991), Hacker et al. (1995), Irwin (1994), Ramp et al. (1977), and Ramp et al. (1979). Pluton names are as follows: WR - White Rock, W - Wimer, GP - Grants Pass, IR - Illinois River plutonic complex, BK - Buckskin Peak, GB - Grayback, SM - Squaw Mountain, A - Ashland, VB - Vesa Bluffs, S - Slinkard, TR - Thompson Ridge, BM - Bear Mountain, BP - Bear Peak, PP, Pony Peak, SV - Summit Valley, WC - Wooley Creek, RP - Russian Peak.



rifting across a Middle Jurassic arc complex and arc basement rocks which collectively formed parts of the WTrPz belt. The belt of RCT rocks in the WJB is therefore interpreted to represent a rifted fragment of the WTrPz belt that was carried outboard of spreading centers as the Josephine ophiolite formed. This composite Josephine/RCT lithosphere later served as the depositional basement for the Rogue-Galice overlap sequence and formed the country rock for the Illinois River plutonic complex (IRPC), interpreted to represent the plutonic roots of the Rogue River island arc.

Despite its ties to the older terranes of the Klamath Mountains province, parts of the Josephine ophiolite may have experienced northward displacements on the order of 500-1000 km. For example, faunal studies of hemipelagic strata which overly Josephine pillow lavas indicate a change from equatorial to boreal faunas prior to the Middle Oxfordian of Galice flysch deposits (Pessagno and Blome, 1990). Also, paleomagnetic data from Josephine ophiolite rocks suggests the ophiolite may have experienced a similar degree of northward transport (Smith and Harper, in review, 1995). Large magnitude northward displacements suggest that Josephine spreading centers were oriented perpendicular to the continental margin, a geometry supported by the east-west striking orientation, in present day coordinates, of sheeted mafic dikes of the Josephine ophiolite (Harper, 1984). The paleontologic and paleomagnetic evidence for 500-1000 km of displacement over ~5 m.y. require 1/2 spreading rates of 10-20 cm/yr, typical of rates at fast-spreading centers and in apparent conflict with some of the geologic features of the Josephine ophiolite which are most typical of ophiolitic crust generated at slow- to intermediate-spreading (Alexander and Harper, 1992).

The structural framework of the WJB was previously considered to be an imbricate "thrust" stack of moderately to steeply eastward subterranean units separated by regionally extensive faults (e.g., Blake et al., 1985). However, recent investigations indicate that the subterranean units are not wholly fault-bounded, and therefore do not warrant subterranean status. Instead, recent field investigations indicate that the primary structural features of the

WJB are regional scale tight folds with faulting secondary and most often occurring along the limbs of regional folds (Figure 3-2; also see Chapter 2). Though, structurally complex, the WJB is therefore considered to represent a largely intact fragment of marginal basin oceanic lithosphere.

Folding and faulting of WJB rocks signals the onset of Late Jurassic regional deformation interpreted to mark the beginning of the Nevadan orogeny in the province. As a result of early Nevadan shortening, the WJB was folded and faulted into a series of tight folds and underthrust beneath the older Klamath terranes of the WTrPz belt. Structural features associated with the tectonic collapse of the Josephine marginal ocean basin are intruded by ~150 Ma dikes plutons marking the end of early Nevadan deformation. Harper et al. (1994) present data which indicate Nevadan deformation continues, at least locally until the Early Cretaceous.

Condrey Mountain Schist

The Condrey Mountain Schist (CMS) occurs in a structural window beneath the WTrPz belt and consists of transitional greenschist-blueschist facies metasediments, metavolcanic, and rare occurrences of metagabbro and metadiabase (Figure 3-2). Two competing interpretations exist for correlating rocks of the CMS with lower grade terranes of the region. One interpretation focuses on lithologic similarities and suggests that the CMS represents the higher metamorphic grade equivalents of the WJB, specifically the Galice Formation and ophiolitic rocks that may be correlative with the RCT or the Josephine ophiolite (Hotz, 1979; Saleeby and Harper, 1994). A second interpretation focuses on the apparent age data and suggests that, despite their gross lithologic similarities, the CMS and WJB rocks cannot be related because of distinct differences in radiometric ages; therefore, a fundamental tectonic boundary must occur between the CMS and the WJB (Hill, 1984, 1985; Helper, 1986).

Western Paleozoic and Triassic belt

The WTrPz belt (Figure 3-1), as defined by Irwin (1972), contains of a series of thrust fault bounded oceanic terranes that primarily consist of an assortment of Permian to Triassic, amphibolite- to greenschist-facies metavolcanic and metasedimentary rocks, and metaperidotite. In the southern part of the Klamath Mountains province, the terranes occur in a moderately eastward dipping thrust sequence comprised of, from west to east, the RCT (e.g., Wright and Wyld, 1994), the western Hayfork terrane (WHT; e.g., Wright and Fahan, 1988), the Sawyers Bar terrane defined by Ernst (1990) and Ernst and Hacker (1993) as a composite of the previously termed eastern Hayfork, Salmon River, and North Fork terranes, and the Stuart Fork terrane (e.g., Goodge, 1989; 1990).

With the exception of the RCT, the terranes of the WTrPz belt contain sedimentary rocks with detrital grains (e.g., zircon) recycled from cratonic North America (Miller and Saleeby, 1987) indicating that the WTrPz belt terranes probably represent primitive arcs, ocean basins, and subduction complexes along the western North American continental margin, in a setting perhaps analogous to the modern western Pacific (e.g., Wright and Wyld, 1994; Miller and Saleeby, in press, 1995). Rocks of the WHT, are interpreted to represent a Middle Jurassic volcanoplutonic arc complex and are constructed, at least in part, upon the older terranes of the WTrPz belt complex (Harper and Wright, 1984; Wright and Fahan, 1988). WHT magmatism follows an ~20 m.y. hiatus in the province and represents the early phase that occurred during the amalgamation of the WTrPz belt (Hacker et al., 1994; Wright and Wyld, 1988). Thus the WHT and related rock represents the early phase of a more prolonged episode of Jurassic arc magmatism in the region.

Until recently the Oregon portion of the WTrPz belt remained undivided, apparently suffering from the "state-line effect" barrier against continuing California regional contacts northward across the border. Recent work by Donato et al. (in press, 1995) has recognized RCT and WHT rocks in Oregon, and with more work in the region a similar degree of subdivision of the California portion of the WTrPz belt may eventually be

achieved (Figure 3-2). On the contrary, the apparent lesser degree of imbrication of the northern WTrPz belt may reflect a genuine decrease in the degree of shortening and thrusting from south to north across the province. The thrust faults that bound the various terranes of the WTrPz belt deform ~167 Ma metavolcanic rocks of the WHT and are themselves intruded by ~164 Ma plutons (Wright and Fahan, 1988). This Middle Jurassic contractile episode is distinct from the aforementioned Nevadan thrusting and essentially amalgamated the WTrPz belt. With the exception of the relatively few plutons in the WJB, this deformational event formed the composite “country rock” for the post-164 Ma plutons of the province.

Post-164 Ma plutons

The numerous post-164 Ma large plutons (Figure 3-2) and countless smaller intrusions emplaced into the WTrPz belt have been interpreted to represent subduction generated magmas (e.g., Hamilton, 1969; and Davis et al., 1978). Some workers have subdivided the post-164 Ma plutons into as many as four separate plutonic belts based primarily on radiometric age data (Hotz, 1971; Irwin, 1985). The belts, termed the Shasta Bally, the Wooley Creek, the Greyback, and the Grants Pass plutonic belts, are broadly drawn parallel to structural trends in the country rocks though the plutons are clearly discordant with respect to these older structures and brings into question the relevance of drawing the boundaries parallel to these trends. Additionally, more recent U/Pb zircon apparent ages determined from plutons of several belts appear to overlap. These new data combined with the apparent inconsistencies in the various belt designations, invite a re-examination of the spatial and temporal patterns of magmatism, the focus of part of the “Discussion” section below.

Geochronologic Data

Methods and analytical procedures

U/Pb zircon age data are presented in Table 3-1. Notes on the analytical procedures and assessment of uncertainties are given in the footnotes of Table 3-1. A more in depth discussion of procedures and uncertainties is given in Appendix 2. Discussion of the zircon data centers on $^{207}\text{Pb}/^{206}\text{Pb}$ versus $^{238}\text{U}/^{206}\text{Pb}$ concordia plots (Terra and Wasserburg, 1972). For samples that are concordant, and are of a restricted age range, the graphic relations are shown in a plot where equivalent segments of concordia are stacked with a common abscissa (Figure 3-3). This plot facilitates close examination of relations between concordia and error bars, which is particularly useful for geologically related samples.

In the discussion of the zircon data, internal concordance is defined as agreement of the U/Pb and Pb/Pb ages of an individual analyses within analytical uncertainty. It is expressed graphically by the intersection of the error bars with concordia. External concordance is defined as agreement, or graphic overlap, in internally concordant ages from multiple fractions of a given sample or from multiple samples collected from the same rock unit. Externally concordant ages are considered to be accurate approximations of igneous crystallization ages inasmuch as the effects of multi-stage isotopic evolution are heterogeneous within map-scale units and have been observed to vary with the physical properties of zircon. Treatment of discordant samples requires the application of a discordance mechanism model, e.g., the loss or inheritance of radiogenic Pb, which is best developed by assessment of the isotopic systematics in the geological context of the sample.

Age determinations by the $^{40}\text{Ar}/^{39}\text{Ar}$ incremental heating method are listed in Table 3-2. The analyses were conducted by B.R. Hacker at Stanford University in 1993 following the analytical procedures summarized by Harrison and Fitz Gerald (1986). The

Table 3-1. URANIUM-LEAD ISOTOPIC DATA

| Size (μm) [†] | Zircon fraction properties ^{††} | Wt. (mg) [Ⓞ] | U (ppm) | $^{206}\text{Pb}^*$ (ppm) | Atomic ratios | | | | Apparent Ages (m.y.) [§] | | |
|--|--|--------------------------|------------|------------------------------|---|--|--|---|--|---|----------|
| | | | | | $\frac{^{206}\text{Pb}^*}{^{204}\text{Pb}}$ | $\frac{^{206}\text{Pb}^*}{^{238}\text{U}}$ | $\frac{^{207}\text{Pb}^*}{^{235}\text{U}}$ | $\frac{^{207}\text{Pb}^*}{^{206}\text{Pb}^*}$ | $\frac{^{207}\text{Pb}^*}{^{235}\text{U}}$ | $\frac{^{207}\text{Pb}^*}{^{206}\text{Pb}^*}$ | |
| 1. IR-4: Agmatitic diorite, Illinois River plutonic complex (123°50'53.5" W, 42°23'19.5"). | | | | | | | | | | | |
| 45-64 ² | Stubby prisms, lt tan. | 3.0 | 335.1 | 7.06 | 9.553 | 0.02433(16) | 0.16541 | 0.04933(18) | 155.0 | 155.4 | 163 (8) |
| 64-80 ² | <2:1 only, clear w/rare incl. | 4.2 | 192.5 | 4.09 | 11,074 | 0.02453(16) | 0.16659 | 0.04927(19) | 156.3 | 156.5 | 160 (9) |
| 80-100 ² | Bi-modal 95% 1:1, 5% >4:1. | 2.2 | 218.6 | 4.67 | 6,774 | 0.02468(17) | 0.16769 | 0.04931(14) | 157.2 | 157.4 | 162 (7) |
| 2. IR-3: Massive hornblende diorite, Illinois River plutonic complex (123°48'21" W, 42°22'18.5"). | | | | | | | | | | | |
| 64-80 ³ | Tan w/rare incl., 2:1, Fr>Eu. | 4.2 | 118.7 | 2.55 | 5,306 | 0.02484(17) | 0.16880 | 0.04931(12) | 158.2 | 158.4 | 162 (6) |
| 80-100 ³ | Lt. tan w/rare incl., 2:1, Fr=Eu. | 4.6 | 191.7 | 4.17 | 5,733 | 0.02513(17) | 0.17051 | 0.04922(11) | 160.0 | 159.9 | 158 (5) |
| 3. 93DY-YB-8: Pegmatitic hornblende-biotitetonalite, Illinois River plutonic complex (123°51'44" W, 42°23'53.5"). | | | | | | | | | | | |
| <64 ⁴ | Eu>Fr, 3:1, clear w/micro incl. | 0.95 | 185.7 | 3.96 | 2,503 | 0.02465(13) | 0.16680 | 0.04910(13) | 157.0 | 156.6 | 152 (6) |
| 4. IR-1: Foliated biotite tonalite, Illinois River plutonic complex (123°46'57" W, 42°21'14.5"). | | | | | | | | | | | |
| 45-64 ⁴ | >3:1 w/clear incl., Eu>Fr. | 3.9 | 247.8 | 5.09 | 8,615 | 0.02368(16) | 0.16122 | 0.04941(15) | 150.9 | 151.8 | 167 (7) |
| >120 ⁴ | ~3:1, w/clear incl., Eu>Fr. | 6.6 | 259.5 | 5.52 | 3,676 | 0.02456(17) | 0.16669 | 0.04925(15) | 156.4 | 156.5 | 159 (7) |
| 5. 91DY-PP-64: Foliated biotite tonalite, Illinois River plutonic complex (123°46'46" W, 42°19'37"). | | | | | | | | | | | |
| 45-64 ³ | Lt. tan w/rare inclusion. | 1.5 | 609.1 | 11.94 | 10,877 | 0.02264(15) | 0.15474 | 0.04947(24) | 144.4 | 145.8 | 170 (11) |
| 64-80 ³ | 3:1 to 5:1, Eu>Fr. | 5.1 | 366.2 | 7.70 | 4,407 | 0.02430(16) | 0.16649 | 0.04924(19) | 154.8 | 155.0 | 159 (9) |
| 6. IR-2: Trondhjemite gneiss layer in amphibolite, Illinois River plutonic complex (123°46'57" W, 42°21'07.5"). | | | | | | | | | | | |
| 64-80 ² | Cloudy, opaque grains, Eu>Fr. | 4.7 | 457.8 | 9.98 | 2,735 | 0.02519(17) | 0.17087 | 0.04923(13) | 160.3 | 160.2 | 158 (6) |
| 7. 91DY-PP-9B: Trondhjemite dike in amphibolite-grade metamorphosed dike complex (123°46'40" W, 42°18'36"). | | | | | | | | | | | |
| 45-64 ³ | Lt. Tan, stubby prisms. | 2.5 | 231.1 | 5.00 | 4,323 | 0.02500(17) | 0.16979 | 0.049289(15) | 159.2 | 159.2 | 161 (7) |
| 64-80 ³ | | 5.6 | 366.2 | 8.00 | 5,292 | 0.02524(17) | 0.17127 | 0.04924(11) | 160.7 | 160.5 | 159 (5) |
| 80-100 ³ | | 2.3 | 419.3 | 9.03 | 7,859 | 0.02489(17) | 0.16908 | 0.04929(13) | 158.5 | 158.6 | 161 (6) |

Table 3-1 (continued). URANIUM-LEAD ISOTOPIC DATA

| Size (μm) [†] | Zircon fraction properties ^{††} | Wt. (mg) [@] | U (ppm) | ²⁰⁶ Pb* (ppm) | Atomic ratios | | | | | | Apparent Ages (m.y.) \S | |
|---|--|--------------------------|------------|-----------------------------|---|--|--|--|--|--|--|--|
| | | | | | ²⁰⁶ Pb/ ²⁰⁴ Pb | ²⁰⁶ Pb* ²³⁸ U | ²⁰⁷ Pb* ²³⁵ U | ²⁰⁷ Pb* ²⁰⁶ Pb* | ²⁰⁶ Pb* ²³⁸ U | ²⁰⁷ Pb* ²³⁵ U | ²⁰⁷ Pb* ²³⁵ U | ²⁰⁷ Pb* ²⁰⁶ Pb* |
| 8. 92DY-WIM-3: Biotite granodiorite, main stage of Wimer pluton (123°07'16.5" W, 42°37'32"). | | | | | | | | | | | | |
| 64-80 ¹ | 2:1, incl. free, Fr>Eu. | 3.6 | 417.5 | 9.09 | 13,435 | 0.02515(17) | 0.17129 | 0.04941(13) | 160.2 | 160.5 | 167 (6) | |
| 100-120 ¹ | 3:1, incl. free, Fr>Eu. | 10.3 | 359.5 | 7.84 | 13,568 | 0.02520(17) | 0.17148 | 0.04938(09) | 160.4 | 160.7 | 166 (4) | |
| 9. 92CB-AP-79: Biotite-hornblende quartz monzodiorite, intermediate stage of Ashland pluton. (Lat./Long.?) | | | | | | | | | | | | |
| <64 ³ | <3:1, inclusion-rich. | 1.0 | 665.7 | 14.39 | 3,841 | 0.02497(17) | 0.16991 | 0.04937(22) | 159.0 | 159.3 | 165 (10) | |
| <80 ³ | Clear, Eu>Fr, 5:1 grains. | 0.5 | 585.2 | 12.83 | 2,737 | 0.02533(17) | 0.17205 | 0.04927(20) | 161.3 | 161.2 | 161 (10) | |
| 80-100 ² | Clear w/micro-inclusions. | 2.7 | 189.9 | 4.02 | 1,984 | 0.02448(17) | 0.16631 | 0.04930(12) | 155.9 | 156.2 | 162 (6) | |
| 10. 92CB-AP-80: Hornblende-biotite granite, late stage of Ashland pluton. (Lat./Long.?) | | | | | | | | | | | | |
| <45 ² | 2:1 to 8:1, Fr=Eu, clear. | 1.0 | 1,527 | 29.46 | 9,811 | 0.02228(15) | 0.15109 | 0.04920(27) | 142.1 | 142.9 | 156 (13) | |
| 45-64 ² | 3:1 to 7:1, incl-rich, fractures. | 2.9 | 871.9 | 17.96 | 876 | 0.02380(17) | 0.16106 | 0.04910(12) | 151.7 | 151.6 | 152 (6) | |
| 64-80 ² | 2:1 to 8:1, Fr=Eu, clear. | 0.7 | 1,838 | 38.44 | 8,706 | 0.02416(20) | 0.16380 | 0.04919(08) | 153.9 | 154.0 | 156 (4) | |
| 11. 92CB-TR-4: Biotite-hornblende-pyroxene gabbro, main stage of Thompson Ridge pluton. (Lat./Long.?) | | | | | | | | | | | | |
| 45-64 ² | Fr=Eu, v. lt. tan w/clear incl. | 2.3 | 442.7 | 9.74 | 6,519 | 0.02541(17) | 0.17238 | 0.04921(09) | 161.8 | 161.5 | 158 (4) | |
| 64-80 ² | 3:1, Fr>Eu w/ rare clear incl. | 5.2 | 160.6 | 3.53 | 774 | 0.02536(19) | 0.17242 | 0.04933(40) | 161.5 | 161.5 | 163 (19) | |
| 80-100 ² | Fr=Eu, clear, inclusion free. | 4.2 | 268.1 | 5.91 | 1,870 | 0.02546(18) | 0.17280 | 0.04925(21) | 162.1 | 161.9 | 160 (10) | |
| 12. 92CB-GBP-1688: Hornblende diorite, main stage of Grayback pluton. (Lat./Long.?) | | | | | | | | | | | | |
| 45-64 ¹ | 1:1 to 3:1, incl-rich. | 2.3 | 292.7 | 6.36 | 8,002 | 0.02510(17) | 0.17062 | 0.04933(23) | 159.8 | 160.0 | 163 (8) | |
| 64-80 ¹ | 1:1 to 5:1, Eu>Fr, clear. | 3.2 | 109.3 | 2.36 | 8,847 | 0.02490(17) | 0.16921 | 0.04931(12) | 158.6 | 158.7 | 162 (6) | |
| 80-100 ¹ | <2:1, pink-tan. | 1.6 | 887.1 | 19.29 | 3,267 | 0.02512(17) | 0.17035 | 0.04921(41) | 159.9 | 159.7 | 158 (19) | |
| 13. 92CB-GBP-154: Hornblende-biotite granodiorite, late stage of Grayback pluton. (Lat./Long.?) | | | | | | | | | | | | |
| 45-64 ⁴ | 1:1, Eu>Fr, clear, incl. free. | 3.8 | 288.8 | 6.15 | 2,108 | 0.02462(17) | 0.16668 | 0.04912(10) | 156.8 | 156.5 | 153 (5) | |
| 64-80 ⁴ | 1:1, v. lt. tan w/sm. clear incl. | 2.5 | 448.4 | 9.32 | 9,382 | 0.02401(16) | 0.16294 | 0.04923(15) | 153.0 | 153.3 | 159 (7) | |
| >80 ⁴ | 2:1, w/small clear incl. | 0.8 | 344.5 | 7.24 | 8,447 | 0.02429(13) | 0.16480 | 0.04923(10) | 154.7 | 154.9 | 159 (6) | |

Table 3-1 (continued). URANIUM-LEAD ISOTOPIC DATA

| Size (μm) [†] | Zircon fraction properties ^{††} | Wt. (mg) [@] | U (ppm) | ²⁰⁶ Pb (ppm) | Atomic ratios | | | | Apparent Ages (m.y.) [§] | | |
|---|--|--------------------------|------------|----------------------------|--|--|--|--|--|--|----------|
| | | | | | ²⁰⁶ Pb/ ²³⁸ U | ²⁰⁷ Pb/ ²³⁵ U | ²⁰⁶ Pb/ ²⁰⁷ Pb* | ²⁰⁷ Pb/ ²⁰⁶ Pb* | ²⁰⁷ Pb/ ²³⁵ U | ²⁰⁶ Pb/ ²⁰⁷ Pb* | |
| 14. 91DY-JM-11: Plagiogranite dike cutting serpentinitized peridotite of the Onion Camp complex (123°48'35" W, 42°14'45"). | | | | | | | | | | | |
| 45-64 ³ | 1:1 to 4:1 w/clear incl., Eu>Fr. | 2.3 | 198.3 | 4.67 | 9,855 | 0.02723(15) | 0.18604 | 0.04957(13) | 173.2 | 173.3 | 175 (6) |
| 64-100 ³ | 1:1 to 4:1 w/clear incl., Eu>Fr. | 1.3 | 215.2 | 5.08 | 8,002 | 0.02725(15) | 0.18650 | 0.04965(15) | 173.4 | 173.6 | 178 (7) |
| 15. 93DY-JM-10: Plagiogranite dike cutting serpentinitized peridotite of the Onion Camp complex (123°48'35.5" W, 42°14'35.5"). | | | | | | | | | | | |
| <45 ² | Clear, Eu>Fr, 2:1 to 5:1. | 2.3 | 379.8 | 8.37 | 13,361 | 0.02547(17) | 0.17444 | 0.04970(12) | 162.1 | 163.3 | 181 (6) |
| 45-64 ² | Clear, Eu>Fr, 2:1 to 5:1. | 1.4 | 726.6 | 16.69 | 12,111 | 0.02654(18) | 0.18107 | 0.04950(55) | 168.9 | 169.0 | 171 (26) |
| 64-80 ² | Clear, Eu>Fr, 2:1 to 5:1. | 0.8 | 562.3 | 13.21 | 8,013 | 0.02760(17) | 0.18817 | 0.04947(18) | 175.5 | 175.1 | 170 (8) |

[†] Fractions separated by grain size and magnetic properties. Magnetic properties are given as non-magnetic split on Franz Isodynamic Separator for 1.7 amps with side/front slopes of; ¹ 0.5/20, ² 1/20, ³ 2/20, or ⁴ 5/20. Dissolution and chemical extraction technique modified from Krogh (1973).

^{††} All samples are hand-picked to 99.9% purity prior to dissolution. Abbreviations are: Eu=euhedral grains; Fr=fregmented grains; ratios given are the respective length:width ratios of euhedral zircon grains; incl.=inclusion; Lt=light.

[@] Due to uncertainties in weight of sample, U-Pb concentration may be in error, use of mixed ²⁰⁵Pb-²³⁰Th-²³⁵U spike ensures age of sample is correct.

* Radiogenic/nonradiogenic correction based upon 40 picogram blank Pb (1:18.78;15.61;38.50) and initial Pb approximations: 206/204=18.6; 207/204=15.6; 208/204=38.2.

[§] Decay constants used in age calculation: $\lambda^{238}\text{U} = 1.55125 \times 10^{-10}$, $\lambda^{235}\text{U} = 9.98465 \times 10^{-10}$ (Jaffey and others, 1971); $^{238}\text{U}/^{235}\text{U}$ atom=137.88. Uncertainties (\pm) in radiogenic ratios calculated by quadratic sum of total derivatives of ²³⁸U and ²⁰⁶Pb* concentration and ²⁰⁷Pb*/²⁰⁶Pb* equations with error differentials defined as follows: (1) Isotope ratio determinations from standard errors (β/n) of mass spectrometer runs plus uncertainties in fractionation corrections based on multiple runs of NBS 981, 983, and U500 standards; (2) Spike concentrations from range of deviations in multiple calibrations with normal solutions; (3) Spike compositions from external precisions of multiple isotope ratio determinations; (4) Uncertainty in natural ²³⁸U/²³⁵U from Chen and Wasserburg (1981); and (5) Nonradiogenic Pb isotopic compositions from uncertainties in isotope ratio determinations of blank Pb and uncertainties in composition of initial Pb from estimates of regional variations based on references given above and consideration of rock type.

Figure 3-3. Stacked segments of $^{207}\text{Pb}/^{206}\text{Pb}$ versus $^{238}\text{U}/^{206}\text{Pb}$ concordia diagrams after Terra and Wasserburg (1972) showing concordant to discordant data points with concordia. (A) plots data from the Illinois River plutonic complex (IRPC), (B) plots data from IRPC dikes and samples from the Wimer and Ashland plutons, and (C) plots data from the Thompson Ridge and Greyback plutons, plus two samples from dikes cutting Onion Camp complex peridotite (WJB).

Figure 3-3A.

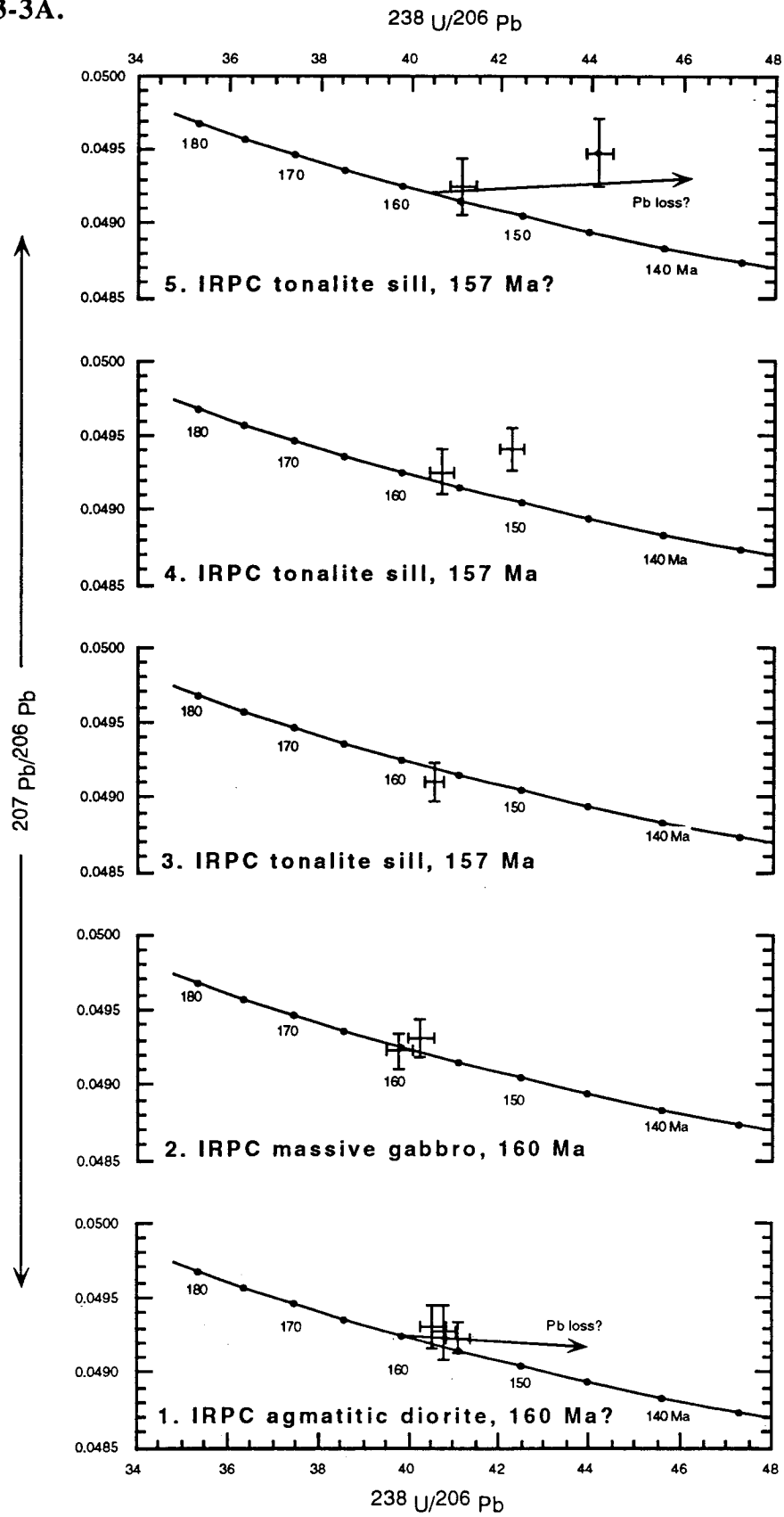


Figure 3-3B.

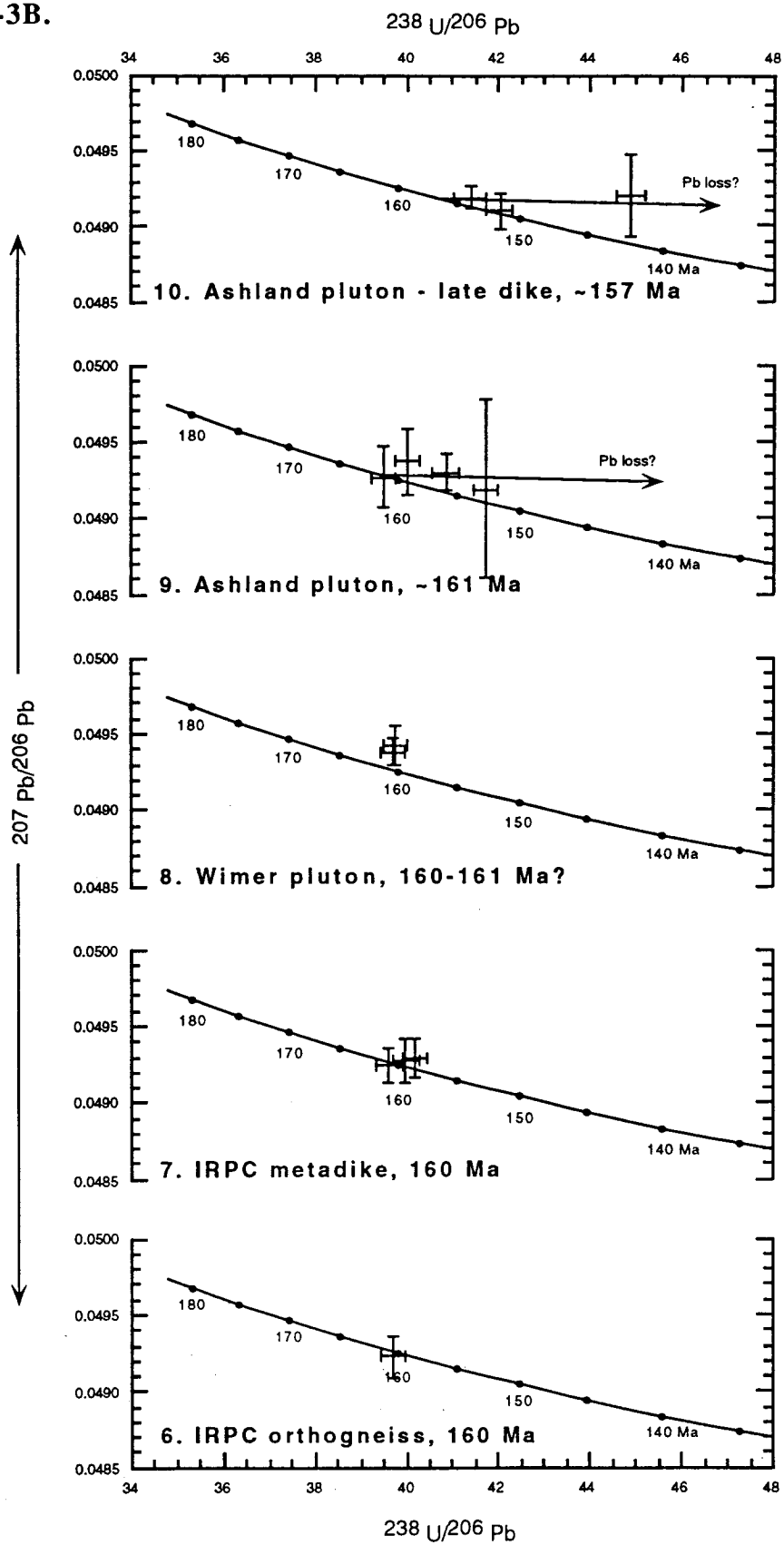
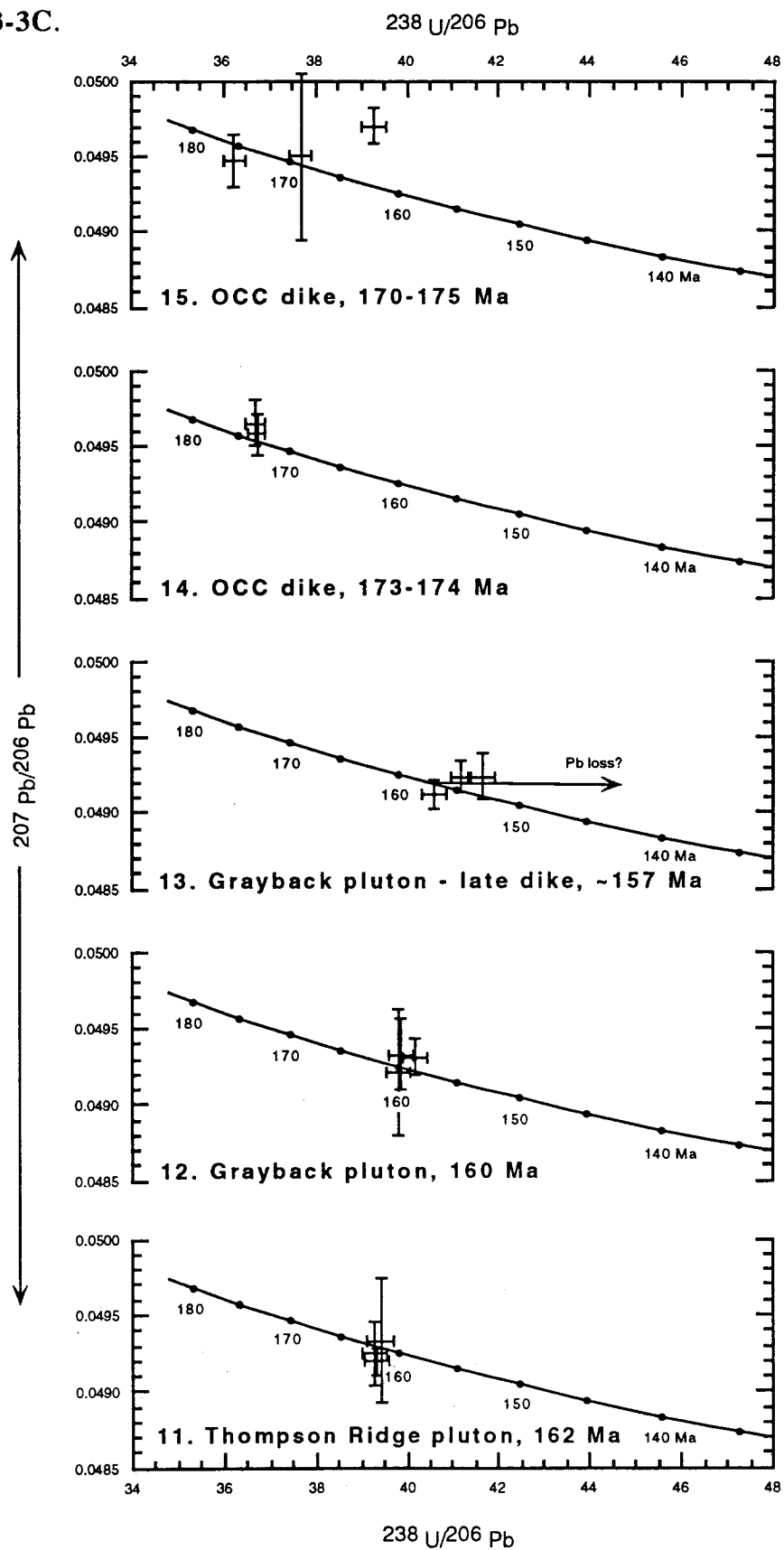


Figure 3-3C.



ages were calculated using the decay constants and isotopic abundances recommended by Stieger and Jager (1977).

The $^{40}\text{Ar}/^{39}\text{Ar}$ ages were determined from plateaus defined by ten or more incremental heating steps per sample. The plateaus may yield ages that are too old if the trapped component of Ar has a nonatmospheric composition (atmospheric $^{40}\text{Ar}/^{39}\text{Ar} = 295.5$) which can be determined by plotting $^{36}\text{Ar}/^{40}\text{Ar}$ versus $^{39}\text{Ar}/^{40}\text{Ar}$ to define an isochron whose x- and y-intercepts give the trapped and radiogenic Ar components (McDougall and Harrison, 1988). In the eight samples for which ages are reported here, the trapped component of Ar was found to be essentially atmospheric, and the plateau ages are considered reasonable age approximations (B.R. Hacker, personal communication, 1993).

The $^{40}\text{Ar}/^{39}\text{Ar}$ ages represent cooling ages unless the mineral, in this case hornblende, crystallized at temperatures below its closure temperature. Closure temperatures are estimated to be $\sim 500^\circ\text{C}$ for igneous hornblende, but for metamorphic hornblende, especially those which exhibit exsolution, the closure temperature may be significantly lower (Harrison and Fitz Gerald, 1986). The $^{40}\text{Ar}/^{39}\text{Ar}$ ages on igneous hornblende will be similar to crystallization ages only if cooling occurred rapidly (e.g., lavas or shallow dikes). Hornblende from plutonic bodies, particularly from plutons consisting of two or more phases, may have remained at elevated temperatures and therefore will yield ages substantially younger than the age of crystallization.

Data

An extensive body of radiometric age data exists for the igneous and metamorphic rocks exposed in the WJB and WTrPz belt of California and Oregon (Hacker and Ernst, 1994; Hacker et al., 1995). The following discussion presents the new U-Pb zircon and $^{40}\text{Ar}/^{39}\text{Ar}$ geochronologic data for pre-Nevadan plutons, amphibolite bodies, and dikes in Oregon with a brief discussion of the important geologic features of the samples and the rock units they represent. Then, in an overview of the entire Jurassic geochronometric data

Table 3-2. Summary of $^{40}\text{Ar}/^{39}\text{Ar}$ apparent ages.

| Lithologic Unit | Station | Lat/Long | Description | Mineral | Plateau Age ^a , Ma |
|--|------------|-----------------------------|---|------------|-------------------------------|
| <i>Rogue Formation</i> | 89-PP-4 | 42°18'10" N 123°46'51" W | Illinois River falls; crystal and lithic tuff breccia | hornblende | 153.4 ± 0.6 |
| <i>Illinois River plutonic complex</i> | 92-PP-70 | 42°15'43" N 123°52'11" W | Chetco River; norite | hornblende | 155.3 ± 0.5 |
| <i>Illinois River plutonic complex dikes</i> | 89-PP-12C | 42°18'38" N 123°46'51" W | Illinois River; hornblendite | hornblende | 156.0 ± 0.5 |
| | 89-PP-15 | 42°19'32" N 123°46'38" W | Illinois River; gneissic hornblende- biotite quartz diorite | hornblende | 156.3 ± 0.6 |
| <i>Briggs Creek amphibolite</i> | 91CR-9B | 42°24'04" N 123°44'50" W | Briggs Creek; metagabbro | hornblende | 156.8 ± 0.5 |
| | 91EDM-72A | 42°21'37" N 123°44'42" W | Soldier Creek; hornblende schist | hornblende | 157.9 ± 0.5 |
| <i>Onion Camp complex</i> | 91-EDM-81A | 42°20'40" N 123°39'40" W | Squaw Mountain; amphibolite gneiss | hornblende | 169.6 ± 0.5 |
| | 90-EDM-10 | 42°18'58" N 123°40'46" W | Squaw Mountain; hornblende schist | hornblende | 173.1 ± 0.6 |

set, these new data are considered in terms of the new constraints and insights they provide regarding the Jurassic geologic and tectonic evolution of the Klamath Mountains.

Specifically, these new data help to define: 1) the areal extent of the Late Jurassic magmatic arc, and 2) the two distinct and relatively short lived contractile deformational episodes that punctuated a relative continuum of Middle and Late Jurassic oceanic arc magmatism.

Middle and Late Jurassic Volcanoplutonic Arc Rocks

Rogue Formation. The Rogue Formation consists of a stratified sequence of basaltic to dacitic, calc-alkaline and arc-tholeiite volcanogenic rocks including lava, volcanic breccia, and volcanogenic turbidites (Chapter 2). Basal Rogue Formation strata are typically intercalated with Late Callovian to Early Oxfordian hemipelagic strata of the Galice Formation and are overlain by Middle Oxfordian to Kimmeridgian flysch deposits of the Galice Formation (Pessagno and Blome, 1990). In the central Illinois River drainage area, Rogue Formation strata appear to have been deposited directly upon a serpentinite matrix melange containing ophiolitic blocks that include pillow lava and interbedded Callovian chert (Chapter 2).

Saleeby (1984) obtained a concordant U/Pb age of 157 ± 1.5 Ma from zircon in dacitic tuff breccia in the type Rogue Formation (along the Rogue River) collected from a stratigraphic position located a few hundred meters below the contact with the overlying Galice Formation flysch. Prismatic, brown hornblende obtained from an ~1 meter thick lithic crystal tuff breccia collected below the Illinois River Falls yield an $^{40}\text{Ar}/^{39}\text{Ar}$ age of 153.4 ± 0.6 Ma. The deposits occur ~500 m stratigraphically above an interpreted conformable depositional contact upon serpentinite and serpentinitized peridotite. Its stratigraphic position relative to the Oxfordian/Kimmeridgian flysch of the Galice Formation is unknown because overlying deposits are truncated by the Chetco Pass fault.

Unless the thickness of the Rogue Formation is <1 km, the relatively younger apparent age of Rogue Formation strata at Illinois River Falls appears to occur at a deeper stratigraphic level in the Formation than the 157 Ma sample from the Rogue River, at least

relative to its basal contact. This apparent paradox in ages between the two localities, which occur ~75 km apart, can be reconciled either by a north to south progradation of volcanogenic strata, by a progressive onlap of Rogue strata onto a basement high in the central Illinois River area, or by a combination of both. Field and stratigraphic relations indicate that the considerable topographic relief characterized the Rogue-Galice ocean basin in the Late Middle Jurassic (Chapter 2) and the coarse, fragmental nature of Rogue Formation strata suggests that lateral variability was common. Thus the 153 and 157 Ma ages are considered representative ages for Late Jurassic arc volcanism in general agreement with the known radiometric ages of arc plutons in the region (discussed below).

Illinois River plutonic complex (IRPC). The IRPC forms the northwestern portion of the WJB in Oregon (Figure 3-2) and is a reversely zoned calc-alkaline to calcic plutonic body with coarsely crystalline gabbro (troctolite and norite) at its core mantled by medium grained gabbro (hornblende gabbro and norite), diorite, and subordinate quartz diorite (Jorgenson, 1970; Garcia, 1982; Chapter 2). Commingled low-K, biotite tonalite and garnet, two-mica tonalite form a late stage sill-like body at the roof of the complex. Both the main phase rocks and the late stage low-K tonalite have experienced dynamic amphibolite facies metamorphism that deformed the complex into an elongate NE-SW trending domal structure. Post-tectonic hornblende gabbro pegmatoid forms an ~0.5-1.0 km thick sill beneath the roof rocks at the southwestern extent of the complex. Metaperidotite, metagabbro, amphibolite gneiss, amphibolite schist, and subordinate impure quartzite, interpreted to represent Triassic to Middle Jurassic composite oceanic crust and mantle lithosphere, form the roof and wallrocks of the complex. Refer to Chapter 2 for a more detailed discussion of the IRPC.

U/Pb zircon data from the main phase of the complex and the late stage tonalite are shown in Figure 3-3. The main phase plutonic rocks, Samples 1 and 2, are both internally and externally concordant at ~157 and ~160 Ma respectively. Sample 1 is a hornblende-biotite quartz diorite with abundant ellipsoidal to highly flattened gabbroic enclaves.

Volumetrically, this lithology comprises <1% of the observed outcrops in the IRPC. The silicic host material is the most evolved rock type of the main phase plutonic rocks (see Chapter 2), consistent with the interpretation that Sample 1 represents magma that crystallized toward the end of the main phase plutonic rocks. Sample 2 is a hornblende diorite that occurs with hornblende gabbro and norite comprising the great bulk of the plutonic complex, and is considered to represent the best approximation for the crystallization age of the main phase of the IRPC.

Samples 3, 4, and 5 represent analyses of the low-K tonalite body. The U/Pb zircon data are yield internally concordant apparent ages of ~155-157 Ma for one size fraction from each sample (Table 3-1 and Figure 3-3). However, Samples 4 and 5 also include internally discordant fractions such that collectively the data are externally discordant. Factors which may have affected the isotopic systematics include a loss of radiogenic Pb during brittle deformation associated with displacement across the Chetco Pass fault, located ~0.5 km away, inheritance or entrainment of older zircon, or a combination of both factors. Geochemical data support the notion that the low-K tonalites exhibit a distinctive geochemical signature (high Sr/Y) consistent with their possible derivation as a partial melt from a garnet amphibolite. The amphibolitic wallrocks of the IRPC probably contain, at least in part, Triassic metabasalt and metasediments that conceivably could provide a source of older zircon for the low-K tonalites if they indeed formed as partial melts (Chapter 2). Field relations clearly indicate that the low-K tonalite sill intrudes that main phase gabbro and diorite and is therefore younger than 157 Ma consistent with the internally concordant ages of 155-157 Ma.

Samples 6 and 7 are quartz dioritic amphibolite grade metamorphosed dikes intruding the peridotite wallrocks of the IRPC. Samples 6 and 7 are internally and externally concordant at 160 Ma. Collectively the metamorphosed dikes are interpreted to have intruded the peridotite during the early phase of the main stage IRPC intrusion.

$^{40}\text{Ar}/^{39}\text{Ar}$ age determinations for rocks of the IRPC include recrystallized igneous hornblende from a main phase norite sample, igneous hornblende from a gabbroic dike intruding the peridotite wallrocks of the complex, and metamorphic hornblende from a quartz dioritic amphibolite gneiss encased in peridotite (Table 3-2). All three apparent ages overlap within error (1σ) at 155-156 Ma. Collectively, these data suggest that the IRPC and its immediate wallrocks cooled below approximately 450-500°C shortly after the late stage crystallization of the IRPC, at ~155-157 Ma. These cooling ages also tightly constrain the amphibolite grade dynamic recrystallization of IRPC rocks and metamorphism of its wallrocks to have occurred between 155 and 157 Ma.

Previously reported U/Pb and K/Ar data are in general agreement with new data reported here. U/Pb age determinations include 155 ± 2 Ma (late dike) and 166 ± 2 Ma (main phase) for rocks of the Rum Creek metagabbro (Saleeby, 1984) which is considered to form part of the wallrock complex of the IRPC. In view of the new age data from the IRPC, the 166 Ma age is considered to represent the crystallization age of ophiolitic crust that form part of the county rock of the IRPC. The 155 Ma sample is strikingly similar in age to the main body of the IRPC, and it seems likely that it represents an IRPC related dike or small intrusion in the metagabbro. Hotz (1971) reported three K/Ar hornblende ages reported for the IRPC and its wallrocks that, when recalculated using standardized decay constants (Steiger and Jager, 1977), are 154-155 Ma and are essentially equivalent in age to the $^{40}\text{Ar}/^{39}\text{Ar}$ reported here. Dick (1976) reports slightly older K/Ar ages, 158 ± 4 Ma and 161 ± 3 Ma for IRPC rocks from the southern part of the complex. Only the older of the two ages conflicts with the cooling history indicated by the new data and may reflect a slight problem with excess Ar.

Ashland pluton. The normally zoned Ashland pluton is a calc-alkaline pluton that intrudes rocks of the WTrPz belt (Figure 3-2). Detailed field and petrologic study of the pluton (Gribble et al., 1990) indicate that the Ashland pluton was formed through a

series of compositionally distinct magma pulses in two distinct stages. Stage I magmas include an earliest pulse of hornblende gabbro and two-pyroxene gabbro, followed by a suite of tonalitic rocks, and finally by a suite of K_2O - and P_2O_5 -rich quartz monzodioritic rocks. Stage II granodiorite and granite intrude the monzodioritic rocks and are themselves intruded by latest stage aplitic and granitic dikes.

Both Samples 9 and 10 exhibit discordance patterns with upper intercept, internally concordant data to indicate Stage I rocks are indeed older than Stage II rocks, in support of the field relations (Figure 3-3). The crystallization ages of Stage I quartz monzodiorite, Sample 9, and of Stage II hornblende-biotite granite, Sample 10, are interpreted to be ~161-162 Ma and ~156 Ma respectively. The discordance patterns are similar to those of the IRPC low-K tonalite samples and the Greyback late stage granodiorite sample. In addition the Ashland pluton rocks exhibit Sr and O isotopic data similar to the Greyback pluton (Barnes et al., 1992). Therefore, the discordance of the Ashland pluton samples is considered to reflect similar processes, the inheritance of older zircon either through partial melting or assimilation of Klamath crustal rocks. Samples 9 and 10 exhibit a pronounced Pb loss with respect to U signature that may reflect metamictization as a result of the relatively high U concentrations (Table 3-1).

Hacker et al., (1995) report an $^{40}Ar/^{39}Ar$ apparent age for hornblende of 152.0 ± 1.2 Ma, and previous K/Ar data for samples from the Ashland pluton yield a wide range of apparent ages from ~150-170 Ma for hornblende and ~136-155 Ma for biotite. The older K/Ar ages, >155 Ma for hornblende and >150 Ma for biotite conflict with the zircon and $^{40}Ar/^{39}Ar$ apparent ages, and may reflect problems with excess Ar or an analytical problem as well. Like the IRPC and Greyback-Thompson Ridge plutonic bodies, the geochronometric data from rocks of the Ashland pluton suggest that it remained hot (>500°C) for ~10 m.y.

The Wimer pluton has received relatively little study in the region (sample 8). It occurs along the NNE trend of the Greyback-Thompson Ridge belt, though its overall

quartz dioritic and tonalitic composition is more silicic than the Greyback-Thompson Ridge bodies. Preliminary U/Pb zircon data from the pluton yield internally discordant and externally concordant data with U/Pb ages of 160 Ma and Pb/Pb ages of 166-167 Ma (Table 3-1). Assuming these data reflect a slight inheritance of radiogenic Pb, the Wimer pluton is most likely 155-160 Ma, and therefore represents another Late Jurassic pluton related to the Greyback-Thompson Ridge and Ashland plutons. In order to confirm this, however, additional zircon fractions need to be analyzed.

Greyback - Thompson Ridge plutonic belt. The Greyback and Thompson Ridge plutons (Figure 3-2) are the largest and next to largest, respectively, of four intrusions that comprise an approximately linear, NNE striking zone of intrusion within the WTrPz belt of southern Oregon. The plutons appear to intrude a high angle fault zone separating greenschist facies volcanogenic metasedimentary rocks and ophiolitic melange on the west, correlable with rocks of the western Hayfork and Rattlesnake Creek terranes, respectively, from amphibolite facies Rattlesnake Creek terrane on the east (Donato et al., in review; Tomlinson, 1993). Swarms of mafic to felsic dikes occupy the zones between the three southernmost plutons indicating their cogenetic nature. The Greyback and Thompson Ridge plutons are calc-alkaline to calcic intrusions that consist of medium- to coarse-grained gabbro, diorite, quartz diorite, tonalite, and rare olivine clinopyroxenite. The Greyback pluton has been studied in the greatest detail and consists of an early, reversely zoned tonalite to gabbro that was intruded by synplutonic noritic and gabbroic magmas (Barnes et al., in review). Late stage activity was characterized by the intrusion of tonalitic and granitic dikes, many of which contain mafic enclaves and hybrid zones.

U/Pb zircon data from main phase diorite and gabbro of the Thompson Ridge-Greyback system, Samples 11 and 12, and late stage Greyback granodiorite, Sample 13, yield internally and externally concordant data at ~162-160 Ma and ~157 Ma respectively (Table 3-1 and Figure 3-3). The late-stage granodiorites in the Greyback show Sr and oxygen isotopic data that can be explained either by 1) the partial melting of "young" crustal

rocks in the deep Klamath crust (e.g., graywackes, possibly with detrital zircon from cratonal North America or older Klamath terranes or 2) the assimilation of primitive metasedimentary rocks, possibly the aforementioned wackes (Barnes et al., 1992). Also, Sample 13 contains locally abundant mafic magmatic enclaves, which argues for some kind of interaction between the granodioritic melt and a mafic end member.

Previously reported K/Ar age determinations of Greyback pluton rocks include a 153 ± 5 Ma on hornblende and 141 ± 4 Ma on biotite (Hotz, 1971). More recently, Hacker et al, (1995) report $^{40}\text{Ar}/^{39}\text{Ar}$ ages on hornblende of 157.3 ± 1.4 Ma for a sample from the Greyback pluton and 153.9 ± 0.8 Ma and 154.1 ± 0.5 Ma for samples from the Thompson Ridge pluton. The hornblende ages suggest that the Greyback-Thompson Ridge plutonic system may have remained hot ($>500^\circ\text{C}$) for ~ 6 -9 Ma following the crystallization of the main plutonic phases of the plutons and ~ 0 -3 Ma following the crystallization of late stage intrusions.

Basement rocks of the Middle to Late Jurassic volcanoplutonic arc

Briggs Creek amphibolite. The Briggs Creek amphibolite body (BCA) consists primarily of amphibolite gneiss and hornblende schist with subordinate micaceous and garnetiferous quartzite, gneissic gabbro, and meta-serpentinite and is interpreted to represent a fragment of relatively low P/T metamorphosed oceanic crust (Coleman and Lanphere, 1991). Field relations and minor and trace element geochemical data suggest that the BCA represents the higher grade metamorphosed equivalents of the Onion Camp complex (Chapter 2).

Three $^{40}\text{Ar}/^{39}\text{Ar}$ apparent ages of metamorphic hornblende range from ~ 156 to ~ 158 Ma (Table 3-2) which conflict with previously determined K/Ar hornblende ages of ~ 138 -131 Ma (Coleman and Lanphere, 1991). One of the K/Ar samples was re-analyzed by the $^{40}\text{Ar}/^{39}\text{Ar}$ method and yielded a plateau age of 156 Ma and an isochron age of ~ 155 Ma suggesting that the K/Ar ages may reflect Ar loss, or an analytical problem as well (Hacker

et al, 1995). Thus age data suggest that the BCA cooled below $\sim 450^{\circ}\text{C}$ by 156-158 Ma, approximately 1-2 Ma prior to the $^{40}\text{Ar}/^{39}\text{Ar}$ ages obtained from the main phase rocks of the IRPC and its immediately adjacent wallrocks. This subtle difference in apparent cooling ages may reflect the gradual relaxing of isotherms during cooling of the IRPC from the more distal BCA toward the plutonic body. Finally, though the BCA rocks apparently cooled beneath the closure temperature of hornblende at ~ 156 -158 Ma, structural features and ubiquitous greenschist facies retrogression indicate that the BCA unit continued to experience penetrative deformation until perhaps as young as ~ 150 Ma when undeformed mafic and intermediate dikes cut the regional foliation.

Onion Camp complex. The Onion Camp complex (OCC) consists of serpentinitized peridotite and an overlying serpentinite matrix melange with blocks of greenschist to amphibolite facies metavolcanic and metasedimentary rocks cut by heterogeneous mafic intrusive complexes. On the basis of field relations and geochemical signatures, the complex is correlated with the Rattlesnake Creek terrane of the WTrPz belt (Chapter 2; Yule and Saleeby, 1992). A stratified sequence of interlayered volcanogenic, hemipelagic, and olistostromal strata overlie the OCC which is interpreted to represent a rifted fragment of the RCT that became separated from the WTrPz belt during regional extension and the generation of the Josephine inter-arc basin (Chapter 2). Prior to this report, the only previously reported age control for these rocks consisted of a Late Triassic age determination obtained from a radiolarian chert locality near Onion Camp (Roure and DeWever, 1983).

Two samples of amphibolite gneiss obtained from complexly folded bodies of amphibolite located near Squaw Mountain yield $^{40}\text{Ar}/^{39}\text{Ar}$ hornblende plateau ages of 169.6 ± 0.5 Ma and 173.1 ± 0.6 Ma (Table 3-2). Evidence of apparent regional metamorphic cooling of Middle Jurassic age is exceedingly rare in the Klamath Mountains province, a peculiarity considering the fact that the province experienced pronounced shortening and thrust imbrication during this time (Wright and Fahan, 1988). The only other known

Middle Jurassic ages not related to arc magmatism include an amphibolite in the RCT near Preston Peak that yielded an $^{40}\text{Ar}/^{39}\text{Ar}$ isochron age of 175.5 ± 2.5 Ma (G.D. Harper, personal communication, age determined from same sample which yielded a K/Ar hornblende age of $\sim 190 \pm 7$ Ma, in Gorman, 1985) and the K/Ar hornblende age of 165 ± 3 Ma from amphibolite tectonite in the Preston Peak ophiolite (Saleeby et al., 1982).

Additional age constraint is provided by felsic dikes that intrude serpentinized peridotite of the Onion Camp complex (Table 3-1 and Figure 3-3). U/Pb zircon data from Sample 14 yields internally and externally concordant U/Pb apparent ages of ~ 173 Ma with slightly older Pb/Pb ages of ~ 175 Ma. Data for Sample 15 exhibit discordant behavior but two internally concordant, but externally discordant fractions suggest an age of ~ 170 - 175 Ma, consistent with the concordant apparent age of Sample 14. The relatively high U concentrations of Sample 15 may explain its discordance pattern (Table 3-1). Collectively, the $^{40}\text{Ar}/^{39}\text{Ar}$ and U/Pb data establish the age of the Onion Camp complex as pre-Middle Jurassic, consistent with the independent field and geochemical data that correlate the OCC rocks with the Rattlesnake Creek terrane.

Geochronologic overview

The radiogenic age data presented in this paper combined with a wealth of pre-existing age data provide an opportunity to re-examine the temporal and spatial variability of Middle Jurassic to Cretaceous arc magmatism and metamorphism in the Klamath Mountains province, and to re-evaluate the concept of Jurassic orogeny in the province. Specifically, previous workers have subdivided the Middle Jurassic to Cretaceous plutons of the province into six belts separated primarily on the basis of apparent age data and spatial distribution (Irwin, 1985). However, four of these belts, the Chetco, Grants Pass, Greyback, and Wooley Creek belts, contain plutons, dated by the U/Pb zircon method during this study, whose apparent ages overlap and bring into question the relevance of

these belt designations. In addition the Ar/Ar apparent ages determined for amphibolite tectonites in the WJB are distinct from those ages determined for amphibolites from other terranes of the Klamath Mountains province and suggest that cooling of amphibolite belts was spatially and temporally variable in the region, a feature that must be incorporated into a model for the Jurassic geologic and tectonic evolution of the province.

Figure 3-4 shows a plot of a total of 238 separate geochronometric analyses, subdivided by gross lithology and age dating method, for Middle Jurassic to Early Cretaceous rocks of the Klamath Mountains province. These data include the ages reported in this article plus most of the previously published geochronometric data reported by numerous workers (the data are tabulated in Hacker et al., 1993; also see caption to Figure 3-4 for individual author references). Some K/Ar data (< 10 analyses) were omitted from Figure 3-4 when more recent Ar/Ar age determinations provided distinctly different ages for the same or related rock sample and the K/Ar data were thus interpreted as flawed, probably due to excess Ar, Ar loss, or possible analytical error.

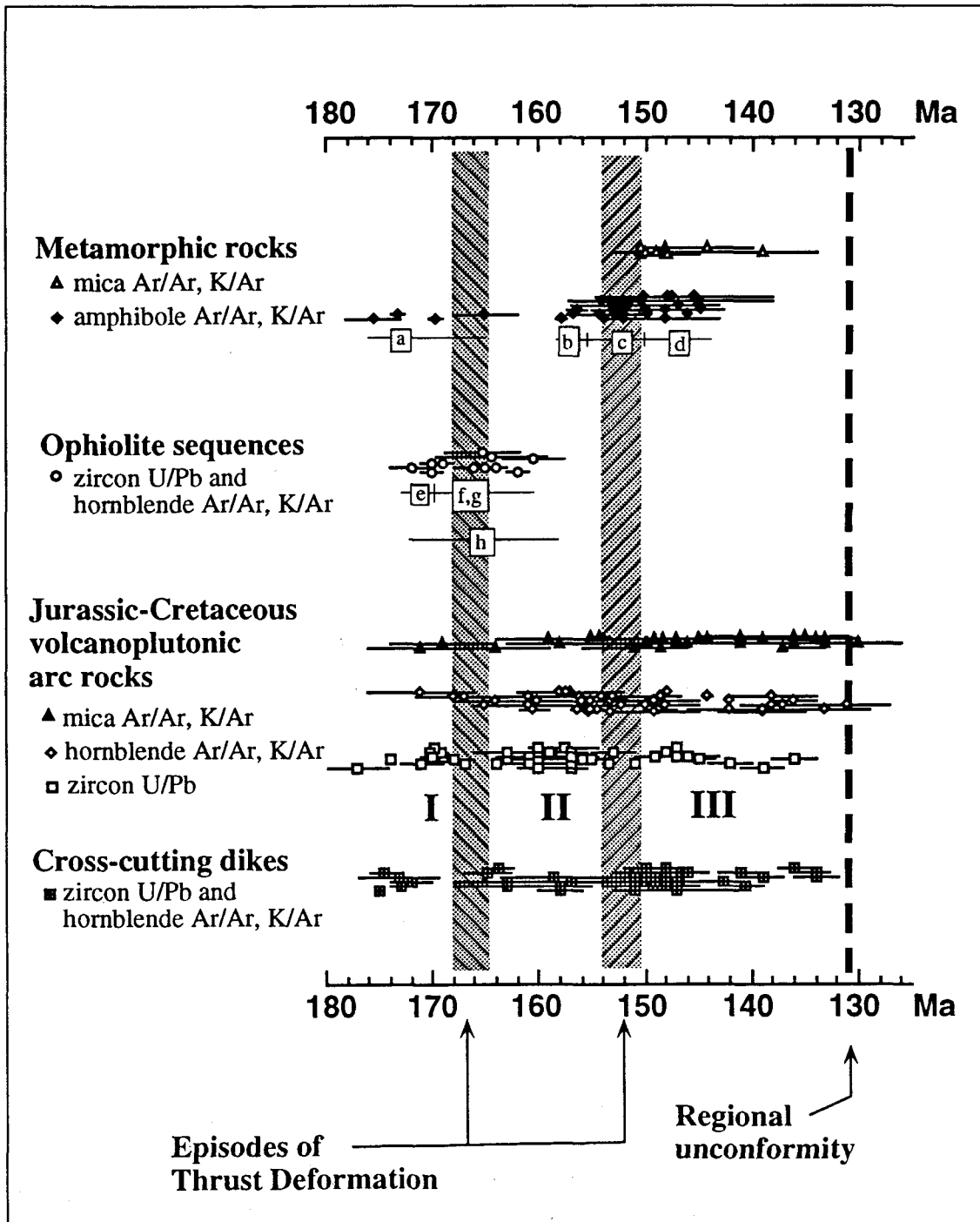
To a first order, the following features are evident from the age data shown in Figure 3-4: 1) a continuum of volcanoplutonic arc magmatism from ~175-135 Ma, 2) ophiolite generation from ~172-162 Ma, and 3) two ~10 m.y. periods of cooling recorded in metamorphic rock units, one in the Middle Jurassic that is only locally preserved, and a more widespread Late Jurassic cooling episode. Superimposed on these data are the approximate timing of regional dynamic metamorphism and active thrust faulting in the Klamath Mountains province, a Middle Jurassic event as outlined by Wright and Fahan (1988), and another occurring ~10 m.y. later in the Late Jurassic (e.g., Harper et al., 1994). Note that the Middle Jurassic thrusting event also coincides with ophiolite generation (Figure 3-4) and suggests that synchronous extensional and contractile tectonism characterized the Middle Jurassic tectonic evolution of the province.

Figure 3-4. Middle Jurassic to Early Cretaceous geochronometric data of the Klamath Mountains province. Error bars shown are 1σ analytical error for Ar/Ar and K/Ar data, and 2σ analytical error for concordant U/Pb zircon data; U/Pb zircon data shown without error bars are approximate ages interpreted from discordant data as reported by authors.

1) Hornblende (n=39) and biotite (n=11) Ar/Ar and K/Ar apparent age data of metamorphic rocks are primarily from amphibolite facies mafic rocks with a few analyses of greenschist and transitional greenschist-blueschist facies rocks; (a) data from amphibolites of the “rift-edge” facies of the Josephine marginal ocean basin (see text), (b) data from amphibolites of Briggs Creek amphibolite, western Jurassic belt (WJB), (c) data from amphibolites of the Rattlesnake Creek terrane sensu latu, Marble Mountains sensu strictu, western Paleozoic and Triassic belt (WTrPz belt), and (d) data from amphibolites of the May Creek terrane, WTrPz belt. 2) U/Pb zircon (n=8) and Ar/Ar hornblende (n=3) apparent age data of ophiolite sequences including the Josephine ophiolite sensu strictu and related ophiolitic rocks occurring in the Klamath Mountains province and in outliers of WJB rocks in southwesternmost Oregon (e.g., Blake et al., 1985); (e) 170-172 Ma China Peak dike complex and metadiorite of the Condrey Mountain schist (Saleeby and Harper, 1993), (f) 169 Ma Snow Camp ophiolite and 164 Ma Wild Rogue ophiolite (Saleeby, 1984), and (g) the 166 Ma Rum Creek metagabbro (Saleeby, 1984), 164 Ma Preston Peak ophiolite, and 162 Ma Josephine ophiolite sensu strictu (Saleeby and Harper, 1993). 3) U/Pb zircon (n=48), Ar/Ar and K/Ar hornblende (n=45) and biotite (n=33) ages of plutons and subordinate related volcanogenic rocks (western Hayfork terrane and Rogue Formation). Data suggest the province experienced a continuum of subduction related magmatism spanning ~30 m.y. Collectively the Klamath Mountains “batholith” consists of three phases, labeled I, II, and III, subdivided on the basis of age data, areal distribution patterns (Figure 4), and geochemical data (see text for discussion). Phase I lasted from ~177-167 Ma, phase II from ~165-153 Ma, and phase III from ~150-135 Ma. 4) U/Pb

zircon, Ar/Ar and K/Ar apparent age data for cross-cutting dikes (n=41) generally considered related to arc magmatism on the basis of geochemistry, though conceivably some of the ~175-160 Ma dikes may be related to ophiolite genesis.

Age data are from this report (Tables 1 and 2 and numerous other investigators tabulated in Hacker et al., (1993a) and Hacker et al., (1995), including Barnes et al., (1986); Brouxel et al., (1989); Davis et al., (1965); Dick (1976); Evernden and Kistler (1970); Gray (1985); Hacker et al., (1993b); Helper et al., (1989); Hotz (1971); P. Hotz in Ramp (1984); Kays et al., (1977); Lanphere et al., (1968); M.A. Lanphere in Irwin (1985); Renne and Scott (1988); Saleeby (1984); Saleeby (1990); Saleeby et al., (1982); Saleeby and Harper, (1993); Snoke et al., (1981); Ohr (1987); Welsh (1982); Wright and Fahan (1988); Wright and Wyld (1986).



Middle Jurassic to Early Cretaceous volcanoplutonic arc rocks

Following an ~20 m.y. hiatus, arc magmatism in the Klamath Mountains province was re-established by ~175 Ma (Wright and Fahan, 1988; Wright and Wyld, 1994). Though the age data indicate that arc magmatism continued essentially uninterrupted for ~40 m.y., a closer examination of the age data determined from cross-cutting dikes and from plutonic and volcanic rocks (and U/Pb zircon ages) reveals that relatively short-lived, amagmatic breaks occur at ~167-164 Ma and ~153-150 Ma (Figure 3-4). The zircon ages of the arc volcanoplutonic series were primarily obtained from plutonic rocks with subordinate data from related volcanic rocks (see caption to Figure 3-4). The apparent gaps in the data are considered genuine since the database is essentially complete; the only Jurassic to Cretaceous plutons not dated by U/Pb zircon methods are the White Rock and the Vesa Bluffs plutons whose Ar/Ar and K/Ar ages suggest they do not overlap the age of either of the two amagmatic periods (Hotz, 1971; and Hacker et al., 1995). Moreover, the apparent amagmatic breaks coincide with known tectonic events and distinct changes in pluton geochemical and isotopic signatures (discussed below) suggesting that a fundamental reorganization of the arc batholith occurs at this time. On this basis, the volcanoplutonic arc rocks of the Klamath province are subdivided into three phases, labeled I, II, and III on Figure 3-3.

It is interesting to note that the Ar/Ar and K/Ar age data overlap the apparent amagmatic breaks in the zircon age data and illustrate the ambiguity in interpreting the amphibole and mica ages. For example, the cooling age could represent 1) normal, isobaric cooling of a plutonic body following its intrusion, or 2) premature “quenched” cooling related to a particular tectonic process. In batholithic belts where continuous magmatism is punctuated by compressional and extensional events, one might expect to see both types of cooling reflected in the data. This indeed appears to be the case for plutonic

rocks of the Klamath Mountains province based on the distribution of amphibole and mica cooling ages with respect to age (Figure 3-4). Specifically, the apparent continuum of cooling ages from ~170-130 Ma suggests that cooling of the plutons varied greatly in time and place and is likely related, at least in part, to the isobaric cooling of individual plutonic centers rather than regional metamorphic events. Additionally, the clustering of biotite cooling ages immediately following Late Jurassic thrusting event suggests that regional tectonism also, in part, controlled the cooling ages recorded in the region. Thus interpreting the timing and duration of distinct regional tectonic events in the province must be viewed through a “background” of cooling ages related to areally and temporally variable arc magmatism.

Middle to Late Jurassic ophiolite sequences

Compared to the volcanoplutonic arc rocks, sparse age data exist for the Middle to Late Jurassic ophiolite sequences of the Klamath Mountains province, collectively referred to here as the Josephine ophiolite *sensu lato* (Figure 3-4). However, the age data were obtained from ophiolite sequences occurring over the entire region and represent a relatively thorough sampling of the ophiolite, thus the spread in ages exhibited in Figure 3-4 is probably close to delineating the extensional episode that produced the ophiolite sequences, though further age determinations may widen this range. The range in age of the Klamath ophiolites is essentially identical to the range in ages reported for the Coast Range ophiolite of California (Figure 3-4, and in Saleeby, 1992) and suggests that the Josephine and Coast Range ophiolites are related. The ophiolites represented by the age data in Figure 3-4 include the Josephine ophiolite *sensu strictu* (Harper, 1984), and a number of separate, partial to complete ophiolite sequences occurring in the WJB, in related outliers in western Oregon, and in the Rattlesnake Creek terrane that, collectively with the Josephine ophiolite, are considered to have once floored a marginal ocean basin fringing western North America (e.g., Saleeby, 1994). Included with the Josephine ophiolite “*sensu lato*” is the Preston

peak ophiolite (Snoke, 1977), the Devil's Elbow ophiolite (Wright and Wyld, 1986), the Wild Rogue (Marial) and Snow Camp ophiolites (Blake et al., 1985), and the China Peak mafic metadikes and metagabbro of the Condrey Mountain schist (Saleeby and Harper, 1993).

The inclusion of the China Peak dike complex with the Josephine ophiolite *sensu lato* conflicts with the interpretation of other investigators (e.g., Hacker et al., 1995; Helper, 1986) who consider the complex to be equivalent with intrusive rocks of the western Hayfork terrane. This correlation is based primarily on the apparent overlap in age between WHT rocks and the dike complex combined with the fact that the China Peak complex lies on strike with the WHT volcanic rocks. Exclusion of the China Peak dike and metagabbro ages from the Josephine ophiolite *sensu lato* restrict the age of ophiolite genesis to ~169-160 Ma, only slightly different than the ~172-170 Ma range if they are included. In either case, it is apparent that ophiolite genesis in the Klamath province is ongoing before, during and after the Middle Jurassic thrusting event and underscores the areal variation in tectonic regime that must have typified the Klamath Mountains province in the Middle Jurassic. This contemporaneity between extension and contractile tectonism must be incorporated into any model for the Jurassic tectonic evolution of the province.

Metamorphic rocks

Age determinations of metamorphic rocks of the Klamath Mountains province in general were obtained from low P/T amphibolite facies metamorphic terranes that probably formed at depth within the hot, active oceanic arc environment. The ages are regarded as cooling ages which record either 1) the extinguishing of the arc by extensional or contractile tectonic processes, 2) the isobaric cooling of the arc, or 3) a combination of both.

With the exception of the four analyses which yield Middle Jurassic ages, the geochronometric data obtained from metamorphic rocks of the Klamath Mountains province are Late Jurassic in age (Figure 3-4). The Middle Jurassic cooling ages are

obtained from amphibolite tectonites which occur in parts of the Rattlesnake Creek terrane interpreted to represent the “rift-edge” facies of the Josephine ophiolite (Snook, 1977; and Chapter 2); two samples are from the rifted fragment of RCT in the WJB and two are from the region referred to as the Preston Peak ophiolite (Saleeby et al., 1982; and Harper, personal communication, 1995). In addition these samples occur in regions which were not widely intruded by post-164 plutons (Figure 3-2) and therefore probably record Middle Jurassic cooling in response to tectonism. Given that the Middle Jurassic amphibolites occur in a “rift-edge” tectonic setting, it seems likely that they record cooling in response to extension, and perhaps record the earliest phases of rifting which eventually formed the Josephine marginal ocean basin. With only four age analyses, it is difficult to determine whether the ~10 m.y. range in apparent age is genuine or an artifact of sparse data. Three of the analyses are relatively high precision $^{40}\text{Ar}/^{39}\text{Ar}$ hornblende ages ranging from 169-175 Ma, with a fourth relatively poorly constrained K/Ar age of ~165 Ma. Even if the 165 Ma age is rejected as too young, the Ar/Ar data suggest that the Middle Jurassic cooling is temporally and spatially variable.

Similar to the Middle Jurassic data, the Late Jurassic amphibolite ages span a relatively wide time period, >10 m.y. for both the biotite and amphibole data (Figure 3-4). However, an interesting trend with respect to sample location is contained within the Late Jurassic amphibole data (Figure 3-4). Specifically, WJB amphibolites yield the oldest ages (~158-155 Ma, this report), amphibolites in the central WTrPz belt (Marble Mountains area) yield intermediate (~155-148 Ma, Hacker et al., 1995), and amphibolites in the northern WTrPz belt (May Creek terran of Donato, 1991) amphibolites yield the youngest ages (~144-148 Ma, Hacker et al., 1995). Differences in the local and regional geology help explain these apparently distinct clusters of ages. The amphibolites in the WJB and WTrPz belts are separated by the Orleans-Preston Peak fault which has experienced displacements of 100 km or greater (Jachens et al., 1986), thus slightly older ages in the WJB may represent the early phases of cooling that swept east/southeastward (present

coordinates) across the province during Nevadan thrusting. This concept seems at odds with the central and northern WTrPz belt data which, if anything, suggest a south to north cooling trend. However, Early Cretaceous plutons intrude the northern WTrPz belt amphibolites, but are absent in the central WTrPz belt amphibolites, suggesting that the relatively young northern belt ages may record a post-deformational cooling age while the WJB and central belt amphibolite ages record the temporal and spatial variation of Nevadan underthrusting in the region.

Discussion

Klamath Mountains batholithic belt (KMBB)

The Middle Jurassic to Cretaceous volcanoplutonic rocks of the Klamath Mountains province define a virtual continuum of oceanic arc magmatism over an ~40 m.y. period that appears to occur in three distinct phases, with each phase separated by a short-lived contractile tectonic event. Each phase also exhibits distinct geochemical and isotopic characteristics in support of the three-fold subdivision of the arc rocks (Barnes et al., 1992). Other general features of the plutons include 1) magma genesis linked to subduction, 2) the presence of numerous composite magmatic centers which were active for ~5-10 m.y., e.g., the Greyback-Thompson Ridge chain of plutons, and 3) a distinct discordance of most plutons with respect to regional structural features, particularly the post-164 Ma plutons. The aforementioned traits are typical of long-lived batholithic systems and suggest that the Middle Jurassic to Cretaceous oceanic arc rocks of the Klamath Mountains province in essence comprise an oceanic arc batholithic complex.

The Klamath Mountains batholithic belt (KMBB) represents a distinctly different type of long-lived batholithic system from the well known, composite batholiths of the Cordillera, e.g., the Peninsular Ranges, Sierra Nevada, and Coast batholiths. In comparison, the KMBB has country rock to pluton ratios of ~1-2, as opposed to <0.05 in the composite batholiths, and contains relatively small numbers and sizes of plutons. The

composite batholiths are believed to have developed above a subduction zone at an ocean/continent convergent boundary experiencing relatively high rates of strongly coupled subduction (Andean type of continental margin, Dickinson, 1976). In contrast, the KMBB is considered to represent a long-lived batholithic system that developed above a subduction zone at a loosely coupled ocean/ocean convergent boundary. In modern settings (e.g. the Marianas region), loosely coupled subduction boundaries are characterized by retreating subduction trenches (hinge roll-back) and extension in the overriding plate, and generally occur where very old (>150 m.y.) oceanic lithosphere is being subducted. By analogy with the modern western Pacific, Panthalassan oceanic lithosphere being subducted beneath the Middle and Late Jurassic Sierran-Klamath region would probably generate similar sorts of arc systems.

Because of the striking differences between the KMBB and the great Cordilleran batholiths, the former may serve as a model for Middle Jurassic to Early Cretaceous magmatism in the Cordillera. The following discussion describes the magmatic history and the three phases of the KMBB, labeled I, II, and III below, and describes some of its distinctive features. If the KMBB is indeed representative of Cordilleran wide magmatism during the Middle Jurassic to Early Cretaceous, similar sorts of features should be apparent, namely the broadly three magmatic phases with distinctive geochemical and isotopic signatures and evidence for distinct tectonic events separating each phase.

Magmatic history of the KMBB

Phase I. Phase I plutons are generally restricted to the southern portion of the Klamath mountains province and form a narrow, north-trending belt (Figure 3-5 A) and include the composite Ironside Mountain batholith (Charlton, 1979), the Forks of Salmon pluton (Hotz, 1971), and related small plutons in the southern part of the province. Coeval metavolcanic rocks occur to the north along the trend of the phase I (Ironside Mountain belt) plutons and are considered to represent their extrusive equivalents (Charlton, 1979).

U/Pb zircon ages from the plutonic rocks cluster at ~169-170 Ma and K/Ar hornblende ages from the metavolcanic rocks range from ~167-177 Ma (Figure 3-4, data from Wright and Fahan, 1988). Compositions of the plutonic rocks primarily range from gabbro to quartz monzodiorite with subordinate granodiorite and granite (Charlton, 1979). They are calc-alkalic and contain higher contents of K₂O and Rb (at lower SiO₂ contents) than any of the younger phase plutons (Barnes et al., 1992). Limited isotopic data exist for phase I rocks, but the metavolcanic rocks have high ϵ_{Nd} and low ϵ_{Sr} values that plot within the field for mantle-derived basalts (within the “mantle array”) and a $\delta^{18}O$ value of 10.2 ‰ (Barnes et al., 1992). The narrow belt of the phase I magmatic rocks relative to later phases is probably due to Middle Jurassic thrusting and contractile deformation which resulted in the amalgamation of terranes to form the WTrPz belt and formed a gently eastward dipping imbricate thrust stack which served as the country rock for later plutons of the KMBB.

Phase II. Phase II magmatism ranges in age from ~164-153 Ma (Figure 3-4) and primarily occurs within the older terranes of the WTrPz belt. Notable exceptions include the IRPC of the WJB and possibly the Middle Jurassic Castle Crag pluton (Figure 3-5 B) which intrudes the eastern Klamath terrane and has yielded K/Ar biotite and hornblende ages ranging from 175-162 Ma (Lanphere et al., 1968). Compositions of phase II plutons are calc-alkaline to calcic and include gabbroic to dioritic plutons with varying amounts of more evolved compositions ranging from quartz monzodiorite to granite. Relative to phase I, phase II plutons have lower K₂O and Rb, lower ϵ_{Nd} and higher ϵ_{Sr} values, and relatively high $\delta^{18}O$ values indicating that phase II plutons probably include assimilated metasedimentary rocks or partial melts derived from metasediments (Barnes et al., 1992).

Phase III. Magmatism associated with phase III of the KMBB is more widely distributed than the previous phases and is represented by plutons ranging in age from ~150-135 Ma (Figures 3-4 and 3-5 C). The ages of phase III plutons are generally Latest Jurassic in the WJB and in the western portion of the WTrPz belt, and tend to young

Figure 3-5. Magmatic and tectonic evolution of the Klamath Mountains batholithic belt. Generalized maps of the Klamath Mountains province showing the areal distribution of the three phases of the Klamath Mountains batholith. A) shows phase I (177-167 Ma) plutons along the trend of the Ironside Mountain batholith. B) shows phase II (164-153 Ma) which occur north of the Salmon “tectonic” line. Also note the thrust faults which formed immediately prior to phase II magmatism (167-164 Ma). C) shows phase III (150-135 Ma) which occurs throughout the province and in general progresses across the province from WNW to ESE.

Figure 3-5 A.

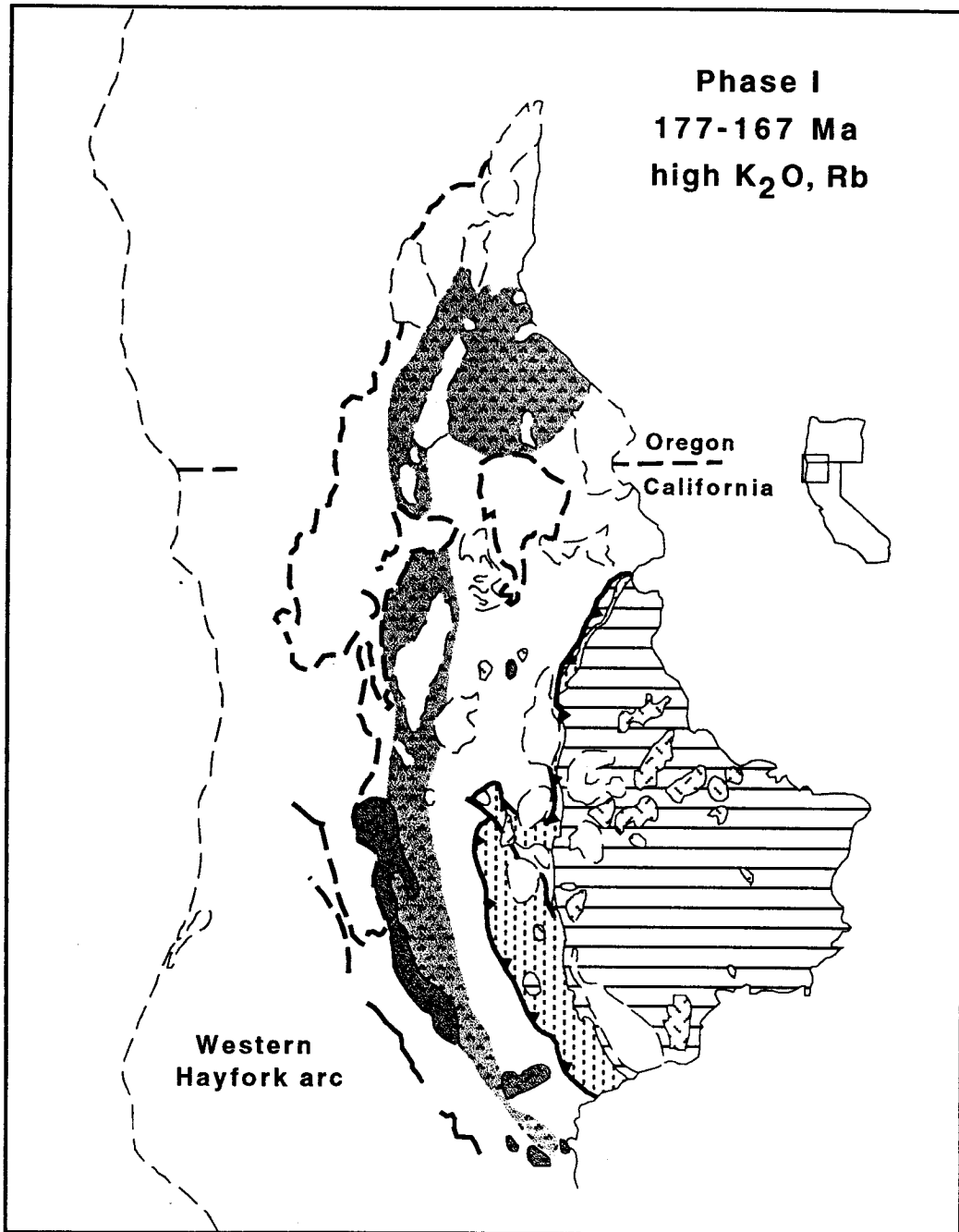


Figure 3-5 B.

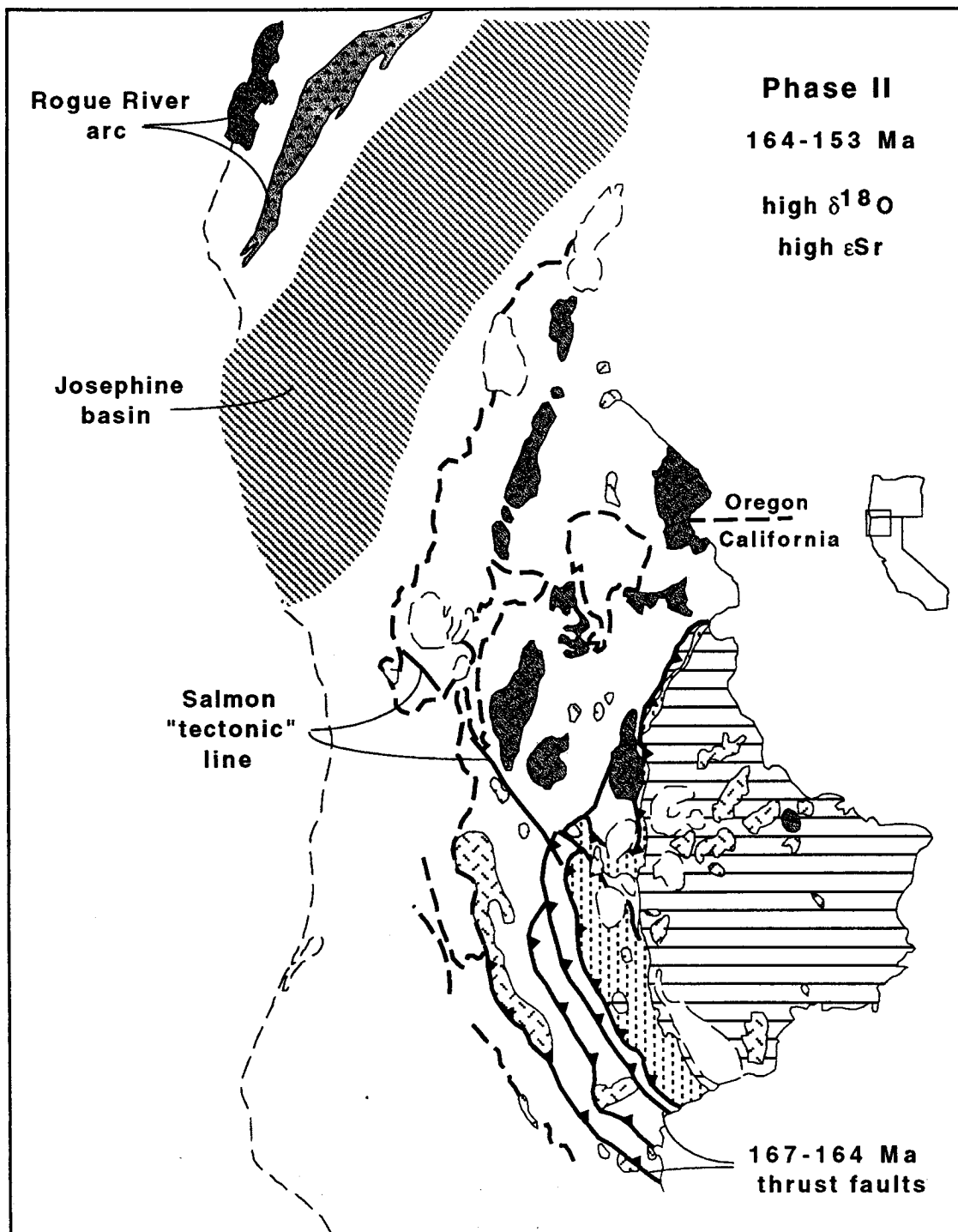
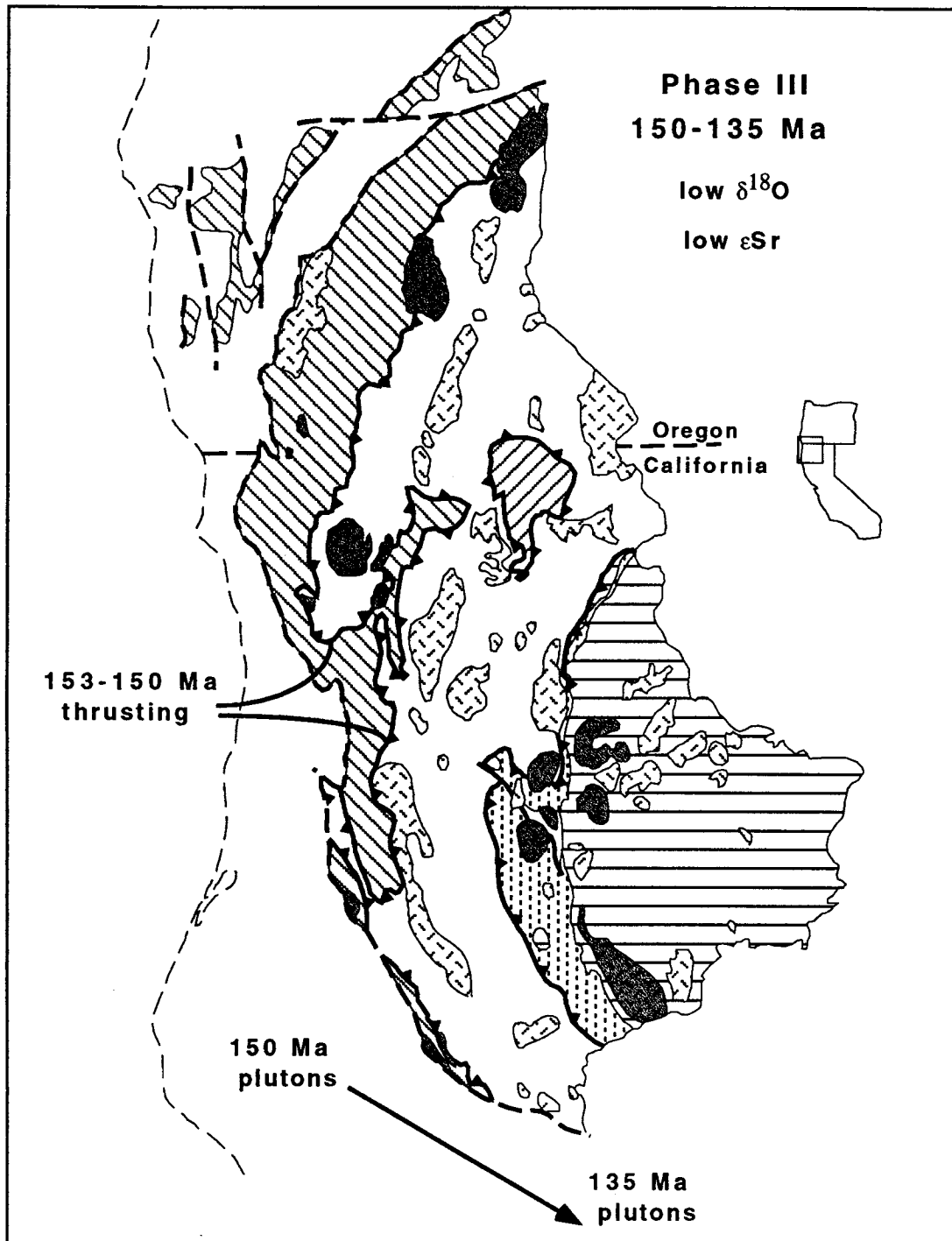


Figure 3-5 C.



toward the eastern part of the province suggesting that arc magmatism migrated from west to east across the province during this time (Figure 3-5 C). Phase III plutons are dominated by tonalite-trondhjemite plutons from ~150-140 Ma (e.g., the White Rock, Pony Peak, Craggy Peak, Sugar Pine, Caribou Mountain, and Canyon Creek plutons) but also contain one diorite-tonalite-granodiorite (the Deadman Peak pluton). Tonalite-trondhjemite magmatism was followed by the intrusion of dioritic to granodioritic plutons at ~140-135 Ma (the Grants Pass, Yellow Butte, and Shasta Bally plutons). Phase III tonalite-trondhjemite plutons are calcic with the lowest K_2O and Rb contents of all plutonic suites whereas the diorite-granodiorite plutons are calc-alkalic and are similar in K_2O and Rb to the phase II plutons (Barnes et al., 1992). The isotopic signatures of phase III plutons are distinctly different from phase II plutons with relatively high ϵ_{Nd} and low ϵ_{Sr} values and low high $\delta^{18}O$ values. Barnes et al. (1992) interpret these data to indicate that phase III plutons show little evidence of assimilation of metasedimentary crust but display trace-element evidence consistent with an origin by partial melting of young ophiolite rocks underthrust beneath the region at ~150 Ma.

Distinctive features of the KMBB

The Salmon tectonic line. Phase II plutons are conspicuously absent in the southern third of the province southwest of a vaguely defined northwest-trending zone that parallels much of the Salmon River, a zone referred to by Irwin (1985) as the Salmon tectonic line (Figure 3-5 B). However, since no offset and no deformation related to displacement has been documented with this zone, the Salmon “tectonic” line is considered a non-tectonic feature and instead is interpreted to represent the fore-arc edge of a NW-trending magmatic arc. This interpretation implies that the axis of arc magmatism rotated ~30-45° counter-clockwise relative to the north trending axis of phase I magmatism, and

probably resulted from Middle Jurassic thrusting, Middle Jurassic extension related to ophiolite genesis, or a combination of both.

Parallel arc and back-arc magmatism. Another intriguing feature of phase II magmatism involves the apparent juxtaposition of parallel magmatic arcs, specifically the occurrence of the IRPC located directly to the west of the WTrPz belt phase II plutons (Figure 3-5 B). The IRPC, as part of the Late Jurassic Rogue River “active” island arc complex (Garcia, 1979; 1982), and the phase II plutons which intrude the “remnant arc” WTrPz belt, are considered to have developed on opposite sides of the Josephine marginal ocean basin (Chapter 2; Snoke, 1977; Saleeby and others, 1982; Harper and Wright, 1984). Assuming the plutons represent magmas generated by subduction related processes, a reasonable assumption based on geochemical data, one of two tectonic scenarios is required: 1) the active and remnant arc regions of the Josephine marginal ocean basin were each situated above separate east-dipping subduction zones, one beneath the arc and another beneath the back-arc, or 2) the active and the remnant arc were situated above the same east-dipping subduction zone. The first case requires the back-arc subduction of young, buoyant Josephine oceanic lithosphere beneath the remnant arc, an unlikely scenario given that <10 m.y. old oceanic lithosphere resists subduction and generally forms shallow to flat subduction zones incapable of generating subduction related magmas. The second scenario requires that the “active” and “remnant” arc regions formed at different locations along the strike of a single subduction zone and were juxtaposed by significant left-lateral displacement (>100 km) across the Orleans-Preston Peak fault. This is consistent with the Josephine ophiolite having formed at oceanic spreading centers with spreading directed parallel to the subduction zone, a scenario is supported by 1) the east-west striking orientation, present day coordinates, of sheeted mafic dike complexes indicating north-south directed extension of the Josephine ophiolite (Harper, 1984), 2) faunal data from overlapping sedimentary strata that indicate the Josephine ophiolite experienced northward displacements on the order of 500-1000 km (Pessagno and Blome,

1990), and 3) a component of thrust displacement as great as 100 km for the Orleans-Preston Peak fault (Jachens et al., 1986).

If the single subduction zone model is accepted, then the IRPC and WTrPz phase II plutons, though similar in age, represent widely separated magmatic centers. Furthermore, it is intriguing to speculate whether related arc plutons formed a continuous or semi-continuous arc connecting the two regions, or if subduction generated magmas between the two regions were incorporated into oceanic spreading centers of the Josephine ophiolite. Such a “commingling” of magmas generated by subduction and oceanic spreading related processes would be expected to blur the distinction between inter-arc basin and arc magma in suprasubduction tectonic settings and may help to explain the non-MORB-like geochemical and isotopic characteristics often exhibited by ophiolites that form in marginal ocean basin situated above subduction zones.

Summary of the KMBB

The representative features of the KMB include 1) the amagmatic breaks during the Late Middle and Late Jurassic, 2) a physical realignment and relocation of the magmatic arc axis, and 3) the systematic changes in geochemical and isotopic signatures during three distinct phases of arc magmatism. These features represent the effect of two, short-lived thrusting episodes in the Middle and Late Jurassic. The effects of thrusting realigned and reshaped the arc magmatic axis. At depth the thrusting emplaced and/or removed material which probably interacted with the subduction generated magmas to produce the geochemical and isotopic signatures observed.

Jurassic orogeny in the Klamath Mountains province

Three competing views of Jurassic orogeny in the Klamath Mountains province have been proposed.

One view points to the relatively short-lived contractile deformational episodes evident in the rock record, particularly the Middle Jurassic thrusting event described by Wright and Fahan (1988; termed the “Siskiyou” event by Coleman et al., 1988) and the Nevadan thrusting described by numerous workers (e.g., Harper et al., 1994).

Another view submits that the orogenic episodes last much longer than the relatively short-lived thrusting events based on detailed investigation of temporally variable, yet local structural features that indicate regional stress fields remained constant for extended periods of time. For example Harper et al., 1994; Saleeby et al., 1989; and Edelman et al., 1989 suggest that rather than a relatively short-lived orogenic episode, the Nevadan orogeny instead endures for ~20 m.y., from ~155-135 Ma.

A third opinion focuses on an ever expanding database of radiometric age determinations that indicate the timing and location of arc magmatism, pluton and metamorphic cooling, and ophiolite genesis is highly variable in the Klamath Mountains province (Hacker et al., 1995). Based primarily on the age data, this opinion questions the usefulness of defining distinct time periods for orogeny in a region where orogenic activity appears to vary greatly in time and location.

This article incorporates aspects of all three views. Specifically, the Klamath Mountains province is considered to have experienced a continuum of spatially and temporally variable orogenic activity that lasted from ~175-135 Ma that was most likely related to magmatic and tectonic processes characteristic of a long-lived oceanic arc. This ~40 m.y. orogeny was punctuated by distinct, relatively short-lived episodes of regional contractile and/or extensional tectonism, namely the Middle Jurassic Siskiyou thrusting event and the contemporaneous Middle Jurassic to Late Jurassic “Josephine” extensional episode, and the Late Jurassic Nevadan thrusting event. In this view, Middle Jurassic to Early Cretaceous orogeny in the Klamath Mountains (and in the Sierra Nevada foothills) converges on the more classic cases of long-lived orogenies used to describe the European-

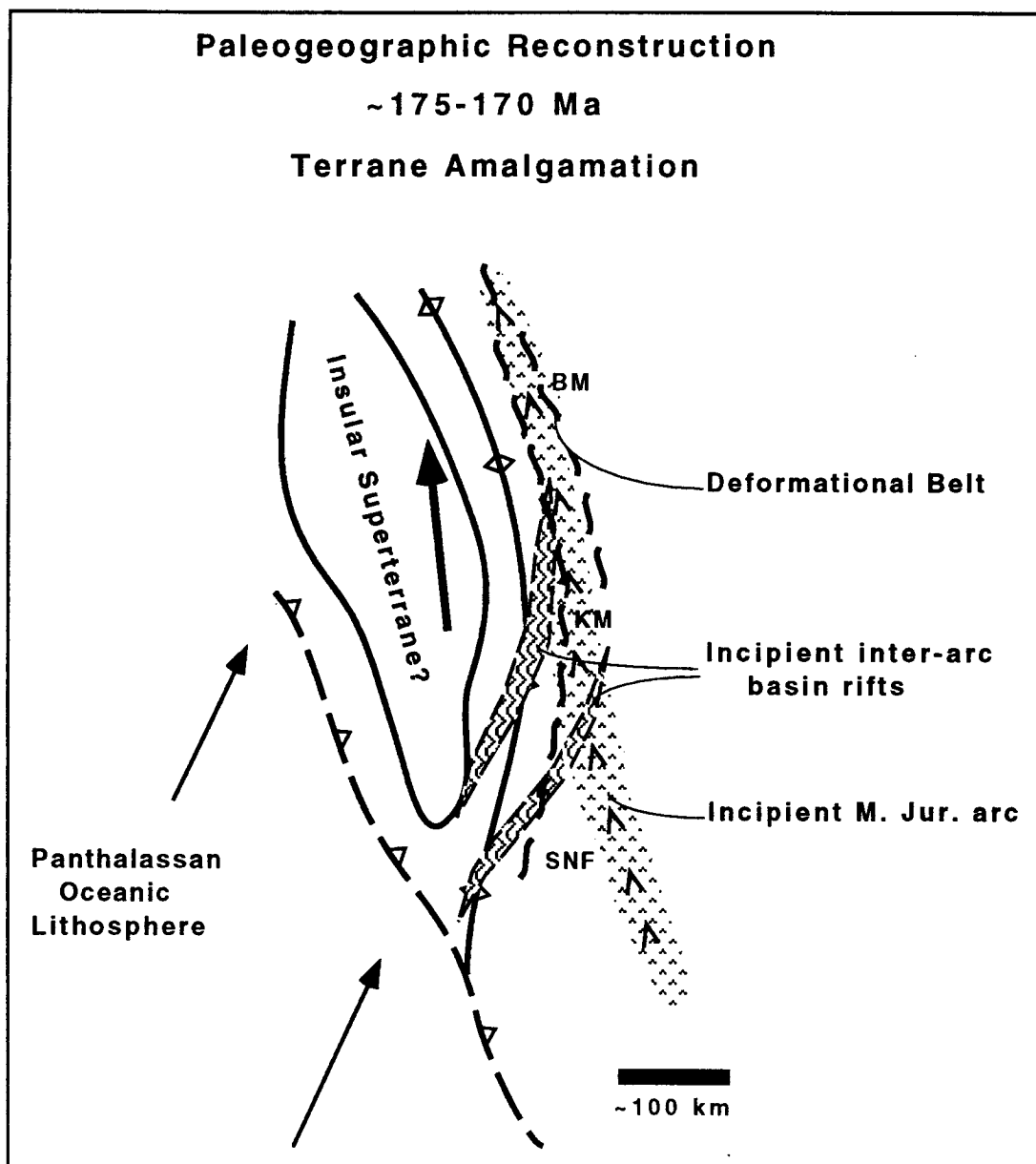
American continental collisional belts (e.g., the Taconic, Acadian, and Alleghenian orogenies).

Tectonic and paleogeographic reconstructions

A series of reconstructions are depicted in Figure 3-6 A-C which are, in general, similar to previous versions of a model for the Jurassic tectonic evolution of the province (e.g., Harper and Wright, 1984; Saleeby and Harper, 1993; Saleeby, 1994). The principal features of this model include: 1) a Middle Jurassic arc built across a sequence of older Klamath terranes, 2) a Late Middle to Late Jurassic marginal ocean basin generated by the rifting apart of the pre-existing arc complex to form an active arc, inter-arc basin, and remnant arc triad, and 3) the Late Jurassic tectonic collapse and imbrication of the marginal ocean basin as it is underthrust beneath the remnant arc terrane during the Nevadan orogeny. However, several important modifications to this model are incorporated into Figures 5 and represent an attempt to resolve some of the ambiguities of the previous model and to incorporate the new data presented and discussed above. The three figures are not drawn to scale; please note the approximate scale bars.

Middle Jurassic (175-170 Ma). Figure 3-6 A is essentially the same view as shown in Saleeby and Harper (1993) for 169 Ma. Here it depicts a time in the Klamath Mountains province when terrane amalgamation was the principal result of tectonism along the margin of western North America. This process clearly involved all of the pre-Middle Jurassic terranes of the Klamath-Sierran region, and may also have included the Insular Superterrane, now situated in the coastal Pacific northwest region (e.g., Saleeby 1992). Prior to terrane amalgamation, the western North American margin probably consisted of a succession of loosely coupled oceanic arcs, basins, and subduction zones that probably resembled the modern southwest Pacific margins of Asia and/or Australia. At ~175 Ma something caused this system to coalesce resulting in regional deformation and metamorphism, thrust faulting (proto-Siskiyou faults), arc magmatism, and localized

Figure 3-6 A. Tectonic and Paleogeographic reconstruction at ~175-170 Ma. The Middle Jurassic tectonic was characterized by the re-establishment of arc magmatism, the amalgamation of oceanic terranes with ties to the western North American margin, regional deformation and metamorphism. The figure invokes the collision of the Insular Superterrane with the continental margin at this time to produce these effects, but they may more simply reflect plate re-organization and intensified convergence across the plate boundary at this time.



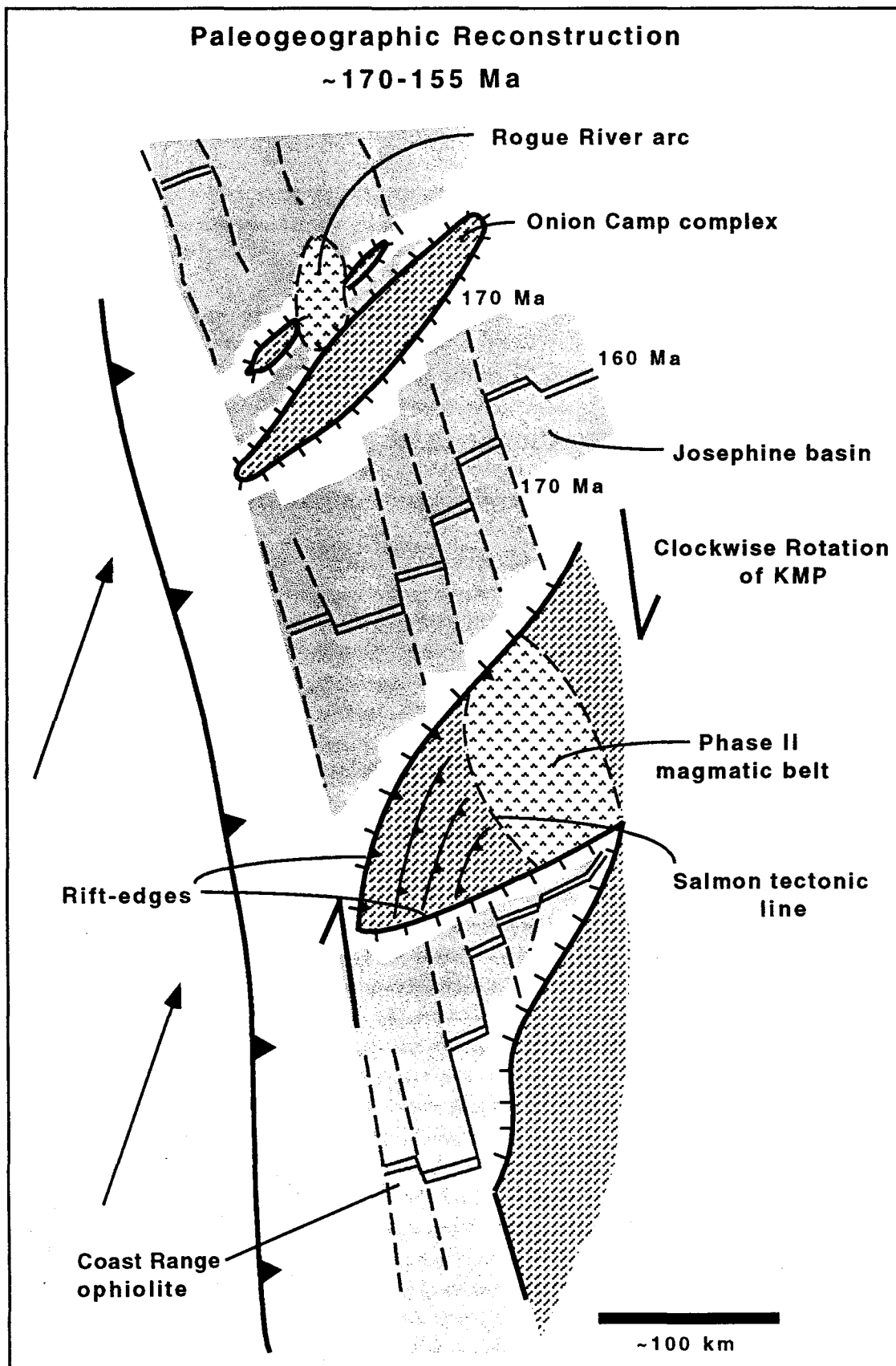
extension, perhaps as a result of a relative change in plate motions or a collision (e.g., the Insular Supeterrane).

The specific features of the Klamath Mountains province which formed during this time, and in some cases continued to be active following terrane amalgamation, include: 1) the early phases of arc magmatism mark the beginning of the ~40 m.y. Klamath Mountains oceanic arc batholith (phase I magmas); 2) the China Peak complex, the Wild Rogue ophiolite, and perhaps the Squaw Mountain amphibolite cooling ages record the initiation of extension leading to the opening and formation of the Josephine (and Coast Range) marginal ocean basins; and 3) contractile deformation and regional metamorphism. It must be noted that the amphibolite tectonites of the Squaw Mountain and Preston Peak areas probably formed as a result of this contractile deformation. However, it remains unclear whether the cooling ages record this event or later cooling related to extension.

Late Middle to Late Jurassic (170-155 Ma). Figure 3-6 B represents a time when the Klamath Mountains was shaped by continued arc and inter-arc basin magmatism, and by clockwise rotation of the province (prior to 164 Ma). These processes are envisioned to reflect either broadly distributed right-lateral shear across the region or strain partitioning at the subduction zone with right-lateral transtension in the arc. Both cases require highly right-oblique convergence across the Farallon/North American or Kula/North American plate boundary during this time.

The principal difference between Figure 3-6 B and the previous model is the depiction of the Josephine marginal ocean basin with margin parallel spreading and margin parallel offset of pre-existing oceanic lithosphere. In the most reconstructions (e.g., Saleeby and Harper, 1993; Harper et al., 1994) spreading is shown directed parallel to the basin margins, but the older lithosphere was offset perpendicular to the margins, a kinematically unfeasible solution. The Andaman Sea region provides a likely modern analog. As depicted in Figure 3-6 B, this geometry indicates that the Rogue River island arc complex may have been far removed from the Klamath Mountains province *sensu*

Figure 3-6 B. Tectonic and Paleogeographic reconstruction at ~170-155 Ma. The Middle to Late Jurassic sketch shows the development of right oblique spreading, clockwise rotation of the KMP and thrusting, and phase II arc magmatism in the Klamaths sensu strictu and to the north in the vicinity of the Onion Camp complex rift fragment. Abbreviations include (RCT=Rattlesnake Creek terrane, WHT=western Hayfork terrane, SBT=Sawyer's Bar terrane, IRPC=Illinois River plutonic complex, RC=Rum Creek metagabbro).

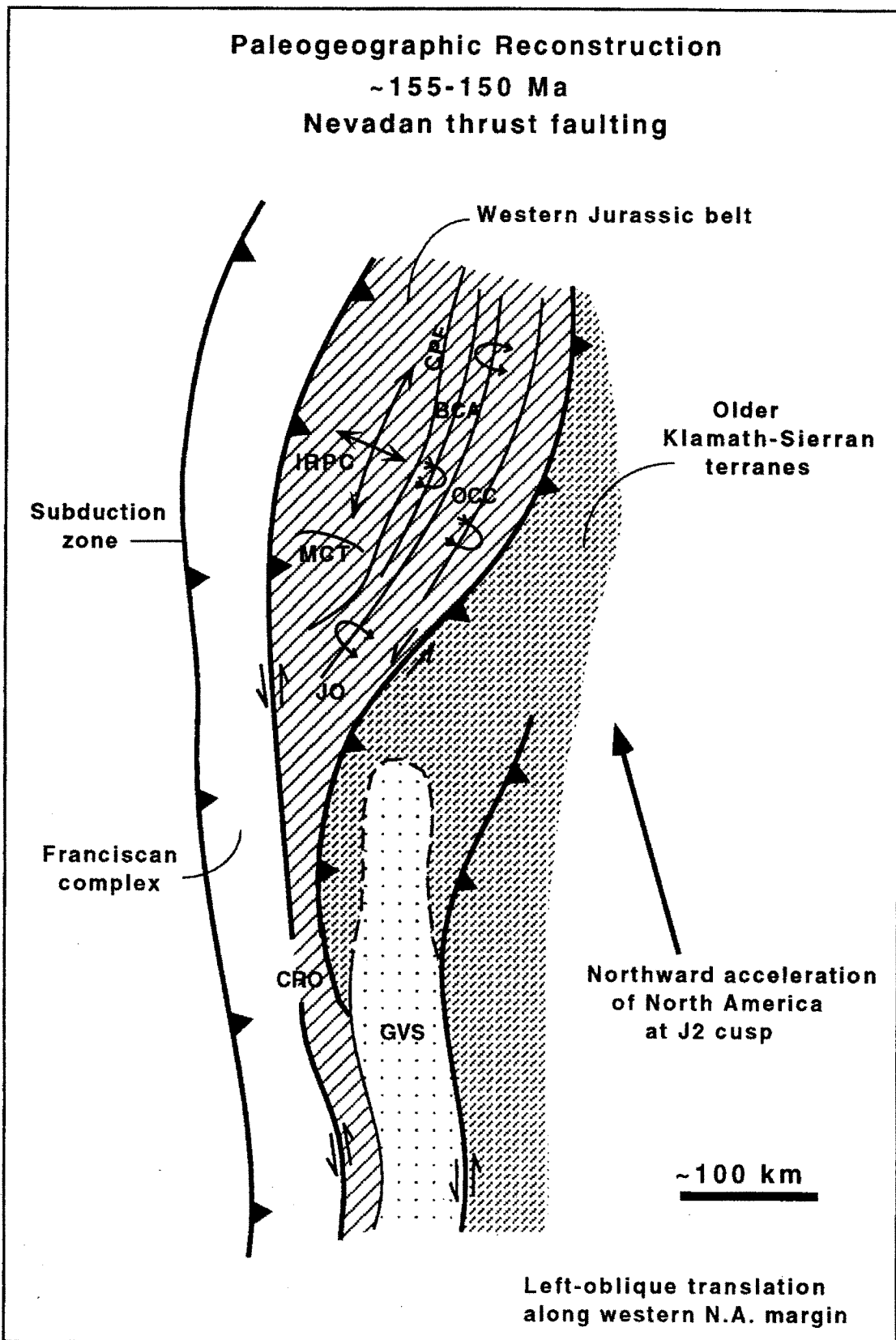


strictu. Another important benefit of Figure 3-6 B is that both the Rogue arc and the phase II plutons of the WTrPz belt form above the same subduction zone. As a consequence, the Middle Jurassic “remnant arc” is never removed from the active arc region helping to explain how subduction-related magmatism continues essentially uninterrupted in the region.

Another distinction between Figure 3-6 B and other models is the generation of both the Josephine and Coast Range ophiolites in separate basins, on either side of the Klamath Mountains province. This geometry keeps the province in the region of arc Late Jurassic arc magmatism and helps to explain how the Klamaths end up in a Cretaceous fore-arc setting relative to the Sierra Nevada during the Cretaceous (see Figure 3-6 B). Differential spreading between the two ophiolites could provide a mechanism by which the province rotates clockwise by $\sim 30\text{-}45^\circ$ relative to the axis of arc magmatism, thus creating the Salmon “tectonic” line (Irwin, 1985; and Hacker et al., 1995). It is conceivable that the clockwise rotation of the province resulted in continued displacement across the terrane-bounding faults of the WTrPz belt and may explain why the displacements seem greatest in the southern Klamaths, i.e., in the region furthest from the rotation pole. The cross-stitching phase II plutons indicate that the displacement, and perhaps rotation, ceased by ~ 164 Ma, a time when Josephine-Coast Range spreading was probably occurring at its maximum rate.

Latest Jurassic (155-150 Ma). At the time depicted by Figure 3-6 C, the province experienced regional contractile deformation and metamorphism associated with the early Nevadan orogeny and resultant tectonic collapse and imbrication of the Josephine ocean basin. This episode marks a profound change from right-oblique transtension to left-oblique transpression along the North American plate boundary during this time, and is temporally coincident with other reported cases of left lateral transtension and transpression in the Sierran foothills (Wolf and Saleeby, 1993, 1995) in the southwestern U.S. and Mexico (i.e., the Mojave-Sonoran megashear; Silver and Anderson, 1975).

Figure 3-6 C. Tectonic and Paleogeographic reconstruction at ~155-150 Ma. Large magnitude left-oblique tectonic collapse of the Josephine basin, perhaps accommodating left-lateral displacement along the continental margin at this time. Abbreviations of units referred to in text include: WRO=Wild Rogue ophiolite, SCO=Snow Camp ophiolite, BCA=Briggs Creek amphibolite, IRPC=Illinois River plutonic complex, MCT=Madstone Cabin thrust, CPF=Chetco Pass fault, JO=Josephine ophiolite, OCC=Onion Camp complex, CRO=Coast Range ophiolite, and GVS=Great Valley sequence.



The chief differences between Figure 3-6 C and the earlier models involve a relatively high order of left-oblique convergence across and/or beneath the Klamath Mountains province on Nevadan structures during tectonic collapse of the Josephine basin. As depicted in Figure 3-5B, the Rogue arc and the WTrPz belt may have been widely separated at the maximum extent of the Josephine basin, perhaps by as much as 500-1000 km if the faunal and paleomagnetic data are accurate. If correct, this scenario requires large magnitude left-lateral displacements across Nevadan structures to juxtapose the Rogue arc and the rest of the Klamath Mountains province. The Preston Peak/Orleans thrust system is constrained to have experienced thrust displacements as much as 100 km or greater (Jachens, 1986), but the magnitude of left-lateral displacement is unconstrained and could conceivably be much greater. It is particularly interesting to consider such large magnitude left-lateral displacements in light of the Mojave-Sonora megashear. Specifically, left-lateral displacement in the southwestern U.S. across the Mojave-Sonora megashear may feed northwestward into a series of structures (folds and faults) that formed during the left-oblique tectonic collapse of the Josephine basin or series of basins.

In Figure 3-6 C, the Klamath Mountains province, remains elevated with respect to the region to the south (the Coast Range ophiolite) helping to explain the apparent onlap of Early Cretaceous Great Valley sequence strata. To the north, erosion of the Klamath "highlands" supplied flysch detritus to the Josephine basin as it was underthrust beneath the region.

By ~150 Ma thrust displacements ceased as evidenced by numerous cross-cutting intrusive bodies and signaled the beginning of the third magmatic phase of the Klamath Mountains batholith. Over the next 15 m.y., plutonism appears to have migrated eastward across the province.

SUMMARY AND CONCLUSIONS

The new age data presented here help to complete an extensive database of radiometric ages and provides the following insight and constraint regarding the geologic and tectonic evolution of the Klamath Mountains province:

1. The WJB, previously considered to consist entirely Late Middle Jurassic and Late Jurassic oceanic arc and ophiolitic rocks, also contains pre-Middle Jurassic rocks which occur as screens in the Josephine ophiolite and form part of the depositional basement and country rock for the volcanoplutonic rocks of the Rogue River island arc complex. These older rocks are correlative with rocks of the Rattlesnake Creek terrane and confirm a model for the Jurassic tectonic evolution of the Klamath Mountains province. The model portrays the WJB as a marginal ocean basin that formed in response to rifting across an older arc and arc basement terrane, the WTrPz belt. As a result, a rifted fragment of older oceanic arc lithosphere was carried outboard of the marginal ocean basin spreading centers.

2. The U/Pb zircon age data from Oregon plutons are essentially the same age defining a NW-SE trending belt of plutons which contrast previously held views in favor of NE-SW trending plutonic belts in the northern Klamaths (e.g., Irwin, 1985).

3. Middle Jurassic to Cretaceous arc magmatism in the province is essentially continuous with subtle, relatively amagmatic breaks occurring at ~167-164 Ma and ~153-150 Ma, coincident with the Siskiyou and Nevadan regional thrusting events and maximum Josephine spreading. These breaks also coincide with an areal redistribution of arc magmatism, and in effect define three phases of arc magmatism in the province, with each phase characterized by distinct geochemical and isotopic signatures.

4. When viewed collectively, the Middle Jurassic to Cretaceous plutons of the Klamath Mountains province can be viewed as a long-lived (~40 m.y.) oceanic arc batholithic complex. The "Klamath Mountains batholith" is distinctly different from the giant Cretaceous and Tertiary Cordilleran batholiths, and may provide a model for

batholithic belts formed above loosely coupled, convergent ocean/ocean plate boundaries characterized by slab roll-back and extension in the overriding plate. Moreover, the style of arc magmatism so well preserved in the Klamath Mountains province may serve as archetype for Jura-Cretaceous magmatism throughout the western Cordillera.

5. Jurassic to Early Cretaceous orogeny in the province is best characterized as a product of contrasting orogenic styles. One style is characterized by an ~40 m.y. continuum of spatially and temporally variable arc magmatism (~175-135 Ma) and inter-arc basin (~173-160 Ma) magmatism and associated localized metamorphism and deformation. This background of orogenic activity is punctuated by distinct, short-lived contractile deformational events, the ~167-164 Ma Siskiyou and ~153-150 Ma Nevadan thrusting events.

6. The geologic and tectonic evolution of the Josephine marginal ocean basin indicates that the Jurassic construction of the Klamath Mountains province was the product of essentially two temporally distinct tectonic regimes. The first was characterized by broadly distributed right-oblique shear across the region resulting the north-directed extension (present day coordinates), contemporaneous oceanic arc and ophiolite genesis, with relative clockwise rotation and amalgamation of pre-Middle Jurassic Klamath terranes. The second was characterized by left-oblique shear across the region resulting the tectonic collapse and underthrusting of the WJB beneath the WTrPz belt. The abrupt change from right-oblique to left-oblique shear appears to have occurred at approximately 155-157 Ma related to the J2 cusp (May and Butler, 1986).

REFERENCES

- Barnes, C.G., Petersen, S.W., Kistler, R.W., Prestvik, T., and Sundvoll, B., 1992, Tectonic implications of isotopic variation among Jurassic and Early Cretaceous plutons, Klamath Mountains, *Geol. Soc. Amer. Bull.*, **104**, 117-126.
- Blake, M.C., Jr., D.C. Engebretson, A.S. Jayko, and D. L. Jones, 1985, Tectonostratigraphic terranes in southwest Oregon, in: *Tectonostratigraphic Terranes of the Circum-Pacific Region*, Earth Sci. Ser., edited by D.G. Howell, pp. 147-157, Circum-Pacific Council for Energy and Mineral Resources, Houston, Tex.
- Charleton, D.W., 1979, Geology of part of the Ironside Mountain quadrangle, northern California, Klamath Mountains, Ph.D. dissertation, 542pp., UCSB.
- Coleman, R.G., Manning, C.E., Mortimer, N., Donato, M.M., and Hill, L.B., 1988, Tectonic and regional metamorphic framework of the Klamath Mountains and adjacent Coast Ranges, California and Oregon, in: Ernst, W.G. (ed.), *Metamorphism and Crustal Evolution of the Western United States*, Rubey vol. VII, Prentice Hall, Englewood Cliffs, NJ, 1061-1096.
- Coleman, R. G., and M. Lanphere, 1991, The Briggs Creek amphibolite, Klamath Mountains, Oregon: Its origin and dispersal, *N. Z. J. Geol. Geophys.*, **34**, 271-284.
- Davis, G.A., Monger, J.W.H., and Burchfiel, B.C., 1978, Mesozoic construction of the Cordilleran "collage," central British Columbia to central California, in: D.G. Howell and K.A. McDougall (eds.), *Mesozoic paleogeography of the western U.S.*, Pacific Section, Society of Economic Paleontologists and Mineralogists Pacific Coast Paleogeography Symposium **1**, 1-32.
- Dick, H.J.B., 1976, The origin and emplacement of the Josephine Peridotite of southwestern Oregon, Ph.D. dissertation, Yale University, 409p.
- Edelman, S.H., and W.D. Sharp, 1989, Terranes, early faults, and pre-Late Jurassic amalgamation of the western Sierra Nevada metamorphic belt, California, *Geol. Soc. of Am. Bull.* **101**, 1420-1433.
- Ernst, W.G., 1990, Accretionary terrane in the Sawyers Bar area of the Western Triassic and Paleozoic belt, central Klamath Mountains, northern California, *Geol. Soc. Amer. Spec. Paper*, **255**, 297-306.
- Garcia, M.O., 1979, Petrology of the Rogue and Galice formations, Klamath Mountains, Oregon: Identification of a Jurassic island-arc sequence, *Jour. Geol.*, **87**, 29-41.
- Garcia, M.O., 1982, Petrology of the Rogue River island-arc complex, southwest Oregon, *Amer. Jour. Sci.*, **282**, 783-807.
- Goode, J.W., 1990, Tectonic evolution of a coherent Late Triassic subduction complex, Stuart Fork terrane, Klamath Mountains, northern California, *Geol. Soc. Amer. Bull.*, **102**, 86-101.
- Gorman, C.M., 1985, Geology, geochemistry and geochronology of the Rattlesnake Creek terrane, west-central Klamath Mountains, California, M.S. thesis, University of Utah, 111p.

- Hacker, B.R., and Ernst, W.G., 1993, Jurassic orogeny in the Klamath Mountains: A geochronological analysis, in Dunne, G.C., and McDougall, K.A. (eds.) *Mesozoic paleogeography of the western United States-II, Pacific Section, Society of Economic Paleontologists and Mineralogists*, 37-59.
- Hacker, B.R., Donato, M.M., Barnes, C.G., McWilliams, M.O., and W.G. Ernst, 1995, Timescales of orogeny: Jurassic construction of the Klamath Mountains, *ectonics*, v. 14, 677-703.
- Hamilton, W., 1969, Mesozoic California and the underflow of Pacific mantle, *Geol. Soc. Amer. Bull.* **80**, 2409-2430.
- Hamilton, W., 1978, Mesozoic tectonics of the western United States, in *Mesozoic Paleogeography of the Western United States*, edited by D.G. Howell and K.A. McCougall, pp. 33-70, Society of Economic Paleontologists and Mineralogists, Pacific Section, Los Angeles, Calif.
- Harper, G.D., 1980, The Josephine ophiolite-remains of a late Jurassic marginal basin in northwestern California, *Geology*, **8**, 333-337.
- Harper, G.D., 1984, The Josephine ophiolite, *Geol. Soc. Amer. Bull.* **95**, 1009-1026.
- Harper, G.D., and Wright, J.E., 1984, Middle to Late Jurassic tectonic evolution of the Klamath Mountains, California-Oregon, *Tectonics* **3**, 759-772.
- Harper, G.D., Saleeby, J.B., and Heizler, M., 1994, Formation and emplacement of the Josephine ophiolite, and the age of the Nevadan orogeny in the Klamath Mountains, California-Oregon: U/Pb zircon and $^{40}\text{Ar}/^{39}\text{Ar}$ geochronology, *J. Geophys. Res.*, **99**, 4293-4321.
- Harrison, T. M., and J. D. Fitz Gerald, 1986, Exsolution in hornblende and its consequences for $^{40}\text{Ar}/^{39}\text{Ar}$ age spectra and closure temperature, *Geochimica Cosmochimica et Acta*, **50**, 247-253.
- Helper, M.A., 1986, Deformation and high P/T metamorphism in the central part of the Condrey mountain window, north-central Klamath Mountains, California and Oregon, *Geol. Soc. Amer. Memoir*, **164**, 125-141.
- Hill, L. B., 1984, A tectonic and metamorphic history of the north-central Klamath Mountains, California, Ph.D. dissertation, 248 pp., Stanford Univ., Stanford, Calif.
- Hill, L.B., 1985, Metamorphic, deformational and temporal constraints on terrane assembly, northern Klamath Mountains, California, in: Howell, D.G. (ed.), *Tectonostratigraphic Terranes of the Circum-Pacific Region*, Circum-Pacific Council for Energy and Mineral Resources, Houston, TX, Earth Science Series, **1**, 173-186.
- Hotz, P.E., 1971a, Geology of lode gold districts in the Klamath Mountains, California and Oregon, *U.S. Geol. Survey Bull.*, **1290**, 91p.
- Hotz, P. E., 1979, Regional metamorphism in the Condrey Mountain quadrangle, north-central Klamath Mountains, California, *U. S. Geol. Surv. Prof. Pap.*, 1086.

- Irwin, W.P., 1972, Terranes of the western Paleozoic and Triassic belt in the southern Klamath Mountains, California, in: *U.S. Geol. Survey Prof. Paper*, **800-C**, 103-111.
- Irwin, W.P., 1985a, Age and tectonics of plutonic belts in accreted terranes of the Klamath Mountains, California and Oregon: in D.G. Howell (ed.), *Tectonostratigraphic terranes of the Circum-Pacific Region*, *Circum-Pacific Council for Energy and Mineral Resources*, Earth Science Series 1, 187-199.
- Jachens, R.C., Barnes, C.G., and Donato, M.M., 1986, Subsurface configuration of the Orleans fault: Implications for deformation in the western Klamath Mountains, California, *Geol. Soc. Amer. Bull.*, **97**, 388-395.
- Jorgenson, D.B., 1970, Petrology and Origin of the Illinois River Gabbro, a part of the Josephine Peridotite-Gabbro Complex, Klamath Mountains, Southwestern Oregon, Ph.D., University of California, Santa Barbara, 195 pp.
- Krogh, T.E., 1973, A low contamination method for the hydrothermal decomposition of zircon and extraction of U and Pb for isotopic age determinations, *Geochim. Cosmochim. Acta*, v. 37, 485-494.
- Lanphere, M.A., Irwin, W.P., and Hotz, P.E., 1968, Isotopic age of the Nevadan orogeny and older plutonic and metamorphic events in the Klamath Mountains, California, *Geol. Soc. Amer. Bull.*, **79**, 1027-1052.
- Miller, M.M., and Saleeby, J.S., 1991, Permian and Triassic paleogeography of the Eastern Klamath arc and Eastern Hayfork subduction complex, Klamath Mountains, California, *Paleozoic Paleogeography of the Western United States-II, Pacific Section SEPM*, **67**, 643-652.
- Pessagno, E.A., and Blome, C.D., 1990, Implications of new Jurassic stratigraphic, geochronometric, and paleolatitudinal data from the western Klamath terrane (Smith River and Rogue Valley subterrane), *Geology*, **18**, 665-668.
- Roure, F., and DeWever, P., 1983, Decouverte de radiolarites du Trias dans l'unité occidentale des Klamath, sud-ouest de l'Oregon, U.S.A.: Consequences sur l'âge des peridotites de Josephine, *Comptes Rendus de l'Académie des Sciences (Paris)*, **297**, 161-164.
- Saleeby, J.B., 1984, Pb/U zircon ages from the Rogue River area, western Jurassic belt, Klamath Mountains, Oregon, *Geol. Soc. Amer. Abstr. with Prog.*, **16**, 331.
- Saleeby, J.B., 1992, Petrotectonic and paleogeographic settings of the U.S. Cordilleran ophiolites, in *DNAG, v.G-3, The Cordilleran Orogen: Conterminous U.S.*, 653-683.
- Saleeby, J.B., Geary, E.E., Paterson, S.R., and O.T. Tobisch, 1989a, Isotopic systematics of Pb/U (zircon) and $^{40}\text{Ar}/^{39}\text{Ar}$ (biotite-hornblende) from rocks of the central Foothills terrane, Sierra Nevada, California, *Geol. Soc. Amer. Bull.*, **101**, 1481-1492.
- Saleeby, J.B., and G.D. Harper, 1993, Tectonic relations between the Galice Formation and the schists of Condrey Mountain, Klamath Mountains, northern California, in *Mesozoic Paleogeography of the Western United States*, vol. II, edited by G. Dunne

- and K. McDougall, pp. 61-80, Society of Economic Paleontologists and Mineralogists, Pacific Section, Los Angeles, California.
- Saleeby, J.B., Harper, G.D., Snoke, A.W., and Sharp, W.D., 1982, Time relations and structural-stratigraphic patterns in ophiolite accretion, west central Klamath Mountains, California, *J. Geophys. Res.* **87**, 3831-3848.
- Silver, L.T. and T.A. Anderson, 1974, Possible left-lateral early to middle Mesozoic disruption of the southwestern North American craton margin, *Geol. Soc. Am. Abstr with Prog.*, v.6, 955-956.
- Snoke, A.W., 1977, A thrust plate of ophiolitic rocks in the Preston Peak area, Klamath Mountains, California, *Geol. Soc. Amer. Bull.*, **88**, 1641-1659.
- Steiger, K.H. and Jager, E., 1977, Subcommittee on geochronology: Convention on use of decay constants in geo- and cosmo-chronology, *Earth Planet. Science Lett.*, **36**, 359-362.
- Terra, F. and Wasserburg, G.J., 1972, U/Pb systematics in lunar basalts, *Earth Planet. Science Lett.*, **17**, 65-78.
- Tomlinson, S.L., 1993, Tectonostratigraphy of the Bolan Lake area, Klamath Mountains, Oregon, M.S. thesis, Texas Tech Univ., 84p.
- Wolf, M.B. and J.B. Saleeby, 1992, Jurassic Cordilleran dike swarm/shear zones: implications for the Nevadan orogeny and North American plate motion, *Geology*, v. 14, p. 671-674.
- Wright, J.E., and Fahan, M.R., 1988, An expanded view of Jurassic orogenesis in the western United States Cordillera: Middle Jurassic (pre-Nevadan) regional metamorphism and thrust faulting within an active arc environment, Klamath Mountains, California, *Geol. Soc. Amer. Bull.*, **100**, 859-876.
- Wright, J. E., and S. J. Wyld, 1986, Significance of xenocrystic Precambrian zircon contained within the southern continuation of the Josephine ophiolite: Devils Elbow ophiolite remnant, Klamath Mountains, northern California, *Geology*, **14**, 671-674.
- Wright, J. E., and S. J. Wyld, 1994, The Rattlesnake Creek Terrane, Klamath Mountains, California: an early Mesozoic volcanic arc and its basement of tectonically disrupted oceanic crust, *Geol. Soc. Am. Bull.*, **106**, 1033-1056.
- Wyld, S.J., and Wright, J.E., 1988, The Devils Elbow ophiolite remnant and overlying Galice Formation: New constraints on the Middle to Late Jurassic evolution of the Klamath Mountains, California, *Geol. Soc. Amer. Bull.*, **100**, 29-44.
- Yule J.D., Saleeby, J.S., Jones, D.L., and Silk, M., 1992, Correlation of basement terranes across the Late Jurassic Josephine inter-arc basin, southwestern Oregon and Northern California: *Geol. Soc. Am. Abs. With Prog.*, v. 24, n.5, p. 93.

CHAPTER 4

STRUCTURAL FRAMEWORK

OF MARGINAL OCEAN BASIN LITHOSPHERE:

AN EXAMPLE FROM THE KLAMATH MOUNTAINS,

OREGON

Abstract

The western Klamath Mountains province exposes one of the world's best preserved accreted examples of composite marginal ocean basin lithosphere that formed adjacent western North America in the Middle to Late Jurassic. The so-called Josephine basin, complete with an inter-arc basin ophiolite sequence, overlapping sedimentary deposits, and oceanic island arc and remnant arc complexes, provides a unique opportunity to directly view the structural framework and features of marginal basin oceanic lithosphere which are otherwise obscured in modern settings beneath the ocean and/or thick accumulations of surficial deposits. The direct observation of these features contributes insight and constraint on poorly characterized features of oceanic lithosphere including the nature of the transition between inter-arc basin and oceanic arc crust and mantle lithosphere, the framework and thickness of oceanic island arc crust, and the relative ages of mantle lithosphere and the overlying crustal rocks. Specific findings reported in this article include 1) the recognition of two distinct generations of peridotite contained within the Josephine peridotite massif, one associated with the Josephine ophiolite sequence (Harper, 1984) and older peridotite associated with the Rattlesnake Creek terrane (RCT) (Wright and Wyld, 1994), 2) the designation of a rift-edge facies (after Snoke, 1977) to help reconstruct the tectonic history and paleogeographic configuration marginal ocean basins, and 3) the

characterization of at least two “end-member” types of oceanic island arc crust. The juxtaposition of two generations of mantle peridotite represents the first known example of an intraperidotite contact and suggests that rifting of the RCT related to the formation of the Josephine ophiolite involved both the crust and underlying mantle lithosphere.

Collectively, the oceanic features described herein emphasize the complementary and sometimes competing roles that extension, convergence, and magmatism play in shaping marginal ocean basin lithosphere.

Introduction

A significant proportion of oceanic lithosphere that gets accreted to continental margins is generally considered to have originated in marginal ocean basin tectonic settings, above subduction zones in oceanic arcs, basins, and ridges that fringe continental margins. In observing the geologic relations in accreted oceanic terranes, it is often easiest to focus on the accretion-related structural features and tectonic processes rather than the more subtle features which formed in the oceanic setting. Yet it is important to examine the oceanic features accreted terranes because they provide a unique opportunity for direct observation of subsurface framework of oceanic lithosphere. This paper will focus on the oceanic structural, stratigraphic, and petrologic features of marginal ocean basin lithosphere that is exceptionally well preserved and exposed in the Klamath Mountains province of northern California and southern Oregon.

The Jurassic construction of the Klamath Mountains province of California and Oregon is widely regarded as an archetypal example of the accreted fringing oceanic terranes to a continental margin. Moreover, the province is unique in that its Jurassic accretionary history is essentially unobscured by subsequent tectonism and magmatism, and over 25 years of intensive study and reflection has generated an abundance of information regarding the accretionary tectonic history of the Klamaths. Thus the accretion-related processes and structures are relatively well understood and can be

removed to gain a more clear understanding of the general structural framework that characterized the Jurassic Josephine marginal ocean basin lithosphere in its oceanic setting.

In general, the findings of this study suggest that much of the structural and stratigraphic complexity characteristic of the Klamath Mountains terranes is oceanic in origin. More specifically, the findings discussed below include 1) the first known documented example of an intraperidotite boundary separating two distinct generations of mantle peridotite, 2) the description of transitional “rift-edge” facies (after Snoke, 1977) that occurs between oceanic island arc and inter-arc basin crust, and 3) the characterization of oceanic island arc crust as a function of time and rate dependent magmatic and tectonic processes.

Features of marginal ocean basins

The accreted Middle to Late Jurassic oceanic arc and inter-arc basin rocks of the Klamath Mountains province, collectively referred to here as the Josephine marginal ocean basin, are considered to have originated in a setting somewhat analogous to the modern day Marianas region of the western Pacific or the Andaman Sea region of southeast Asia (e.g., Uyeda, 1974; Karig, 1971; Snoke, 1977; Saleeby et al., 1982; Harper and Wright, 1984). Figure 4-1 shows the principal petrotectonic elements of these regions, an active arc, remnant arc, and intervening inter-arc basin, in a generalized cross-section of these regions drawn perpendicular to the subduction zone. Note that the Andaman Sea and Mariana regions represent end member types of inter-arc basins with spreading oriented parallel and perpendicular to the subduction trench, respectively.

Studies of the general features of modern marginal ocean basin lithosphere has contributed much to our understanding of their structural features and general structural framework (e.g., Karig, 1971). Considering most marginal basin oceanic lithosphere is either underwater and/or buried by thick surficial deposits, these studies must rely on remote sensing techniques to image the lithospheric structures which are inaccessible to

GENERALIZED CROSS SECTION OF AN ISLAND ARC SYSTEM

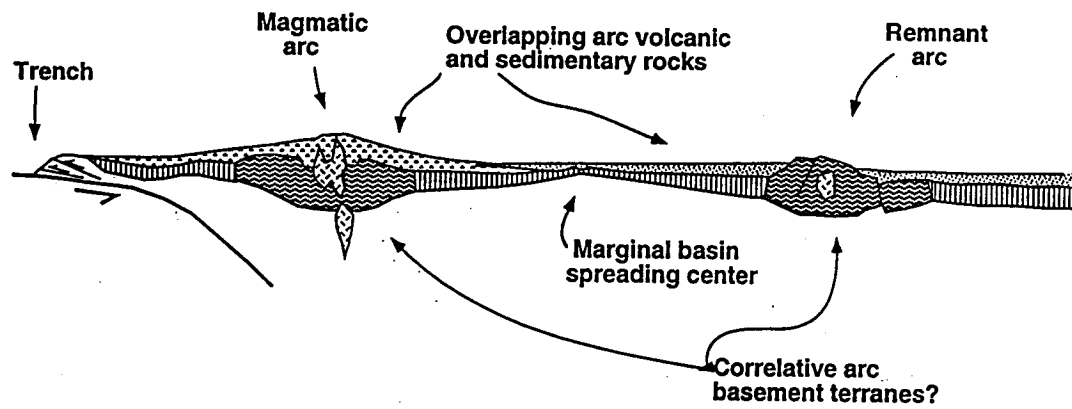


Figure 4-1. Generalized cross-section across a marginal ocean basin. Modified from Karig (1971).

direct observation. As a consequence, a number of fundamental questions regarding the structural framework and tectonic evolution of marginal ocean basin lithosphere remain unresolved. Specifically, little is known regarding 1) the age of the mantle lithosphere relative to overlying crustal sequences and the nature of the boundary between lithospheric and asthenospheric mantle, 2) the nature of the transition between inter-arc basin ophiolite and oceanic arc crust, 3) the character of apparently thickened crust and lithosphere in oceanic arcs (and remnant arcs) and the relative similarities and/or differences between the active and remnant arc basement lithologies. Accretion-related structures, with cumulative structural relief of >15 km, expose all stratigraphic levels of Josephine basin lithosphere and provide a unique opportunity to address these issues by directly observing the oceanic features in the field.

Geologic overview of the Josephine marginal ocean basin

The petrotectonic elements of the Josephine marginal ocean basin are exposed in the western Jurassic belt (WJB) and in part of the western Paleozoic belt (WTrPz belt; Figure 4-2). These elements include the Rogue River “active” arc complex and the Josephine inter-arc basin ophiolite which primarily comprise the WJB, and the western Hayfork “remnant” arc and its arc basement, the Rattlesnake Creek terrane (RCT), which chiefly forms the western portions of the WTrPz belt. In the southern half of the province, the outcrop belt of the WJB and WTrPz belt is relatively narrow but widens considerably to the north in southern Oregon, the region which serves as the focus for the following discussion (Figure 4-3). Here the WJB contains a rift-fragment of the RCT as part of the Rogue River arc basement, a lithotectonic link between the active arc region of the WJB and the remnant arc region of the WTrPz belt. It must be emphasized, however, that the remnant arc of the WTrPz belt continued to be a locus for “active-arc” magmatism contemporaneous with magmatism in the Rogue River arc of the WJB. These two regions of Late Jurassic arc magmatism are considered representative different parts of the same

Figure 4-2. Geologic index map of (part) of the Klamath Mountains province. Note the outline of Figure 4-3. Also note the line A-A' which is the approximate line of cross-section used to draw Figure 4-6.

The province is characterized by fault-bounded, arcuate thrust belts consisting of lithologically distinct eugeoclinal rocks. These belts (terrane) display a general age progression across the province with rocks as old as Early Paleozoic on the east to mainly Late Jurassic on the west (Irwin, 1960, 1966, 1981). The terranes of the Klamath Mountains are intruded by calc-alkaline plutons of chiefly Mesozoic age (Lanphere and others, 1968; Hotz, 1971; Wright, 1981; also see Chapter 3) and are overlain with an angular unconformity by Lower Cretaceous strata of the Great Valley Sequence (Irwin, 1981). Eastward dipping thrust faults of regional extent bound the principal terranes of the province (Irwin, 1964; Davis, 1969; Davis and others, 1978) and are interpreted to have formed through time during accretionary periods related to the subduction of oceanic materials beneath an overriding continental margin (Hamilton, 1969; Saleeby and others, 1982; and Ando and others, 1982).

Figure 4-3. Small scale, generalized map of Plate 1 showing the primary structural features. Note that, for the sake of clarity, antiformal axial traces have been omitted from the map. In general, an anticlinal regional structure accompanies each synclinal trace. Refer to text for a detailed discussion. Locations referred to in text and on Figure 4-5; EDM=Eight Dollar Mountain, CR=Chetco River, WB=Whetstone Butte, 6C=Sixmile Creek, SC=Shan Creek, and HC=Hellgate Canyon.

oceanic island arc system (as discussed in Chapter 3). For the sake of discussion below, the Late Jurassic arc plutons of the WTrPz belt are collectively referred to informally as the Siskiyou arc after the Siskiyou Mountains in the Oregon-California border region where many of the Late Jurassic arc plutons occur.

Fossil and geochronometric data (see Chapter 3; and e.g., Wright and Fahan, 1988; Pessagno and Blome, 1990; Saleeby and Harper, 1993; Hacker et al., 1993; Harper et al., 1994) constrain the life-cycle of the Josephine marginal basin to an ~15-20 m.y. period during the Middle and Late Jurassic (Figure 4-4). Ages constrain the “birth” of the Josephine basin and early ophiolite genesis to the Middle Jurassic, contemporaneous with waning arc magmatism in the western Hayfork arc. Ophiolite genesis appears to have continued until the Late Jurassic roughly coeval with arc magmatism and sedimentation in the Josephine basin. At ~155 Ma, the arc appears to have been extinguished as the basin was imbricated and thrust beneath the WTrPz belt terranes at the onset of Nevadan thrust faulting. By ~150 Ma, Nevadan thrusts were intruded by small plutons constraining the “death” or tectonic collapse of the Josephine basin to have occurred between ~155 and 150 Ma. The resulting deformation produced regional scale folds and faults that control the map patterns exhibited in Figure 4-3. For example, the northeast-trending belts of peridotite extending from the main peridotite mass to the south are interpreted as gently NNE plunging, tight antiformal structures with upright to slightly inclined axial planes. Other primary structural features include a moderately to steeply SE dipping regional foliation and high angle faults oriented subparallel to the regional foliation that display both normal and reverse displacements and are interpreted to have formed along highly attenuated limbs of regional scale folds.

With this understanding of the accretion related structures, the stratigraphic order of the Josephine basin can be recognized. In general, the rocks of the Josephine basin occur in distinctive lithologic associations that define the following three tiered stratigraphic succession (Figure 4-5): 1) a basal layer comprised of two types of variably serpentized

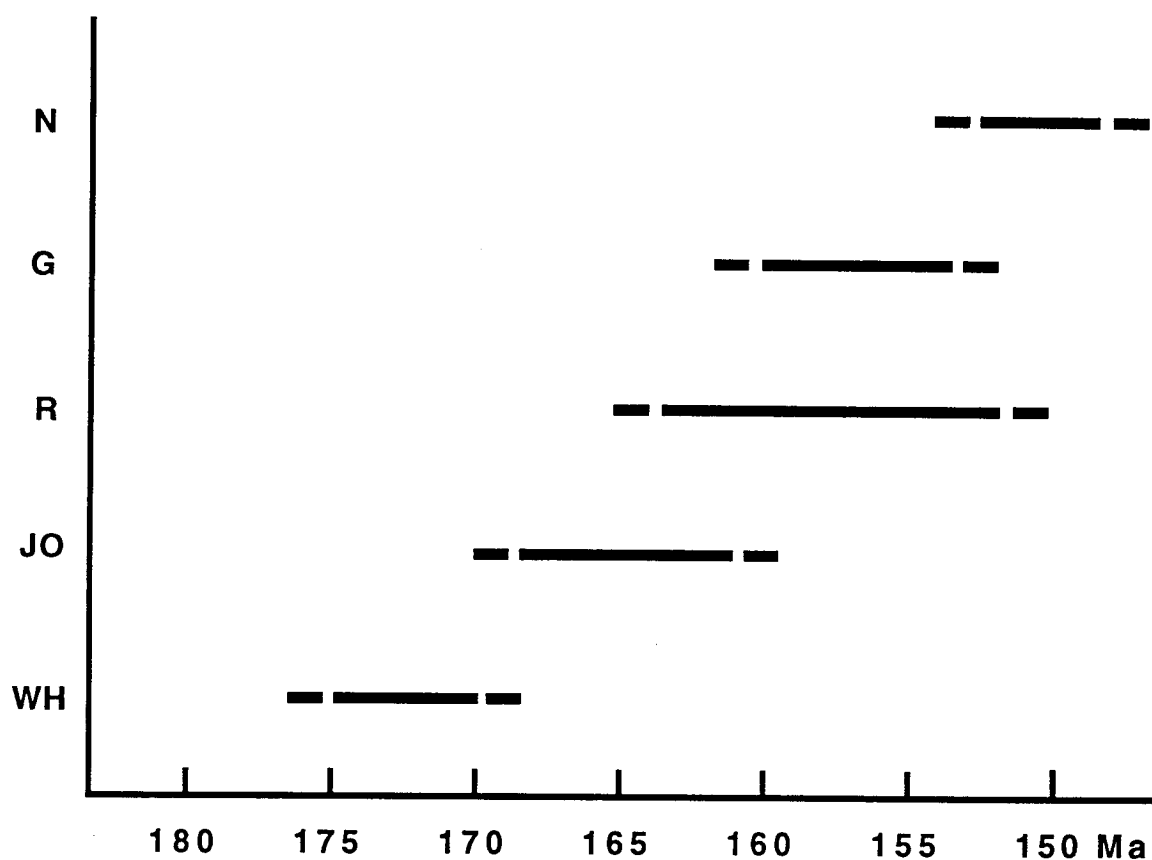
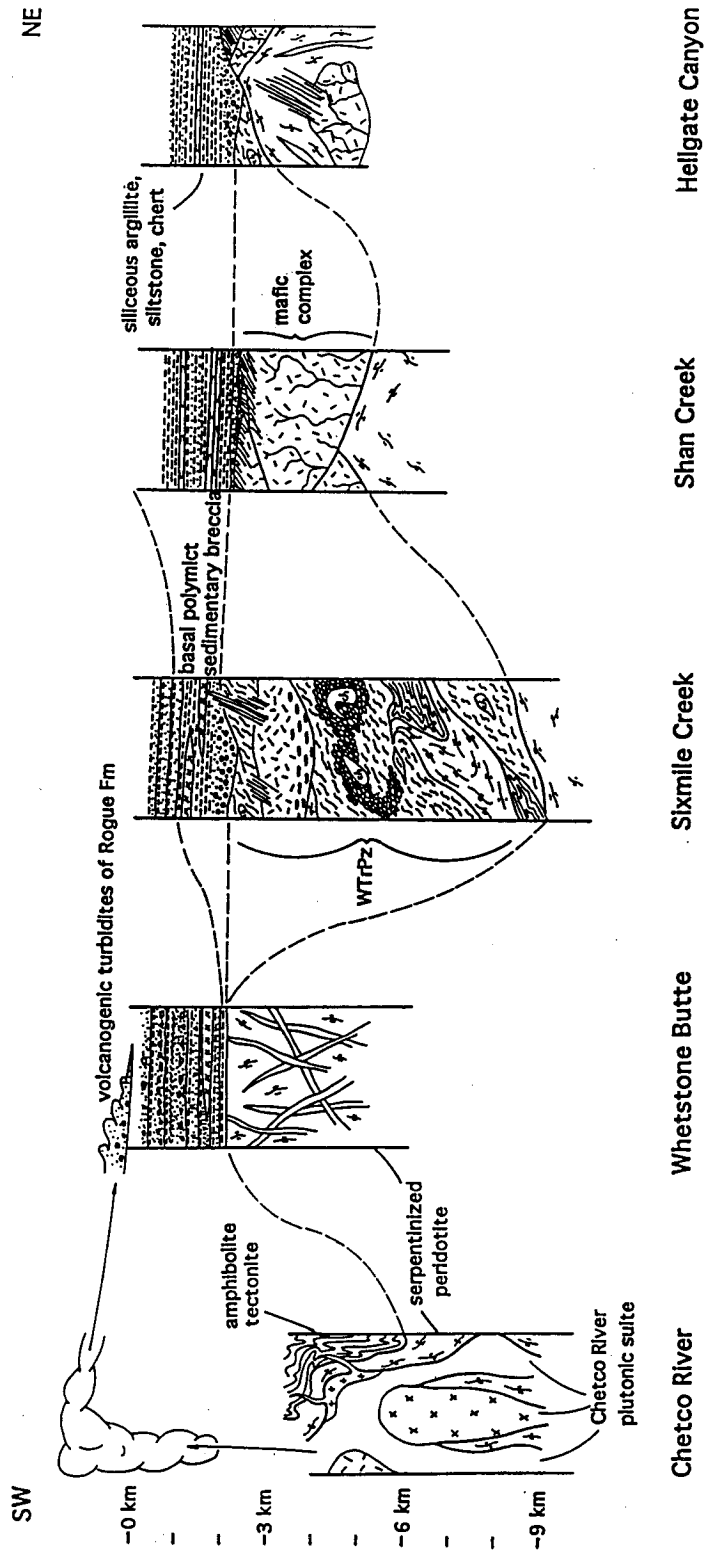


Figure 4-4. Plot of the range in known age data for the petroTECTONIC elements of the Josephine marginal ocean basin; WH=volcanoplutonic arc rocks of the western Hayfork terrane, JO=Josephine ophiolite *sensu strictu* and *sensu latu*, R=Rogue River volcanoplutonic arc rocks including ages for the Illinois River plutonic complex, the Rogue Formation, and the cross-stitching Middle to Late Jurassic plutons of the WTrPz belt, G=hempelagic and flysch sedimentary overlap strata of the Galice Formation, N=approximate timing of displacement across Nevadan thrust faults.

Figure 4-5. A) Diagrammatic columnar sections from five locations within the WJB illustrate the generalized three tiered stratigraphy of the belt. See Figure 4-3 for the locations of the stratigraphic columns.

Diagrammatic Columnar Sections of Rogue-Josephine Marginal Basin Lithosphere



peridotite, the Josephine and RCT peridotite masses; 2) an intermediate layer consisting of a variably metamorphosed, heterogeneous, and highly fragmented oceanic crustal rocks belonging to the Josephine ophiolite and the RCT; and 3) an upper layer comprised of overlapping sedimentary and volcanogenic strata derived from several sources including the fringing active magmatic arc, the remnant arc and continental margin, and localized intra-basinal fault scarps. Plutonic rocks of the active arc intrude the basal and intermediate stratigraphic layers, with scarce dikes and sills intruding the basal part of the overlap sequence.

Distinctive features of the Josephine marginal ocean basin

Intraperidotite contact

The Josephine peridotite, one of the largest peridotite masses in the world, is exposed over an ~700 km² region of the California-Oregon border region in the western Klamath Mountains province. The peridotite is interpreted to represent the residue of partial melting (Dick, 1976) and presumably formed during the genesis of the Late Jurassic Josephine ophiolite sequence (Harper, 1984). However, radiometric age data and field relations described in Chapters 2 and 3 indicate that at least part of the Josephine peridotite is pre-Middle Jurassic in age. Specifically, serpentinized peridotite that forms a northeast trending finger-like extension from the main peridotite mass (Figures 4-2 and 4-3) is cut by felsic dikes which yield ~175 Ma U/Pb zircon ages (data listed in Table 3-1, Chapter 3). Continuous exposure of this “older” peridotite is traceable ~10 km to the southwest into the Josephine peridotite mass *sensu strictu*, without crossing any obvious structural break.

These relations suggest that either the Josephine peridotite is ≥ 10 m.y. older than previously suspected or that two generations of mantle peridotite occur in the region. The latter possibility is supported by a number of geologic relations distinguishing two types of peridotite in the region, listed in Table 4-1, and implies that some sort of pre-accretion intra-peridotite contact separates pre-Middle Jurassic peridotite from Late Jurassic peridotite

Table 4-1

Distinguishing features of the Josephine and Rattlesnake Creek terrane peridotite masses

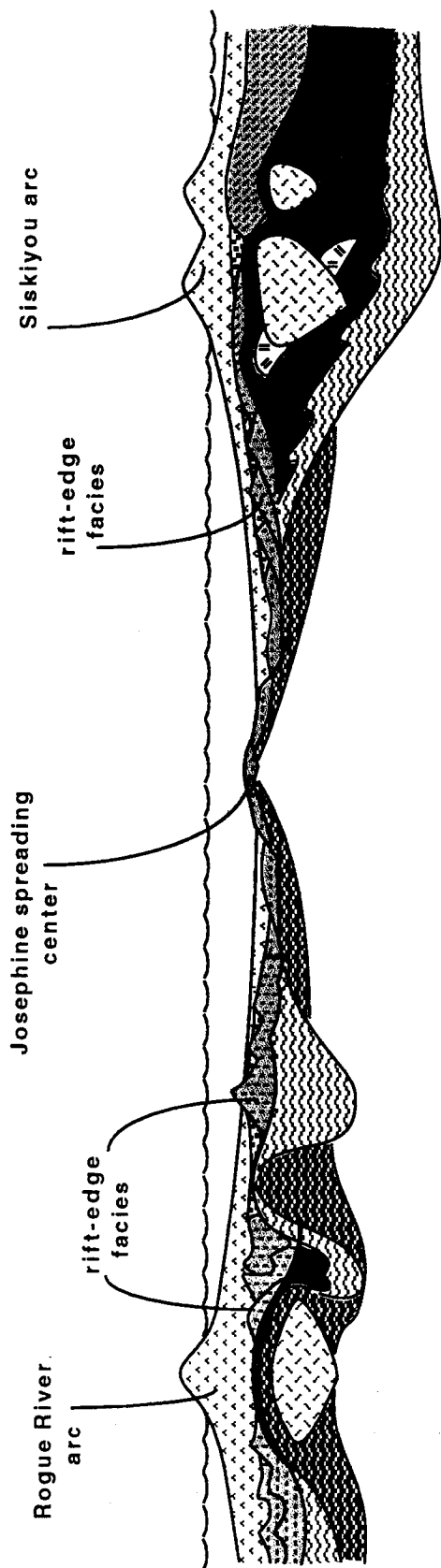
| <u>Rattlesnake Creek terrane (RCT)</u> | <u>Josephine peridotite</u> |
|--|--|
| 1. Completely to moderately serpentized (>50%). | 1. Moderately to nonserpentized, with pristine harzburgite and dunite locally common. |
| 2. Amphibolite facies penetrative fabric, now mostly serpentized; associated with Middle Jurassic (~175 Ma) amphibolite tectonites. | 2. Absence of amphibolite facies penetrative fabric. |
| 3. Exposed on the seafloor as evidenced by the nonconformable overlap of Rogue Fm strata. | 3. ----- |
| 4. Anastomosing regional Nevadan shear foliations common. | 4. Anastomosing regional Nevadan shear foliations rare. |
| 5. At least Middle Jurassic in age, but may be Triassic in age by association with crustal rocks of the RCT. Cut by numerous generations of dikes ranging in age from ~175-150 Ma. Podiform chromite rarely present. | 5. Probably Late Jurassic in age, the age of the crustal sequence of the Josephine ophiolite. Less commonly intruded by dikes whose ages range from ~160-150 Ma. Podiform chromite locally abundant. |
| 6. Rare rodingite dikes. | Rodingite dikes common. |

of the Josephine ophiolite sequence. This boundary is depicted in cross-section view in Figure 4-6.


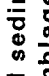




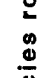
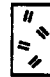


The notion of an intraperidotite contact raises some intriguing questions regarding 1) how exactly the oceanic juxtaposition of two generations of mantle peridotite occurs, and 2) what characterizes the nature of the boundary between intra-oceanic peridotite masses. A clue as to how the RCT and Josephine peridotite masses were juxtaposed is evident from the map distribution of the two units. In Figure 4-2, note that the older RCT peridotite only occurs bordering the crustal rocks of the RCT suggesting that the RCT crust and peridotite comprise a composite “screen” of older oceanic lithosphere contained within the Josephine ophiolite, befitting the model described above for the Jurassic tectonic evolution of the Josephine basin. Specifically, the observed map distribution of RCT peridotite is an expected result if the Josephine basin formed by rifting apart the crust and mantle rocks of the western Hayfork arc basement (RCT). Given this scenario it is conceivable that the contact between the Josephine and the RCT peridotite masses may represent the contact between lithospheric and asthenospheric mantle prior to the generation of the Josephine ophiolite.

Though these two types of peridotite are clearly distinguishable in the field, the nature of the boundary was not studied in detail, mostly because its significance was not realized until after the completion of field work when the radiometric ages of the cross-cutting dikes were determined. In the field, the nature of the boundary appears gradational without obvious shearing or faulting. It is typically marked by a distinct vegetation change where hillslopes underlain by RCT peridotite are less vegetated than those underlain by Josephine peridotite. In addition, RCT peridotite forms relatively rounded and subdued topographic features when compared to the more resistant, steep and blocky slopes characteristic of the Josephine peridotite. A prime example of these differences occurs in the vicinity of Eight Dollar Mountain, a conical mountain located at the northeasternmost extent of the Josephine peridotite (Figure 4-3), where the peak and its upper slopes consist

Figure 4-6. Simplified, cross-section drawn from north-northwest to south-southeast across the reconstructed Josephine marginal ocean basin (e.g., Figure 4-2 and Figure 3-5 B, Chapter 3). Note that the inter-arc basin is foreshortened in this view to give equal emphasis to the various components, namely, the Rogue arc, the Josephine ophiolite, and the Siskiyou arc. Also note that the cross-section is drawn with a vertical exaggeration of ~3.



EXPLANATION

-  ophiolite crustal sequence
-  volcanic and sedimentary overlap assemblage
-  "rift-edge facies" (see text)
-  "remnant" arc composite crust
-  Post-164 Ma plutons
-  amphibolite facies rocks
-  Josephine peridotite
-  Pre-164 Ma plutons
-  basal ophiolite breccia
-  pre-Josephine peridotite

of relatively fresh Josephine peridotite, and the lower slopes and river drainages to the west and east consist of serpentized RCT peridotite. These features suggest the boundary in essence represents a “serpentinization front,” perhaps consistent with the notion that low angle, ductile shearing across this boundary juxtaposed relatively serpentized, low temperature peridotite against relatively unserpentinized, high temperature peridotite. However, this scenario is highly speculative and future research is needed to gain a better understanding of this boundary.

Inter-arc basin rift-edge facies

Most generalized depiction's of modern marginal ocean basins (e.g., Figure 4-1) show sharp boundaries separating inter-arc basin and oceanic arc/remnant arc crust. In accreted ancient examples, Snoke (1977) described a more gradual transition or “rift-edge facies” for rocks in the remnant arc region of the Josephine basin near Preston Peak in northern California. A “matching” rift-edge facies has also been recognized beneath deposits of the Rogue River arc on the opposite margin of the Josephine basin in the central Illinois River drainage, Oregon (Yule and Saleeby, 1992; Chapter 2). In addition to providing a more realistic view of the transition between inter-arc basin and oceanic island arc crust, the concept of a rift-edge facies can help to reconstruct the tectonic history and paleogeographic configuration of accreted fragments of marginal ocean basin sequences. For instance, in the case of the Josephine basin, the occurrence of rift-edge facies rocks in both the WJB and the WTrPz belt provides an lithotectonic linkage between two fault bounded terranes and suggests that rifted fragments of the WTrPz belt (RCT) were carried northward during spreading, a view supported by apparent spreading geometries deduced from the Josephine ophiolite (Harper and Wright, 1984).

The distinctive features of the Josephine rift-edge facies include 1) cross-cutting heterogeneous mafic intrusive complexes, 2) ubiquitous hydrothermal alteration and

accompanying cataclastic “hydrofracture” textures, 3) locally thick accumulations of olistostromal deposits, and 4) direct and/or indirect evidence of normal faulting.

Mafic intrusive complexes. The mafic intrusive complexes cover areas ranging from outcrop- to kilometer-scale and principally consist of hydrothermally altered gabbro and sheeted dikes of diabase and basalt. They exhibit features typical of the intermediate to shallow crustal levels of ophiolite sequences and are, by analogy, considered to be miniature ophiolite sequences intruding variable country rock lithologies including peridotite, amphibolite, and greenschist grade metavolcanic and metasedimentary rocks of the RCT. In support of this interpretation, radiometric ages obtained from the rift-edge facies mafic complexes are coeval with the ages determined from the main body of the Josephine ophiolite (e.g., Saleeby and Harper, 1993).

Alteration/deformation features. With the exception of the overlapping sedimentary strata, rift-edge facies rocks are vein-filled and thoroughly altered, primarily under static greenschist and sub-greenschist facies conditions; the common replacement minerals are epidote-chlorite-sauserite-sphene-prehnite-calcite-quartz-sulfides, and common vein mineralogies are prehnite-calcite-quartz, and epidote-chlorite-quartz. In addition, all lithologies (including peridotite and amphibolite) exhibit cataclastic fragmentation textures featuring random networks of rock fragments cemented by vein materials interpreted to have formed by hydrofracturing processes. The alteration and fragmentation textures clearly cut earlier dynamic metamorphic textures in the mantle lithosphere and crustal lithologies, but are conspicuously absent in the overlapping synorogenic sediments. These relations tightly constrain the alteration episode to have occurred concurrently with or shortly following the intrusion of the mafic intrusive complexes, consistent with the interpretation that the alteration and fragmentation textures record the rift-related tectonism and magmatism associated with the opening of the Josephine basin.

Olistostromal deposits. The basal overlapping strata of the rift-edge facies primarily consist of impure chert, argillite and siltstone interbedded with locally thick, but laterally discontinuous deposits comprised of poly lithologic conglomeratic grit, debris flow breccia, and megabreccia with individual clasts measuring >100 m in size. Clast lithologies in the breccia vary in proportions, but are predominantly ophiolitic with secondary metavolcanic and metasedimentary schist and semischist. Age data is poorly constrained but is presumably Late Jurassic based on a probable Kimmeridgian age determined from radiolarian chert interbeds (M. Silk, personal communication, 1992). The breccia deposits are interpreted to represent talus breccia deposits derived from submarine in probable normal, transform, and/or transfer fault dominated basins which were otherwise accumulating pelagic and hemipelagic sediments.

Extensional faulting. Evidence for faulting is largely circumstantial because of the complexities of trying to identify normal faults in a region affected by later contractile deformation and thrust faulting. However, small scale normal offsets, e.g., of layering in sediments and dike margins, are locally observed in some rift-edge facies outcrops. Several indirect pieces of evidence indicate that the rift-edge facies rocks were tectonically denuded, at least locally. For example, the nonconformable overlap of RCT mantle peridotite by Rogue Formation volcanogenic strata suggests that the RCT crust was exposed at the surface, probably by a low-angle normal fault. In addition, considerable topographic relief is necessary to generate the olistostromal deposits which may have been shed from normal fault scarps, though transform and/or transfer faults are also likely candidates.

It is important to point out that some features of the rift-edge facies are common to the rocks of the Josephine ophiolite. Specifically, the hydrothermal alteration and small scale extensional faulting common to rift-edge facies rocks is also evident in the ophiolite (Alexander and Harper, 1992); however, the ophiolite sequence generally lacks the degree of brittle fragmentation and hydrofracture textures that typify the rift-edge facies rocks.

Secondly, olistostromal deposits are often deposited on the Josephine ophiolite instead of rift-edge facies rocks (e.g., the Lems Ridge olistostrome, Ohr, 1987; the Devil's Elbow ophiolite, Wright and Wyld, 1986), but they include RCT detritus (Ohr, 1987) indicating a proximity to an older source. Thus the features of the rift-edge facies and similar features associated with the Josephine ophiolite reflect the high degree hydrothermal alteration and brittle fragmentation processes which affected rocks of the Josephine marginal ocean basin.

Oceanic arc crust

A wealth of observational, analytical, and remote sensing data has led to the general understanding that oceanic island arc crust consists of a relatively thick composite of oceanic rocktypes of variable age and proportion. The primary components include subduction-derived plutons, related arc volcanic rocks, and ophiolitic crust (Figure 4-1) whose complex and multi-component nature reflect various, and sometimes competing processes that actively shape oceanic arc crust. These processes include arc magmatism, contractile deformation, and extension which, depending on the relative duration and rate, will produce a variety of arc types. For example, relatively thick composite oceanic arc crust will result from high rates of arc magma supply, long-lived fixed arc magmatism, and/or relatively high convergence rates; whereas thin oceanic arc crust will result from the opposite situation, low rates of magma supply, short-lived arc magmatism, and/or unstable extension-dominated tectonic settings.

The Klamath Mountains province contains a variety of arc complexes deformed and exposed at all stratigraphic levels thereby providing a unique opportunity to directly observe the roots of oceanic arc systems to see how their structural framework may vary as a function of time and rate dependent magmatic and tectonic processes. The following discussion will focus on the Late Jurassic, coeval Rogue River and Siskiyou arc complexes which essentially represent two "end-member" types of oceanic island arcs (Figure 4-6). Specifically, the Rogue arc contains a single arc plutonic complex, is relatively short-lived,

and intrudes thin ophiolitic crust and mantle. In contrast, the Siskiyou arc contains multiple generations of plutons, is relatively long-lived, and intrudes an imbricate thrust stack of older oceanic terranes.

Rogue River arc. The Rogue River arc (Figure 4-6) consists of coeval arc volcanic and plutonic rocks (160-153 Ma) which overlie and intrude a heterogeneous aggregation of rocks related to the Rattlesnake Creek terrane (RCT) and the Josephine ophiolite (JO). Specifically, the Rogue volcanic rocks nonconformably overlap serpentinite matrix melange containing crustal blocks of RCT and JO lithologies. The country rocks of the arc plutonic complex consist chiefly of peridotite(!) and amphibolite tectonite. Field relations suggest that the arc plutonic complex intruded the uppermost mantle lithosphere beneath rift-edge facies rocks which were <5 km thick. The crustal rocks in the roof of the arc pluton were heated and deformed in ductile extensional shear zones as material was displaced from the roof toward the margins of the pluton where they accumulated as polydeformed amphibolite and gneiss (Chapter 2). Thus the minimal thickening of oceanic crust in the Rogue arc appears to result entirely from the intrusion and eruption of a single arc magmatic system which lasted a relatively short period of time. It is important to note the occurrence of mantle peridotite within the Rogue arc “crust” and whether a seismic survey of a modern analog to the Rogue type arc would reveal this structural complexity.

Siskiyou arc. The features which distinguish the Siskiyou arc from the Rogue arc essentially reflect the composite nature and multi-stage history of the host oceanic crust terrane. Specifically, the country rocks of the Late Jurassic (~164-155 Ma) Siskiyou plutons are the products of 1) the construction of a Middle Jurassic (~177-167 Ma) arc that was probably very similar to a Rogue-type arc, i.e., arc magmas intruding and deposited upon an ophiolitic/primitive arc melange, and 2) a distinct episode of compression and thrust faulting at ~167-164 Ma which resulted in crustal thickening and terrane amalgamation to form the WTrPz belt (Wright and Fahan, 1988). Thus the Late Jurassic Siskiyou arc plutons were merely adding to an already substantial thickness of oceanic

crust. The thickness of the Siskiyou arc crust is difficult to constrain because its deepest levels were tectonically eroded during Nevadan underthrusting of the Josephine ophiolite, but it seems likely that crustal thicknesses may have reached ~30 km based on evidence in the Siskiyou plutons for assimilation of metasedimentary rocks or mixing with crustal melts at deep crustal levels (Barnes et al., 1992).

Thus the Late Jurassic Rogue and Siskiyou arcs represent two distinct types of oceanic island arc crust and illustrate how the rates and duration of magmatism and competing extensional and compressional tectonism can affect its formation. It is intriguing to consider the effect of forming and intra-arc basin ophiolite that is situated above or along the magmatic arc axis, similar to the paleogeographic reconstruction envisioned for the Josephine basin (Chapter 3). With this geometry it is conceivable that the inter-arc basin ophiolite magmas are, in part, subduction-derived magmas, a highly speculative hypothesis that may be testable carefully designed geochemical and isotopic analyses. If this is a viable magmatic process, it may help to explain the apparent paucity of typical oceanic island arc magmatism that is contemporaneous with the Late Jurassic Josephine and Coast Range ophiolites (Saleeby, 1994).

Conclusions

The western Klamath Mountains province exposes a well preserved accreted fragment of mostly intact, albeit structurally complex, Middle to Late Jurassic marginal ocean basin lithosphere that provides an exceptional opportunity to directly observe the structural features and framework of oceanic island arcs and inter-arc basins. Rocks of the Josephine basin reveal features emphasizing the complementary and sometimes competing roles that tectonic and magmatic processes play in shaping marginal basin oceanic lithosphere. More specifically, in the Josephine ocean basin, extension-related processes have the most profound effect by outpacing ophiolitic magmatism which results in 1) the brittle fragmentation of the ophiolitic and rift-edge facies rocks, 2) the creation of fault

scarps which spawn olistostromal deposits, and 3) the compression of thermal gradients which drives extensive hydrothermal systems resulting in the ubiquitous alteration and vein network systems. In addition, the recognition of two generations of mantle peridotite contained within a single peridotite mass emphasizes that the rifting of an oceanic terrane can involve the crust and its underlying mantle lithosphere.

In the oceanic arc crust, the relative rates and duration of tensional, convergent, and magmatic processes will control the type of arc crust that is generated. Thin arc crust (<10 km thick), like that observed in the Rogue arc, will result in short-lived arc magmatic systems built on juvenile and highly extended oceanic crust. The more common example of oceanic crust, based on comparisons with modern oceanic arcs, is the Siskiyou arc which seems to have resulted from long-lived (>10 m.y.) arc magmatism and tectonically thickened crust.

References

- Alexander, R.J. and Harper, G.D., 1992, The Josephine ophiolite, an ancient analog for oceanic lithosphere formed at intermediate-spreading ridges, in *Ophiolites and Their Modern Oceanic Analogues*, edited by B. Parsons and P. Browning, pp. 3-38, Blackwell Scientific Publ., Oxford.
- Barnes, C.G., Petersen, S.W., Kistler, R.W., Prestvik, T., and Sundvoll, B., 1992, Tectonic implications of isotopic variation among Jurassic and Early Cretaceous plutons, Klamath Mountains, *Geol. Soc. Amer. Bull.*, **104**, 117-126.
- Dick, H.J.B., 1976, The origin and emplacement of the Josephine Peridotite of southwestern Oregon, Ph.D. dissertation, Yale University, 409p.
- Hacker, B. R., Ernst, W. G., and McWilliams, M. O., 1993, Genesis and evolution of a Permian-Jurassic magmatic arc/accretionary wedge, and reevaluation of terranes in the central Klamath Mountains, *Tectonics*, **12**, 387-409.
- Harper, G.D., 1984, The Josephine ophiolite, *Geol. Soc. Amer. Bull.* **95**, 1009-1026.
- Harper, G.D., and Wright, J.E., 1984, Middle to Late Jurassic tectonic evolution of the Klamath Mountains, California-Oregon, *Tectonics* **3**, 759-772.
- Karig, D.E., 1971, Origin and development of marginal basins in the western Pacific, *J. Geophys. Res.*, v. 76, 2542-2560.
- Ohr, M., 1987, Geology, geochemistry and geochronology of the Lems Ridge olistostrome, Klamath Mountains, California, M.S. thesis, SUNY Albany, 278p.
- Pessagno, E.A., and Blome, C.D., 1990, Implications of new Jurassic stratigraphic, geochronometric, and paleolatitudinal data from the western Klamath terrane (Smith River and Rogue Valley subterrane), *Geology*, **18**, 665-668.
- Saleeby, J.B., Harper, G.D., Snoke, A.W., and Sharp, W.D., 1982, Time relations and structural-stratigraphic patterns in ophiolite accretion, west central Klamath Mountains, California, *J. Geophys. Res.* **87**, 3831-3848.
- Saleeby, J.B., and G.D. Harper, 1993, Tectonic relations between the Galice Formation and the schists of Condrey Mountain, Klamath Mountains, northern California, in *Mesozoic Paleogeography of the Western United States*, vol. II, edited by G. Dunne and K. McDougall, pp.61-80, Society of Economic Paleontologists and Mineralogists, Pacific Section, Los Angeles, California.
- Snoke, A.W., 1977, A thrust plate of ophiolitic rocks in the Preston Peak area, Klamath Mountains, California, *Geol. Soc. Amer. Bull.*, **88**, 1641-1659.
- Uyeda, S., 1977, Some basic problems in the trench-arc-back arc system, in *Islands Arcs Deep Trenches and Back-arc Basins*, Maurice Ewing Series 1, edited by Manik Talwani and Walter C. Pitman, III, pp. 1-14, American Geophysical Union, Washington D.C.
- Wright, J.E., and Fahan, M.R., 1988, An expanded view of Jurassic orogenesis in the

western United States Cordillera: Middle Jurassic (pre-Nevadan) regional metamorphism and thrust faulting within an active arc environment, Klamath Mountains, California, *Geol. Soc. Amer. Bull.*, **100**, 859-876.

Wright, J.E., and Wyld, S.J., 1986, Significance of xenocrystic Precambrian zircon contained within the southern continuation of the Josephine ophiolite: Devils Elbow ophiolite remnant, Klamath Mountains, northern California, *Geology*, **14**, 671-674.

Wright, J. E., and Wyld, S. J., 1994, The Rattlesnake Creek terrane, Klamath Mountains, California: an early Mesozoic volcanic arc and its basement of tectonically disrupted oceanic crust, *Geol. Soc. Am. Bull.*, **106**, 1033-1056.

Yule, J.D., Saleeby, J.B., Jones, D.L., and Silk, M., 1992, Correlation of basement terranes across the Late Jurassic Josephine inter-arc basin, southwestern Oregon and northern California, *Geol. Soc. Amer. Abs. with Programs*, **24**, 5, 93.

APPENDIX 1

GEOLOGIC MAP OF THE CENTRAL ILLINOIS RIVER AREA, JOSEPHINE AND CURRY COUNTIES, OREGON

Introduction

The geologic map area encompasses approximately 800 square kilometers of a region that lies to the west of U.S. Highway 199 and to the west of Grants Pass and Cave Junction, Oregon. The region is underlain by surficial deposits and by stratified, intrusive, and variably metamorphosed crust and mantle derived rocks of Triassic to Late Jurassic age. These rocks were studied during a comprehensive, detailed geologic mapping project of the Eight Dollar Mountain and Pearsoll Peak 7.5' topographic quadrangles, and portions of the Cave Junction, Chetco Peak, Chrome Ridge, Galice, Josephine Mountain, Onion Mountain, Selma, and York Butte 7.5' topographic quadrangles.

The region exposes one of the world's best preserved examples of composite, marginal ocean basin lithosphere. These rocks were accreted to the North American margin in the Late Jurassic subsequent to their genesis in an oceanic setting. The rocks of the study area consist of stratified sedimentary and volcanic rocks, multiply deformed greenschist to amphibolite grade metamorphosed sedimentary and volcanic rocks, shallow level intrusive rocks, plutonic intrusive complexes, and two generations of variably serpentinitized tectonized mantle peridotite. The chief tectonostratigraphic elements are: 1) a complete to partial ophiolite sequence, 2) rifted fragments of older oceanic crust and mantle lithosphere, 3) the plutonic roots and wallrocks of an oceanic magmatic arc, and 4) a stratified overlap assemblage comprised of pelagic, hemipelagic, and flysch strata, olistostromal deposits, and arc volcanogenic rocks whose age and geochemistry suggest a genetic linkage with the arc plutonic complex.

Parts of the study area and surrounding regions have been the cite of numerous previous geologic field mapping projects (e.g., Dick, 1975; Page et al., 1981a, 1981b; Ramp, 1977, 1984, 1986). Please refer to Plate 1 and the "Index to geologic mapping" for work that was modified during this study, and for a listing of other sources of geologic mapping in the study area.

The rocks of the field area have been subdivided on the geologic map and in this text into map units based on guidelines recommended by the North American Commission on Stratigraphic Nomenclature (1983).

SEDIMENTARY AND (OR) VOLCANIC ROCKS consist of stratified rocks, and their moderately deformed and metamorphosed equivalents, that obey the law of superposition. These include Quaternary deposits, the Galice Formation, the Rogue Formation, deposits of the Fiddler Mountain olistostrome complex, and lavas of the Josephine ophiolite.

REGIONALLY METAMORPHOSED AND (OR) DEFORMED ROCKS consist of metasedimentary, metavolcanic, and (or) metaplutonic rocks that do not obey the law of superposition. Included in this category are the amphibolite of Briggs Creek, all rocks of the Onion Camp complex, and the Josephine peridotite.

INTRUSIVE ROCKS, plutonic, hypabyssal rocks have been subdivided on the basis of their emplacement age and (or) composition. These include late-stage small intrusions and dikes, rocks of the Illinois River plutonic complex, and the intrusive section Josephine ophiolite. The International Union of Geological Sciences Subcommittee on Systematics of Igneous Rocks (Streckeisen, 1976) was utilized to classify these rocks. Radiometric ages have been calculated or recalculated with the decay constants and abundances recommended by the International Union of Geological Sciences Subcommittee on Geochronology (Steiger and Jager, 1977). The Decade of North American Geology Time Scale (Palmer, 1983) has been used to relate these radiometric dates to the geologic time scale.

General Explanation of Plates 1-11

Plate 1 is a generalized geologic map of the entire study area, drawn at a scale of 1:96,000 and compiled from Plates 2-11. Plates 2-11 are larger scale geologic maps (1:24,000) of varying portions of USGS 7.5 ' topographic quadrangles. Figure A1-1 shows the areal distribution of the quadrangle maps. Cross-sections are included on Plate 1. Structural symbols are omitted on Plate 1 for the sake of clarity. Please refer to the explanation of Plates 2-11 and to Plates 2-11 themselves for structural information.

The rocks belonging to each map unit are described below in the Description of Map Units. Geologic units that have not been assigned to map units include mafic to intermediate dikes and, in the case of Plate 1, surficial deposits that occur at too small of a scale to be shown on the maps. The dikes and surficial deposits are described in the Description of Map Units for Plates 2-11. Major faults in the area are discussed in Chapter 2. Tables A1-1, A1-2, and A1-3 outline the basic information about each of the geochemical, paleontologic, and geochronologic samples analyzed during this study.

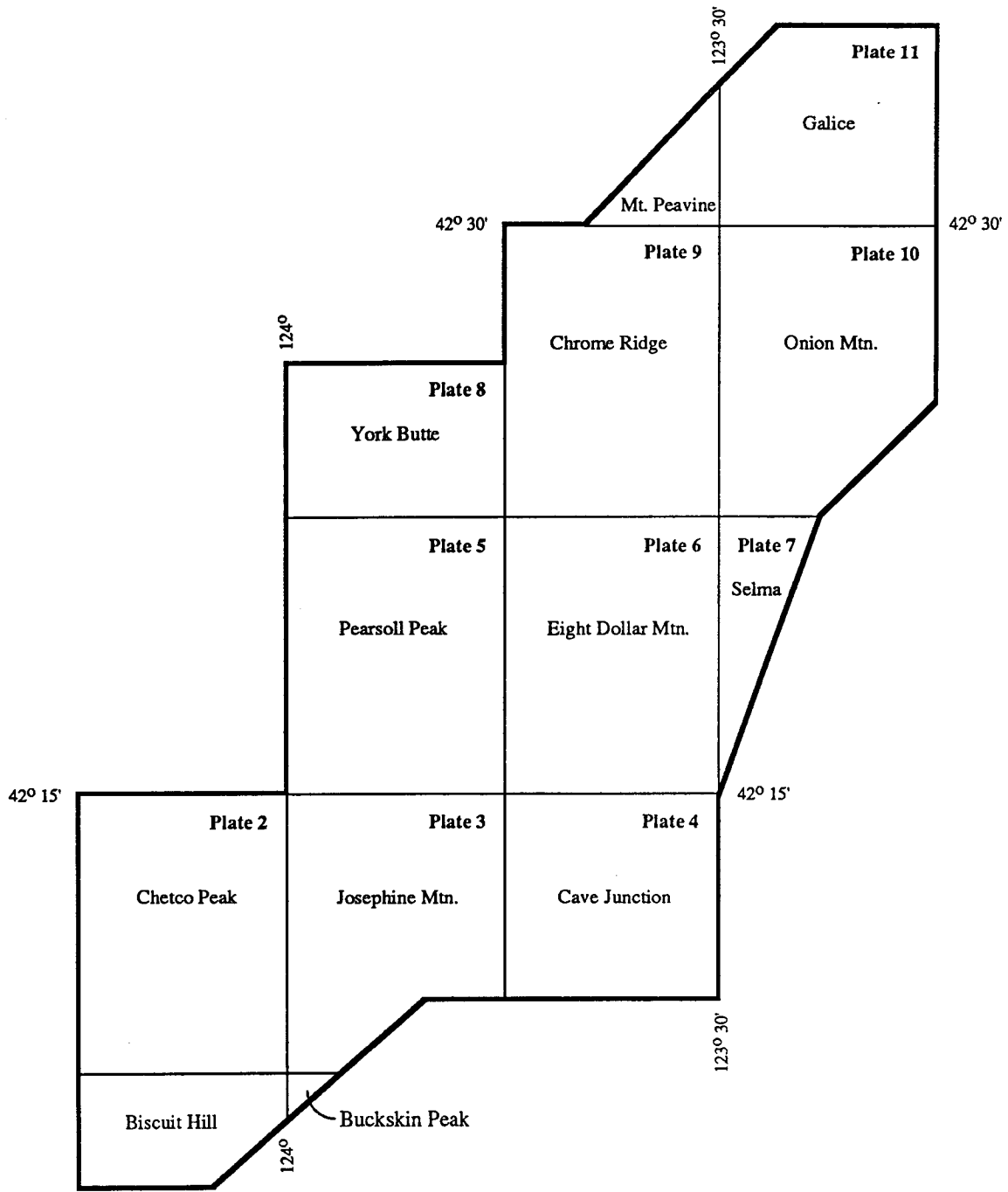


Figure A1-1. Outline of the study area showing the boundaries of USGS 7.5' topographic maps.

Table A1-1. Geochemical samples and localities.Illinois River plutonic complex

| Station | Lithology | Latitude (°N) deg/min/sec | Longitude (°W) deg/min/sec | Remarks |
|-----------|--------------------------|------------------------------|-------------------------------|--|
| 1. CP-4 | Troctolite | 42/14/29 (42.241) | 123/53/01 (123.884) | Layers in outcrop defined by |
| 2. YB-6 | Troctolite | 42/22/41 (42.378) | 123/48/53 (123.815) | |
| 3. PP-70 | Norite | 42/15/43 (42.262) | 123/52/14 (123.871) | Ar/Ar sample (155.3 ± 0.5 Ma). |
| 4. YB-13 | Norite | 42/23/29 (42.391) | 123/50/25 (123.840) | |
| 5. YB-7 | Norite | 42/22/32 (42.376) | 123/49/02 (123.817) | |
| 6. YB-9 | Homblende gabbro | 42/23/27 (42.391) | 123/51/47 (123.863) | |
| 7. IR-3 | Homblende gabbro | 42/18/36 (42.310) | 123/48/18 (123.805) | Zircon sample. Homogenous with local ultramafic xenoliths. |
| 8. IR-4 | Granodiorite | 42/23/20 (42.389) | 123/50/53 (123.848) | Zircon sample (~160 Ma). Agmatitic with mafic enclaves. |
| 9. PP-17 | Tonalite- trondhemite | 42/19/40 (42.328) | 123/46/45 (123.779) | |
| 10. PP-48 | Tonalite- trondhemite | 42/19/37 | 123/46/45 (123.779) | |
| 11. PP-62 | Tonalite- trondhemite | 42/16/11 (42.270) | 123/51/09 (123.853) | |
| 12. PP-64 | Tonalite- trondhemite | 42/19/37 (42.327) | 123/46/46 (123.780) | Zircon sample (~157 Ma). |
| 13. PP-69 | Tonalite- trondhemite | 42/21/47 (42.363) | 123/47/06 (123.785) | |
| 14. PP-9A | Dike | 42/18/36 (42.310) | 123/46/40 (123.778) | Zircon sample (~157 Ma) . Felsic orthogneiss dike in amphib. facies dikes. |
| 15. PP-14 | Dike | 42/19/23 (42.323) | 123/46/47 (123.780) | Hornblendite dike cutting peridotite roof rocks of the plutonic complex. |

Rogue Formation

| Station | Lithology | Latitude (°N) deg/min/sec | Longitude (°W) deg/min/sec | Remarks |
|------------|-----------------|------------------------------|-------------------------------|--|
| 1. PP-6 | Massive flow | 42/17/42 (42.287) | 123/45/03 (123.751) | Cpx-rich massive lava cut by dioritic dikes in outcrop along Illinois River. |
| 2. EDM-49 | Massive flow | 42/20/22 (42.339) | 123/40/55 (123.682) | |
| 3. EDM-51B | Massive flow | 42/20/37 (42.344) | 123/41/41 (123.695) | |
| 4. EDM-59 | Massive flow | 42/21/27 (42.357) | 123/42/52 (123.714) | Flow unit interbedded with volcanic breccia. |
| 5. G-9 | Massive flow | 42/34/14 (42.571) | 123/32/27 (123.541) | |
| 6. S-38 | Massive flow | 42/18/14 (42.304) | 123/43/09 (123.719) | |

Table A1-1 (continued). Geochemical samples and localities.Rogue Formation (continued)

| Station | Lithology | Latitude (°N) deg/min/sec | Longitude (°W) deg/min/sec | Remarks |
|------------|-----------|------------------------------|-------------------------------|--|
| 7. S-18 | Tuff | 42/17/37 (42.294) | 123/43/12 (123.740) | Collected at opposite the confluence of Hoover Gulch and the Illinois River. |
| 8. EDM-48C | Tuff | 42/20/51 (42.348) | 123/40/48 (123.680) | |
| 9. EDM-51A | Tuff | 42/20/37 (42.344) | 123/41/41 (123.695) | |
| 10. 6MiRd | Sill | 42/18/48 (42.313) | 123/43/12 (123.720) | Clinopyroxene-rich sill intruding volcanogen. turbidite in basal Rogue Fm. |
| 11. EDM-84 | Sill | 42/20/00 (42.333) | 123/40/39 (123.678) | Clinopyroxene-rich sill intruding slaty argillite of the Galice Fm. |

Josephine ophiolite

| Station | Lithology | Latitude (°N) deg/min/sec | Longitude (°W) deg/min/sec | Remarks |
|------------|--------------------|------------------------------|-------------------------------|--|
| 1. PP-27 | Dike | 42/16/25 (42.274) | 123/46/07 (123.769) | Collected from fragmented and folded(?) sheeted mafic dike complex |
| 2. PP-33 | Dike | 42/15/52 (42.264) | 123/49/03 (123.818) | Ditto PP-27. |
| 3. PP-44A | Dike | 42/17/18 (42.288) | 123/48/05 (123.801) | Upper west fork of Rancherie Creek |
| 4. OM-1A | Dike | 42/27/31 (42.459) | 123/31/18 (123.522) | |
| 5. S-2 | Dike | 42/19/43 (42.329) | 123/36/57 (123.616) | Collected from road metal quarry exposing sheeted dikes and pillows. |
| 6. EDM-88A | Dike | 42/17/45 (42.296) | 123/43/40 (123.728) | EDM-88A and 88B collected from the same outcrop, Illinois River. |
| 7. EDM-88B | Dike | 42/17/45 (42.296) | 123/43/40 (123.728) | |
| 8. G-17B | Dike | 42/32/26 (42.541) | 123/30/10 (123.503) | Riverside exposure immediately downstream from Hog Ck. boat launch. |
| 9. S-1 | Pillow lava | 42/20/46 (42.346) | 123/36/37 (123.610) | Collected from same road metal quarry as S-2. |
| 10. G-17A | Pillow lava | 42/32/26 (42.541) | 123/30/09 (123.503) | Riverside exposure immediately downstream from Hog Ck. boat launch. |
| 11. W-1D | Pillow lava | 42/29/41 (42.495) | 123/29/04 (123.484) | River polished exposure on east side of Rogue River. |
| 12. JM-6 | Massive greenstone | 42/14/31 (42.242) | 123/45/53 (123.765) | Collected from Fiddler Mountain. |

Onion Camp complex

| Station | Lithology | Latitude (°N) deg/min/sec | Longitude (°W) deg/min/sec | Remarks |
|---------|-------------|------------------------------|-------------------------------|---|
| 1. CP-3 | Pillow lava | 42/14/11 (42.236) | 123/47/46 (123.796) | Collected from road metal quarry near Onion Camp. |

Table A1-1 (continued). Geochemical samples and localities.Onion Camp complex (continued)

| Station | Lithology | Latitude (°N) deg/min/sec | Longitude (°W) deg/min/sec | Remarks |
|------------|--------------------|------------------------------|-------------------------------|--|
| 2. OM-8 | Pillow lava | 42/26/26 (42.441) | 123/35/44 (123.596) | |
| 3. EDM-83A | Pillow lava | 42/17/20 (42.289) | 123/37/33 (123.728) | River polished exposure of pillow lavas adjacent the Illinois River. |
| 4. EDM-83B | Pillow lava | 42/17/20 (42.289) | 123/37/33 (123.728) | River polished exposure of pillow lavas adjacent the Illinois River. |
| 5. EDM-87 | Pillow lava | 42/17/48 (42.297) | 123/43/42 (123.728) | |
| 6. G-14C | | 42/32/37 (42.544) | 123/30/40 (123.511) | Roadcut in opposite Hellgate Canyon overlook, Rogue River gorge. |
| 7. OM-11 | Massive greenstone | 42/27/55 (42.465) | 123/35/44 (123.596) | Collected from quarry near Onion Mountain. |
| 8. OM-14 | Massive greenstone | 42/29/52 (42.498) | 123/32/36 (123.543) | |
| 9. G-14A | Massive greenstone | 42/32/37 (42.544) | 123/30/40 (123.511) | Roadcut in opposite Hellgate Canyon overlook, Rogue River gorge. |
| 10. CP-45 | Massive greenstone | 42/13/12 (42.220) | 123/48/22 (123.806) | Collected from cirque wall above Babyfoot Lake. |
| 11. CR-22 | Massive greenstone | 42/25/38 (42.427) | 123/37/33 (123.626) | |
| 12. JM-11 | Dike | 42/14/45 (42.246) | 123/48/35 (123.800) | Zircon sample (~173-174 Ma). Plagiogranite dike cutting OCC peridotite near Whetstone Butte. |

Table A1-2. Paleontologic samples and localities.

| Station | Description | Latitude (°N) & Longitude (°W) deg/min/sec | Interpreted Age | Species List |
|----------|---|--|---|---|
| 1. PP-45 | Gray argillaceous chert with calcareous nodules; N35E, 51SE. | 42/17/13.5 123/48/19.5 | Late Jurassic (Callovian) | Eurcyrtidiellum pustulatum Parvicingula Archaeodictyomitra sp. Hsuum sp. |
| 2. CP-37 | Tightly folded white-gray chert; N46E, 31SE. | 42/14/28.5 123/47/37.5 | Late Jurassic (Upper Kimmeridgian - Lower Tithonian?) | Lupherium sp. Praeconocaryomma magnimamma Large spheres (unidentifiable) |
| 3. CP-5 | Locality of Roure and DeWever (1983). Isolated exposure of well-bedded red chert; N20E, 39SE. | 42/14/19 123/46/52.5 | Upper Triassic (?) - Bajocian | probable Conoptums |

Table A1-3. Geochronologic samples and localities.

| Station | Age (Ma) | Latitude (°N) deg/min/sec | Longitude (°W) deg/min/sec | Remarks |
|------------|---------------|------------------------------|-------------------------------|---|
| 1. PP-4 | 153.4 ± 0.6 † | 42/18/10 | 123/46/51 | Illinois River falls. Rogue Fm, crystal and lithic tuff breccia. |
| 2. PP-70 | 155.3 ± 0.5 † | 42/15/43 | 123/52/11 | Confluence of Slide Creek with Chetco River. IRPC, norite. |
| 3. PP-12C | 156.0 ± 0.5 † | 42/18/38 | 123/46/51 | Illinois River. Hornblendite dike cutting Pearsoll Peak peridotite. |
| 4. PP-15 | 156.3 ± 0.6 † | 42/19/32 | 123/46/38 | Illinois River. Hb-bio meta qtz diorite dike cutting Pearsoll Peak peridotite. |
| 5. CR-9B | 156.8 ± 0.5 † | 42/24/04 | 123/44/50 | Briggs Creek. Metagabbro in Briggs Creek amphibolite body. |
| 6. EDM-72A | 157.9 ± 0.5 † | 42/21/37 | 123/44/42 | Soldier Creek. Hornblende schist, Briggs Creek amphibolite body. |
| 7. EDM-81A | 169.6 ± 0.5 † | 42/20/40 | 123/39/40 | Squaw Mtn. Amphibolite gneiss, Onion Camp complex. |
| 8. EDM-10 | 173.1 ± 0.6 † | 42/18/58 | 123/40/46 | Squaw Mtn. Amphibolite gneiss, Onion Camp complex. |
| | 159.5 ± 0.5 ‡ | 42/22/18.5 | 123/48/21 | Illinois River. Massive hornblende gabbro. |
| 10. IR-4 | 159.2 ± 1.2 ‡ | 42/23/19.5 | 123/50/53.5 | Illinois River. Granodiorite with mafic enclaves. |
| 11. YB-8 | 157.1 ± 0.9 ‡ | 42/23/53.5 | 123/51/44 | Illinois River. Biotite-hornblende tonalite. |
| 12. IR-1 | 156.5 ± 1.2 ‡ | 42/21/14.5 | 123/46/57 | Illinois River. Biotite-hornblende tonalite. |
| 13. PP-64 | >154.9 ‡ | 42/19/37 | 123/46/46 | Near Sourdough Flat. Biotite-hornblende tonalite. |
| 14. IR-2 | 160.3 ± 1.3 ‡ | 42/21/07.5 | 123/46/57 | Illinois River. Felsic leucosome in amphibolite gneiss and schist cutting Pearsoll Peak peridotite. |
| 15. PP-9B | 160.1 ± 0.5 ‡ | 42/18/36 | 123/46/40 | Felsic metadike in amphibolite facies mafic dike complex cutting Pearsoll Peak peridotite. |
| 16. PP-9A | ~160 ± 10 | 42/18/36 | 123/46/40 | Same outcrop as PP-9B, different metadike. |
| 17. S-3 | 150.0 ± 0.5 ‡ | 42/15/11.5 | 123/44/30 | Near Fiddler Mountain. Dacite dike cutting regional Nevadan foliation. |
| 18. JM-10 | 175.3 ± 2.0 ‡ | 42/14/35.5 | 123/48/35.5 | Near Whetstone Butte. Plagiogranite dike cutting serp. perid. of the OCC. |
| 19. JM-11 | 173.2 ± 0.7 ‡ | 42/14/45 | 123/48/35 | Near Whetstone Butte. Plagiogranite dike cutting serp. perid. of the OCC. |
| 20. EDM-89 | ??? ‡ | 42/17/48 | 123/43/40.5 | Illinois River. Plagiogranite body associate with sheeted mafic dikes intruding metavolc. rocks of the OCC. |

† hornblende, $^{40}\text{Ar}/^{39}\text{Ar}$.

‡ zircon, U-Pb.

GEOLOGIC MAP EXPLANATION

PLATE 1

Symbols

(see Plate 1 for explanation of symbols)

Rock Units

Q Quaternary fluvial deposits of the Illinois River and Rogue River valleys.

h d Late stage (post regional deformation) hornblende-rich dikes and small intrusions.

Overlap Sequence - Includes sedimentary and volcanogenic rocks deposited upon rocks of both the Josephine ophiolite and the Onion Camp terrane.

J g *Galice Formation*. (Late Jurassic). Consists of Callovian hemipelagic deposits grading upward into Oxfordian-Kimmeridgian flysch deposits. Lower pelagic and hemipelagic strata interfinger with strata of the Rogue Formation. Flysch deposits and overlap deposits of the Rogue Formation.

J r *Rogue Formation*. (153.4 ± 0.6 Ma, Ar/Ar amphibole; 157 ± 1.5 Ma (Saleeby, 1984)). Consists of basaltic to andesitic volcanogenic turbidites, volcanic breccias, and lava flows.

J f m *Fiddler Mountain Olistostrome*. Consists of chert (ch), argillite (arg), and pebble conglomerate interbedded with breccia and megabreccia deposits whose clasts primarily consist of basalt, diabase, gabbro with subordinate chert, serpentine, and peridotite clasts. Clasts range in size from coarse sand to >500 m. Not shown on the map are scattered exposures of relatively thin ophiolite clast and serpentinite clast sand and breccia deposits that occur at the base of the Rogue and

Galice Formations. Chert yields poorly preserved Late Jurassic(?) radiolaria (M. Silk, personal communication).

Illinois River plutonic complex. (Illinois River gabbro of Jorgenson, 1970; intrusive portion of the Chetco River complex of Hotz, 1971). Radiometric age determinations made during this study include ~157 Ma (Jtt) and ~160 Ma (Jgd), U/Pb zircon, and 155-156 Ma (Jgd), Ar/Ar amphibole.

Jog Layered olivine gabbro and two-pyroxene gabbro form the core of the plutonic complex.

Jgd The main phase of the plutonic complex consisting of foliated to massive biotite hornblende quartz diorite, hornblende gabbro-diorite, and norite.

Jfl Marginal facies consisting of flaser quartz diorite, diorite, and gabbro with shallowly inclined, NE-SW trending lineations and steeply dipping foliations occur along the eastern margin of the plutonic complex.

Jtt Commingled biotite tonalite and two-mica garnet trondhjemite that comprise a deformed sill that forms the top of the plutonic complex. Sub-horizontal foliations and shallow NE-SW trending lineations are common (exposed beneath Pearsoll Peak and at Pine Flat).

Jpeg Nondeformed hornblende gabbro pegmatoid sill with distinctive comb structure exposed at the southern border of the complex beneath the Madstone Cabin fault.

Country rocks of the Illinois River plutonic complex. Predominantly amphibolite facies mafic and ultramafic rocks.

bcag Briggs Creek amphibolite, a large continuous body of amphibolite gneiss

and schist, and subordinate impure metaquartzite occurs in the drainages of Briggs Creek. Radiometric age determinations for the Briggs Creek amphibolite made during this study fall in the range between 156-158 Ma (Ar/Ar amphibole). Field relations and geochemical data suggest that the protolith terrane for these rocks is composite in nature and consists of crustal rocks from both the Josephine ophiolite (Jjo) and the Onion Camp terrane (JTroc). In the southwestern part of the map near Pearsoll Peak and Dry Butte, fragments of amphibolite facies ophiolitic crust (Jog?) are represented by local exposures of gneissic meta-gabbro (mg) underlain by metapyroxenite (py). The metapyroxenite consists mostly of cumulate textured wehrlite and clinopyroxenite. Elsewhere, meta-peridotite (pd) comprised of harzburgite, dunite, and local podiform chromite occur as screens and roof rocks for the plutonic complex. This peridotite wallrock, including the extensive Pearsoll Peak and Chrome Ridge peridotite bodies, are interpreted to represent disconnected fragments of the Josephine peridotite.

ag Smaller bodies of amphibolite that occur beneath the Madstone Cabin fault and exhibit structures and lithologies that are essentially identical to the Briggs Creek amphibolite. On this basis, in combination with similar geochemical affinities (Harper et al., in press), these southern amphibolite bodies are interpreted as equivalent, but disconnected fragments of the Briggs Creek amphibolite.

Josephine ophiolite (162-166 Ma, U-Pb zircon, Saleeby, 1984). On the basis of distinctive age and field relations, these rocks are interpreted as northern extensions of the type Josephine ophiolite exposed in northern California (Harper, 1984).

Jjo The crustal sequence (Jjo) consists of scarce layered gabbro, massive gabbro, sheeted mafic dikes, and pillow lavas and lava breccias. Chert interbedded with calcareous pelagic and hemipelagic strata and pillow lava yield Callovian

radiolaria (Yule et al., 1992); essentially identical to the age relations described in the type Josephine section (Pessagno and Blome, 1990).

J j p The mantle lithosphere portion of the ophiolite, named the Josephine peridotite by Dick (1976). Consists of virtually pristine tectonized harzburgite, dunite, and podiform chromite, and partially to wholly serpentized peridotite.

s s p Highly sheared and completely serpentized Josephine peridotite along and near the Madstone Cabin thrust fault.

Onion Camp complex, herein named for rocks exposed in the NW corner of the Fiddler Mountain 7.5' topographic quadrangle where Roure and DeWever (1983) reported a Triassic age from chert collected near Onion Camp. Cherts collected for this study from the same locality of Roure and DeWever (1983) yield mostly amorphous radiolaria with scarce Triassic to Middle Jurassic forms (Yule et al., 1992). The combination of Triassic(?)–Jurassic fossil ages with distinctive lithologic and geochemical traits correlate rocks of the Onion Camp terrane with rocks known as the Rattlesnake Creek and Marble Mountains terranes in the western Paleozoic and Triassic belt of the Klamath Mountains.

J T r o c Greenschist facies crustal rocks of the Onion Camp complex, including greenstone, pillow lava and interbedded red chert, heterogeneous mafic intrusive rocks, and intercalated meta-argillite, metachert, and metatuff.

a m Amphibolite gneiss, schist, and impure quartzite. Progenitor materials are constrained to be the greenschist facies rocks of the complex (JTroc).

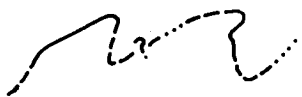
s p Serpentized peridotite and serpentinite of the Onion Camp complex. Peridotite near Whetstone Butte is intruded by ~175 Ma dikes. Near Squaw Mountain, the sinuous nature of the contact between the amphibolite and peridotite illustrates the complex folding history experienced by rocks in the Onion Camp

terrane. Boundary between the Onion Camp peridotite (sp) and the Josephine peridotite (Jjp) is typically marked by a distinct vegetation change. The boundary represents an intra-peridotite boundary separating two, distinct bodies of peridotite; the OCC sp cut by ~175 Ma dikes, and the Jjp presumably formed during ophiolite genesis at 160-165 Ma.

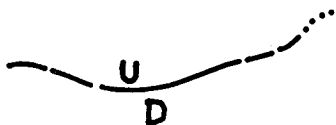
ssp Sheared serpentinite. Only the largest serpentinite bodies are shown on the map because numerous exposures of sheared, black serpentinite cannot be shown at this scale. The degree of serpentinization and shearing increases toward the contacts with crustal rocks and near fault contacts where highly sheared serpentinitized peridotite occurs (ssp).

GEOLOGIC MAP EXPLANATIONPLATES 2-11

Symbols



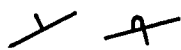
lithologic contact, solid where known, dashed where inferred, and dotted where concealed



high angle fault, solid where known, dashed where inferred, and dotted where concealed



thrust fault, solid where known, dashed where inferred, and dotted where concealed



strike and dip of bedding, upright and overturned



strike and dip of foliation, foliation with lineation



approximate strike and dip of shear foliation



strike, dip, and lineation of S-C planes in sheared serpentinite



strike and dip of igneous layering



trend and plunge of fold axes

Rock Units

Quaternary deposits

- Qal** Unconsolidated silt, sand, and gravel alluvial deposits occupying modern stream and river channels, and associated low terraces and flood plains.
- Qt** River terrace deposits. Elevated, weakly consolidated silt, sand, and gravel alluvial deposits common in wider portions of present day river valleys (e.g. the Illinois River Valley and the Rogue River valley). Deposits represent older, uplifted (or abandoned) river channel and flood plain deposits that occur within 100 meters elevation of current stream levels. Diller (1907) referred to these deposits as auriferous gravels of the Third Cycle of Erosion.
- Qls** Landslide debris, arrows show general direction of downslope movement. Landslides are often rooted in zones of sheared serpentinite, the ubiquitous rocktype throughout the map area. For example, a number of large landslides are rooted in the sheared serpentinite along the Madstone Cabin and Pearsoll Peak thrust faults (Pearsoll Peak and Chetco Peak 7.5' quadrangles). Landslides are also common on oversteepened slopes where mass wasting is widespread.
- Qtc** Talus cone deposits, or rock fall deposits common on the eastern flank of Eight Dollar Mountain.
- Qgt** Glacial till. Unconsolidated, unsorted debris covering the broad slopes in valleys beneath small, north facing cirques near Vulcan Peak, Pearsoll Peak, and Babyfoot Lake (Chetco Peak, Pearsoll Peak quadrangles, and Fiddler Mountain, respectively).

Old river gravel deposits - precise age unknown. The deposits consist of weakly to moderately consolidated alluvial material occurring high above modern streams associated with remnants of ancient fluvial systems. In extreme cases, boulders and cobbles exposed in roadcuts are completely weathered to saprolite. Both the high and moderate level Quaternary (?) fluvial deposits described below illustrate the relatively recent tectonic uplift that has affected this part of southwestern Oregon. The rates of uplift and the presence or lack of evidence for neotectonic activity are important questions that more careful study of the Quaternary-Holocene sediments and nearby faults may resolve.

Qog A north trending set of outcrops that expose ancient fluvial gravels occur on the divides between Onion, Swede, Soldier, and Sixmile Creeks in the southwestern and northwestern parts of the Chrome Ridge and Eight Dollar Mountain 7.5' quadrangles, respectively. Diller (1907) referred to these deposits as auriferous gravels of the Second Cycle of Erosion because they occur at elevations approximately 1500 feet below the Klamath peneplain (gravels from this First Cycle of Erosion occur to the west of Pearsoll Peak at Gold Basin and north of York Butte at Mud Spring), and 2000-2500 feet above alluvial deposits of the present day Illinois and Rogue Rivers. He also noted the north-south trending outcrop pattern defined by these deposits and suggested that they were deposited by an ancestral Illinois River that flowed northward from its present course above the mouth of Sixmile Creek to enter the Rogue River near Galice. These ancient fluvial deposits closely follow the trace of the Chetco Pass Fault, parallel the regional structural trend of the map units, and occur immediately to the west of broad upland areas characterized by low relief and deep soil profiles (e.g. Swede Basin). In combination, these relations suggest that the ancestral Illinois River occupied the western part of a broad, fault-bounded valley analogous to the modern Illinois River valley south of the map area near Cave Junction.

Qorg Remnants of old river gravels that occur as flat benches at approximately 1400 to 1600 feet elevation on the valley slopes of the modern Illinois River and Deer Creek in the southern portion of the Eight Dollar Mountain 7.5' quadrangle. Diller (1907) referred to these deposits as auriferous gravels of the Third Cycle of erosion.

Latest Jurassic

hd Mafic to intermediate dikes and small intrusions. Radiometric age determinations cluster at 150 Ma and include U-Pb zircon, Ar-Ar and K-Ar amphibole and biotite (?) apparent ages (this study; Dick, 1976; and Harper and Saleeby, in press). Dike textures range from coarse porphyritic to aphanitic. Acicular hornblende crystals are characteristic, though not always diagnostic. Phenocrysts in mafic dikes include clinopyroxene, stubby to acicular hornblende, and plagioclase feldspar. In intermediate dikes, acicular hornblende, plagioclase feldspar, and quartz phenocrysts occur. The quartz phenocrysts, in some cases, are resorbed.

The late stage dikes are most common in the southern part of the map area, particularly in the vicinity of Fiddler Mountain and Canyon Peak in the Josephine Mountain 7.5' quadrangle. These dikes most commonly intrude serpentized portions of the Josephine peridotite and surrounding rocks of the Onion Camp terrane. They rarely occur west of the Chetco Pass fault and are scarce in the Galice and Rogue Formations. Larger bodies of 150 Ma intrusions exist to the south of the map area suggesting that the locus for 150 Ma magmatism lay to the south.

Field and petrographic relations distinguish the late stage dikes from older dikes and intrusions. The 150 Ma dikes never exhibit the brittle fragmentation textures and the ubiquitous greenschist facies hydrothermal alteration that is diagnostic of older intrusive rocks. In addition, they cut across the pervasive

regional foliation and therefore place a pre-150 Ma age constraint on the timing of regional compressional deformation. The late stage dikes are typically shallowly dipping. Where they intrude serpentinitized peridotite, they are not rodingitized suggesting that they were emplaced after serpentinitization occurred. Deformation and serpentinitization of peridotite did occur post-150 Ma as evidenced by a slight degree of rodingitization and the fact that the dikes are cut by faults in serpentinite shear zones.

Late Middle to Late Jurassic

Note: Refer to Chapter 2 for a more detailed description of the following rock units.

Galice Formation. (Late Jurassic). Consists of Callovian hemipelagic deposits grading upward into Oxfordian-Kimmeridgian flysch deposits (Pessagno and Blome, 1990). Lower pelagic and hemipelagic strata interfinger with strata of the Rogue Formation. Flysch deposits overlap deposits of the Rogue Formation.

Jg graywacke, siltstone, shale and chert.

Jgs siltstone, shale and chert.

Rogue Formation. (153.4 ± 0.6 Ma, Ar/Ar amphibole; 157 ± 1.5 Ma (Saleeby, 1984). Consists of basaltic to andesitic volcanogenic turbidites, volcanic breccias, and lava flows.

Jru Rogue Formation, undivided.

Jrm massive lava and volcanic breccia.

Jrb well-bedded volcanogenic turbidites.

Jrsd mafic to intermediate sills and dikes.

Fiddler Mountain Olistostrome. Consists of chert, argillite, and pebble conglomerate interbedded with breccia and megabreccia deposits whose clasts primarily consist of basalt, diabase, gabbro with subordinate chert, serpentine, and peridotite clasts.

Jol olistostromal deposits, undivided.

Jchar chert and slaty argillite. Chert yields poorly preserved Late Jurassic(?) radiolaria (Yule et al., 1992).

Jcgl polymict conglomerate with mostly ophiolite derived clasts. Clasts range in size from coarse sand to >500 m.

Illinois River plutonic complex. (Illinois River gabbro of Jorgenson, 1970; intrusive portion of the Chetco River complex of Hotz, 1971). Radiometric age determinations made during this study include ~157 Ma (Jtt) and ~160 Ma (Jgd), U/Pb zircon, and 155-156 Ma (Jgd), Ar/Ar amphibole.

Jirpc Undivided rocks of the plutonic complex.

Jog Layered olivine gabbro and two-pyroxene gabbro form the core of the plutonic complex. Cumulate textures are common. Orbicular gabbro rare.

Jirgb The main phase of the plutonic complex consisting of foliated to massive biotite hornblende quartz diorite, hornblende gabbro-diorite, and norite.

Jflgb Marginal facies consisting of flaser quartz diorite, diorite, and gabbro with shallowly inclined, NE-SW trending lineations and steeply dipping foliations occur along the eastern margin of the plutonic complex.

Jtt Commingled biotite tonalite and two-mica garnet trondhjemite that comprise a deformed sill that forms the top of the plutonic complex. Sub-horizontal foliations and shallow NE-SW trending lineations are common (exposed beneath Pearsoll Peak and at Pine Flat).

Josephine ophiolite (162-166 Ma, U-Pb zircon, Saleeby, 1984). On the basis of distinctive age and field relations, these rocks are interpreted as northern extensions of the type Josephine ophiolite exposed in northern California (Harper, 1984). Chert interbedded with calcareous pelagic and hemipelagic strata and pillow lava yield Callovian radiolaria (Yule et al., 1992); essentially identical to the age relations described in the type Josephine section (Pessagno and Blome, 1990).

Jjcr Rocks of the crustal sequence of the ophiolite, undivided, including layered and massive gabbro, sheeted mafic dikes, and pillow lavas and lava breccias. Most often the sequence is incomplete and appears to have been tectonically disrupted. Where complete, the sequence never exceeds 2 km in thickness.

Jjpl pillow lava and lava breccia.

Jjsd sheeted mafic dikes.

Jjgb massive gabbro.

Jjcg cumulate gabbro.

jpd The mantle lithosphere portion of the ophiolite, named the Josephine peridotite by Dick (1976). Consists of virtually pristine tectonized harzburgite, dunite, and podiform chromite, and partially to wholly serpentized peridotite.

jspd massively serpentized peridotite. Cross-cutting ~175 Ma dikes near Whetsone Butte (Plate 3) suggest that at least part of the Josephine peridotite is older than the crustal section of the ophiolite. Instead, this map unit may represent part of the Onion Camp complex.

Country rocks of the Illinois River plutonic complex. Predominantly amphibolite facies mafic and ultramafic rocks.

JTram Briggs Creek amphibolite, a large continuous body of amphibolite gneiss and schist, and subordinate impure metaquartzite occurs in the drainages of Briggs Creek. Radiometric age determinations for the Briggs Creek amphibolite made

during this study fall in the range between 156-158 Ma (Ar/Ar amphibole). Field relations and geochemical data suggest that the protolith terrane for these rocks is composite in nature and consists of crustal rocks from both the Josephine ophiolite (Jjcr) and the Onion Camp complex (WTrPz).

spd serpentinized harzburgite and dunite of unknown association.

pd unserpentinized harzburgite, dunite, and local podiform chromite of unknown association occurring as screens and roof rocks for the plutonic complex. Interpreted as disconnected fragments of the Josephine peridotite.

Triassic to Middle Jurassic

Onion Camp complex, herein named for rocks exposed in the NW corner of the Fiddler Mountain 7.5' topographic quadrangle where Roure and DeWever (1983) reported a Triassic age from chert collected near Onion Camp. Cherts collected for this study from the same locality of Roure and DeWever (1983) yield mostly amorphous radiolaria with scarce Triassic to Middle Jurassic forms (Yule et al., 1992). The combination of Triassic(?)–Jurassic fossil ages with distinctive lithologic and geochemical traits correlate rocks of the Onion Camp terrane with rocks known as the Rattlesnake Creek and Marble Mountains terranes in the western Paleozoic and Triassic belt of the Klamath Mountains.

WTrPz Onion Camp complex, undivided, correlated with the Rattlesnake Creek and Marble Mountains terrane based on distinctive lithologic, geochemical, age, and structural data. Late Triassic to Early Jurassic radiolarian chert collected near Onion Camp (Plate 3).

mvs greenschist facies metavolcanic and metasedimentary rocks including greenstone, pillow lava and interbedded red chert, heterogeneous mafic intrusive rocks, and intercalated meta-argillite, metachert, and metatuff.

ch isolated blocks of red chert generally associated with massive and pillow lava.

mc metadiabase and metagabbro complex.

- am** amphibolite gneiss, schist, and impure quartzite. Progenitor materials are constrained to be the greenschist facies rocks of the complex (mvs).
- spd** massively serpentinized peridotite.
- sp** sheared serpentinite.

References

- Dick, H.J.B., 1976, The origin and emplacement of the Josephine Peridotite of southwestern Oregon, Ph. D. dissertation, Yale University, 409p.
- Diller, J.S., 1907, The Mesozoic sediments of southwestern Oregon, *Am. Jour. Sci.*, **23** 401-421.
- Harper, G.D., 1984, The Josephine ophiolite, *Geol. Soc. Amer. Bull.*, **95**, 1009-1026.
- Harper, G.D., and Saleeby, J.B., 1994, Formation and emplacement of the Josephine ophiolite, and the age of the Nevadan orogeny in the Klamath Mountains, California-Oregon: U/Pb and $^{40}\text{Ar}/^{39}\text{Ar}$ geochronology, *J. Geophys. Res.*, **99**, 4293-4321.
- Harper, G.D., Grady, K., and Coulton, A.J., in press, 1995, *Tectonics*, Origin of the amphibolite "sole" of the Josephine ophiolite: Emplacement of a cold ophiolite over a hot arc.
- Hotz, P.E., 1971, Geology of lode gold districts in the Klamath Mountains, California and Oregon, *U.S. Geol. Survey Bull.*, **1290**, 91p.
- Jorgenson, D.B., 1970, Petrology and origin of the Illinois River gabbro, a part of the Josephine peridotite-gabbro complex, Klamath Mountains, southwestern Oregon, Ph.D. dissertation, University of California, Santa Barbara, 195 p.
- North American Commission on Stratigraphic Nomenclature, 1983, North American Stratigraphic Code: American Association of Petroleum Geologists Bulletin, v. 67, no. 5, pp., 841-875. Page et al., 1981a
- Page, N.J., Gray, F., Cannon, J.K., Foose, M.P., Lipin, B., Moring, B.C., Nicholson, S.W., Sawline, M.G., Till, A., and W.P. Ziemianski, 1981, Geologic map of the Kalmiopsis wilderness area, Oregon, *U. S. Geol. Surv. Misc. Field Studies Map MF-1240-A*.
- Pessagno, E.A., and Blome, C.D., 1990, Implications of new Jurassic stratigraphic, geochronometric, and paleolatitudinal data from the western Klamath terrane (Smith River and Rogue Valley subterrane), *Geology*, **18**, 665-668.
- Ramp, L., 1977, Geology, mineral resources, and rock material of Curry County, Oregon, *Oregon Dept. Geol. and Mineral Industries Bull.*, **88**, 47p.
- Ramp, L. and Peterson, N.V., 1979, Geology and mineral resources of Josephine County, Oregon, *Oregon Dept. Geol. and Mineral Industries Bull.*, 100, 45 p.
- Ramp, L., 1984, Geologic map of the southeast quarter of the Pearsoll Peak quadrangle, Curry and Josephine Counties, Oregon, *Oregon Dept. Of Geol. And Mineral Industries Geol. Map Series GMS-30*, scale 1:24,000.
- Ramp, 1986 Geologic map of the northwest quarter of the Cave Junction quadrangle, Josephine County, Oregon, *Oregon Dept. Of Geol. And Mineral Industries Geol. Map Series GMS-38*, scale 1:24,000.
- Roure, F., and DeWever, P., 1983, Decouverte de radiolarites du Trias dans l'unité

occidentale des Klamath, sud-ouest de l'Oregon, U.S.A.: Consequences sur l'age des peridotites de Josephine, *Comptes Rendus de l'Academie des Sciences (Paris)*, **297**, 161-164.

Saleeby, J.B., 1984, Pb-U zircon ages from the Rogue River area, western Jurassic belt, Klamath Mountains, Oregon, *Geol. Soc. Amer. Abstr. with Prog.*, **16**, 331.

Steiger, R.H., and Jager, E., 1977, Subcommittee on geochronology: convention on the use of decay constants in geo- and cosmochemistry: *Earth and Planetary Science Letters*, v. 36, p. 350-362.

Streckeisen, A., 1976, To each plutonic rock its proper name: *Earth Science Reviews*, v. 12, pp. 1-33.

Palmer, A.R., 1983, The Decade of North American Geology Time Scale: *Geology*, v. 11, pp. 503-504.

Yule, J.D., Saleeby, J.B., Jones, D.L., and Silk, M., 1992, Correlation of basement terranes across the Late Jurassic Josephine inter-arc basin, southwestern Oregon and northern California, *Geol. Soc. Amer. Abs. with Programs*, **24**, 5, 93.

APPENDIX 2

U/Pb Geochronologic Methods

Laboratory Methods

Zircon separation. Geochronologic samples collected from the central Illinois River drainage area ranged from 10 to 50 kg of homogenous rock that sampled from a single outcrop. The samples were broken into fist-sized samples on the outcrop and, along river exposures, washed to remove soil. Zircons were separated from the rock mechanically and with heavy liquids, sieved to <165 micron, and separated magnetically on a Frantz isodynamic separator. The least magnetic fractions at a side-slope of 5° or less, a forward slope of 10°, and a current setting of 1.7 amps were acid washed in warm concentrated HNO₃ for 30 minutes, and rinsed at least four times in warm, once distilled water followed by reagent-grade acetone. The zircon population was sieved in various size fractions using silk screens that were disposed of after each use. Each zircon fraction was hand-picked in reagent-grade acetyl alcohol under a binocular microscope, resulting in a population consisting of greater than 99.9% zircon. Composite zircon grains and zircons with inclusions, fractures, and staining were discarded. The zircons were weighed (within 5%), placed into a previously cleaned Teflon (TFE) capsule, and rinsed in warm ultraclean HNO₃ for 15 minutes.

Zircon dissolution and isolation of U and Pb. The procedures for dissolving zircon and isolating U and Pb are similar to those described by Krogh (1973). Significant changes from Krogh's procedure include: 1) the zircons is dissolved in HF and then redissolved in HCl in a Teflon capsule; 2) a mixed ²³⁵U-²⁰⁸Pb tracer is added after the HCl solution has been aliquoted and the sample and spike are placed on a hot plate overnight to equilibrate; 3) Uranium is removed from the columns with 0.5 N HBr, rather than H₂O; and 4) a mixed ²⁰⁵U-²³⁰Th-²³⁵U tracer is used for small samples (less than 2 mg)

then added to a HF solution, diluted with concentrated HNO₃, and then placed on a hot plate overnight to equilibrate. Finally, the solution is evaporated and re-equilibrated with 6N HCl overnight on a hot plate again.

Mass spectrometry. Isotopic analyses were conducted on a 35-cm VG 90° extended geometry-sector multicollector with an accelerating voltage of ~8 kV. Pb was loaded with H₃PO₄ silica gel (Cameron and others, 1969) onto a previously outgassed rhenium filament and pre-heated in a laminar-flow hood. Isotopic data were collected during a 20-minute interval during which ²⁰⁸Pb (or ²⁰⁵Pb), ²⁰⁷Pb, and ²⁰⁶Pb were measured on separate faraday cup collectors and ²⁰⁴Pb was measured on a separate Daly multiplier. Filament temperatures averaged 1500°C and the current signal averaged ~10⁻¹¹ amps (~10⁻¹¹ ohm resistor) of ²⁰⁶Pb and decreased slightly during the course of the run. Uranium was loaded with H₃PO₄ and graphite and was analyzed as uranium metal. Filament temperatures were ~1950-2000°C. Uranium isotopic data were collected on a multicollector faraday cup, with a signal current ranging from 10⁻¹¹ to 10⁻¹² amps (10⁻¹¹ ohm resistor). For most samples, 50 sets of isotope ratios were measured, with each measurement representing a 5-second integration. NBS Pb and U standards were routinely analyzed throughout the study and did not vary significantly from given NBS values.

Data analysis. The following values have been used in adjusting the measured isotopic ratios and in the age calculations:

1) The composition and concentration of ²³⁵U - ²⁰⁸Pb tracer were measured and the compositions are as follow: ²⁰⁸Pb/²⁰⁶Pb = 1448 ± 26, ²⁰⁸Pb/²⁰⁷Pb = 4025 ± 242, ²⁰⁸Pb/²⁰⁴Pb = 9400 ± 1128 and ²³⁵U/²³⁸U = 17.27 ± 0.05. Determination of the Pb and U concentrations are: 7.6944 x 10⁻⁷ ± 1.8‰ Pb moles/g, and 1.908 x 10⁻⁸ ± 3‰ U moles/g tracer.

2) The composition and concentration of a mixed ²⁰⁵Pb-²³⁰Th-²³⁵U tracer were measured and the compositions are: ²⁰⁵Pb/²⁰⁷Pb = 3669 ± 210, ²⁰⁵Pb/²⁰⁶Pb = 3035 ± 125,

$^{205}\text{Pb}/^{204}\text{Pb} = 12264 \pm 1200$ and $^{235}\text{U}/^{238}\text{U} = 2080 \pm 21$. Determination of the Pb and U concentrations are: $0.4537 \times 10^{-9} \pm 6\%$ Pb moles/g, and $2.78 \times 10^{-9} \pm 5\%$ U moles/g tracer.

3) The isotopic composition of the unspiked aliquot was adjusted for $0.04 \pm .02$ ng blank lead with a composition of $^{206}\text{Pb}/^{204}\text{Pb} = 18.78 \pm 0.30$, $^{207}\text{Pb}/^{204}\text{Pb} = 15.61 \pm 0.22$, and $^{208}\text{Pb}/^{204}\text{Pb} = 38.5 \pm 0.60$. The amount of blank Pb was determined by isotope dilution analysis of a typical dissolution and chemical separation without zircon. The blank composition was determined through the isotopic analysis of acids and dust particles in the lab.

4) Blank U is in the 20 ng range which is negligible for U concentration determinations.

5) The isotopic composition of the spiked aliquot was adjusted for blank Pb by balancing both the $^{206}\text{Pb}/^{204}\text{Pb}$ and $^{206}\text{Pb}/^{207}\text{Pb}$ of the spiked and unspiked aliquots. Additional Pb blank in the spiked aliquot was assigned the composition cited above.

6) Common Pb remaining after correction for blank Pb is interpreted as the initial Pb, and is assigned a composition of: $^{206}\text{Pb}/^{204}\text{Pb} = 18.6 \pm 1.5$, $^{207}\text{Pb}/^{204}\text{Pb} = 15.6 \pm 0.4$, and $^{208}\text{Pb}/^{204}\text{Pb} = 38.0 \pm 2.0$ (as reported for Mesozoic samples by Doe and Zartman, 1979).

7) Constants used are: $\lambda^{238}\text{U} = 1.55125 \times 10^{-10}$; $\lambda^{235}\text{U} = 9.8485 \times 10^{-10}$; and $^{238}\text{U}/^{235}\text{U}$ (atomic) = 137.88 (Jaffey, et al., 1971; Steiger and Jager, 1977).

Table A2-1. Isotopic composition of Pb in NBS standard.

| Sample | $^{206}\text{Pb}/^{204}\text{Pb}$ | $^{206}\text{Pb}/^{207}\text{Pb}$ | $^{206}\text{Pb}/^{208}\text{Pb}$ |
|--|-----------------------------------|-----------------------------------|-----------------------------------|
| NBS 983 (given values) | 2695 ± 145 | 14.0447 ± 0.0079 | 73.43 ± 0.13 |
| Lunatic II Caltech 12 runs, 100 ng, JBS <i>ff</i> = 1%/AMU | 2729 ± 50 | 14.048 ± 0.010 | 73.43 ± 0.13 |
| UCSB MAT 261 3 runs, 100 ng, JBS <i>ff</i> = 1%/AMU | 2751 ± 20 | 14.048 ± 0.008 | 73.142 ± 0.731 |
| UCSB MAT 261 7 runs, (Mattinson, 1987) | 2742 | 14.063 | 73.626 |
| MAT 261 Factory with static daly JBS, 50 ng | 2748 ± 21 | 14.0390 ± 0.0090 | 73.346 ± 0.290 |
| VG-354 Factory with static daly JBS, 10 ng | 2703 ± 16 | 14.0340 ± 0.0060 | 73.057 ± 0.010 |
| JBS, 100ng | 2750 ± 10 | 14.0360 ± 0.0020 | 73.072 ± 0.007 |
| VG SECTOR-MS 25 ng, 7 runs, JBS | 2729 | 14.040 | 73.053 |
| VG SECTOR-MS 25 ng, 14 runs, JDY | 2704 ± 12 | 14.0468 ± 0.0093 | 73.105 ± 0.276 |

Isotopic compositions measured by the VG mass spectrometer at Caltech, by other mass spectrometers at Caltech, the University of California at Santa Barbara, and by mass spectrometers at VG and Finnegan MAT factories. Internal precisions for all runs given as 1σ . Uncertainties for actual samples are probably higher, due to minor variations in sample purity.

Table A2-2. Isotopic composition of U in NBS standard.

| Sample | $^{235}\text{U}/^{238}\text{U}$ |
|---|---------------------------------|
| NBS 500 (given values) | 0.99969 ± 0.050 |
| VG SECTOR-MS 2 runs, 50 ng, JBS (Std. error %) | 0.99795 (0.0088) |
| VG SECTOR-MS 2 runs, 100 ng, JBS (Std. error %) | 0.9977 (0.0379) |
| VG SECTOR-MS 2 runs, 100 ng, JBS (Std. error %) | 0.99985 (0.0147) |
| VG SECTOR-MS 8 runs, 100 ng, JDY (Std. error %) | 1.0005 (0.0141) |

Isotopic composition measured by the VG mass spectrometer at Caltech. Internal precisions for all runs given as 1σ . Uncertainties for actual samples are probably higher, due to minor variations in sample purity.

References

- Cameron, A.E., Smith, D.H., and Walker, R.L., 1969, Mass spectrometry of nanogram-size samples of lead: *Analytical Chemistry*, v. 41, p.525-526.
- Doe, B.R., and Zartman, R.E., 1979, Plumbotectonics, the Phanerozoic, in Barnes, H.L., eds., *Geochemistry of hydrothermal ore deposits*: Wiley Interscience, New York, p. 22-70.
- Jaffey, A.H., Flynn, K.F., Glendenin, L.E., Bentley, W.C., and Essling, A.M., 1971, Precision measurement of half-lives and specific activities of ^{235}U and ^{238}U : *Physical Reviews C*, v. 4, p. 1889-1906.
- Krogh, T.E., 1973, A low-contamination method for hydrothermal decomposition of zircon and extraction of U and Pb for isotopic age determinations: *Geochimica et Cosmochimica Acta*, v. 37, p. 485-494.
- Mattinson, J.M., 1987, U-Pb ages of zircons: a basic examination of error propagation: *Chemical Geology*, v. 66, p. 151-162.
- Steiger, R.H., and Jager, E., 1977, Subcommittee on geochronology: convention on the use of decay constants in geo- and cosmochemistry: *Earth and Planetary Science Letters*, v. 36, p. 350-362.